SMOOTH VARIABLE STRUCTURE FILTERING: THEORY AND APPLICATIONS

SMOOTH VARIABLE STRUCTURE FILTERING: THEORY AND APPLICATIONS

By

STEPHEN ANDREW GADSDEN, B.ENG.MGT.

A Thesis
Submitted to the School of Graduate Studies
in Partial Fulfilment of the Requirements
for the Degree of Doctor of Philosophy
in Mechanical Engineering

McMaster University

Doctor of Philosophy (2011) McMaster University

(Mechanical Engineering) Hamilton, Ontario

TITLE: Smooth Variable Structure Filtering: Theory and Applications

AUTHOR: Stephen Andrew Gadsden, B.Eng.Mgt. (McMaster University)

SUPERVISOR: Dr. Saeid R. Habibi

NUMBER OF PAGES: xv, 205

Dedicated to the memory of Colin D. di Cenzo, C.M., C.D., M.Sc., D.Sc., F.C.A.E., 1923-1992.

An inspiration of mine to undertake the field of engineering.

Abstract

Filtering strategies play an important role in estimation theory, and are used to extract knowledge of the true states typically from noisy measurements or observations made of the system. The name 'filter' is appropriate since it removes unwanted noise from the signal. In 2007, the smooth variable structure filter (SVSF) was introduced. This filter is based on the sliding mode control and estimation techniques, and is formulated in a predictor-corrector fashion. The SVSF makes use of an existence subspace and of a smoothing boundary layer to keep the estimates bounded within a region of the true state trajectory. This creates a robust and stable estimation strategy. The research presented in this thesis focuses on advancing the development and implementation of the SVSF.

In its original form, the SVSF does not utilize a state error covariance matrix, which is a measure of the accuracy of the state estimates. Therefore, the first major contribution of this research is the formulation of an SVSF strategy with a covariance derivation. This creates a number of research opportunities that can only be pursued and rely on the availability of the error covariance matrix. In an effort to further improve the estimation accuracy, a time-varying smoothing boundary layer is created by minimizing the covariance. This contribution significantly improves the SVSF, and provides a mechanism for combining the SVSF with other popular estimation strategies. A linear system example with the presence of uncertainties is studied which demonstrates that the proposed SVSF improves the estimation accuracy by approximately 20%. Furthermore, a new model-based fault detection strategy is created based on the interacting multiple model (IMM) method. This new method (IMM-SVSF) is applied on an experimental apparatus for the purposes of fault detection. It is able to improve upon the fault detection probability by $10-30\%$ (depending on the fault), when compared with the most commonly used strategy. The IMM-SVSF method is also found to work extremely well for target tracking problems, demonstrating an improvement of roughly 40%. This research results in a number of novel contributions, and significantly advances the development of the SVSF.

Acknowledgements

The author would like to express his gratitude to his supervisor, Dr. Saeid R. Habibi, for his guidance, advice, and support during the course of his research and the writing of this dissertation. Furthermore, special gratitude must be conveyed to fellow graduate students Mohammed El Sayed, Kevin McCullough, Yu Song, and Mohammad Al-Shabi for their kind assistance, technical expertise, and support during this research.

Financial support provided by the School of Graduate Studies, the Department of Mechanical Engineering, and the Ontario Graduate and National Sciences and Engineering Research Council scholarships is acknowledged and greatly appreciated (OGS and NSERC, respectively).

I would also like to express my gratitude to my parents, Eileen and Stephen, and siblings, Tricia, Christian, and Domenique, for their encouragement and support throughout my entire academic career. Furthermore, without the loving support of my fiancée, Yu Sun Chung, this work would not have been possible. 항상 변함없이 나를 지원해주는 정유선에세 항상 고맙고 함께할 우리의 미래를 기대합니다.

Table of Contents

List of Figures

List of Tables

List of Nomenclature

A	Linear system matrix
A_E	EHA piston area
B or G	Input gain matrix
B_E	EHA load friction
C	Linear measurement matrix
C_M	Controllability matrix
D_P	EHA pump displacement
e_x	State error vector (unless otherwise stated)
e_y	Artificial measurement (or innovation) error vector
e_z	Measurement (or innovation) error vector
f	Nonlinear system (or process) function
F	Linearized system (or process) matrix
G_{EHA}	EHA transfer function
h	Nonlinear measurement function
H	Linearized measurement matrix
i	Index value
I	Identity matrix
j	Index value
J	Fisher Information Matrix (FIM)
k	Step value (for recursive process)
K	Gain value (used by filter)
L	EHA leakage coefficient
m	Number of measurements
M	EHA load mass
M_3	Third-order moments
M_4	Fourth-order moments

M_P	Matrix consisting of second and fourth-order moments
n	Number of states
O_M	Observability matrix
P	State error covariance matrix
Q	System noise covariance matrix
r	Number of models (or modes)
R	Measurement noise covariance matrix
S	Innovation covariance matrix
T	Sample rate
u	Input to the system (scalar or vector)
v	Measurement noise (scalar or vector)
V	Lyapunov function
V_0	EHA initial cylinder volume
w	System noise (scalar or vector)
W	Weights (usually for sigma or cubature points)
x	States or parameters (scalar or vector)
X	Propagated states (usually for sigma or cubature points)
y	Artificial measurement (scalar or vector)
z	Measurements (scalar or vector)
$\bar{a}$ or $diag(a)$	Creation of a square matrix with diagonal elements of some vector a
$\bar{A}$ or $diag(A)$	Creation of a vector with diagonal elements of some matrix A
$\|a\|$	Absolute value of some parameter a
$\|a\|_{Abs}$	Absolute value of some vector or matrix a
$E\{a\}$	Expectation of some random vector or parameter a
$k+1\|k$	Subscript, a priori (before the fact) value
$k+1\|k+1$	Subscript, a posteriori (after the fact) value
$\mathcal{N}(\mu, \sum)$	Gaussian distribution with μ mean, and $\sum$ covariance
$p(a)$	Probability of some value a
p_{ij}	Mode transition matrix (a designer value)

$sat(a)$	Saturation of some value a (such that $-1 \leq a \leq 1$)
$sign(a)$	Signum function of some value a (such that a may equal -1, 0, or 1)
$\circ$	Schur product (element by element matrix multiplication)
$*$	Convolution operator
β	Existence subspace value (SVSF)
β_e	EHA effective bulk modulus
γ	'Memory' or convergence rate (SVSF)
ψ	Smoothing boundary layer value (SVSF)
μ_j	Mode probabilities
$\mu_{i\|j}$	Mixing probabilities
Λ_j	Likelihood function
a^T	Transpose of a vector or matrix a
a^+	'Pseudoinverse' of some vector a
^	Estimated value of some state or parameter
$\sim$	Error of some state or parameter

Chapter 1

Introduction

This chapter provides an introduction to the research performed; including the problem statement, research contributions and novelty, and organization of the thesis.

1.1 Problem Statement

Estimation theory is considered to be a part of signal processing and statistics. It involves finding a value of some parameter of interest, which affects the output of a system, often in the presence of inaccurate or uncertain observations. The purpose of estimation, as described by Bar-Shalom et al. in [28], can be one of many reasons: determination of planet orbit parameters, statistical inference, aircraft traffic control system (i.e., tracking), use in control plants with uncertainties (i.e., parameter identification or state estimation), message retrieval from noisy signals (i.e., communication theory), and also signal and image processing. The ability to successfully control a mechanical or electrical system depends on the knowledge of the true states or parameters of interest. For example, consider a linear mechanical system, where the dynamics such as position, velocity, and acceleration are defined to be the states of interest. The state dynamics, or how the system operates with time, may be captured by using a state representation as follows:

$$x_{k+1} = Ax_k + Bu_k + w_k \tag{1.1.1}$$

Where x_k defines the system states, A is the linear system matrix, B is the input gain matrix, u_k is the corresponding input to the system, and w_k refers to the system noise present in the system. To understand the behaviour of a system, elements from the state vector need to be observed or measured. Sensors placed in the environment are used to measure the states of interest. A relationship exists between the measurements and the states, and may be defined as follows:

$$z_{k+1} = Cx_{k+1} + v_{k+1} \tag{1.1.2}$$

Where z_k defines the measurements, C refers to the linear measurement matrix, and v_k refers to the measurement noise present in the sensors. Unless otherwise stated, it is assumed in this thesis that the system and measurement noises are modeled as Gaussian noise, with zero mean and covariance's Q_k and R_k, respectively as follows:

$$p(w_k) \sim \mathcal{N}(0, Q_k) \tag{1.1.3}$$

$$p(v_k) \sim \mathcal{N}(0, R_k) \tag{1.1.4}$$

Therefore, it is the role of a filter to extract knowledge of the true states typically from noisy measurements or observations made of the system, and form state estimates $\hat{x}_k$. The name 'filter' is appropriate since it removes unwanted noise from the signal. Typically, in solving linear estimation problems, the system and measurement dynamics are model based and may be described by discrete-time equations, such as (1.1.1) and (1.1.2). The concept of filter applies equally well to nonlinear systems and measurements, defined respectively by:

$$x_{k+1} = f(x_k, u_k) + w_k \tag{1.1.5}$$

$$z_{k+1} = h(x_{k+1}) + v_{k+1} \tag{1.1.6}$$

Where f and h represent the nonlinear system and measurement models, respectively. The most popular and well-studied estimation method is the Kalman filter (KF), which was introduced in the 1960s [29,30]. As will be explained later in Chapter 2, the KF yields a statistically optimal solution for linear estimation problems, as defined by (1.1.1) and (1.1.2), in the presence of Gaussian noise.

The KF is formulated in a predictor-corrector manner, and is implemented recursively. The states are first estimated using the system model, termed as a priori estimates, meaning 'prior to' knowledge of the observations. A correction term is then added based on the innovation (also called residuals or measurement errors), thus forming the updated or a posteriori (meaning 'subsequent to' the observations) state estimates. The KF has been broadly applied to problems covering state and parameter estimation, signal processing, target tracking, fault detection and diagnosis, and even financial analysis [31,32]. The success of the KF comes from the optimality of the Kalman gain in minimizing the trace of the a posteriori state error covariance matrix. The trace is taken because it represents the state error vector in the estimation process [33]. A number of different methods have extended the classical KF to nonlinear systems, with the most popular and simplest method being the extended Kalman filter (EKF) [34,35]. The EKF is conceptually similar to the KF; however, requires linearization of the nonlinear system and measurements models. The optimality of the KF comes at a price of stability and robustness. The KF assumes that the system model is known and linear, the system and measurement noises are zero mean Gaussian, and the states have initial conditions with known means and variances [34,28]. However, the previous assumptions do not always hold in real applications. If these assumptions are violated, the KF may yield suboptimal results and can become unstable [36].

In 2007, the smooth variable structure filter (SVSF) was introduced and is based on variable structure theory and sliding mode concepts [37]. It implements a switching gain to converge the estimates to within a boundary of the true states, referred to as the existence subspace. As demonstrated in the literature, and to be reinforced throughout this thesis, the SVSF provides a robust and stable estimate to modeling uncertainties and errors [37,38]. This is particularly advantageous when the system model is not well-defined or known to the user. The SVSF also offers other advantages which will be explored throughout this thesis. However, since the filtering strategy is relatively new, a number of research opportunities exist with the SVSF. It is therefore the goal of this research to further advance and develop the SVSF; in particular, to improve its performance and increase the number of its useful applications.

1.2 Research Contributions and Novelty

The main research involves the field of state and parameter estimation, with a concentration on further developing the SVSF. In its current form, the SVSF is a sub-optimal filtering strategy (i.e., it does not yield an optimal state estimate in terms of estimation error), however it is very robust and stable to modeling uncertainties and errors. Expanding on the current form of the SVSF yields many more opportunities and applications for this new filter. The general overview of the research is shown in the following figure. In its current form, the SVSF is not a classical filter in the sense that it does not have or make use of a covariance matrix, which is a measure of the state estimation error. Therefore, the first main contribution of this research is the creation of a covariance formulation for the SVSF.

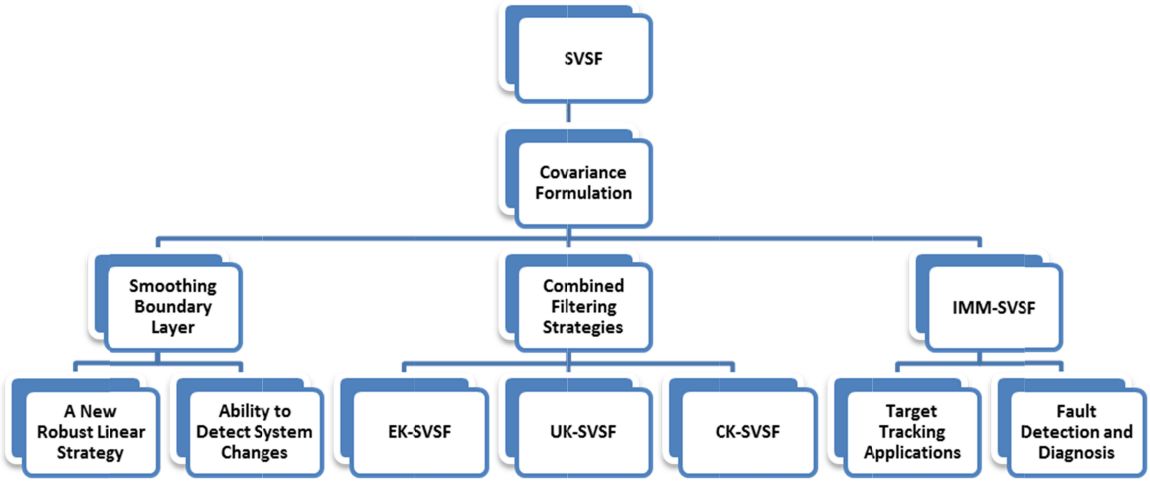

Figure 1.2.1. Research Flowchart

The addition of the covariance creates many new opportunities for research, including the development of equations for the smoothing boundary layer (SBL), which would make the widths time-varying (i.e., changing widths based on the errors and modeling uncertainties present in the estimation process). The boundary layer widths would then be calculated at each time step, as opposed to using some predetermined, fixed conservative width throughout the estimation process.

A time-varying SBL increases the overall estimation accuracy of the SVSF, and creates a mechanism for the SVSF to be combined with other Kalman-based filtering strategies to further improve accuracy while maintaining robustness to uncertainties. Furthermore, a time-varying SBL provides another indicator of performance, including the ability to detect system changes. Another contribution of this research is the formulation of an interacting multiple model (IMM) method based on the SVSF filtering strategy. This methodology can be applied on target tracking, as well as fault detection and diagnosis problems. The IMM-SVSF methodology makes use of a finite number of models (i.e., based on the system behaviour), and the robustness of the SVSF strategy, to create a more accurate estimation method.

These contributions are significant to the development of the SVSF, as well as to the body of knowledge in the estimation field. To summarize the research, the contributions may be broken down into primary and secondary research goals, as follows.

Primary Contributions:

1. Covariance derivation for the SVSF estimation strategy (linear and nonlinear systems).
2. Time-varying SBL widths, based on minimizing the trace of the state error covariance.
3. Formulation of the IMM-SVSF (based on the covariance derivation for the SVSF) with applications for fault detection and diagnosis of mechanical and electrical systems, as well as target tracking problems.

The following secondary contributions are only possible due to the primary contributions, and are listed as follows.

Secondary Contributions:

1. Proposal of a smoothing boundary layer matrix, as opposed to a vector, which is important for the calculation of a time-varying SBL.
2. Creation of a new robust filtering strategy for linear systems, based on combining elements of the KF with the SVSF.

3. Development of the time-varying smoothing boundary layer creates another indicator of performance. In particular, the widths may be used to determine the presence of modeling uncertainties, as well as detect any changes in the system.

4. Combination of the SVSF with other nonlinear estimation strategies to increase the overall estimation accuracy while maintaining stability (i.e., extended KF, unscented KF, and cubature Kalman filter).

5. A better understanding of how the SVSF behaves according to its smoothing boundary layer, and the presence of modeling uncertainties.

The advancements of the SVSF, as outlined above, are validated through a number of computer experiments (typically mechanical systems and target tracking examples). Furthermore, an experimental setup (the electrohydrostatic actuator) was used to further demonstrate the theory developed in this thesis.

1.3 Organization of the Thesis

This thesis is organized as follows. Chapter 2 reviews the main literature on conventional estimation forms such as the Kalman filter. Furthermore, it provides an overview of the popular multiple model methods, and briefly discusses sliding mode estimation. In Chapter 3, the SVSF is described in detail, including its predecessors. A covariance derivation for the SVSF is provided in Chapter 4, and is applied to both linear and nonlinear systems. Two computer experiments are provided in order to demonstrate the results of this chapter.

A new form of the SVSF based on minimizing the trace of the covariance is derived and discussed in Chapter 5. This allows the SVSF to be combined with other filtering strategies (such as the Kalman filter, extended and unscented Kalman filter, and cubature Kalman filter) to increase the overall accuracy and robustness of the estimation process. Chapter 6 introduces the IMM form of the SVSF. This new strategy, referred to as the IMM-SVSF, is used primarily for two applications: target tracking (i.e., radars and global position systems), and fault detection and diagnosis of mechanical and electrical systems (i.e., an electrohydrostatic actuator).

Recommendations for future research work and concluding remarks are made in the final chapter. Furthermore, a number of conference and journal publications have been prepared during the research process and development of this thesis [1-27]. These papers are a result of research directly and indirectly related to the work presented in the following chapters.

Chapter 2

Literature Review

Estimation theory is an important tool for the successful control of mechanical and electrical systems. This chapter provides a comprehensive review of a number of conventional estimation strategies (i.e., Kalman-based methods). The concepts of multiple model methods are also reviewed. Finally, the chapter concludes with introducing and providing an overview of sliding mode estimation methods.

2.1 A (Very) Brief History of Estimation Theory

Modern control theory relies on reliable state estimates in order to provide accurate and safe control of mechanical and electrical systems. Estimation theory is therefore an important tool for providing accurate state and parameter estimates. The development of estimation techniques spans nearly five centuries, and involves a number of contributors from a variety of fields. The following figure shows the lifelines of a number of important contributors to the field of estimation, and who are famous in their own right [39]. Girolamo Cardano made the first major contribution by providing an accurate analysis of probabilities, and also helped to formulate the law of large numbers [34]. His work on general probability was developed further by Pascal, Fermat, Huygens, and Bernoulli [34]. Thomas Bayes would later derive his famous rule for statistical inference, which forms the basis for some Bayesian estimation techniques [32]. During the nineteenth century, it became apparent that probabilistic theory could be used to study and even model natural phenomena and systems [39].

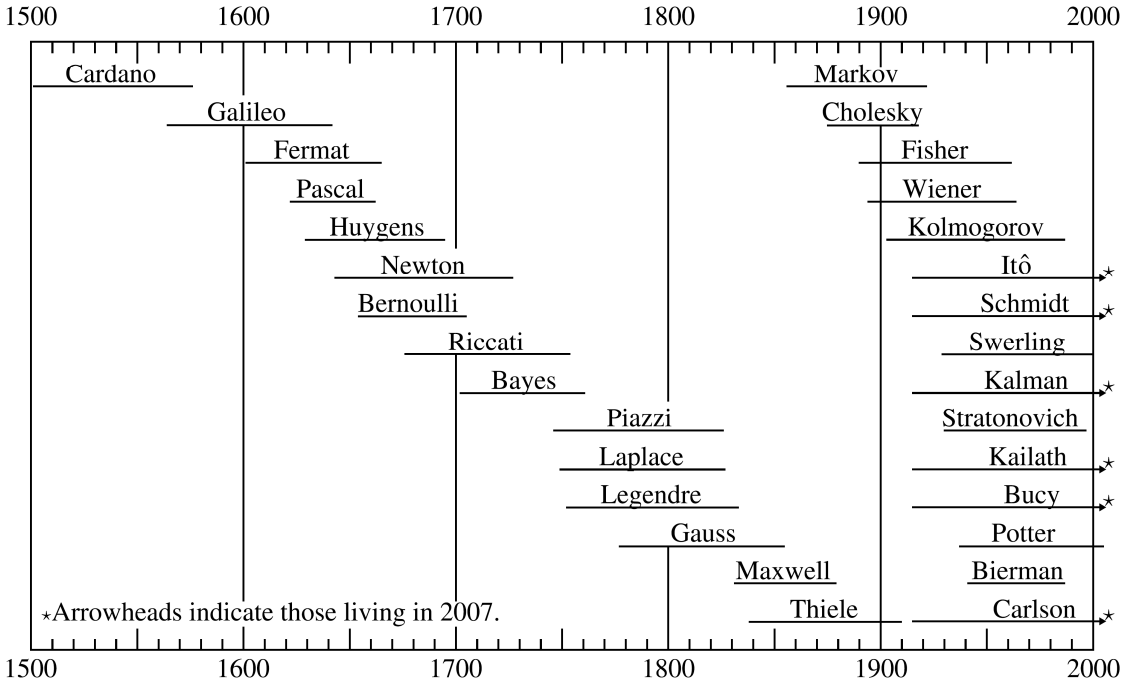

Figure 2.1.1. Lifelines of Important Contributors to Estimation Theory [39]

Based on probability and statistical methods, Andrei Markov developed the Markov process or chain [28]. This theory states that the instantaneous variation with time of the probability distribution of system states is determined by its current distribution, which includes the effects of all the past events of the system [39]. Another very important contributor to the field of estimation was Andrei Kolmogorov, who helped formulate the mathematical basis of probability and random processes [39]. In fact, his work, along with Norbert Wiener, founded the basics of estimation; including the theory of prediction, filtering, and smoothing. The concept of prediction refers to estimation methods that use measurements or observations prior to the time that the state of the system is to be estimated, or $t_{obs} < t_{est}$ [28]. Filters use measurements up to and including the time of interest, or $t_{obs} \leq t_{est}$. Finally, smoothers make use of measurements beyond the desired time of interest, such that the estimate is refined further, or $t_{obs} > t_{est}$ [28].

During the 1940s, Wiener worked on developing an automatic controller for directing antiaircraft fire, based on noisy radar information [39]. His work ultimately led to the derivation of an optimal estimator, based on continuous-time [40]. Meanwhile, Kolmogorov independently derived an optimal linear predictor for discrete-time systems [28,41]. Their work would later be referred to as the Wiener-Kolmogorov filter[1], a predecessor to the popular Kalman filter [34].

2.2 The Wiener-Kolmogorov Filter

The Wiener-Kolmogorov filter (WF) is a statistical estimation method that estimates the state of a system in an effort to minimize the mean square estimation error [39]. The WF solution is based on scalar measurements and stationary signals, with known spectral properties subject to white noise [42]. The goal of the WF (and most filters) is to remove unwanted noise from a measurement or signal [34]. The following figure summarizes the WF process.

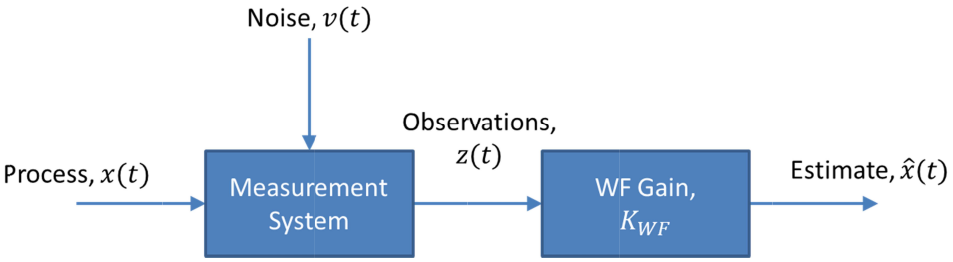

Figure 2.2.1. Summary of the WF Estimation Process (Adapted from [28])

Based on the above figure, consider the following measurement $z(t)$, which is a function of the noise free signal $x(t)$ and the noise $v(t)$ [28]:

$$z(t) = x(t) + v(t) \tag{2.2.1}$$

[1] In some literature, it is also known simply as the Wiener filter (WF) [34]. However, since Kolmogorov did in fact develop the concept independently to Wiener, this thesis will refer to it as the Wiener-Kolmogorov filter. Note that Kolmogorov published his results one year prior to when Wiener developed his version [41]. However, it did not become immediately popular in Western literature due to Kolmogorov's work being published first in Russian [34].

An estimate of the signal $\hat{x}(t)$ may be obtained using a gain K_{WF}, as follows:

$$\hat{x}(t) = K_{WF}(t) * z(t) \tag{2.2.2}$$

Where $*$ refers to the convolution operator. The solution that yields the estimate $\hat{x}(t)$ of the process is obtained in the frequency domain, where the gain K_{WF} is a transfer function calculated by using Fourier transforms [28]. This process attempts to minimize the mean square error. The WF gain may be defined by [34,42]:

$$K_{WF}(t) = \mathcal{F}^{-1}\left[\frac{S_z - S_v}{S_z}\right] \tag{2.2.3}$$

Where $\mathcal{F}^{-1}$ refers to the inverse Fourier transform. Furthermore, S_z and S_v refer to the Fourier transforms of the measurement and noise autocorrelations, respectively (i.e., the power spectrums) [34,42]. During the 1950s, a significant amount of work was put into developing the WF strategy [43,44]. In particular, NASA was interested in implementing estimation strategies for space navigation problems [45].

2.3 The Kalman Filter

In 1960, Rudolph Kalman presented a new approach to linear filtering and prediction problems, which would later become known as the Kalman filter (KF) [29]. This method was successfully applied by NASA for their lunar and Apollo missions, and quickly became the 'workhorse' of estimation [34,46]. The KF yields a statistically optimal solution for linear estimation problems, as defined by (1.1.1) and (1.1.2), in the presence of Gaussian noise defined by (1.1.3) and (1.1.4). The KF is a model based method, derived in the time domain and a discrete-time setting. A continuous-time version was developed by Kalman and Bucy, and is consequently referred to as the Kalman-Bucy filter [47]. However, this thesis is concerned only with discrete-time estimation problems.

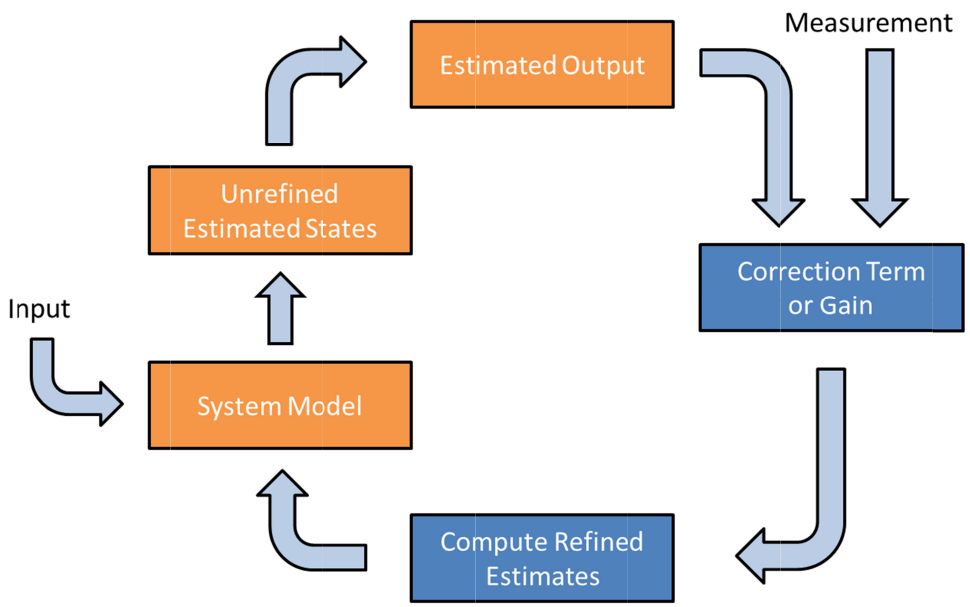

Figure 2.3.1. Overview of the Predictor-Corrector Method

Like many other filters, the KF is formulated in a predictor-corrector manner. The general form of a predictor-corrector method is shown in the above figure. The states are first estimated using the system model and input, termed as a priori estimates, meaning 'prior to' knowledge of the observations. A correction term is then added based on the innovation (also called residuals or measurement errors), thus forming the updated or a posteriori (meaning 'subsequent to' the observations) state estimates.

The KF has been broadly applied to problems covering state and parameter estimation, signal processing, target tracking, fault detection and diagnosis, and even financial analysis [31,32]. The success of the KF comes from the optimality of the Kalman gain in minimizing the trace of the a posteriori state error covariance matrix [29]. The trace is taken because it represents the state error vector in the estimation process [33]. The KF implements the state space representation, which allows the method to be easily computed recursively using computers [39]. The following section summarizes the main KF process.

2.3.1 The KF Equations

The following five equations form the core of the KF algorithm, and are used in an iterative fashion. Equations (2.3.1.1) and (2.3.1.2) define the a priori state estimate $\hat{x}_{k+1|k}$ based on knowledge of the system A and previous state estimate $\hat{x}_{k|k}$, and the corresponding state error covariance matrix $P_{k+1|k}$, respectively.

$$\hat{x}_{k+1|k} = A\hat{x}_{k|k} + Bu_k \tag{2.3.1.1}$$

$$P_{k+1|k} = AP_{k|k}A^T + Q_k \tag{2.3.1.2}$$

The Kalman gain K_{k+1} is defined by (2.3.1.3), and is used to update the state estimate $\hat{x}_{k+1|k+1}$ as shown in (2.3.1.4). The gain makes use of an innovation covariance S_{k+1}, which is defined as the inverse term found in (2.3.1.3).

$$K_{k+1} = P_{k+1|k}C^T\left(CP_{k+1|k}C^T + R_{k+1}\right)^{-1} \tag{2.3.1.3}$$

$$\hat{x}_{k+1|k+1} = \hat{x}_{k+1|k} + K_{k+1}\left(z_{k+1} - C\hat{x}_{k+1|k}\right) \tag{2.3.1.4}$$

The a posteriori state error covariance matrix $P_{k+1|k+1}$ is then calculated by (2.3.1.5), and is used iteratively, as per (2.3.1.2).

$$P_{k+1|k+1} = (I - K_{k+1}C)P_{k+1|k} \tag{2.3.1.5}$$

The derivation of the KF is well documented, with details available in [29,30,33]. The optimality of the KF comes at a price of stability and robustness. The KF assumes that the system model is known and linear, the system and measurement noises are white, and the states have initial conditions with known means and variances [28,34]. However, the previous assumptions do not always hold in real applications. If these assumptions are violated, the KF yields suboptimal results and can become unstable [36]. Furthermore, the KF is sensitive to computer precision and the complexity of computations involving matrix inversions [39].

2.3.2 Overcoming Issues with the KF

This section summarizes methodologies for overcome issues with the KF (i.e., strict assumptions, numerical stability, and matrix inversions). As demonstrated in literature, the state error covariance matrix must be symmetric and positive-definite in order to properly represent the statistics for state vector components [48]. In linear algebra, a symmetric matrix is defined as a square matrix which is equal to its corresponding transpose. Consider a symmetric matrix P, then the following is satisfied:

$$P = P^T \tag{2.3.2.1}$$

A symmetric matrix P is considered positive-definite if the following is satisfied:

$$b^T P b > 0 \tag{2.3.2.2}$$

Where b is a non-zero vector with real entries. Essentially, the above two definitions ensure that the off-diagonal elements of the state error covariance matrix are equal to each other (i.e., $p_{ij} = p_{ji}$), and that the elements along the diagonal are real and positive values (i.e., the square of each estimation error is guaranteed to be positive). Factored-form (or square-root) filters help to ensure numerical stability [49,50,51]. The square-root formulation makes use of three powerful linear algebra techniques: QR decomposition, Cholesky factor updating, and efficient least squares [52,53]. The covariance matrix is broken up into factored terms, which are propagated forward and updated at each measurement [48]. The factors are multiplied together reforming the covariance matrix, thus ensuring it to be positive definite. The two most popular square-root filters are Potter's square-root filter and Bierman-Thornton's UD filter [54]. The UD filter has similar accuracy to Potter's strategy, however is less computationally expensive [34]. Introduced in the late 1970s, UD filtering is based on transformation methods that involve an upper triangle covariance factorization (2.3.2.3) [55,56]. Although the UD strategy is considered a type of square-root filter, no square roots are actually calculated; where the covariance P is defined by:

$$P = UDU^T \tag{2.3.2.3}$$

Where U is an upper triangle matrix with diagonal elements that are unity (all 1), and $D = diag(d_1, \dots, d_n)$. The matrices U and D are referred to as the UD factors of the covariance matrix P. A number of different strategies exist to perform UD decomposition (i.e., to create U and D matrices) [39]. Further to the UD strategy, numerical stability for filtering strategies can be improved by factoring the covariance matrix into Cholesky factors [57]. This was discovered when attempting to improve the stability of the KF when dealing with finite-precision arithmetic [39]. Essentially the nature of the KF remains the same; however, an equivalent statistical parameter is used and is found to be less sensitive to round-off errors [58]. Increasing the arithmetic precision reduces the effects of round-off error, which improves the overall stability of the filter.

Another strategy which can be used to overcome KF instabilities involves imposing boundaries on the state estimate by a priori or designer knowledge of the system [28]. For example, given the upper bounds on the level of parameter or modeling uncertainty, the KF gain may be bounded to help improve estimation stability [28]. Furthermore, the a priori and a posteriori state error covariance matrices may be modified to include the effects of modeling uncertainty. The addition of modeling uncertainties increases the covariance value, which makes sense intuitively since the presence of uncertainties generally increases the estimation error. For example, consider the modified a priori covariance matrix $P_{k+1|k}$ defined as follows [28]:

$$P_{k+1|k} = \hat{A}P_{k|k}\hat{A}^T + Q_k + \tilde{A}X_k\tilde{A}^T + \hat{A}Y_{k|k}\hat{A}^T + \tilde{A}Y_{k|k}^T\tilde{A}^T \tag{2.3.2.4}$$

Equation (2.3.2.4) represents the a priori state error covariance matrix when modeling error is present in the estimation process [28]. Note that the last three terms have been added to the original covariance calculation (2.3.1.2), which increases the magnitude of the covariance matrix (by capturing the additional modeling uncertainties). The matrix X_k refers to a mean square value (MSV) matrix (or a correlation matrix), and represents the expectation of the true states x_k, or $E\{x_k x_k^T\}$. The matrix $Y_{k|k}$ is the cross-term between the true states x_k and the error of the states $\tilde{x}_k$, or $E\{x_k \tilde{x}_k^T\}$. The corresponding a posteriori covariance matrix $P_{k+1|k+1}$ is redefined as follows [28]:

$$\begin{aligned} P_{k+1|k+1} = {} & \left(I - K_{k+1}\hat{C}\right)P_{k+1|k}\left(I - K_{k+1}\hat{C}\right)^T + K_{k+1}R_{k+1}K_{k+1}^T \\ & + K_{k+1}\tilde{C}X_{k+1}\tilde{C}^T K_{k+1}^T - \left(I - K_{k+1}\hat{C}\right)Y_{k+1|k}\tilde{C}^T K_{k+1}^T \\ & - K_{k+1}\tilde{C}Y_{k+1|k}^T\left(I - K_{k+1}\hat{C}\right) \end{aligned} \tag{2.3.2.5}$$

Note that the matrices X_k and $C_{k|k}$ also need to be calculated recursively in order to update the state error covariance matrix. The correlation matrix X_k is initialized and calculated using the following equations, respectively [28]:

$$X_0 = E\{x_0 x_0^T\} = \hat{x}_{0|0}\hat{x}_{0|0}^T + P_{0|0} \tag{2.3.2.6}$$

$$X_{k+1} = AX_kA^T + Q_k \tag{2.3.2.7}$$

The cross-term $Y_{k|k}$ is initialized and calculated (predicted and updated) using the following three equations, respectively [28]:

$$Y_{0|0} = P_{0|0} = P_0 \tag{2.3.2.8}$$

$$Y_{k+1|k} = AX_kA^T + AY_{k|k}^T\tilde{A}^T + Q_k \tag{2.3.2.9}$$

$$Y_{k+1|k+1} = \left(I - K_{k+1}\hat{C}\right)Y_{k+1|k} - K_{k+1}\tilde{C}X_{k+1} \tag{2.3.2.10}$$

The previous equations summarize a methodology for calculating the state error covariance matrix for the KF process, in the presence of modeling error. Note that the calculation of the matrices requires knowledge of the true matrices A, C, Q, and R. In most cases, these matrices are not available; however, their nominal values may be used to represent an average scenario [28]. Furthermore, the true state values x_k are also required in order to calculate X_k and $Y_{k|k}$. Therefore, the previous equations may only be used practically for studying the sensitivity of the KF to modeling errors (i.e., how it changes the size of the covariance matrix) [28]. Other methodologies for improving the KF robustness to modeling errors include the addition of fictitious process (system) noise, and using a fading memory strategy [34,42]. Essentially, modifying the system noise matrix by adding a fictitious amount is done when less confidence is placed in the system model used by the filter [34]. This in turn causes the filter to place more emphasis on the measurements, and less on the system model which may be incorrect [34,59,60].

Typically, tuning is done by trial and error since the modeling errors are almost always unknown (if they were known no tuning would be required!) [42]. A fading memory strategy is a simple way for the filter to 'forget' measurements in the distant past, and place more emphasis on the information available now [34]. It is important to note that this causes the KF to lose optimality, however it helps to overcome robustness and stability issues. Consider the following modification to the a priori state error covariance (2.3.1.2) [34,61,62]:

$$P_{k+1|k} = \alpha A P_{k|k} A^T + Q_k \tag{2.3.2.11}$$

Where α is some positive constant, typically slightly larger than 1 (i.e., $\alpha = 1.01$). The value may be selected based on how much of the past measurements are desired (i.e., how much one wants the filter to 'forget') [34]. This strategy has been shown to improve the KF performance in terms of robustness to modeling error [42]. A time-varying value for α has also been proposed, in an effort to further improve upon the performance [28,42].

In addition to the methods presented earlier, the KF performance may be improved numerically by implementing the 'Joseph form' of the a posteriori state error covariance matrix [34,39]. Suppose that (2.3.1.5) is presented as follows [34]:

$$P_{k+1|k+1} = (I - K_{k+1}C)P_{k+1|k}(I - K_{k+1}C)^T + K_{k+1}R_{k+1}K_{k+1}^T \tag{2.3.2.12}$$

The form (2.3.2.12) was formulated in the 1960s by Peter Joseph, and has been shown to be more stable and robust than the simpler form (2.3.1.5) [63,64]. The Joseph stabilized version of the a posteriori covariance equation guarantees that it will always be symmetric positive definite, provided that the a priori covariance matrix is symmetric positive definite [34]. Note that the simpler form (2.3.1.5) does not guarantee symmetry or positive definiteness [28]. The simpler form of the KF a posteriori covariance is calculated when the Kalman gain equals the optimal value. Equation (2.3.1.5) is typically used in practice because it is computationally cheaper, however can lead to numerical instabilities [34]. As will be described later in Chapter 4, the Joseph form of the a posteriori covariance (2.3.2.12) will be used throughout this thesis.

Another simple methodology for improving the numerical stability of the state error covariance matrix involves forcing the covariance to be symmetric and initializing it appropriately [34]. For example, after the a posteriori covariance value has been calculated, it may be modified as follows [34,42]:

$$P_{k+1|k+1} = (P_{k+1|k+1} + P_{k+1|k+1}^{\mathrm{T}})/2 \tag{2.3.2.13}$$

Other ways involve forcing the off-diagonal terms to be equivalent to each other (i.e., $P_{ij} = P_{ji}$), or forcing the eigenvalues of $P_{k+1|k+1}$ to be positive [34]. Note that these solutions do not result in major improvements, however they should always be implemented since they are relatively straightforward and easy [34]. Furthermore, it is important to use an appropriate initial covariance value such that it does not experience large or abrupt changes throughout the estimation process [42].

The Gaussian assumption for the noise (which is done for a simpler derivation) may also cause instabilities. One method for overcoming this sometimes strict assumption is to model the non-Gaussian probability distribution with a Gaussian sum (i.e., a finite number of well-designed Gaussian probability distributions). Although this increases the computational complexity of the filter, this method has been shown to work very well [65].

Despite issues with robustness and instability, the KF remains one of the most popular and well-studied filter since it was introduced in the 1960s [30,32]. The optimality of the KF for linear estimation problems makes it an attractive choice for state estimation [34]. However, in some cases the KF strategy may fail, typically due to finite precision arithmetic and modeling errors [66]. To summarize the KF strategy, it is important to note that the KF relies on the following strict assumptions [34]:

- The system under study is linear.
- Matrices A, C, Q, and R, are exactly known.
- The system and measurement noises (w and v) are zero-mean with a Gaussian distribution (Q and R), and are completely uncorrelated.

If any of these assumptions are violated, the KF yields suboptimal results and can become unstable [36]. However, this section introduced a number of methodologies for improving the KF performance and stability. These strategies may be summarized by the following list [34]:

- Increase arithmetic precision.
- Utilize a form of square root filtering (i.e., UD filtering or Cholesky factorization).
- Force P to be symmetric at each time step.
- Initialize P appropriately.
- Implement a fading memory strategy.
- Add fictitious system noise.

The above list is by no means inclusive. However, these strategies are the most popular in terms of improving the KF performance [34].

2.4 Nonlinear Estimation Strategies

In nature, all systems are in fact nonlinear, as described by the following system and measurement equations.

$$x_{k+1} = f(x_k, u_k) + w_k \tag{2.4.1}$$

$$z_{k+1} = h(x_{k+1}) + v_{k+1} \tag{2.4.2}$$

Due to the success of the KF with linear applications, it was natural to expand on the method for nonlinear systems and measurements. The first such expansion led to a perturbation form of the KF (PKF), also known as the linearized KF (LKF) [67,68,69]. The PKF was the predecessor to the now popular extended Kalman filter (EKF), which was originally called the Kalman-Schmidt filter [70]. Following the development of the EKF, an unscented form (UKF) was created in an effort to capture a greater estimate of the nonlinearities [36,71].

More recently, the cubature KF (CKF) was proposed to further improve upon the estimation accuracy for nonlinear systems and measurements [72]. Other popular nonlinear estimation strategies include the H-infinity filter and the particle filter (PF) [31,73]. The PF may also be known as Monte Carlo filters [31], interacting particle approximations [74], bootstrap filters [75], condensation algorithms [76], and survival of the fittest methods [77], to name a few. Although these filters are effective and offer other advantages (and disadvantages), only the Kalman-based filters will be reviewed in this thesis.

2.4.1 The Perturbation Kalman Filter

The perturbation Kalman filter (PKF) estimates the state of nonlinear dynamic systems by linearizing its nonlinearities [68]. Linearization techniques are used to simulate linear behaviour locally about a point of interest. Assuming that the function of interest is differentiable, then a Taylor series expansion may be used for linearization [42]. In general, a Taylor series expansion of some function f about a point x is defined as follows [68]:

$$f(x+\Delta x) = f(x) + f^1(x)\Delta x + \frac{f^2(x)}{2!}\Delta x + \cdots + \frac{f^n(x)}{n!}\Delta x \tag{2.4.1.1}$$

Where f^i is the i^{th} derivative of f with respect to x, evaluated at the linearization point x, and where Δx is the perturbation [68]. The PKF estimates the states by combining a nominal trajectory state with an estimate of the perturbation. It is based on the assumption that the system and measurement can be modeled respectively by [34]:

$$x_{k+1} = x_k^{nom} + \Delta x_k \tag{2.4.1.2}$$

$$z_{k+1} = z_{k+1}^{nom} + \Delta z_{k+1} \tag{2.4.1.3}$$

Where the nominal states and measurements are found by $x_{k+1}^{nom} = f(x_k^{nom})$ and $z_{k+1}^{nom} = h(x_{k+1}^{nom})$, respectively. Note that a nominal trajectory is defined as a trajectory in which the random variables take on their expected values [68]. The true values will not follow the nominal trajectory exactly due to the presence of random noise (system or measurement), which are referred to as perturbations [68].

The system and measurement perturbations are approximated respectively as follows [34]:

$$\Delta x_{k+1} \approx F_k \Delta x_k + w_k \tag{2.4.1.4}$$

$$\Delta z_{k+1} \approx H_{k+1} \Delta x_{k+1} + v_{k+1} \tag{2.4.1.5}$$

Note that the matrices F_k and H_{k+1} are Jacobian matrices with partial derivatives of the system $f(x)$ or measurement $h(x)$ function with respect to the state x or measurement z, respectively. These are evaluated at the nominal state value x_k^{nom}, as follows [68]:

$$F_k = \left. \frac{\partial f(x)}{\partial x} \right|_{x=x_k^{nom}} \tag{2.4.1.6}$$

$$H_{k+1} = \left. \frac{\partial f(x)}{\partial x} \right|_{x=x_{k+1}^{nom}} \tag{2.4.1.7}$$

The PKF is initialized with the perturbation estimate $\widehat{\Delta x}_0$ and uncertainty P_0. The initial estimate is usually set to zero. The PKF calculates the a priori perturbation estimate and covariance respectively as follows [68]:

$$\widehat{\Delta x}_{k+1|k} = F_k \widehat{\Delta x}_{k|k} \tag{2.4.1.8}$$

$$P_{k+1|k} = F_k P_{k|k} F_k^T + Q_k \tag{2.4.1.9}$$

Similar to the standard KF structure, the PKF gain is calculated as follows [68]:

$$K_{k+1} = P_{k+1|k} H_{k+1}^T \left(H_{k+1} P_{k+1|k} H_{k+1}^T + R_{k+1} \right)^{-1} \tag{2.4.1.10}$$

The a posteriori perturbation estimates and covariance are then calculated respectively as follows [68]:

$$\widehat{\Delta x}_{k+1|k+1} = \widehat{\Delta x}_{k+1|k} + K_{k+1} \left(z_{k+1} - h(x_{k+1}^{nom}) - H_{k+1} \widehat{\Delta x}_{k+1|k} \right) \tag{2.4.1.11}$$

$$P_{k+1|k+1} = (I - K_{k+1} H_{k+1}) P_{k+1|k} \tag{2.4.1.12}$$

It is important to note that the PKF estimates the state perturbations. The a priori and a posteriori full state estimates are respectively defined by:

$$\hat{x}_{k+1|k} = x_{k+1}^{nom} + \widehat{\Delta x}_{k+1|k} \tag{2.4.1.13}$$

$$\hat{x}_{k+1|k+1} = x_{k+1}^{nom} + \widehat{\Delta x}_{k+1|k+1} \tag{2.4.1.14}$$

If the nonlinearities present in the estimation process are very mild, then the PKF method will work very well. However, using a nominal trajectory implies that the state trajectories are known in advance, which is often not the case [68]. If this is the case, then the Jacobian matrices may be calculated offline, saving computational resources. However, if the state perturbations are not small, then the PKF will yield large estimation errors [68]. Furthermore, in practice, the deviation of the actual trajectory from the nominal trajectory generally increases over the course of the estimation process [39].

2.4.2 The Extended Kalman Filter

The extended Kalman filter (EKF) builds on the concepts of the PKF. Instead of using a static nominal trajectory, the EKF utilizes the state estimate trajectory which is updated at each time step [68]. Conceptually, the EKF is very similar to the standard KF. The nonlinear system and measurement functions (f and h, respectively) are used to predict the state estimates and predicted measurements. However, it is not possible to use these functions to calculate the predicted and updated state error covariance matrices. Similar to the PKF, the EKF requires that the functions f and h be linearized (as per its Jacobian). Although this allows the KF to handle mildly-nonlinear estimation problems, it introduces a number of instabilities. For example, the linearization process may overlook unmodeled nonlinear modeling uncertainties, which may cause the estimate to go unstable [39]. Furthermore, the calculation of the Jacobian increases the computational complexity of the filter. The partial derivatives are used to compute linearized system and measurement matrices F and H, respectively found as follows [39]:

$$F_k = \left.\frac{\partial f(x)}{\partial x}\right|_{x=\hat{x}_{k|k},u_k} \tag{2.4.2.1}$$

$$H_{k+1} = \left.\frac{\partial h(x)}{\partial x}\right|_{x=\hat{x}_{k+1|k}} \tag{2.4.2.2}$$

Equations (2.4.2.1) and (2.4.2.2) essentially linearize the nonlinear system or measurement functions around the current state estimate [30]. This comes at a loss of optimality, as the KF gain is no longer considered to be the best solution to the estimation problem [33]. The EKF process may be summarized by the following seven equations. The state estimate $\hat{x}_{k+1|k}$ is predicted using the nonlinear system model (2.4.2.3), and the corresponding state error covariance matrix $P_{k+1|k}$ is found (2.4.2.4).

$$\hat{x}_{k+1|k} = f\left(\hat{x}_{k|k}, u_k\right) \tag{2.4.2.3}$$

$$P_{k+1|k} = F_k P_{k|k} F_k^T + Q_k \tag{2.4.2.4}$$

The measurement error (or innovation) $\tilde{y}_{k+1}$ is then found (2.4.2.5), based on the nonlinear measurement model h, followed by the measurement error (innovation) covariance matrix S_{k+1} (2.4.2.6).

$$\tilde{y}_{k+1} = z_{k+1} - h\left(\hat{x}_{k+1|k}\right) \tag{2.4.2.5}$$

$$S_{k+1} = H_{k+1} P_{k+1|k} H_{k+1}^T + R_{k+1} \tag{2.4.2.6}$$

The near-optimal KF gain K_{k+1} is calculated (2.4.2.7). This gain is then used in conjunction with the predicted state estimate $\hat{x}_{k+1}$ and the measurement error $\tilde{y}_{k+1}$ to update the state estimate (2.4.2.8).

$$K_{k+1} = P_{k+1|k} H_{k+1}^T S_{k+1}^{-1} \tag{2.4.2.7}$$

$$\hat{x}_{k+1|k+1} = \hat{x}_{k+1|k} + K_{k+1} \tilde{y}_{k+1} \tag{2.4.2.8}$$

Finally, the state error covariance matrix is updated as per (2.4.2.9).

$$P_{k+1|k+1} = (I - K_{k+1} H_{k+1}) P_{k+1|k} \tag{2.4.2.9}$$

Equations (2.4.2.1) through (2.4.2.9) form the EKF estimation process. The linearization process of (2.4.2.1) and (2.4.2.2) introduces uncertainties that can sometimes cause the filter to go unstable [35]. However, for mildly nonlinear systems, the EKF provides a very good estimate of the states, and is relatively easy to implement [34].

2.4.3 The Unscented Kalman Filter

The next major progression of KF theory involved the introduction of the sigma-point Kalman filter (SPKF) [34]. The SPKF is based on a weighted statistical linear regression strategy which linearizes the nonlinear model statistically [78,79]. Essentially, SPKF methods draw a certain number of points (referred to as sigma points) from the projected probability distribution of the states [42]. These points are then projected using the nonlinear system model, in an effort to obtain an a posteriori estimate for the probability distribution. Note that this strategy avoids the requirement of linearization, which generally leads to a more accurate estimation strategy since it avoids the calculation of Jacobian matrices [80,81].

The most popular type of SPKF is the unscented Kalman filter (UKF) [36,71]. A number of different forms exist, and include [42]: the unscented [34,71], general unscented [34,80], simplex unscented [34,81,82,83], and spherical unscented [34,83]. The standard UKF method will be presented and discussed in this thesis [71]. The UKF strategy makes use of a deterministic sampling technique referred to as the unscented transform. It is well established in literature that this method provides a more accurate estimate of the state mean and covariance than the EKF [39]. As shown in the following figure, a finite number of weighted sample points (selected about the mean) are propagated through the nonlinear functions, which create an approximate solution to the mean and covariance of the desired estimate [36,71].

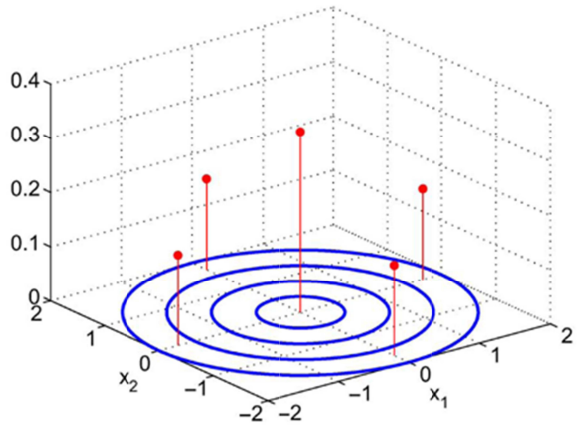

Figure 2.4.1. Distribution of Sigma Point Set for the UKF in 2-D Space [72]

The following equations help summarize the UKF estimation method [71]. The first step to applying the UKF is to generate the sigma points. The n-dimensional random variable x_k with mean $\hat{x}_{k|k}$ and covariance $P_{k|k}$ may be approximated by $2n+1$ sigma points. The initial sigma points (corresponding sample and weight) may be calculated as follows:

$$X_{0,k|k} = \hat{x}_{k|k} \tag{2.4.3.1}$$

$$W_0 = \kappa/(n+\kappa) \tag{2.4.3.2}$$

The next n number of sigma points may be calculated as follows:

$$X_{i,k|k} = \hat{x}_{k|k} + \left(\sqrt{(n+\kappa)P_{k|k}}\right)_i \tag{2.4.3.3}$$

$$W_i = 1/[2(n+\kappa)] \tag{2.4.3.4}$$

Likewise, the remaining n number of sigma points may be found as:

$$X_{i+n,k|k} = \hat{x}_{k|k} - \left(\sqrt{(n+\kappa)P_{k|k}}\right)_i \tag{2.4.3.5}$$

$$W_{i+n} = 1/[2(n+\kappa)] \tag{2.4.3.6}$$

The parameter κ is a design value (typically a small value, significantly less than 1), $\left(\sqrt{(n+\kappa)P_{k|k}}\right)_i$ is the i^{th} row or column of the matrix square root of $(n+\kappa)P_{k|k}$, and W_i is the weight that is associated with the i^{th} sample point [36]. The sigma points are then propagated through the nonlinear system model (2.4.3.7), and then are used with their corresponding weights to calculate the predicted state estimate (2.4.3.8).

$$\hat{X}_{i,k+1|k} = f\left(X_{i,k|k}, u_k\right) \tag{2.4.3.7}$$

$$\hat{x}_{k+1|k} = \sum_{i=0}^{2n} W_i \hat{X}_{i,k+1|k} \tag{2.4.3.8}$$

From (2.4.3.7) and (2.4.3.8), it is possible to calculate the predicted state error covariance as follows:

$$P_{k+1|k} = \sum_{i=0}^{2n} W_i \left(\hat{X}_{i,k+1|k} - \hat{x}_{k+1|k}\right)\left(\hat{X}_{i,k+1|k} - \hat{x}_{k+1|k}\right)^T \tag{2.4.3.9}$$

Next, the sigma points are propagated through the nonlinear measurement model (2.4.3.10), and the predicted measurement is calculated (2.4.3.11).

$$\hat{Z}_{i,k+1|k} = h\left(\hat{X}_{i,k+1|k}, u_k\right) \tag{2.4.3.10}$$

$$\hat{z}_{k+1|k} = \sum_{i=0}^{2n} W_i \hat{Z}_{i,k+1|k} \tag{2.4.3.11}$$

The measurement (or innovation) covariance is then calculated as follows:

$$P_{zz.k+1|k} = \sum_{i=0}^{2n} W_i \left(\hat{Z}_{i,k+1|k} - \hat{z}_{k+1|k}\right)\left(\hat{Z}_{i,k+1|k} - \hat{z}_{k+1|k}\right)^T \tag{2.4.3.12}$$

Likewise, the cross-covariance (between the state and measurement) is then calculated as follows:

$$P_{xz.k+1|k} = \sum_{i=0}^{2n} W_i \left(\hat{X}_{i,k+1|k} - \hat{x}_{k+1|k}\right)\left(\hat{Z}_{i,k+1|k} - \hat{z}_{k+1|k}\right)^T \tag{2.4.3.13}$$

From (2.4.3.12) and (2.4.3.13), the Kalman gain K_{k+1} may be calculated (2.4.3.14).

$$K_{k+1} = P_{xz.k+1|k} P_{zz.k+1|k}^{-1} \tag{2.4.3.14}$$

The remaining UKF process is conceptually similar to the standard KF or EKF. The updated (or a posteriori) state estimate may be calculated (2.4.3.15), and the updated state error covariance may be found (2.4.3.16).

$$\hat{x}_{k+1|k+1} = \hat{x}_{k+1|k} + K_{k+1}\left(z_{k+1} - \hat{z}_{k+1|k}\right) \tag{2.4.3.15}$$

$$P_{k+1|k+1} = P_{k+1|k} - K_{k+1} P_{zz,k+1|k} K_{k+1}^T \tag{2.4.3.16}$$

By the nature of its derivation, the UKF may appear to be more computationally demanding than the EKF. However, both methods are roughly the same, as the UKF does not require linearization of the nonlinear functions [39]. For mildly nonlinear estimation problems, both the EKF and UKF will yield the same solution [32]. However, the UKF becomes more advantageous when the nonlinearities are increased.

2.4.4 The Cubature Kalman Filter

The next progression in KF theory led to the development of the cubature Kalman filter [72,84]. The CKF uses a third-degree cubature rule to numerically compute Gaussian-weighted integrals, as opposed to the sigma point set used by the UKF [72]. Consider the following figure which illustrates this distribution used to capture the points used by the CKF.

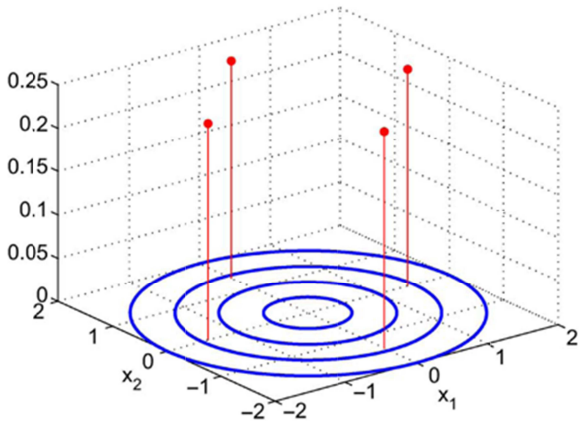

Figure 2.4.2. Third-Degree Spherical-Radial Cubature Point Set for the CKF [72]

The cubature rule approximates an n-dimensional Gaussian weighted integral as follows [72]:

$$\int_{\mathbb{R}^{n_x}} f(x)\mathcal{N}(x;\mu,\sum)dx \approx \frac{1}{2n} f(\mu + \sqrt{\sum}\xi_i) \tag{2.4.4.1}$$

Where a square-root factor of the covariance $\sum$ satisfies the relationship $\sum = \sqrt{\sum}\sqrt{\sum}^T$ and the set of $2n$ cubature points are given by [72]:

$$\xi_i = \begin{cases} \sqrt{n}e_i, & i = 1,2,\dots,n \\ -\sqrt{n}e_{i-n}, & i = n+1, n+2, \dots, 2n \end{cases} \tag{2.4.4.2}$$

Where $e_i \in \mathbb{R}^n$ denotes the i^{th} elementary column vector. According to [72], the third-degree cubature rule is exact for polynomial integrands up to the third degree or for any odd-degree polynomial. As described in [72], the goal of the CKF algorithm is to recursively compute the probability $p(x_{k+1}|z_{1:k+1}) = \mathcal{N}(\hat{x}_{k+1|k+1}, P_{k+1|k+1})$ given the posterior $p(x_k|z_{1:k}) = \mathcal{N}(\hat{x}_{k|k}, P_{k|k})$ at time k. The CKF algorithm described in this section is presented as in [72]. The initial set of cubature points X are calculated based on the previous a posteriori state estimate $\hat{x}_{k|k}$, the previous a posteriori state covariance $P_{k|k}$, and the cubature-point set ξ_i (described earlier):

$$X_{i,k|k} = \sqrt{P_{k|k}}\xi_i + \hat{x}_{k|k} \qquad i = 1,2,\dots,2n \tag{2.4.4.3}$$

These cubature points are then propagated through the system equation, as follows:

$$X^*_{i,k+1|k} = f(X_{i,k|k}, u_k) \qquad i = 1,2,\dots,2n \tag{2.4.4.4}$$

Next, the predicted state $\hat{x}_{k+1|k}$ and predicted state error covariance $P_{k+1|k}$ are calculated, respectively:

$$\hat{x}_{k+1|k} = \frac{1}{2n}\sum_{i=1}^{2n} X^*_{i,k+1|k} \tag{2.4.4.5}$$

$$P_{k+1|k} = \frac{1}{2n}\sum_{i=1}^{2n} X^*_{i,k+1|k} X^{*T}_{i,k+1|k} - \hat{x}_{k+1|k}\hat{x}^T_{k+1|k} + Q_{k+1} \tag{2.4.4.6}$$

The predicted cubature points $X_{i,k+1|k}$ are then evaluated based on the predicted stated $\hat{x}_{k+1|k}$ and predicted state error covariance $P_{k+1|k}$:

$$X_{i,k+1|k} = \sqrt{P_{k+1|k}}\xi_i + \hat{x}_{k+1|k} \qquad i = 1,2,\dots,2n \tag{2.4.4.7}$$

The predicted cubature points $X_{i,k+1|k}$ are then propagated through the measurements $Z_{i,k+1|k}$, and the corresponding predicted measurement is calculated $\hat{z}_{k+1|k}$, respectively as follows:

$$Z_{i,k+1|k} = h(X_{i,k+1|k}, u_{k+1}) \qquad i = 1,2,\dots,2n \tag{2.4.4.8}$$

$$\hat{z}_{k+1|k} = \frac{1}{2n}\sum_{i=1}^{2n} Z_{i,k+1|k} \tag{2.4.4.9}$$

In order to calculate the corresponding cubature Kalman gain W_{k+1}, the innovation covariance $P_{zz,k+1|k}$ and cross-covariance $P_{xz,k+1|k}$ matrices need to be evaluated, respectively as follows:

$$P_{zz,k+1|k} = \frac{1}{2n}\sum_{i=1}^{2n} Z_{i,k+1|k} Z_{i,k+1|k}^T - \hat{z}_{k+1|k}\hat{z}_{k+1|k}^T + R_{k+1} \tag{2.4.4.10}$$

$$P_{xz,k+1|k} = \frac{1}{2n}\sum_{i=1}^{2n} X_{i,k+1|k} Z_{i,k+1|k}^T - \hat{x}_{k+1|k}\hat{z}_{k+1|k}^T \tag{2.4.4.11}$$

The CKF gain may now be calculated as follows:

$$W_{k+1} = P_{xz,k+1|k} P_{zz,k+1|k}^{-1} \tag{2.4.4.12}$$

Finally, the updated states $\hat{x}_{k+1|k+1}$ and corresponding error covariance $P_{k+1|k+1}$ may be found:

$$\hat{x}_{k+1|k+1} = \hat{x}_{k+1|k} + W_{k+1}(z_{k+1} - \hat{z}_{k+1|k}) \tag{2.4.4.13}$$

$$P_{k+1|k+1} = P_{k+1|k} + W_{k+1} P_{zz,k+1|k} W_{k+1}^T \tag{2.4.4.14}$$

The CKF algorithm may be summarized by (2.4.4.1) through (2.4.4.14), and is repeated iteratively. It has been shown to yield more accurate estimation results when compared with the EKF and UKF strategies [72,84].

2.5 Multiple Model Methods

In nature, many systems behave according to a number of different models (modes, or operating regimes). For example, in target tracking, a target may travel straight (i.e., uniform motion) or turn (i.e., undergo a coordinated turn) [28]. Furthermore, a system may experience different types of noises (i.e., white or 'coloured') [39]. In these scenarios, it is desirable to implement adaptive estimation algorithms, which 'adapt' themselves to certain types of uncertainties or models in an effort to minimize the state estimation error [28]. One type of adaptive estimation technique includes the 'multiple model' (MM) algorithm [85]; which include the following: static MM [86], dynamic MM [28], generalized pseudo-Bayesian (GPB) [87,88,89,90], and the interacting multiple model (IMM) [28,91,92].

For the MM methods, a Bayesian framework is used (i.e., probability based). Essentially, based on some prior probabilities of each model being correct (i.e., the system is behaving according a finite number of modes), the corresponding updated probabilities are calculated [28]. Throughout this thesis, it will be assumed that all of the models are linear with the presence of Gaussian noise; however, nonlinear models could be used via linearization [28]. Each MM method requires estimation of the states and their corresponding probability. The most popular strategy that has been implemented in the MM framework remains the KF, and is referred to as the IMM-KF [39]. As such, it forms the basis for comparison in later chapters.

2.5.1 Static Multiple Model Method

The static MM algorithm assumes that the model the system obeys is fixed and that no switching occurs from one mode to another throughout the estimation process [28]. It is important to note that although the model is fixed, each model has its own dynamics, such that the overall estimator remains dynamic [28]. Bayes' formula is used to calculate the updated probability of model j being correct, based on current measurements, as follows [28]:

$$\mu_{j,k+1} = \frac{p\left(z_{k+1}\middle|Z^k, M_j\right)\mu_{j,k}}{\sum_{i=1}^{r} p(z_{k+1}|Z^k, M_i)\mu_{i,k}} \qquad j = 1, \dots, r \tag{2.5.1.1}$$

According to [28], $p\left(z_{k+1}\middle|Z^k, M_j\right)$ is the likelihood function $\Lambda_{j,k+1}$ of mode j at time $k+1$ for model M_j, and can be solved by:

$$\Lambda_{j,k+1} \equiv p\left(z_{k+1}\middle|Z^k, M_j\right) = \mathcal{N}\left(e_{j,z,k+1|k}; 0, S_{j,k+1}\right) \tag{2.5.1.2}$$

Where $e_{j,z,k+1|k}$ and $S_{j,k+1}$ refer to the innovation (or a priori measurement error) and the innovation covariance matrix from the mode-matched filter corresponding to mode j [28]. Equation (2.5.1.2) may be solved as follows [28,39]:

$$\Lambda_{j,k+1} = \frac{1}{\sqrt{\left|2\pi S_{j,k+1}\right|_{Abs}}} exp\left(\frac{-\frac{1}{2} e_{j,z,k+1|k}^T e_{j,z,k+1|k}}{S_{j,k+1}}\right) \tag{2.5.1.3}$$

An estimation method (such as the KF) is used for each model to calculate mode-conditioned state estimates and the corresponding mode-conditioned covariance's [28]. The mode estimates defined by (2.5.1.1) determine the probability of each mode being correct (i.e., being used by the system), and are calculated based on its corresponding likelihood function (2.5.1.2). Note that the total sum of all the mode probabilities (2.5.1.1) is equal to 1. Figure 2.5.1 helps to further explain the static MM estimator.

The output from each filter is used to update the mode probability $\mu_{j,k+1}$, and consequently determine the overall output from the static MM strategy. The mode-conditioned state estimates are then combined to obtain the overall output estimate as follows [28]:

$$\hat{x}_{k+1|k+1} = \sum_{j=1}^{r} \mu_{j,k+1} \hat{x}_{j,k+1|k+1} \tag{2.5.1.4}$$

Finally, the covariance of the combined estimates is defined by [28]:

$$\begin{aligned} P_{k+1|k+1} = \sum_{j=1}^{r} \mu_{j,k+1} \Big\{ & P_{j,k+1|k+1} \\ & + \left(\hat{x}_{j,k+1|k+1} - \hat{x}_{k+1|k+1}\right)\left(\hat{x}_{j,k+1|k+1} - \hat{x}_{k+1|k+1}\right)^T \Big\} \end{aligned} \tag{2.5.1.5}$$

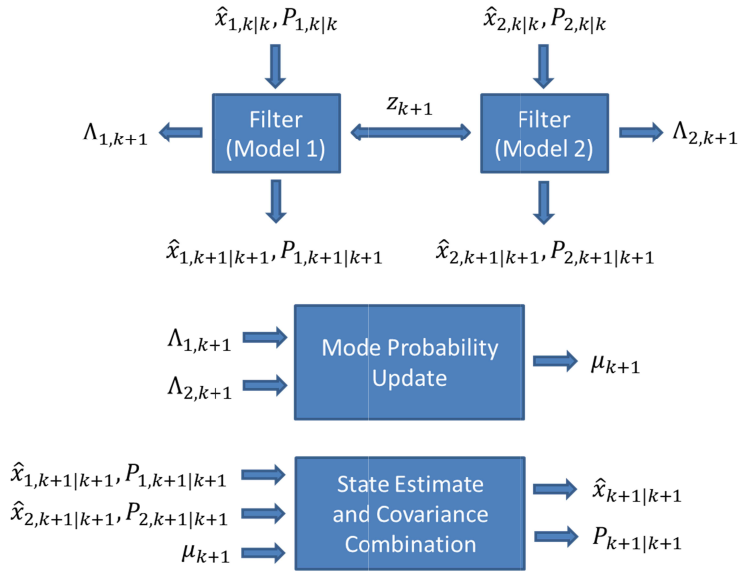

Figure 2.5.1. Static MM Estimator for Two Models (Adapted from [28])

Note that the filters run recursively using their own estimates, and the overall estimates are used for output purposes only [28].

2.5.2 Dynamic Multiple Model Method

A static system model is often not realistic. In the dynamic MM case, the mode the system is operating in can undergo switching with time [28]. For a two system example, at time $k+1$ the system may switch from mode 1 to mode 2, or may simply stay in mode 1. It is assumed that the mode switching (i.e., mode jump process) is a Markov process or chain with known mode transition probabilities referred to as p_{ij} [28]. Furthermore, p_{ij} is assumed to be time-invariant, and is typically a designer parameter. In order to accurately represent the dynamic model switching, the entire mode history (or sequence of models) needs to be kept and stored. However, the number of histories n increases exponentially with time [28]:

$$n = r^k \tag{2.5.2.1}$$

Where r is the number of models and k is the time. For example, for three models and at time 2, there are a total of 9 possible sequences.

The conditional probability distribution function of the state x at time $k+1$ may be found by a Gaussian mixture with an exponentially increasing number of terms, as follows [28]:

$$p\left(x_{k+1}\middle|Z^{k+1}\right)=\sum_{l=1}^{r^{k+1}}p\left(x_{k+1}\middle|M^{k+1,l},Z^{k+1}\right)P\left(M^{k+1,l}\middle|Z^{k+1}\right) \tag{2.5.2.2}$$

Where $P\left(M^{k+1,l}\middle|Z^{k+1}\right)=\mu_{k+1,l}$ refers to the mode history probability, from history l up to time $k+1$. The probability of a mode history is obtained by [28]:

$$\mu_{k+1,l}=\frac{1}{c}p\left(z_{k+1}\middle|M^{k+1,l},Z^{k+1}\right)p_{ij}\mu_{k,s} \tag{2.5.2.3}$$

Where $i=s_k$ is the last model of the parent sequence s, and c is a normalization constant. The dynamic MM method requires conditioning on the entire past history, which means that an increasing number of filters are required, making the approach impractical [28]. According to [28], the only way to avoid the exponentially increasing number of histories is to implement suboptimal techniques. There are two main suboptimal techniques for the dynamic MM method: the generalized pseudo-Bayesian (GPB) strategy, and the interacting multiple model (IMM) estimation algorithm.

2.5.3 Generalized Pseudo-Bayesian Method

The generalized pseudo-Bayesian (GPB) approach combines histories of models that differ in 'older' models [28]. There first-order GPB (GPB1) considers only the possible models in the last time period, whereas the second-order version (GPB2) considers all the possible models in the last two time periods [28,42]. These algorithms require r and r^2 number of filters to operate in parallel, respectively [28]. The GPB1 MM estimator for two models (as an example) is shown in the following figure. Essentially, the filters run recursively using the previous combined state estimates (i.e., the output from the weighted mode-conditioned states).

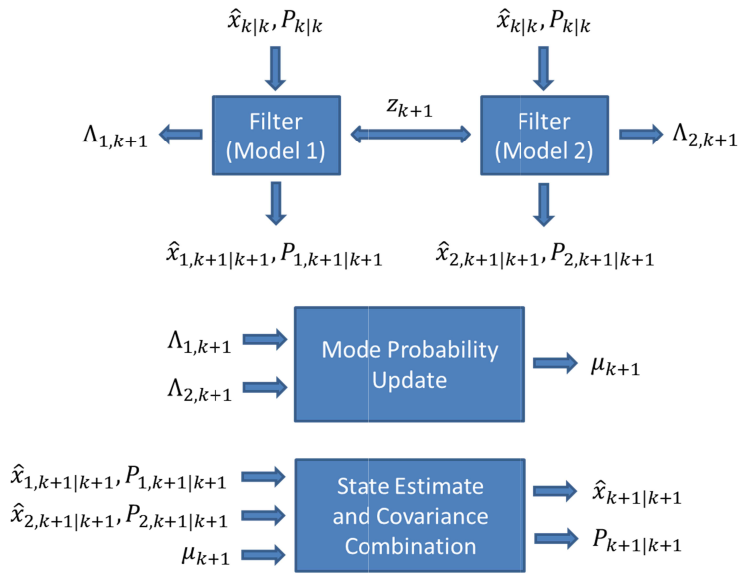

Figure 2.5.2. GPB1 MM Estimator for Two Models (Adapted from [28])

The GPB1 MM estimator may be summarized by the following equations, (2.5.3.1) through (2.5.3.5) [28]. The first step consists of mode-matched filtering. Based on the previous a posteriori combined state estimates $\hat{x}_{k|k}$ and covariance $P_{k|k}$, the mode-matched state estimates $\hat{x}_{j,k+1|k+1}$ and corresponding covariance $P_{j,k+1|k+1}$ are calculated based on M_j. The corresponding likelihood functions are evaluated as follows [28]:

$$\Lambda_{j,k+1} = p\left(z_{k+1} \middle| M_{j,k+1}, \hat{x}_{k+1|k+1}, P_{k+1|k+1}\right) \tag{2.5.3.1}$$

As shown in the previous figure, the next step involves updating the mode probability $\mu_{j,k+1}$ corresponding to M_j, where $j = 1, \ldots, r$ and r is the number of finite models. Based on the mode transition probabilities p_{ij}, the mode probabilities may be updated by [28]:

$$\mu_{j,k+1} = \frac{1}{c}\Lambda_{j,k+1}\sum_{i=1}^{r} p_{ij}\mu_{i,k} \tag{2.5.3.2}$$

Where c is a normalization constant defined as follows [28]:

$$c = \sum_{j=1}^{r} \Lambda_{j,k+1} \sum_{i=1}^{r} p_{ij} \mu_{i,k} \tag{2.5.3.3}$$

Finally, the last step involves combining the state estimates (2.5.3.4) and covariance's (2.5.3.5) from the corresponding filters [28]. This combination stage is similar to that presented in the static MM method section.

$$\hat{x}_{k+1|k+1} = \sum_{j=1}^{r} \mu_{j,k+1} \hat{x}_{j,k+1|k+1} \tag{2.5.3.4}$$

$$\begin{aligned} P_{k+1|k+1} = \sum_{j=1}^{r} \mu_{j,k+1} \Big\{ & P_{j,k+1|k+1} \\ & + \big(\hat{x}_{j,k+1|k+1} - \hat{x}_{k+1|k+1}\big)\big(\hat{x}_{j,k+1|k+1} - \hat{x}_{k+1|k+1}\big)^T \Big\} \end{aligned} \tag{2.5.3.5}$$

The GPB2 MM estimator goes beyond what the GPB1 MM estimator does, and computes the state estimates under each possible current and previous model [28]. This significantly increases the computational complexity of the process [39]. In fact, the structure of the GPB2 algorithm includes r number of estimates and r^2 number of filters. The process may be best described using Figure 2.5.3. The GPB2 MM estimator consists of five main steps: mode-matched filtering, calculation of the merging probabilities, merging stage, mode probability updating, and state estimate and covariance combination. In this case, mode-matched filtering consists of starting with $\hat{x}_{i,k|k}$ and $P_{i,k|k}$, and computing $\hat{x}_{ij,k+1|k+1}$ and $P_{ij,k+1|k+1}$ through a filter matched to $M_{j,k+1}$. Note that there will be r^2 filters, and $i, j = 1, \ldots, r$ [28]. The likelihood functions corresponding to each filter are calculated as follows [28]:

$$\Lambda_{ij,k+1} = p\big(z_{k+1} \big| M_{j,k+1}, \hat{x}_{i,k+1|k+1}, P_{i,k+1|k+1}\big) \tag{2.5.3.6}$$

The next step is to calculate the merging probabilities $\mu_{i|j,k|k+1}$ [28]:

$$\mu_{i|j,k|k+1} = \frac{1}{c_j} \Lambda_{ij,k+1} p_{ij} \mu_{i,k} \tag{2.5.3.7}$$

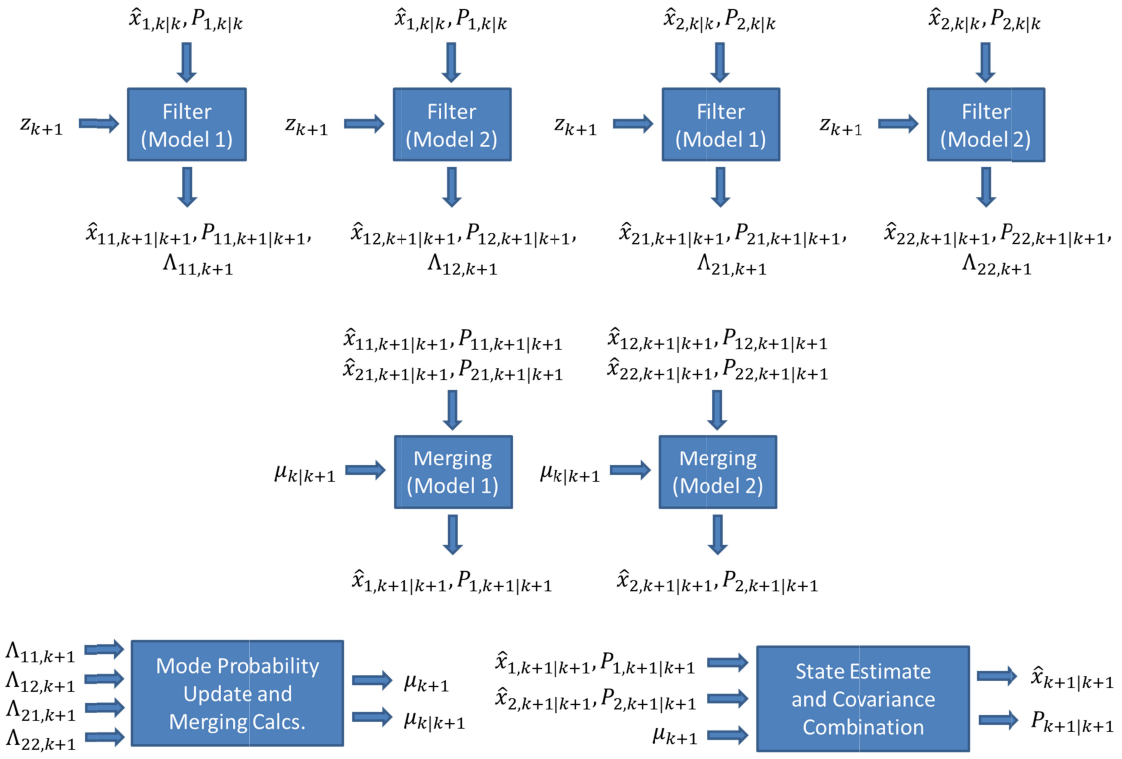

Figure 2.5.3. GPB2 MM Estimator for Two Models (Adapted from [28])

Where:

$$c_j = \sum_{i=1}^{r} \Lambda_{ij,k+1} p_{ij}\, \mu_{i,k} \tag{2.5.3.8}$$

Following this, merging takes place to combine the states and covariance's corresponding to each mode $M_{j,k+1}$. The state estimate corresponding to $M_{j,k+1}$ is calculated as follows [28]:

$$\hat{x}_{j,k+1|k+1} = \sum_{i=1}^{r} \mu_{i|j,k|k+1} \hat{x}_{ij,k+1|k+1} \tag{2.5.3.9}$$

The corresponding covariance is calculated by [28]:

$$P_{j,k+1|k+1} = \sum_{i=1}^{r} \mu_{i|j,k|k+1} \Big\{ P_{ij,k+1|k+1} + \big(\hat{x}_{ij,k+1|k+1} - \hat{x}_{j,k+1|k+1}\big)\big(\hat{x}_{ij,k+1|k+1} - \hat{x}_{j,k+1|k+1}\big)^T \Big\} \tag{2.5.3.10}$$

Next, the mode probabilities are updated using the following two equations [28]:

$$\mu_{j,k+1} = \frac{1}{c} \sum_{i=1}^{r} \Lambda_{ij,k+1} p_{ij} \mu_{i,k} \tag{2.5.3.11}$$

$$c = \sum_{j=1}^{r} \sum_{i=1}^{r} \Lambda_{ij,k+1} p_{ij}\, \mu_{i,k} \tag{2.5.3.12}$$

Finally, like the previous methods, the overall state estimate (2.5.3.13) and covariance (2.5.3.14) are calculated, and are used for output purposes only [28].

$$\hat{x}_{k+1|k+1} = \sum_{j=1}^{r} \mu_{j,k+1} \hat{x}_{j,k+1|k+1} \tag{2.5.3.13}$$

$$P_{k+1|k+1} = \sum_{j=1}^{r} \mu_{j,k+1} \Big\{ P_{j,k+1|k+1} + \big(\hat{x}_{j,k+1|k+1} - \hat{x}_{k+1|k+1}\big)\big(\hat{x}_{j,k+1|k+1} - \hat{x}_{k+1|k+1}\big)^T \Big\} \tag{2.5.3.14}$$

Equations (2.5.3.6) through (2.5.3.14) summarize the GPB2 MM estimator.

2.5.4 The Interacting Multiple Model Strategy

The interacting multiple model (IMM) estimation algorithm is conceptually similar to the GPB2 method, but requires only r number of filters that operate in parallel [28]. The state estimate is calculated under each possible current model, with a mixed initial condition (i.e., a different combination of the previous model-conditioned estimates) [28]. Furthermore, according to and as presented in [28,92], the input to the filter matched to M_j is obtained from an interaction of the r filters, which consists of the mixing of the estimates $\hat{x}_{i,k|k}$ and weightings $\mu_{i|j,k|k}$ (mixing probabilities).

This is equivalent to merging taking place at the beginning of each estimation cycle, which limits the number of filters to r (instead of the GPB2 algorithm which uses r^2 filters) [92]. The IMM strategy has shown to be very effective, and is more computationally efficient than the GPB2 algorithm [28]. Due to its popularity among MM methods, only the IMM estimation strategy will be implemented later in Chapter 6. The following figure helps to explain the IMM method more effectively.

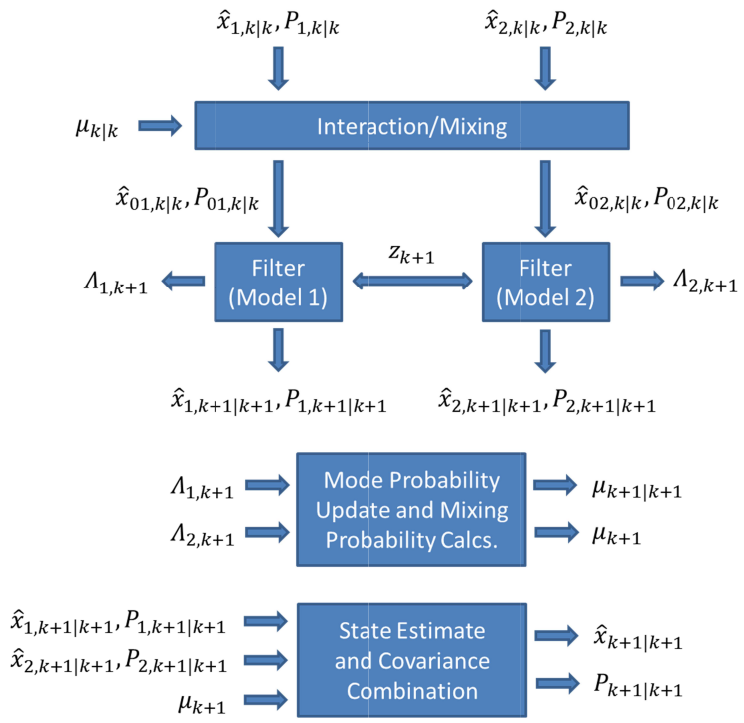

Figure 2.5.4. IMM Estimator for Two Models (Adapted from [28])

The IMM estimator consists of five main steps: calculation of the mixing probabilities, mixing stage, mode-matched filtering, mode probability update, and state estimate and covariance combination. The first step involves calculating the mixing probabilities (i.e., the probability of the system currently in mode i, and switching to mode j at the next step). These are calculated using the following two equations [28]:

$$\mu_{i|j,k|k} = \frac{1}{\bar{c}_j} p_{ij} \mu_{i,k} \tag{2.5.4.1}$$

$$\bar{c}_j = \sum_{i=1}^{r} p_{ij}\, \mu_{i,k} \tag{2.5.4.2}$$

The mixing probabilities $\mu_{i|j,k|k}$ are used in the mixing stage, next. In addition to the mixing probabilities, the previous mode-matched states $\hat{x}_{i,k|k}$ and covariance's $P_{i,k|k}$ are also used to calculate the mixed initial conditions (states and covariance) for the filter matched to M_j. The mixed initial conditions are found respectively as follows [28]:

$$\hat{x}_{0j,k|k} = \sum_{i=1}^{r} \hat{x}_{i,k|k} \mu_{i|j,k|k} \tag{2.5.4.3}$$

$$P_{0j,k|k} = \sum_{i=1}^{r} \mu_{i|j,k|k} \left\{ P_{i,k|k} + \left(\hat{x}_{i,k|k} - \hat{x}_{0j,k|k}\right)\left(\hat{x}_{i,k|k} - \hat{x}_{0j,k|k}\right)^T \right\} \tag{2.5.4.4}$$

The next step involves mode-matched filtering, which involves using (2.5.4.3) and (2.5.4.4) as inputs to the filter matched to M_j. Each filter also uses the measurement z_{k+1} and input to the system u_k (if any). The likelihood functions are calculated for each mode-matched filter as follows [28]:

$$\Lambda_{j,k+1} = \mathcal{N}\left(z_{k+1}; \hat{z}_{j,k+1|k}, S_{j,k+1}\right) \tag{2.5.4.5}$$

Equation (2.5.4.5) may be solved by each filter as follows [28,39]:

$$\Lambda_{j,k+1} = \frac{1}{\sqrt{\left|2\pi S_{j,k+1}\right|_{Abs}}} exp\left(\frac{-\frac{1}{2} e_{j,z,k+1|k}^T e_{j,z,k+1|k}}{S_{j,k+1}} \right) \tag{2.5.4.6}$$

Utilizing the likelihood functions from each filter, the mode probability may be updated by [28]:

$$\mu_{j,k} = \frac{1}{c} \Lambda_{j,k+1} \sum_{i=1}^{r} p_{ij}\, \mu_{i,k} \tag{2.5.4.7}$$

Where the normalizing constant is defined as [28]:

$$c = \sum_{j=1}^{r} \Lambda_{j,k+1} \sum_{i=1}^{r} p_{ij}\, \mu_{i,k} \tag{2.5.4.8}$$

Finally, as before, the overall state estimates (2.5.4.9) and covariance (2.5.4.10) are calculated.

$$\hat{x}_{k+1|k+1} = \sum_{j=1}^{r} \mu_{j,k+1} \hat{x}_{j,k+1|k+1} \tag{2.5.4.9}$$

$$\begin{aligned} P_{k+1|k+1} = \sum_{j=1}^{r} \mu_{j,k+1} \Big\{ & P_{j,k+1|k+1} \\ & + \left(\hat{x}_{j,k+1|k+1} - \hat{x}_{k+1|k+1}\right)\left(\hat{x}_{j,k+1|k+1} - \hat{x}_{k+1|k+1}\right)^{T} \Big\} \end{aligned} \tag{2.5.4.10}$$

Equations (2.5.4.1) through (2.5.4.10) summarize the IMM estimator strategy, and are used recursively. Note that (2.5.4.9) and (2.5.4.10) are used for output purposes only, and are not part of the algorithm recursions [28]. The IMM strategy has successfully been applied to a number of estimation problems [93]; ranging from target tracking in a traffic controller setting [94] to fault detection and diagnosis [95,96]. In fact, both of these applications will be studied later in Chapter 6.

2.6 Sliding Mode Observers

Before continuing to Chapter 3 and discussing the smooth variable structure filter (SVSF), the topic of sliding mode observers (SMOs) is introduced. These observers are based on variable structure control (VSC) and systems, which were introduced in the 1950s [97,98,99]. Essentially, this theory considers systems that contain discontinuities in the differential equations that describe their dynamic state [37]. Variable structure systems contain discontinuity hyperplanes which divide the state space into regions. Within these regions, the dynamic equation governing the system is continuous [37,100]. Hence, the name 'variable structure' is appropriate since the dynamics of a system may be described by a number of distinct equations.

Variable structure theory led to the development of variable structure control. In VSC, the control input is formulated as a discontinuous function of the state vector, such that discontinuity hyperplanes are artificially introduced [37,101]. Consider the following simple example from [37], where $u_i(x,t)$ is a discontinuous input and $s_i(x)$ is referred to as a discontinuity surface:

$$u_i(x,t) = \begin{cases} u_i^+(x,t) & with \quad s_i(x) > 0 \\ u_i^-(x,t) & with \quad s_i(x) < 0 \end{cases} \tag{2.6.1}$$

Therefore, when above the discontinuity surface, the control input is $u_i^+(x,t)$. Conversely, when below the discontinuity surface, the control input is $u_i^-(x,t)$. The most popular form of VSC is sliding mode control (SMC) [98,101]. SMC utilizes a discontinuous switching plane along some desired trajectory, referred to as a sliding surface. The objective is to keep the state values along this surface by minimizing the state errors (difference between the desired trajectory and the estimated or actual values). Ideally, if the state value is off or some distance away from the surface, a switching gain would be used to push the state towards the sliding surface. Once on the surface, the states slide along the surface in what is called a sliding mode [101]. The switching brings inherent stability and robustness to the control strategy, while also introducing chattering (high-frequency switching) that is undesirable in practice and can excite unmodeled dynamics [37]. A boundary layer may be introduced along the sliding surface in order to saturate and smooth out the chattering within a region referred to as the smoothing boundary region [101].

Prior to the 1980s, VSC and SMC methodologies were considered only in the continuous-time domain [42]. In 1985, a discrete-time formulation of SMC was presented [37,102]. Shortly thereafter a stability condition for the discrete SMC was presented, and is now commonly used in discrete controller design [37,103,104]. Since its inception, SMC has become a very popular control methodology, and is the subject of a large amount of research [101]. In the 1980s, SMOs were developed based on variable structure and sliding mode theory [42,105]. Essentially, SMOs work by minimizing the error between the plant (system) and observer models with the help of a switching function [106].

The observer gain is calculated based on the error; such that the system and observer outputs match, and the error surface moves towards zero (in the ideal case) [106]. Similar to VSC, the SMO defines a hyperplane (i.e., a sliding surface) and applies a discontinuous force on the estimate to keep the estimate bounded within an area of the hyperplane, referred to as the existence subspace [42]. The motion consists of three phases: reachability, injection, and sliding [42,107].

The reachability phase consists of forcing the estimates to the hyperplane from some initial conditions, in a finite period of time [42]. Once within the existence subspace, both the injection and sliding phases are present. As the name suggests, the sliding phase forces the estimated errors to slide along a hyperplane towards the origin (ideal case) [42]. The injection phase consists of preventing the estimate from leaving the existence subspace, or in other words, keeping it bounded within an area of the hyperplane [42]. According to [42,105,108], the action of the injection phase enables the observer to be robust enough to overcome uncertainties, modeling errors, and nonlinearities present in the system.

A number of SMOs have been developed since the 1980s [42,105]. The most notable observers include those introduced by Slotine et al. [109,110], Walcott et al. [111,112], Edwards et al. [108], and later by both Tan and Edwards [113]. SMOs have been successfully applied to state and parameter estimation problems, and also fault detection and isolation [42]. Furthermore, a number of developments have generated a large amount of research interest in SMO methods in recent years [105]. A very comprehensive and thorough survey of SMO literature is available in [105]. The following subsections briefly summarize the design of a discontinuous observer, the observer presented by Slotine et al., the Walcott and Zak observer, and finally the Tan and Edwards observer [42].

2.6.1 A Discontinuous Observer

According to [42] and [105], a discontinuous observer is a type of observer that feeds back the output error between the observer and the system as a discontinuous signal. This type of observer may be applied on a continuous linear system and measurement, such as [42]:

$$\dot{x}(t) = Ax(t) + Bu(t) \tag{2.6.1.1}$$

$$z(t) = Cx(t) \tag{2.6.1.2}$$

The system, input, and output matrices (A, B, and C) are time-invariant, where the measurement matrix C is defined by [42,105]:

$$C = [0_{m\times(n-m)} \quad I_{m\times m}] \tag{2.6.1.3}$$

The observer makes use of a discontinuous gain K_s and a sign function of the output error N. The corresponding state estimate $\hat{x}$ is calculated as follows:

$$\dot{\hat{x}}(t) = A\hat{x}(t) + Bu(t) + K_s N \tag{2.6.1.4}$$

The gain K_s is real with dimensions $(n-m)\times m$ and is defined by $K_s = [K_{s,1} \quad I_{m\times m}]^T$ [42]. The function N is defined by $N = \rho sign(e_{\hat{x},2})$, and the output error is calculated by $e_{\hat{x},2}(t) = z(t) - \hat{x}_2(t)$ [42]. According to [42] and [105], the estimated error is defined as follows:

$$\begin{bmatrix}\dot{e}_{\hat{x},1}(t)\\ \dot{e}_{\hat{x},2}(t)\end{bmatrix} = A\begin{bmatrix}e_{\hat{x},1}(t)\\ e_{\hat{x},2}(t)\end{bmatrix} - K_s N \tag{2.6.1.5}$$

Note that the scalar ρ affects the reachability phase of the discontinuous observer, and should be chosen large enough such that the estimated trajectory reaches the sliding surface in a finite period of time [42]. As described earlier, once the estimated trajectory researches the sliding surface, it is bounded within a region and slides along the surface. The discontinuous observer has a few disadvantages. It assumes that there is no noise present, which negatively affects the performance of the observer (since noise is present in nearly every system) [42]. Furthermore, the discontinuous observer approximates nonlinear systems using two parts: a linear and a nonlinear part. The linear part attempts to represent the true system, while the nonlinear part is considered to be uncertainties [42]. This strict assumption holds only if the linear portion is dominant. Finally, this type of SMO is sensitive to the design parameter ρ, which needs to be selected carefully. A large value may lead to chattering, while a small value causes slow convergence [42].

2.6.2 The Slotine et al. Observer

In 1987, Slotine et al. presented an observer that consisted of a linear portion and a discontinuous term [42,110]. According to [42], this observer can be applied to nonlinear systems that have the following form:

$$\dot{x}(t) = Ax(t) + Bu(t) + B\mu(t, z, u) \tag{2.6.2.1}$$

The term $\mu(t, z, u)$ is an unknown nonlinear scalar function. The measurement equation may be defined as (2.6.1.2). For, example consider a system with three states such that the system, input, and measurement matrices may be defined respectively as follows [42]:

$$A = \begin{bmatrix} 0 & 1 & 0 \\ 0 & 0 & 1 \\ 0 & 0 & 0 \end{bmatrix} \tag{2.6.2.2}$$

$$B = [0 \quad 0 \quad 1]^T \tag{2.6.2.3}$$

$$C = [1 \quad 0 \quad 0] \tag{2.6.2.4}$$

The Slotine et al. observer has the following form [42,110]:

$$\dot{\hat{x}}(t) = A\hat{x}(t) + Bu(t) + B\hat{\mu}(t, z, u) + K_l e_z + K_s N \tag{2.6.2.5}$$

$$\hat{z}(t) = C\hat{x}(t) \tag{2.6.2.6}$$

Where, according to [42,110], $\hat{\mu}(t, z, u)$ is a nonlinear estimated function for $\mu(t, z, u)$, $e_z = e_1 = z - \hat{z}$, $N = sign(e_z)$, and the gains are defined by $K_l = [K_{l,1} \quad K_{l,2}]^T$ and $K_s = [K_{s,1} \quad K_{s,2}]^T$. Furthermore, it is important to note that the error in $\hat{\mu}(t, z, u)$, represented by $\Delta\mu$, is assumed to be bounded by $K_{s,2}$ [42]. Slotine et al. reported that the SMO is stable (BIBO) if the gain $K_{s,2}$ is defined to be larger than $|\Delta\mu|$ [42,110]. Furthermore, it was also reported that the addition of the gain $K_{s,1}$ resulted in two types of motion: one prior to reaching the sliding surface and another when the sliding surface has been reached [42,110]. It was determined that the convergence to the sliding surface becomes faster when the gain $K_{s,1}$ is increased [42]. Furthermore, it was found that the gain $K_{l,2}$ affects the reachability of the observer such that when the value is increased, the convergence becomes slower [42,110].

2.6.3 The Walcott and Zak Observer

The Walcott and Zak observer is essentially a modified form of the discontinuous observer, and attempts to accommodate nonlinearities and uncertainties in the system, as well as a multi-input signal [42,111]. Like the previous method, the system is assumed to consist of a linear part and an unknown nonlinear component $\mu(t,z,u)$ [42]:

$$\dot{x}(t) = Ax(t) + Bu(t) + B\mu(t,z,u) \tag{2.6.3.1}$$

The measurement is defined as follows:

$$z(t) = Cx(t) \tag{2.6.3.2}$$

Note that $\mu(t,z,u)$ is bounded by $\rho(t,z,u)$, such that $|\mu(t,z,u)| \leq \rho(t,z,u)$ [42]. The Walcott and Zak observer has a similar structure to the Slotine et al. method, as defined as follows [42,111]:

$$\dot{\hat{x}}(t) = A\hat{x}(t) + Bu(t) + B\hat{\mu}(t,z,u) + K_l e_z + K_s N \tag{2.6.3.3}$$

$$\hat{z}(t) = C\hat{x}(t) \tag{2.6.3.4}$$

However, note that the gains have different formulations, and are defined by [42,111]:

$$N = \rho(t,z,u)sign(C_s e_z) \tag{2.6.3.5}$$

$$K_s = P^{-1}C^T C_s^T \tag{2.6.3.6}$$

$$K_l = \begin{bmatrix} A_{12} \\ A_{22} - A_{22}^s \end{bmatrix} \tag{2.6.3.7}$$

Note that P is a square positive definite matrix and is chosen to satisfy the following condition [42,111]:

$$P(A - K_l C) + (A - K_l C)^T P < 0 \tag{2.6.3.8}$$

Furthermore, C_s is a design matrix used to define the sliding surface as $C_s e_z$, while subject to the following [42,111]:

$$PB = (C_s C)^T \tag{2.6.3.9}$$

Finally, note that A_{22}^s is also a design matrix with negative eigenvalues [42]. To summarize, the Walcott and Zak observer is a modified form of the discontinuous observer but is able to handle multi-input signals and nonlinearities in the system. However, it has several limitations that reduce the number of useful applications for the observer [42,111].

2.6.4 The Tan and Edwards Observer

Presented in 2003, the Tan and Edwards observer (also known as convex parameterization) is an expansion and modification of the Walcott and Zak observer [42,113]. It attempts to increase the number of useful applications, while also reducing the overall design effort [42,113]. For this observer, the system and measurement are structured as follows [42,113]:

$$\dot{x}(t) = Ax(t) + Bu(t) + D\mu(t,z,u) \tag{2.6.4.1}$$

$$z(t) = Cx(t) \tag{2.6.4.2}$$

Where, according to [42], the uncertainty matrix is defined by $D = [0 \quad D_2]^T$, the measurement matrix is $C = [0 \quad T_0]$, and $\mu(t,z,u)$ is a nonlinear function bounded by $\rho(t,z,u)$, such that $|\mu(t,z,u)| \leq \rho(t,z,u)$. Note that if the system matrix is not in canonical form, a transformation must take place to revise the system structure [42]. This type of observer has a similar structure to the previous ones, and is defined by [42,113]:

$$\dot{\hat{x}}(t) = A\hat{x}(t) + Bu(t) + D\hat{\mu}(t,z,u) + K_l e_z + K_s N \tag{2.6.4.3}$$

$$\hat{z}(t) = C\hat{x}(t) \tag{2.6.4.4}$$

However, in this case, the function N is defined by [42,113]:

$$N = \rho(t,z,u)\left|P_0 C_0 \begin{bmatrix} 0 \\ D_2 \end{bmatrix}\right| sign(e_z) \tag{2.6.4.5}$$

The matrix C_0 is the lower portion of the measurement matrix C [42,113]. Furthermore, note that P_0 is a symmetric positive definite matrix defined as a function of the matrix P as follows [42,113]:

$$P = \begin{bmatrix} P_1 & -P_1[K_{s,1} \quad 0] \\ -[K_{s,1} \quad 0]^T P_1 & P_2 + [K_{s,1} \quad 0]^T P_1 [K_{s,1} \quad 0] \end{bmatrix} \tag{2.6.4.6}$$

Where P is designed to satisfy (2.6.3.8) [42,113]:

$$P(A - K_l C) + (A - K_l C)^T P < 0 \tag{2.6.3.8}$$

And the matrix P_0 is defined as follows [42,113]:

$$P_0 = C_0 P_2 C_0^T \tag{2.6.4.7}$$

Furthermore, it is important to note that the sliding gain K_s is defined differently than other observers, as follows [42,113]:

$$K_s = \begin{bmatrix} [K_{s,1} \quad 0] C_0^T \\ C_0^T \end{bmatrix} P_0^{-1} \tag{2.6.4.8}$$

According to [42,113], the gain $K_{s,1}$ is designed such that the term $\left[A_{11} - K_{s,1} A_{21}\right]$ is stable. In order to obtain the linear gain K_l a transformation T_l of the states is required in an effort to transform the measurement matrix into an identity matrix [42,113]:

$$T_l = \begin{bmatrix} I & [K_{s,1} \quad 0] \\ 0 & C_0 \end{bmatrix}^{-1} \tag{2.6.4.9}$$

Performing T_l converts (2.6.4.1) and (2.6.4.2) respectively as follows [42,113]:

$$\dot{x}'(t) = A' x'(t) + B' u(t) + D' \mu(t, z, u) \tag{2.6.4.10}$$

$$z(t) = C' x'(t) \tag{2.6.4.11}$$

Where based on [42,113], $x'(t) = T_l^{-1} x(t) = [x_1(t) \quad x_2(t)]^T$, $A' = T_l^{-1} A T_l$, $B' = T_l^{-1} B$, $C' = C T_l$, $D' = T_l^{-1} D = [0 \quad C_0 D_2]^T$. The gain K_l is defined as follows [42,113]:

$$K_l = \begin{bmatrix} A'_{12} \\ A'_{22} - A^s_{22} \end{bmatrix} \tag{2.6.4.12}$$

The discontinuous gain K_s then takes the following form [42,113]:

$$K_s = \begin{bmatrix} 0 \\ P_0^{-1} \end{bmatrix} \tag{2.6.4.13}$$

Although this observer does require a large number of conditions, it needs less design effort compared to the Walcott and Zak observer [42,105,113]. However, these conditions also limit the number of useful applications for the observer [42,113].

2.7 Summary

Estimation theory is an important tool for the successful control of mechanical and electrical systems. This chapter provided a comprehensive review of a number of conventional estimation strategies (i.e., Kalman-based methods). It was presented that the Kalman filter provides the optimal solution for linear estimation problems. However, it suffers from a number of strict assumptions. If any of these assumptions are violated, the KF yields suboptimal results and can become unstable. However, this chapter also provided an overview of a number of methodologies that may be implemented to improve the KF performance and stability. A number of Kalman-based strategies were presented for handling nonlinear estimation problems. In nature, many systems behave according to a number of different models (modes, or operating regimes). The concept of multiple model (MM) strategies was introduced in an effort to improve upon the estimation results. Finally, a brief overview of sliding mode observers (SMOs) was provided. The following chapter introduces the smooth variable structure filter (SVSF) which is based on concepts closely related to SMOs and variable structure control (VSC), and forms the core of the research presented in this thesis.

Chapter 3

The Smooth Variable Structure Filter

The smooth variable structure filter (SVSF) forms the core of the research for this thesis. This chapter provides an overview of the variable structure filter (VSF), extended variable structure filter (EVSF), and finally introduces the important concepts of the SVSF. A linear computer experiment is used to study and compare the results of the KF and SVSF estimation methods.

3.1 The Variable Structure Filter

The variable structure filter (VSF) was first presented in 2002, and is the predecessor to the smooth variable structure filter (SVSF) [38,114]. It was a new model-based strategy that used concepts closely related to variable structure control. This estimation strategy was presented in an effort to improve upon stability and robustness issues of the popular Kalman filter (KF). As described in Chapter 2, variable structure control (VSC) theory can guarantee stability given some bounded parametric uncertainty [97,98,115]. The most popular form of VSC is that of sliding mode control (SMC), which utilizes a discontinuous switching plane along some desired trajectory [116,117,118,101]. This plane is often referred to as the sliding surface, in which the objective is to keep the state values along this surface in order to minimize the trajectory errors (i.e., difference between the desired trajectory and the estimated or actual values). Ideally, if the state value is off or away from the surface, a switching gain would be used to push the state towards the sliding surface, creating a robust and stable control strategy. Once on the surface, the states slide along the surface in what is called the sliding mode [101].

As presented in Chapter 2, sliding mode concepts have been used for state estimation, and are referred to as sliding mode observers (SMO) or estimators (SME) [105]. Although the VSF uses a discontinuous component to correct estimates like other sliding mode strategies, it differs in its formulation [38]. The VSF uses a predictor-corrector strategy similar to the KF. Given some knowledge of the system prior to time k, it calculates an a priori (or predicted) state estimate $\hat{x}_{k+1|k}$. This state estimate is then updated based on available measurements of the system, thus formulating an a posteriori state estimate $\hat{x}_{k+1|k+1}$. Consider the linear system and measurement equations of (1.1.1) and (1.1.2). The VSF estimation process is summarized as follows [38]. The a priori state estimate is first calculated using the previous time step's a posteriori state estimate and the estimated system model:

$$\hat{x}_{k+1|k} = \hat{A}\hat{x}_{k|k} + \hat{B}u_k \tag{3.1.1}$$

A gain vector K_{k+1}^{VSF} is used to formulate an a posteriori state estimate, as follows:

$$\hat{x}_{k+1|k+1} = \hat{x}_{k+1|k} + K_{k+1}^{VSF} \tag{3.1.2}$$

Where the gain vector K_{k+1}^{VSF} is calculated as a function of the estimated system and measurement matrices $\hat{A}$ and $\hat{C}$, a constant diagonal gain matrix Υ with elements $\Upsilon_{ii} \geq 1$, and an upper bound for both the system and measurement noises W_{Max} and V_{Max} [38]:

$$\begin{aligned} K_{k+1}^{VSF} = \hat{A}^{-1}\hat{C}^{+}\Bigg(\Big|\big|\hat{C}\hat{A}\big|_{Abs}\Big\{\Upsilon\big|\hat{C}\big|_{Abs}\big|e_{z,k+1|k}\big|_{Abs} + \big|\hat{A}^{-1}\hat{C}^{+}\tilde{\xi}_{Max}z_{k+1}\big|_{Abs} \\ + \Big[\big|\hat{C}^{+}\big|_{Abs} + \big|\hat{A}^{-1}\hat{C}^{+}\big|_{Abs}\big(\tilde{\xi}_{Max} + I\big)\Big]V_{Max} + \big|\hat{A}^{-1}\hat{C}^{+}\tilde{\delta}_{Max}u_k\big|_{Abs} \\ + \Big[\big|\hat{A}^{-1}\big|_{Abs} + \big|\hat{A}^{-1}\hat{C}^{+}\tilde{C}_{Max}\big|_{Abs}\Big]W_{Max}\Big\}\Big|_{Abs} \circ sign\big(e_{z,k+1|k}\big)\Bigg) \end{aligned} \tag{3.1.3}$$

Note that the modeling error is denoted by $\sim$, I refers to an identity matrix, and the subscript Max signifies an upper bound. Furthermore, consider that $\xi = CAC^{+}$, $\hat{\xi} = \hat{C}\hat{A}\hat{C}^{+}$, $\tilde{\xi} = \xi - \hat{\xi}$, $\delta = CB$, $\hat{\delta} = \hat{C}\hat{B}$, and $\tilde{\delta} = \delta - \hat{\delta}$. Finally, $\tilde{\xi}_{Max}$, $\tilde{\delta}_{Max}$, and $\tilde{C}_{Max}$ are upper bounds on modeling uncertainties ξ, δ, and C, respectively. The a priori measurement error vector $e_{z,k+1|k}$ is defined as follows:

$$e_{z,k+1|k} = z_{k+1} - C\hat{x}_{k+1|k} \tag{3.1.4}$$

Furthermore, $sign\left(e_{z,k+1|k}\right)$ represents a vector, with elements defined by:

$$sign\left(e_{z,k+1|k}\right) = \begin{bmatrix} sign\left(e_{z_1,k+1|k}\right) \\ \vdots \\ sign\left(e_{z_m,k+1|k}\right) \end{bmatrix} \tag{3.1.5}$$

Note that in general a $sign(e)$ function is defined by:

$$sign(e) = \begin{cases} +1 & e > 0 \\ 0 \quad if & e = 0 \\ -1 & e < 0 \end{cases} \tag{3.1.6}$$

Furthermore, note that $\circ$ refers to the Schur product, such that:

$$a \circ b = \begin{bmatrix} a_1 b_1 \\ a_2 b_2 \\ a_3 b_3 \end{bmatrix} \tag{3.1.7}$$

Where a and b are column vectors with three elements each. Note that the VSF gain results in high frequency switching which limits the performance, as well as introduces chattering in the estimated states [38]. These results may be undesirable when smooth estimates are required. The chattering may be minimized and reduced by the introduction of a smoothing boundary layer ψ [38,118]. It is important to note that outside this boundary layer, the $sign$ function is maintained to ensure robustness and stability. Inside this boundary layer, the VSF gain is interpolated to obtain a smooth function [38]. Hence, consider the following change to the VSF gain:

$$sign\left(e_{z,k+1|k}\right) \rightarrow sat\left(\frac{e_{z_i,k+1|k}}{\psi_i}\right) \tag{3.1.8}$$

Where the saturation function is defined by:

$$sat\left(\frac{e_{z_i,k+1|k}}{\psi_i}\right)=\begin{cases}+1 & \frac{e_{z_i,k+1|k}}{\psi_i}\geq 1\\ \frac{e_{z_i,k+1|k}}{\psi_i} & if \quad -1<\frac{e_{z_i,k+1|k}}{\psi_i}<1\\ -1 & \frac{e_{z_i,k+1|k}}{\psi_i}\leq -1\end{cases} \tag{3.1.9}$$

As described in [38], for the purposes of stability, the VSF gain needs to be large enough to overcome the presence of uncertainties. Therefore, there is a relationship between the magnitude of the VSF gain and the level of uncertainty. Furthermore, the smoothing boundary layer ψ width also needs to be sufficiently large, such that it encompasses the maximum VSF gain values present in the estimation process [38]. The width of this boundary layer also determines the average level of estimation accuracy. Typically, the larger the smoothing boundary layer width, the less accurate the estimate (i.e., more uncertainties present) [38]. This makes sense intuitively, since the presence of fewer uncertainties leads to a more accurate estimate. The boundary layer width is a function of the upper bounds associated with the uncertainties present in the estimation process (i.e., modeling errors, and the system and measurement noises) [38]:

$$\begin{aligned}\psi = \left|\hat{C}^{+}\hat{A}^{-1}\right|_{Abs}\left|\hat{A}\hat{C}\right|_{Abs}\Big\{&\left|\hat{A}^{-1}\hat{C}^{+}\tilde{\xi}_{Max}z_{Max}\right|_{Abs}\\ &+\left[\left|\hat{C}^{+}\right|_{Abs}+\left|\hat{A}^{-1}\hat{C}^{+}\right|_{Abs}\left(\hat{\xi}+\tilde{\xi}_{Max}+I\right)\right]V_{Max}\\ &+\left|\hat{A}^{-1}\hat{C}^{+}\tilde{\delta}_{Max}u_{Max}\right|_{Abs}+\left[\left|\hat{A}^{-1}\right|_{Abs}+\left|\hat{A}^{-1}\hat{C}^{+}\tilde{C}_{Max}\right|_{Abs}\right]W_{Max}\Big\}\end{aligned} \tag{3.1.10}$$

The VSF offers a number of advantages. If the upper bounds of the system uncertainties and noise levels are well-defined, the VSF gain may be easily calculated as per (3.1.3) [42]. Furthermore, the VSF gain provides a robust estimation strategy, and has demonstrated stability to modeling uncertainties [38,114]. However, the VSF strategy does have a few disadvantages. The strategy may only be applied to linear systems, and yields non-optimal estimation results. Furthermore, the estimate may experience chattering, which may be undesirable, depending on the application [38].

3.2 The Extended Variable Structure Filter

In 2006, a modified form of the VSF was introduced, referred to as the extended variable structure filter (EVSF) [119]. Unlike the VSF, the EVSF method may be applied to nonlinear systems and measurements defined by (1.1.5) and (1.1.6) respectively.

$$x_{k+1} = f(x_k, u_k) + w_k \tag{1.1.5}$$

$$z_{k+1} = h(x_{k+1}) + v_{k+1} \tag{1.1.6}$$

The EVSF is formulated in a predictor-corrector fashion, and is conceptually similar to the VSF [119]. The state estimate is first predicted by using the estimated nonlinear system model, as follows:

$$\hat{x}_{k+1|k} = \hat{f}\left(\hat{x}_{k|k}, u_k\right) \tag{3.2.1}$$

The estimate $\hat{x}_{k+1|k}$ is obtained by using the previous state estimate $\hat{x}_{k|k}$, or the initial conditions x_0 at the start of the estimation process. The a priori state estimates are then used to calculate the a priori measurement estimates $\hat{z}_{k+1|k}$, as follows:

$$\hat{z}_{k+1|k} = \hat{h}\left(\hat{x}_{k+1|k}\right) \tag{3.2.2}$$

An EVSF corrective gain K_{k+1}^{EVSF} is then calculated, and used to refine the a posteriori state estimate as follows [119]:

$$\hat{x}_{k+1|k+1} = \hat{x}_{k+1|k} + K_{k+1}^{EVSF} \tag{3.2.3}$$

The EVSF strategy is similar to the extended Kalman filter (EKF), in the sense that it makes use of the linearized system and measurement functions, as follows:

$$\hat{F}_k = \left.\frac{\partial \hat{f}}{\partial x}\right|_{\hat{x}_{k|k}, u_k} \tag{3.2.4}$$

$$\hat{H}_{k+1} = \left.\frac{\partial \hat{h}}{\partial x}\right|_{\hat{x}_{k+1|k}} \tag{3.2.5}$$

The linearization is performed in order to derive the EVSF corrective gain used in (3.2.3). The EVSF corrective gain is defined as follows [119]:

$$K_{k+1}^{EVSF} = \hat{F}_k^+ \hat{H}_{k+1}^+ \Big(\big|\hat{H}_{k+1,Max}\big|_{Abs} \big|\hat{F}_{k,Max}\big|_{Abs} \Big\{ \gamma \big|\hat{H}_{k+1,Max}^+\big|_{Abs} \big|e_{z,k+1|k}\big|_{Abs} + \big|\hat{F}_{k,Max}^{-1}\big|_{Abs} \Big[\big|f(x_k,u_k) - \hat{f}\big(\hat{x}_{k|k},u_k\big)\big|_{Abs} + W_{Max} + \big|\hat{H}_{k+1,Max}^+\big|_{Abs} V_{Max} \Big] \Big\} \circ sign\big(e_{z,k+1|k}\big) \Big) \tag{3.2.6}$$

Note that it is assumed the system under consideration is observable, and has a system output matrix that is positive and constant in its linearized form such that $H_{k+1} = H_k$ [119]. The corrective gained (3.2.6) is conceptually similar to that presented for the VSF (3.1.9), however can be applied for nonlinear systems. The EVSF and VSF strategies have similar advantages and disadvantages [42]. However, one notable disadvantage for the EVSF method is that it requires linearization at each time step in order to calculate the EVSF gain. This results in an increase in numerical effort, as well as reduces the overall estimation accuracy due to the truncation of higher-order terms (i.e., Taylor series approximation) [119]. These disadvantages are similar to the EKF, as discussed earlier in Chapter 2.

3.3 The Smooth Variable Structure Filter

A revised form of the VSF, referred to as the smooth variable structure filter (SVSF), was presented in 2007 [37]. The SVSF strategy is also a predictor-corrector estimator based on sliding mode concepts, and can be applied on both linear or nonlinear systems and measurements. As shown in the following figure, and similar to the VSF, it utilizes a switching gain to converge the estimates to within a boundary of the true state values (i.e., existence subspace) [37]. The SVSF has been shown to be stable and robust to modeling uncertainties and noise, when given an upper bound on the level of unmodeled dynamics and noise [37,38]. The origin of the SVSF name comes from the requirement that the system is differentiable (or 'smooth') [37,42]. Furthermore, it is assumed that the system under consideration is observable [37].

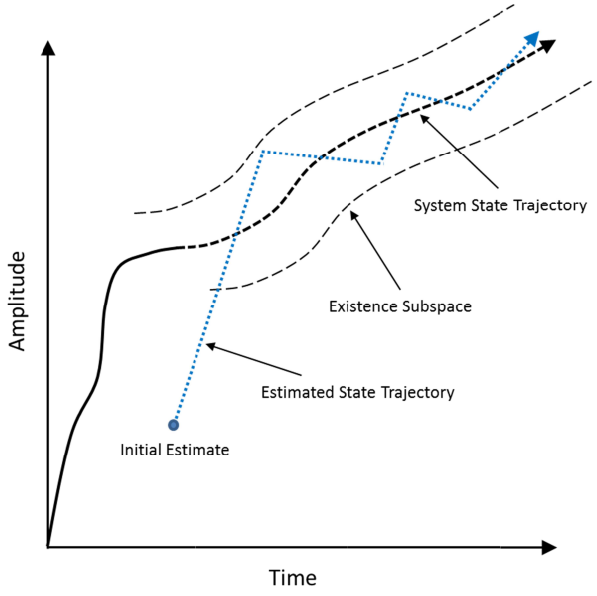

Figure 3.3.1. SVSF Estimation Concept

Consider the following process for the SVSF estimation strategy, as applied to a nonlinear system with a linear measurement equation. The predicted state estimates $\hat{x}_{k+1|k}$ are first calculated as follows:

$$\hat{x}_{k+1|k} = \hat{f}\left(\hat{x}_{k|k}, u_k\right) \tag{3.3.1}$$

Utilizing the predicted state estimates $\hat{x}_{k+1|k}$, the corresponding predicted measurements $\hat{z}_{k+1|k}$ and measurement error vector $e_{z,k+1|k}$ may be calculated:

$$\hat{z}_{k+1|k} = C\hat{x}_{k+1|k} \tag{3.3.2}$$

$$e_{z,k+1|k} = z_{k+1} - \hat{z}_{k+1|k} \tag{3.3.3}$$

Next, the SVSF gain is calculated as follows [37]:

$$K_{k+1}^{SVSF} = C^{+}\left(\left|e_{z,k+1|k}\right|_{Abs} + \gamma\left|e_{z,k|k}\right|_{Abs}\right) \circ sat\left(\frac{e_{z,k+1|k}}{\psi}\right) \tag{3.3.4}$$

The SVSF gain is a function of: the a priori and a posteriori measurement error vectors $e_{z,k+1|k}$ and $e_{z,k|k}$; the smoothing boundary layer widths ψ; the 'SVSF' memory or convergence rate γ with elements $0 < \gamma_{ii} \leq 1$; and the linear measurement matrix C. The SVSF gain is used to refine the state estimates as follows:

$$\hat{x}_{k+1|k+1} = \hat{x}_{k+1|k} + K_{k+1}^{SVSF} \tag{3.3.5}$$

Next, the updated measurement estimates $\hat{z}_{k+1|k+1}$ and corresponding errors $e_{z,k+1|k+1}$ are calculated:

$$\hat{z}_{k+1|k+1} = C\hat{x}_{k+1|k+1} \tag{3.3.6}$$

$$e_{z,k+1|k+1} = z_{k+1} - \hat{z}_{k+1|k+1} \tag{3.3.7}$$

The SVSF process may be summarized by (3.3.1) through (3.3.7), and is repeated iteratively. According to [37], the estimation process is stable and converges to the existence subspace if the following condition is satisfied:

$$\left|e_{k|k}\right|_{Abs} > \left|e_{k+1|k+1}\right|_{Abs} \tag{3.3.8}$$

Note that $|e|_{Abs}$ is the absolute of the vector e, and is equal to $|e|_{Abs} = e \cdot sign(e)$. The proof, as described in [37] and [42], yields the derivation of the SVSF gain from (3.3.8). The stability proof provided in [42] is very clear, and is provided in Appendix 8.1 for completeness.

The SVSF results in the state estimates converging to within a region of the state trajectory, referred to as the existence subspace. Thereafter, it switches back and forth across the state trajectory, as shown earlier in Figure 3.3.1. The existence subspace shown in Figures 3.3.1 through 3.3.3 represents the amount of uncertainties present in the estimation process, in terms of modeling errors or the presence of noise. The width of the existence space β is a function of the uncertain dynamics associated with the inaccuracy of the internal model of the filter as well as the measurement model, and varies with time [37]. Typically this value is not exactly known but an upper bound may be selected based on a priori knowledge.

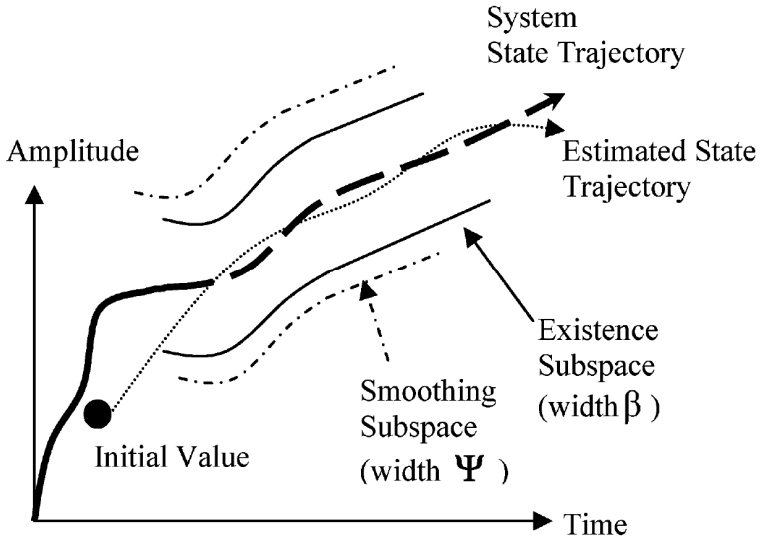

Figure 3.3.2. Smoothed Estimated Trajectory ($\psi \geq \beta$) [37]

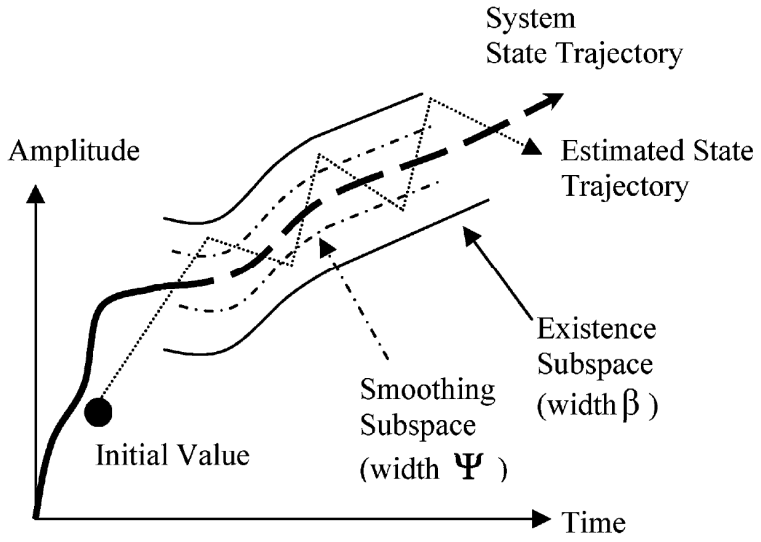

Figure 3.3.3. Presence of Chattering Effect ($\psi < \beta$) [37]

Once within the existence boundary subspace, the estimated states are forced (by the SVSF gain) to switch back and forth along the true state trajectory. As mentioned earlier, high-frequency switching caused by the SVSF gain is referred to as chattering, and in most cases, is undesirable for obtaining accurate estimates [37].

However, the effects of chattering may be minimized by the introduction of a smoothing boundary layer ψ. The selection of the smoothing boundary layer width reflects the level of uncertainties in the filter and the disturbances (i.e., system and measurement noise, and unmodeled dynamics). A time-varying derivation for the SVSF smoothing boundary layer will be explored later in Chapter 5, based on the covariance derivation to be presented in Chapter 4. The effect of the smoothing boundary layer is shown in Figures 3.3.2 and 3.3.3. When the smoothing boundary layer is defined larger than the existence subspace boundary, the estimated state trajectory is smoothed. However, when the smoothing term is too small, chattering remains due to the uncertainties being underestimated. Similar to the VSF strategy, the smoothing boundary layer ψ modifies the SVSF gain as follows [37]:

$$K_{k+1}^{SVSF} = C^{+}\left(\left|e_{z,k+1|k}\right|_{Abs} + \gamma\left|e_{z,k|k}\right|_{Abs}\right) \circ sat\left(e_{z,k+1|k}/\psi\right) \tag{3.3.9}$$

The SVSF gain is considerably less complex than its predecessor (VSF), which allows it to be implemented more easily (mathematically and conceptually). Furthermore, the SVSF estimation process is inherently robust and stable to modeling uncertainties due to the switching effect of the gain. This makes for a powerful estimation strategy, particularly when the system is not well known. Note that for systems that have fewer measurements than states, a 'reduced order' approach is taken to formulate a full measurement matrix [37,120]. Essentially 'artificial measurements' are created and used throughout the estimation process.

3.4 Computer Experiment

This section studies a computer experiment, and compares the KF and SVSF strategies. For linear systems, it is expected that the KF will outperform the SVSF in terms of estimation accuracy. However, the injection of modeling uncertainties will demonstrate the robust performance of the SVSF. A global carbon cycle (GCC) system is used as a linear example, and is shown below as presented in [121] and [122].

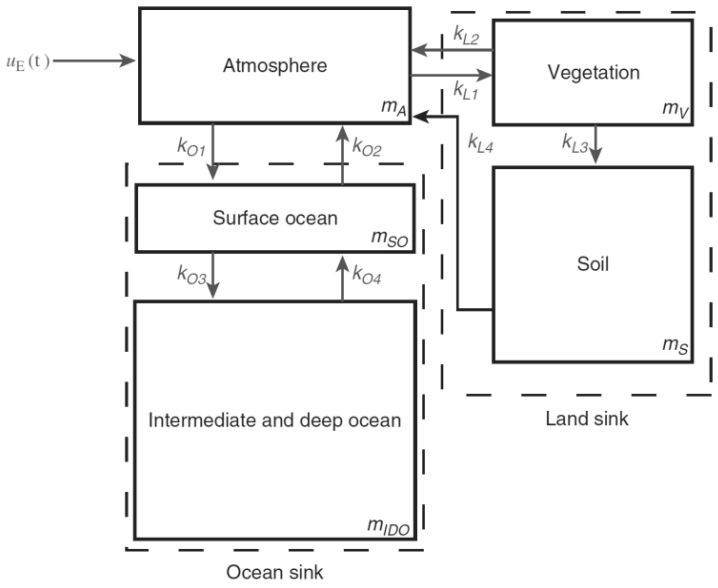

Figure 3.4.1. Global Carbon Cycle [122]

The GCC is used to study climate change and global carbon cycles [121]. As shown in the previous figure, a generic GCC structure is based on a number of reservoir mass balances: atmosphere (m_A), surface ocean (m_{SO}), intermediate and deep ocean (m_{IDO}), vegetation (m_V), and soil (m_S). These reservoirs hold carbon mass, measured in 'gigatonnes' ($1 \times 10^9\ tonnes$) of carbon (GtC). The input u_E to the system is CO_2 emissions ($GtC/year$) from biological sources, such as humans. The arrows in the previous figure represent the net carbon fluxes between boxes (reservoirs) as governed by the exchange coefficients k, and are summarized by the following table [121].

Table 3.4.1. Carbon Fluxes for the Global Carbon Cycle Example

Flux	Land Component (yr^{-1})	Ocean Component (yr^{-1})
1	$k_{L1} = 0.0722$	$k_{O1} = 0.1025$
2	$k_{L2} = 0.0994$	$k_{O2} = 0.5921$
3	$k_{L3} = 0.0871$	$k_{O3} = 0.0708$
4	$k_{L4} = 0.0376$	$k_{O4} = 0.00296$

The mass balance equations may be determined from Figure 3.4.1, and are used to derive a state space representation of the GCC system. The atmospheric mass balance rate may be defined by [121]:

$$\frac{dm_A}{dt} = u_E - (k_{O1} + k_{L1})m_A + k_{L2}m_V + k_{O2}m_{SO} + k_{L4}m_S \tag{3.4.1}$$

Note that the time notation was omitted for simplicity (i.e., $u_E(t)$ becomes u_E). The four remaining reservoir mass balances (surface ocean, intermediate and deep ocean, vegetation, and soil) are defined respectively as follows [121]:

$$\frac{dm_{SO}}{dt} = k_{O1}m_A - (k_{O2} + k_{O3})m_{SO} + k_{O4}m_{IDO} \tag{3.4.2}$$

$$\frac{dm_{IDO}}{dt} = k_{O3}m_{SO} - k_{O4}m_{IDO} \tag{3.4.3}$$

$$\frac{dm_V}{dt} = k_{L1}m_A - (k_{L2} + k_{L3})m_V \tag{3.4.4}$$

$$\frac{dm_S}{dt} = k_{L3}m_V - k_{L4}m_S \tag{3.4.5}$$

Suppose the state vector is defined as $x = [m_A \quad m_{SO} \quad m_{IDO} \quad m_V \quad m_S]^T$, then a discrete-time state space representation for the system (using the values found in Table 3.4.1) with $T = 1\ year$, may be defined as follows:

$$x_{k+1} = \begin{bmatrix} 0.8253 & 0.5921 & 0 & 0.0994 & 0.0376 \\ 0.1025 & 0.3371 & 0.0030 & 0 & 0 \\ 0 & 0.708 & 0.9970 & 0 & 0 \\ 0.0722 & 0 & 0 & 0.8135 & 0 \\ 0 & 0 & 0 & 0.0871 & 0.9624 \end{bmatrix} x_k + \begin{bmatrix} 1 \\ 0 \\ 0 \\ 0 \\ 0 \end{bmatrix} u_E \tag{3.4.6}$$

The corresponding measurement equation is defined by:

$$z_{k+1} = [1 \quad 0 \quad 0 \quad 0 \quad 0]x_{k+1} \tag{3.4.7}$$

For this simulation, system and measurement noise is injected according to (1.1.3) and (1.1.4). The corresponding system and measurement covariance's are defined respectively as follows:

$$Q = 10^{-7} \times diag([1 \quad 1 \quad 1 \quad 1 \quad 1]) \tag{3.4.8}$$

$$R = 1 \times 10^{-5} \tag{3.4.9}$$

The initial states and their estimates are set to zero, based on the assumption that there is no initial carbon present in the system (for the purposes of the computer experiment). The initial state error covariance matrix (used by the KF), is defined as follows:

$$P_{0|0} = 20 \times Q \tag{3.4.10}$$

For this scenario, the SVSF 'memory' or convergence rate and smoothing boundary layers were defined as follows:

$$\gamma = 0.1 \tag{3.4.11}$$

$$\psi = 0.03 \tag{3.4.12}$$

The SVSF smoothing boundary layer was tuned by trial and error in an effort to minimize the state estimation error. The following figure shows the true atmospheric CO_2 concentrations, with the corresponding KF and SVSF estimates, based on an initial impulse response (with amplitude 1).

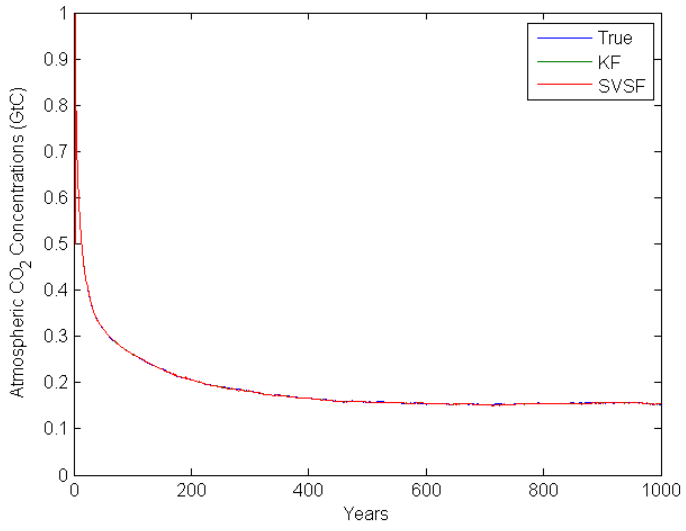

Figure 3.4.2. True and Estimated Atmospheric CO_2 Concentrations, m_A

Note that the estimates are nearly identical, and as such, appear to be overlapping. The KF provides an optimal result (in terms of estimation error) for linear systems; as such, it was expected to outperform the SVSF. A good measure of estimation performance is the root mean square error (RMSE) calculation, which is defined as follows:

$$RMSE_n = \sqrt{\frac{\sum_{i=1}^{m}\left(x_{n,i} - \hat{x}_{n,i}\right)^2}{m}} \tag{3.4.13}$$

Where in this case: n refers to the n^{th} state, m refers to the total number of samples, x refers to the true state value, and $\hat{x}$ refers to the state estimate (from the KF or SVSF). The following table summarizes the RMSE results for this case.

Table 3.4.2. RMSE Results of the Global Carbon Cycle Example

Parameter	KF	SVSF
m_A	8.256×10^{-4}	9.103×10^{-4}
m_{SO}	3.553×10^{-4}	3.568×10^{-4}
m_{IDO}	4.000×10^{-3}	4.000×10^{-3}
m_V	6.120×10^{-4}	6.175×10^{-4}
m_S	8.954×10^{-4}	9.010×10^{-4}

An interesting result occurs when modeling uncertainties are injected into the estimation process half-way through (i.e., at 500 years). Suppose that one of the carbon fluxes used to model the system is incorrectly calculated and used by the filters (i.e., $k_{L1} = 30 \times k_{L1}$). This changes the system defined by (3.4.6), which affects the estimation process. The following two figures illustrate the consequences of the modeling uncertainties. The first figure shows the true atmospheric CO_2 concentrations, with the corresponding KF and SVSF estimates. The second figure shows the corresponding estimation error (i.e., the difference between the true and estimated values). At the inception of the modeling uncertainty, the KF estimate nearly goes unstable, and takes about 500 samples to return to within an acceptable region.

However, due to the corrective action of the SVSF gain, its corresponding estimate remains bounded to within a region of the true state estimate. Although the SVSF estimate is not optimal (as demonstrated by the above table), it is robust in the presence of modeling uncertainties, unlike the KF.

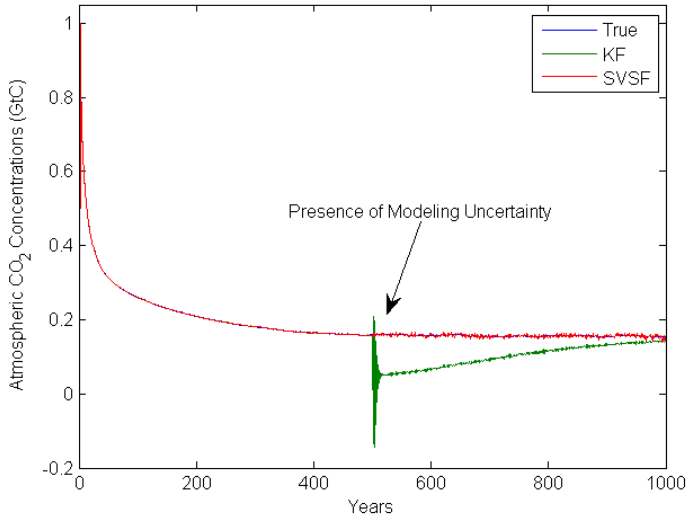

Figure 3.4.3. True and Estimated Values for First State (Uncertainty Case)

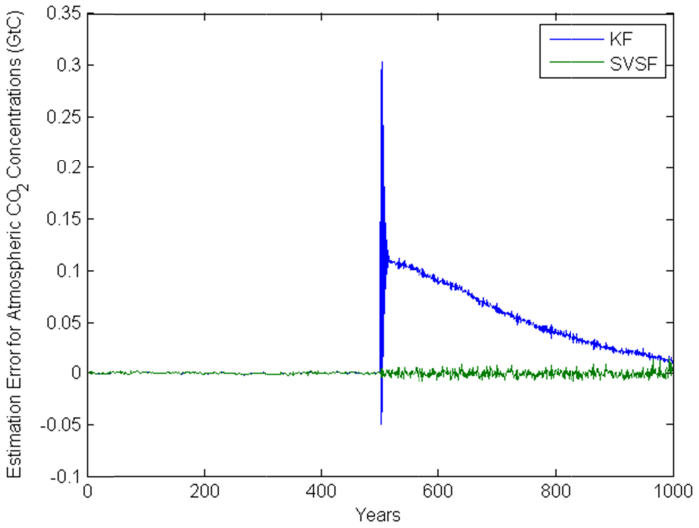

Figure 3.4.4. First State Estimation Error (Uncertainty Case)

Further to the calculation of the RMSE, the Cramér-Rao lower bound (CRLB) may be used as an indicator of the performance of each filter. The CRLB is defined as the inverse of the Fisher information matrix (FIM) J, which quantifies the available information found in the observations about a state [28]. The CRLB provides a lower bound on the achievable variance in the estimation of a parameter. A derivation that can be used for discrete-time filtering is the posterior form (PCRLB) [123,124,125]. This allows meaningful evaluations of estimation techniques, such that the RMSE for each filter can be determined and compared with the PCRLB. Ideally, one would want the RMSE to reach the PCRLB, or be as close as possible. According to [28], the CRLB states that the covariance matrix is bounded as follows:

$$E\{(x-\hat{x})(x-\hat{x})^T\} \geq J^{-1} \tag{3.4.14}$$

The inverse of the PCRLB may be calculated recursively (with initial zero values) [123]:

$$J_{k+1} = \left(AJ_k^{-1}A^T + Q\right)^{-1} + C^T R^{-1} C \tag{3.4.15}$$

The following two figures compare the PCRLB with the KF and SVSF RMSE values for the two cases described earlier (normal and modeling uncertainty).

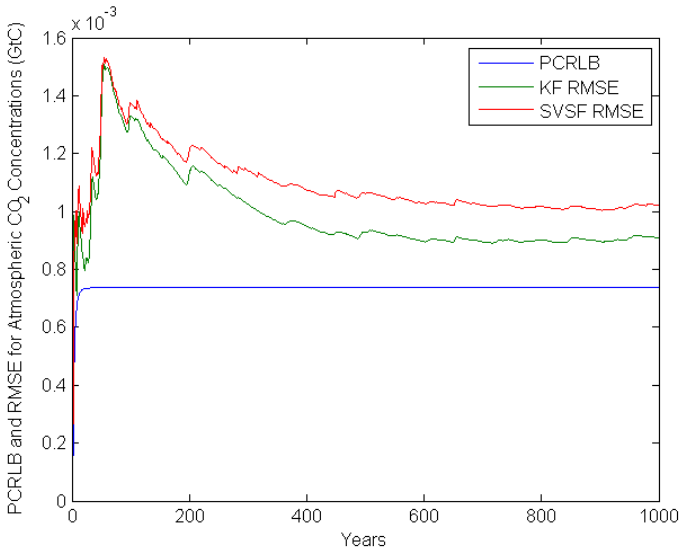

Figure 3.4.5. PCRLB and RMSE for the KF and SVSF Methods (Normal Case)

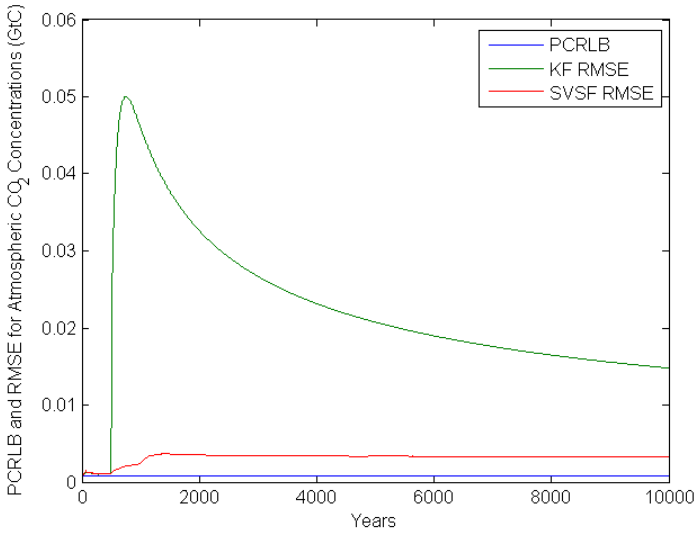

Figure 3.4.6. PCRLB and RMSE for the KF and SVSF Methods (Uncertainty Case)

For the normal case, the KF RMSE is closer to the PCRLB than the SVSF RMSE, which is to be expected, since the KF yields optimal results. The second case clearly shows the SVSF robustness to modeling uncertainties, as the SVSF RMSE is bounded closer to the PCRLB (even after 10,000 samples).

3.5 Summary

This chapter introduced the predecessors to the smooth variable structure filter (SVSF): the variable structure filter (VSF) and its extended form (EVSF). The VSF was derived based on sliding mode and variable structure concepts, and can be applied to linear systems only. The switching gain yields a robust estimation strategy, however this comes at the cost of accuracy (i.e., it is not optimal). The VSF was extended to nonlinear systems and is referred to as the EVSF. The SVSF strategy is also a predictor-corrector estimator based on sliding mode concepts, and can be applied to both linear or nonlinear systems and measurements. The SVSF gain is derived based on a sliding mode concept that creates a very robust estimation strategy. This was demonstrated by the use of a computer experiment, which looked at the RMSE and PCRLB performance metrics.

The SVSF also offers other advantages which will be explored throughout this thesis. Since the filtering strategy is relatively new, a number of research opportunities exist with the SVSF. It is therefore the goal of this research to further advance and develop the SVSF; in particular, to improve its performance and increase the number of its useful applications. The first such development involves the covariance derivation for the SVSF, which is presented in the next chapter.

Chapter 4

Covariance Derivation for the SVSF

This chapter describes the development of the covariance derivation for the SVSF, as applied to both linear and nonlinear systems. Two numerical computer experiments (for linear and nonlinear systems) are presented to provide a comparative study of the SVSF filter with a state error covariance function with other Kalman-based methods.

4.1 Linear Systems

The SVSF in its current form, as described in Chapter 3, does not have or make use of a state error covariance matrix. Error covariance may be used for a variety of reasons: to determine an optimal value of the gain (i.e., such as in the case of the KF); for the implementation of interacting multiple model (IMM) methods that can be used for target tracking or fault detection and diagnosis; or to create other forms such as the information filter formulation (i.e., using the inverse of the covariance) [28]. In statistics and probability theory, a covariance matrix may be defined as a function of two random vectors X and Y. For example, assuming means of $\bar{X}$ and $\bar{Y}$ respectively, a covariance matrix may be defined as follows:

$$cov(X,Y) = E[(X_i - \bar{X})(Y_i - \bar{Y})^T] \tag{4.1.1}$$

Where i refers to the i^{th} element of the vector X or Y. The covariance provides a measure of how random variables are related.

For example, if $cov(X,Y) = 1$ then X and Y are said to be highly correlated. Likewise, $cov(X,Y) = 0$ means that the sets of random variables are uncorrelated. In this thesis, unless otherwise stated, a covariance matrix is assumed to be a function of state estimation errors (i.e., the difference between the actual and estimated state values), and may be defined as the expectation of the error squared, as follows:

$$P = E\{\tilde{x}\tilde{x}^T\} = E\{(x - \hat{x})(x - \hat{x})^T\} \tag{4.1.2}$$

Where x refers to the state, $\hat{x}$ is the corresponding state estimate, and $\tilde{x}$ is the difference between the actual and estimated states. Recall that the SVSF estimation strategy is a predictor-corrector method. As such, it requires an a priori (predicted) and an a posteriori (updated) state error covariance, referred to as $P_{k+1|k}$ and $P_{k+1|k+1}$ respectively. In an effort to find these functions, the following equations must be solved:

$$P_{k+1|k} = E\left\{\left(x_{k+1} - \hat{x}_{k+1|k}\right)\left(x_{k+1} - \hat{x}_{k+1|k}\right)^T\right\} \tag{4.1.3}$$

$$P_{k+1|k+1} = E\left\{\left(x_{k+1} - \hat{x}_{k+1|k+1}\right)\left(x_{k+1} - \hat{x}_{k+1|k+1}\right)^T\right\} \tag{4.1.4}$$

A number of strategies were attempted in an effort to solve both (4.1.3) and (4.1.4). Equation (4.1.4) proved the most difficult, due to the following (expanded) state update equation defined in Chapter 3:

$$\hat{x}_{k+1|k+1} = \hat{x}_{k+1|k} + C^+\left(\left|e_{z,k+1|k}\right|_{Abs} + \gamma\left|e_{z,k|k}\right|_{Abs}\right) \circ sat\left(\frac{e_{z,k+1|k}}{\psi}\right) \tag{4.1.5}$$

The full derivation of $P_{k+1|k+1}$ is provided in Appendix 8.2. It was determined that two equations exist for $P_{k+1|k+1}$, inside and outside the smoothing boundary layer. While outside of the smoothing boundary layer, the a posteriori covariance calculation may be found by:

$$P_{k+1|k+1} = \gamma P_{k|k}\gamma^T + C^{-1}(R_{k+1} + \gamma R_k \gamma^T)C^{-T} \tag{4.1.6}$$

While outside the smoothing boundary layer, the a posteriori state error covariance $P_{k+1|k+1}$ is a function of the previous a posteriori state error covariance $P_{k|k}$, the measurement (output) model C, the SVSF parameter γ, and the measurement noise covariance R_k.

While inside the smoothing boundary layer, solving (4.1.4) using (4.1.5), leads to fourth-order moment calculations (i.e., $E\{\tilde{x}\tilde{x}^T\tilde{x}\tilde{x}^T\}$). The corresponding a posteriori state error covariance may be calculated as follows:

$$P_{k+1|k+1} = P_{k+1|k} - \left(M_{3,1} + M_{3,2}\right)\bar{\psi}^{-1}C^{-T} - C^{-1}\bar{\psi}^{-1}\left(M_{3,3} + M_{3,4}\right) + C^{-1}\bar{\psi}^{-1}M_P\bar{\psi}^{-1}C^{-T} \tag{4.1.7}$$

Where M_3 refers to matrices which consist of third-order moments and M_P is a matrix consisting of second and fourth-order moments, defined as:

$$M_P = M_{4,1} + M_{4,2} + M_{4,3} + M_{4,4} + 4M_{2,2} + 2M_{2,4} + M_{2,10} + 2M_{2,11} + M_{2,13} + M_{2,14} + M_{2,1}\bar{R}_{k+1}^T + \bar{R}_{k+1}\left(M_{2,8} + M_{2,9}\right) + R_{k+1} \circ R_{k+1} + \bar{\gamma}R_{k+1} \circ R_k\bar{\gamma} \tag{4.1.8}$$

Solutions for the second, third, and fourth-order moments are shown in Appendix 8.2. Note that the third and fourth-order moments are calculated recursively. The above derivation is complex, and becomes even more so with an increased number of states. Equation (4.1.7) is cumbersome to compute due to the large number of supporting equations, and is too tedious to implement effectively. In an effort to provide a simplified covariance calculation, an alternative method involving an update equation is proposed. The following revised update equation is similar to the KF strategy. Let:

$$\hat{x}_{k+1|k+1} = \hat{x}_{k+1|k} + K_{k+1}e_{z,k+1|k} \tag{4.1.9}$$

Where the new SVSF gain K_{k+1} is proposed as follows:

$$K_{k+1} = C^{+}diag\left[\left(\left|e_{z,k+1|k}\right|_{Abs} + \gamma\left|e_{z,k|k}\right|_{Abs}\right) \circ sat\left(\frac{e_{z,k+1|k}}{\psi}\right)\right]\left[diag\left(e_{z,k+1|k}\right)\right]^{-1} \tag{4.1.10}$$

To help illustrate (4.1.10), consider a fully measured system $(C = I)$ with three states, such that:

$$K_{k+1} = diag\begin{bmatrix}k_1\\k_2\\k_3\end{bmatrix}\left[diag\begin{pmatrix}e_1\\e_2\\e_3\end{pmatrix}\right]^{-1} \tag{4.1.11}$$

Where:

$$k_i = \left(\left|e_{z_i,k+1|k}\right| + \gamma_i \left|e_{z_i,k|k}\right|\right) \circ sat\left(\frac{e_{z_i,k+1|k}}{\psi_i}\right) \tag{4.1.12}$$

Simplifying (4.1.11) yields:

$$K_{k+1} = \begin{bmatrix} k_1/e_1 & 0 & 0 \\ 0 & k_2/e_2 & 0 \\ 0 & 0 & k_3/e_3 \end{bmatrix} \tag{4.1.13}$$

Substitution of (4.1.13) into the new state update equation of (4.1.9) yields:

$$\hat{x}_{k+1|k+1} = \hat{x}_{k+1|k} + \begin{bmatrix} k_1/e_1 & 0 & 0 \\ 0 & k_2/e_2 & 0 \\ 0 & 0 & k_3/e_3 \end{bmatrix} e_{z,k+1|k} \tag{4.1.14}$$

Note that $e_{z,k+1|k} = [e_1 \quad e_2 \quad e_3]^T$. Simplifying (4.1.14) yields:

$$\hat{x}_{k+1|k+1} = \hat{x}_{k+1|k} + \begin{bmatrix} k_1 \\ k_2 \\ k_3 \end{bmatrix} \tag{4.1.15}$$

Equation (4.1.15) is exactly the same as (3.3.5), or the standard SVSF update equation. Essentially the nature of the SVSF remains the same, as one divides the gain by the a priori output error $e_{z,k+1|k}$, and then multiplies by it again in the update estimate equation (4.1.9).

However, for numerical stability, it is important to ensure that one does not divide by zero in (4.1.7). This can be accomplished using a simple if statement with a very small threshold (i.e., 1×10^{-12}). Introducing the notation of (4.1.9) and (4.1.10) enables one to derive a much simpler covariance derivation. Furthermore, note that the proof of stability for the SVSF is not affected, as the overall corrective gain remains the same as (3.3.5). It is interesting to note that the a priori and a posteriori state error covariance matrices for the SVSF are of similar form to the KF for linear systems, which is to be expected since both filters make use of the same update equation. However, it is important to recognize that although the form of the equations is similar, the applied update gain still differs between the two filters.

4.1.1 A Priori Covariance Calculation

The following presents the derivation of the a priori state error covariance equation for the SVSF for linear systems. It is assumed that the system and measurement matrices are well-defined (i.e., no modeling errors), and are static (i.e., time invariant). The a priori state error covariance matrix may be defined as follows:

$$P_{k+1|k} = E\{\tilde{x}_{k+1|k}\tilde{x}_{k+1|k}^T\} \tag{4.1.1.1}$$

Where, as before, the a priori state error is defined as in (4.1.3). As defined in (1.1.1), the discrete model of the system may be described by the following:

$$x_{k+1} = Ax_k + Bu_k + w_k \tag{1.1.1}$$

Further to (1.1.1), the uncertain estimation model for the system that is used in the prediction stage of the SVSF may be defined as follows:

$$\hat{x}_{k+1|k} = \hat{A}\hat{x}_{k|k} + \hat{B}u_k \tag{4.1.1.2}$$

Substitution of (1.1.1) and (4.1.1.2) into the a priori state error yields:

$$\tilde{x}_{k+1|k} = Ax_k + Bu_k + w_k - \hat{A}\hat{x}_{k|k} - \hat{B}u_k \tag{4.1.1.3}$$

Rearranging (4.1.1.3) yields:

$$\tilde{x}_{k+1|k} = \left(A - \hat{A}\right)x_k + \hat{A}\left(x_k - \hat{x}_{k|k}\right) + \left(B - \hat{B}\right)u_k + w_k \tag{4.1.1.4}$$

Simplifying (4.1.1.4) further yields the following a priori state error equation:

$$\tilde{x}_{k+1|k} = \tilde{A}x_k + \hat{A}\tilde{x}_{k|k} + \tilde{B}u_k + w_k \tag{4.1.1.5}$$

In the absence of modeling errors (i.e., $\hat{A} = A$ and $\hat{B} = B$), the a priori state error equation may be simplified further to (4.1.1.6):

$$\tilde{x}_{k+1|k} = A\tilde{x}_{k|k} + w_k \tag{4.1.1.6}$$

Substitution of (4.1.1.6) into (4.1.1.1) yields the following definition for the a priori state error covariance matrix:

$$P_{k+1|k} = E\left\{\left(A\tilde{x}_{k|k} + w_k\right)\left(A\tilde{x}_{k|k} + w_k\right)^T\right\} \tag{4.1.1.7}$$

Expanding the terms yields:

$$P_{k+1|k} = E\left\{A\tilde{x}_{k|k}\tilde{x}_{k|k}^T A^T + A\tilde{x}_{k|k}w_k^T + w_k\tilde{x}_{k|k}^T A^T + w_k w_k^T\right\} \tag{4.1.1.8}$$

Recall that the system noise w_k is typically modeled as Gaussian noise, such that it is zero-mean with a covariance referred to as Q_k. Furthermore, it is assumed that the system noise w_k and the state errors $\tilde{x}_{k|k}$ are uncorrelated and independent of each other. Based on these assumptions, one may define the following five equations:

$$P(w_k) \sim \mathcal{N}(0, Q_k) \tag{4.1.1.9}$$

$$E\{w_k\} = E\left\{w_k^T\right\} = 0 \tag{4.1.1.10}$$

$$E\left\{w_k w_k^T\right\} = Q_k \tag{4.1.1.11}$$

$$E\left\{w_k\tilde{x}_{k|k}^T\right\} = E\{w_k\}E\left\{\tilde{x}_{k|k}^T\right\} = 0 \tag{4.1.1.12}$$

$$E\left\{\tilde{x}_{k|k}w_k^T\right\} = E\left\{\tilde{x}_{k|k}\right\}E\left\{w_k^T\right\} = 0 \tag{4.1.1.13}$$

Also, it is important to note the definition for the previous time step's a posteriori state error covariance (4.1.1.14).

$$P_{k|k} = E\left\{\tilde{x}_{k|k}\tilde{x}_{k|k}^T\right\} \tag{4.1.1.14}$$

Applying the previous six definitions to (4.1.1.8) yields the solution for the a priori state error covariance for the SVSF, as follows:

$$P_{k+1|k} = AP_{k|k}A^T + Q_k \tag{4.1.1.15}$$

In this case, it is shown that the a priori state error covariance $P_{k+1|k}$ is a function of the previous a posteriori state error covariance $P_{k|k}$, the system model A, and the system noise covariance Q_k.

4.1.2 A Posteriori Covariance Calculation

The a posteriori state error covariance equation may now be obtained using (4.1.1.15). The a posteriori state error covariance matrix is defined as:

$$P_{k+1|k+1} = E\{\tilde{x}_{k+1|k+1}\tilde{x}_{k+1|k+1}^T\} \tag{4.1.2.1}$$

Where the a posteriori state error $\tilde{x}_{k+1|k+1}$ is:

$$\tilde{x}_{k+1|k+1} = x_{k+1} - \hat{x}_{k+1|k+1} \tag{4.1.2.2}$$

The state update and a priori measurement error calculations are respectively defined as follows:

$$\hat{x}_{k+1|k+1} = \hat{x}_{k+1|k} + K_{k+1}e_{z,k+1|k} \tag{4.1.9}$$

$$e_{z,k+1|k} = z_{k+1} - C\hat{x}_{k+1|k} \tag{3.3.3}$$

Substitution of (4.1.9) and (3.3.3) into (4.1.2.2) yields:

$$\tilde{x}_{k+1|k+1} = x_{k+1} - \hat{x}_{k+1|k} - K_{k+1}\left(z_{k+1} - C\hat{x}_{k+1|k}\right) \tag{4.1.2.3}$$

Recall (1.1.2), which states the following definition for the measurement calculation:

$$z_{k+1} = Cx_{k+1} + v_{k+1} \tag{1.1.2}$$

Substitution of (1.1.2) into (4.1.2.3) yields:

$$\tilde{x}_{k+1|k+1} = x_{k+1} - \hat{x}_{k+1|k} - K_{k+1}\left(Cx_{k+1} + v_{k+1} - C\hat{x}_{k+1|k}\right) \tag{4.1.2.4}$$

Equation (4.1.2.4) simplifies to the following:

$$\tilde{x}_{k+1|k+1} = \tilde{x}_{k+1|k} - K_{k+1}\left(C\tilde{x}_{k+1|k} + v_{k+1}\right) \tag{4.1.2.5}$$

Simplifying further yields the following definition for the a posteriori state error equation:

$$\tilde{x}_{k+1|k+1} = (I - K_{k+1}C)\tilde{x}_{k+1|k} - K_{k+1}v_{k+1} \tag{4.1.2.6}$$

Substitution of (4.1.2.6) into (4.1.2.1), and performing the appropriate transpose, yields an equation for the a posteriori state error covariance matrix (4.1.2.7).

$$P_{k+1|k+1} = E\{[(I - K_{k+1}C)\tilde{x}_{k+1|k} - K_{k+1}v_{k+1}][\tilde{x}_{k+1|k}^T(I - K_{k+1}C)^T - v_{k+1}^T K_{k+1}^T]\} \tag{4.1.2.7}$$

Expanding the terms above yields a much more complicated equation, as follows:

$$\begin{aligned} P_{k+1|k+1} = E\{&(I - K_{k+1}C)\tilde{x}_{k+1|k}\tilde{x}_{k+1|k}^T(I - K_{k+1}C)^T \\ &- (I - K_{k+1}C)\tilde{x}_{k+1|k}v_{k+1}^T K_{k+1}^T - K_{k+1}v_{k+1}\tilde{x}_{k+1|k}^T(I - K_{k+1}C)^T \\ &+ K_{k+1}v_{k+1}v_{k+1}^T K_{k+1}^T\} \end{aligned} \tag{4.1.2.8}$$

Recall that the measurement noise v_{k+1} is typically modeled as Gaussian noise, such that it is zero-mean with a covariance referred to as R_{k+1}. Furthermore, it is assumed that the measurement noise v_{k+1} and the state errors $\tilde{x}_{k+1|k}$ are independent of each other. Based on these assumptions, one may define the following five equations:

$$P(v_{k+1}) \sim \mathcal{N}(0, R_{k+1}) \tag{4.1.2.9}$$

$$E\{v_{k+1}\} = E\{v_{k+1}^T\} = 0 \tag{4.1.2.10}$$

$$E\{v_{k+1}v_{k+1}^T\} = R_{k+1} \tag{4.1.2.11}$$

$$E\{v_{k+1}\tilde{x}_{k+1|k}^T\} = E\{v_{k+1}\}E\{\tilde{x}_{k+1|k}^T\} = 0 \tag{4.1.2.12}$$

$$E\{\tilde{x}_{k+1|k}v_{k+1}^T\} = E\{\tilde{x}_{k+1|k}\}E\{v_{k+1}^T\} = 0 \tag{4.1.2.13}$$

Applying the above five definitions to (4.1.2.8) yields the a posteriori state error covariance matrix for the SVSF as follows:

$$P_{k+1|k+1} = (I - K_{k+1}C)P_{k+1|k}(I - K_{k+1}C)^T + K_{k+1}R_{k+1}K_{k+1}^T \tag{4.1.2.14}$$

In this case, it is shown that the a posteriori state error covariance is a function of the SVSF gain K_{k+1}, the a priori state error covariance $P_{k+1|k}$, the measurement model C, and the measurement noise covariance R_{k+1}. Equation (4.1.2.14) is actually known as the Joseph form of the covariance equation, and is valid for any gain value [30].

It may be simplified further if the optimal KF gain value is used [39]. Note that the above strategy for obtaining the state error covariance matrices is well established in literature; it is nonetheless provided here for completeness for the proposed SVSF estimation strategy [30,33].

4.1.3 Proposed Augmented SVSF Estimation Strategy for Linear Systems

This section summarizes the proposed augmented SVSF estimation strategy, which includes the state error covariance calculations for linear systems. There are two stages: prediction and update. The first step is to predict the state estimates (4.1.3.1), calculate the a priori state error covariance (4.1.3.2), and find the corresponding estimation error (4.1.3.3).

$$\hat{x}_{k+1|k} = \hat{A}\hat{x}_{k|k} + \hat{B}u_k \tag{4.1.3.1}$$

$$P_{k+1|k} = \hat{A}P_{k|k}\hat{A}^T + Q_k \tag{4.1.3.2}$$

$$e_{z,k+1|k} = z_{k+1} - C\hat{x}_{k+1|k} \tag{4.1.3.3}$$

The next step involves calculating the corresponding SVSF gain (4.1.3.4), updating the state estimate (4.1.3.5), finding the a posteriori state error covariance (4.1.3.6), and determining the a posteriori measurement error (4.1.3.7) which is to be used in the next iteration.

$$K_{k+1} = C^+ diag\left[\left(\left|e_{z,k+1|k}\right|_{Abs} + \gamma\left|e_{z,k|k}\right|_{Abs}\right) \circ sat\left(\frac{e_{z,k+1|k}}{\psi}\right)\right]\left[diag\left(e_{z,k+1|k}\right)\right]^{-1} \tag{4.1.3.4}$$

$$\hat{x}_{k+1|k+1} = \hat{x}_{k+1|k} + K_{k+1}e_{z,k+1|k} \tag{4.1.3.5}$$

$$P_{k+1|k+1} = (I - K_{k+1}C)P_{k+1|k}(I - K_{k+1}C)^T + K_{k+1}R_{k+1}K_{k+1}^T \tag{4.1.3.6}$$

$$e_{z,k+1|k+1} = z_{k+1} - C\hat{x}_{k+1|k+1} \tag{4.1.3.7}$$

It is important to remind the reader that a 'divide by zero' check should be performed on (4.1.3.4) to avoid division by zero. The proposed SVSF estimation strategy for linear systems may be summarized by (4.1.3.1) through (4.1.3.7). In its current form, it is interesting to point out that the calculation of $P_{k+1|k+1}$ has no effect on the SVSF gain K_{k+1}. However, the SVSF gain does affect the final value of $P_{k+1|k+1}$.

As will be shown later in Chapter 5, the covariance $P_{k+1|k+1}$ may be used to obtain a time-varying smoothing boundary layer ψ_{k+1} that is less conservative and improves the SVSF estimation accuracy by determining a gain K_{k+1} that is closer to its optimal value.

4.2 Nonlinear Systems

In reality, all systems are in fact nonlinear. This section helps to provide a strategy for determining the state error covariance function for the SVSF for nonlinear systems and measurement functions defined respectively as (1.1.5) and (1.1.6). However, it is important to note that throughout this thesis, it is assumed that the measurement matrix is linear, such that the only function requiring linearization would be the system.

$$x_{k+1} = f(x_k, u_k) + w_k \tag{1.1.5}$$

$$z_{k+1} = h(x_{k+1}) + v_{k+1} \tag{1.1.6}$$

Where f and h represent the nonlinear system and measurement models, respectively. It is possible to use the nonlinear functions f and h to predict the state estimates $\hat{x}_{k+1|k}$ and the measurements $\hat{z}_{k+1|k}$. However, these functions may not be directly used to calculate the covariance values [39]. As described in Chapter 2, there are strategies available to extend the KF from linear to nonlinear systems. These same principles will be applied here in an effort to utilize available strategies for calculating $P_{k+1|k+1}$ for the SVSF in the presence of nonlinearities.

4.2.1 Linearization

As made popular by the extended Kalman filter (EKF), the nonlinear system and measurement equations may be linearized and then used to calculate the state error covariance [34]. The partial derivatives are used to compute linearized system and measurement matrices F and H, respectively found as follows [32]:

$$F_k = \left.\frac{\partial f}{\partial x}\right|_{\hat{x}_{k|k}, u_k} \tag{4.2.1.1}$$

$$H_{k+1} = \frac{\partial h}{\partial x}\Big|_{\hat{x}_{k+1|k}} \tag{4.2.1.2}$$

Equations (4.2.1.1) and (4.2.1.2) essentially linearize the nonlinear system or measurement functions around the current state estimate [30]. As mentioned in Chapter 2, linearization introduces uncertainties and errors into the estimation process, which may lead to an unstable estimate [33]. Furthermore, determining a Jacobian of a highly nonlinear function can sometimes be a difficult task. However, linearization proves to be an effective strategy when dealing with mildly-nonlinear functions. Furthermore, as shown by the EKF estimation method, the a priori and a posteriori state error covariance's may be calculated as follows [39]:

$$P_{k+1|k} = F_k P_{k|k} F_k^T + Q_k \tag{4.2.1.3}$$

$$P_{k+1|k+1} = (I - K_{k+1}H_{k+1})P_{k+1|k}(I - K_{k+1}H_{k+1})^T + K_{k+1}R_{k+1}K_{k+1}^T \tag{4.2.1.4}$$

The above two equations are similar to the linear case; however, the system and measurement equations have been linearized. The SVSF strategy for linearization would then be the same as that presented in Section 4.1.3, however the predicted and updated covariance is calculated using (4.2.1.3) and (4.2.1.4) respectively, and the predicted state estimate is calculated by:

$$\hat{x}_{k+1|k} = f\left(\hat{x}_{k|k}, u_k\right) \tag{4.2.1.5}$$

A summary of the SVSF with linearized nonlinear functions is available in Appendix 8.3.

4.2.2 Unscented Transformation

The unscented transform (UT) was made popular by the unscented Kalman filter (UKF), as presented in Chapter 2. The UT is a deterministic sampling technique. A finite number of weighted sample points (referred to as sigma points) are propagated through the nonlinear functions, which create an approximate solution to the mean and covariance of the desired estimate [36,71].

In this case, only the approximation of the covariance is of interest, since the SVSF will handle the state estimate (i.e., mean). The first step to calculating the covariance using the UKF strategy is to generate the desired sigma points. The n-dimensional random variable x_k with mean $\hat{x}_{k|k}$ and covariance $P_{k|k}$ may be approximated by $2n+1$ sigma points. As described in Chapter 2, the initial sigma points (corresponding sample and weight) may be calculated as follows:

$$X_{0,k|k} = \hat{x}_{k|k} \tag{4.2.2.1}$$

$$W_0 = \kappa/(n+\kappa) \tag{4.2.2.2}$$

The next n number of sigma points may be calculated as follows:

$$X_{i,k|k} = \hat{x}_{k|k} + \left(\sqrt{(n+\kappa)P_{k|k}}\right)_i \tag{4.2.2.3}$$

$$W_i = 1/[2(n+\kappa)] \tag{4.2.2.4}$$

Likewise, the remaining n number of sigma points may be found as:

$$X_{i+n,k|k} = \hat{x}_{k|k} - \left(\sqrt{(n+\kappa)P_{k|k}}\right)_i \tag{4.2.2.5}$$

$$W_{i+n} = 1/[2(n+\kappa)] \tag{4.2.2.6}$$

The parameter κ is a design value (typically a small value, significantly less than 1), the last term of (4.2.2.3) or (4.2.2.5) is the i^{th} row or column of the matrix square root of $(n+\kappa)P_{k|k}$, and W_i is the weight that is associated with the i^{th} sample point [71]. The sigma points are then propagated through the nonlinear system or process model (4.2.2.7), and are used to calculate the predicted state error covariance (4.2.2.8).

$$\hat{X}_{i,k+1|k} = f\left(X_{i,k|k}, u_k\right) \tag{4.2.2.7}$$

$$P_{k+1|k} = \sum_{i=0}^{2n} W_i\left(\hat{X}_{i,k+1|k} - \hat{x}_{k+1|k}\right)\left(\hat{X}_{i,k+1|k} - \hat{x}_{k+1|k}\right)^T \tag{4.2.2.8}$$

Note that the state estimate $\hat{x}_{k+1|k}$ is obtained from the SVSF strategy, as opposed to a summation of the weighted sigma points $\hat{X}_{i,k+1|k}$ (i.e., the UKF method).

Since the SVSF state update equation does not change (4.1.3.5), and it is assumed that the measurement matrix is linear or can be linearized as per the earlier section, the updated state error covariance matrix may then be calculated as follows:

$$P_{k+1|k+1} = (I - K_{k+1}H_{k+1})P_{k+1|k}(I - K_{k+1}H_{k+1})^T + K_{k+1}R_{k+1}K_{k+1}^T \tag{4.2.2.9}$$

By the nature of its derivation, the UT may appear to be more computationally demanding. However, this strategy avoids the linearization process, which can cause numerical issues as previously discussed. For mildly nonlinear estimation problems, both linearization and UT may yield the same solution. However, the UT becomes more advantageous when the nonlinearities are increased. The complete SVSF strategy when utilizing the UT will be explored further in Chapter 5.

4.2.3 Cubature Rules

As described in Chapter 2, the use of cubature rules to calculate the state error covariance for the KF was first introduced by the cubature Kalman filter (CKF). The CKF uses a third-degree cubature rule to numerically compute Gaussian-weighted integrals, as opposed to the sigma point set used by the UKF [72]. The cubature rule approximates an n-dimensional Gaussian weighted integral (4.2.3.1).

$$\int_{\mathbb{R}^{n_x}} f(x)\mathcal{N}(x;\mu,\sum)dx \approx \frac{1}{2n}f(\mu + \sqrt{\sum}\xi_i) \tag{4.2.3.1}$$

The term μ refers to the mean of x, $\sum$ refers to the corresponding covariance, and ξ_i refers to the i^{th} cubature point (of $2n$ in total). Note that the square-root factor of the covariance $\sum$ must satisfy the relationship $\sum = \sqrt{\sum}\sqrt{\sum}^T$ [72].

The set of cubature points is given by [72]:

$$\xi_i = \begin{cases} \sqrt{n}e_i, & i = 1,2,\dots,n \\ -\sqrt{n}e_{i-n}, & i = n+1, n+2, \dots, 2n \end{cases} \tag{4.2.3.2}$$

Where $e_i \in \mathbb{R}^n$ denotes the i^{th} elementary column vector. According to [72], the third-degree cubature rule is exact for polynomial integrands up to the third degree or for any odd-degree polynomial. Therefore, it allows a more accurate approximation of the state error covariance matrix when compared with the linearization or UT strategies. For more details on how the cubature points are derived, refer to Chapter 2 or [72]. The initial set of cubature points X are calculated based on the previous a posteriori state estimate $\hat{x}_{k|k}$, the previous a posteriori state covariance $P_{k|k}$, and the cubature-point set ξ_i [72]. Once calculated (4.2.3.3), these cubature points are propagated through the nonlinear system or process model (4.2.3.4).

$$X_{i,k|k} = \sqrt{P_{k|k}}\xi_i + \hat{x}_{k|k} \qquad i = 1,2,\dots,2n \tag{4.2.3.3}$$

$$X^*_{i,k+1|k} = f(X_{i,k|k}, u_k) \qquad i = 1,2,\dots,2n \tag{4.2.3.4}$$

As per the previous section, the predicted estimate is found using the SVSF method $\hat{x}_{k+1|k}$. This value is then used in conjunction with (4.2.3.4) and the system noise covariance matrix Q_k to find the predicted state error covariance matrix (4.2.3.5) [72].

$$P_{k+1|k} = \frac{1}{2n}\sum_{i=1}^{2n} X^*_{i,k+1|k} X^{*T}_{i,k+1|k} - \hat{x}_{k+1|k}\hat{x}^T_{k+1|k} + Q_{k+1} \tag{4.2.3.5}$$

Since the SVSF state update equation does not change (4.1.3.5), and it is assumed that the measurement matrix is linear or can be linearized as per the earlier section, the updated state error covariance matrix may then be calculated as follows:

$$P_{k+1|k+1} = (I - K_{k+1}H_{k+1})P_{k+1|k}(I - K_{k+1}H_{k+1})^T + K_{k+1}R_{k+1}K^T_{k+1} \tag{4.2.3.6}$$

Similar to the linear system case, the aforementioned processes for determining the state error covariance with nonlinear systems do not affect the calculated SVSF gain. However, it is important to reiterate that the SVSF estimation methods presented later in Chapters 5 and 6 would not be possible without the development of a state error covariance function.

4.3 Computer Experiments

The following two sections look at the implementation of the aforementioned strategies on a linear and nonlinear system. The purpose of these computer experiments is to study and compare the state error covariance values calculated by the KF methods and the SVSF.

4.3.1 Linear System

In this section, consider an example found in [39], which deals with a linear, underdamped, second-order system. Consider the following second-order continuous-time dynamic equation with a constant driving term of 12 [39]:

$$\ddot{x}_1(t) + 2\zeta\omega\dot{x}_1(t) + \omega^2 x_1(t) = 12 + w(t) \tag{4.3.1.1}$$

Above, x_1 refers to the displacement, ζ refers to the damping ratio, ω represents the natural frequency of the system, and w refers to system noise. Converting (4.3.1.1) to a discrete-time state space system yields, where $T = 0.001\ sec$ is the sample time:

$$\begin{bmatrix} x_1 \\ x_2 \end{bmatrix}_{k+1} = \begin{bmatrix} 1 & T \\ -\omega^2 T & (1 - 2\zeta\omega T) \end{bmatrix} \begin{bmatrix} x_1 \\ x_2 \end{bmatrix}_k + \begin{bmatrix} 0 \\ 12 \end{bmatrix} T + \begin{bmatrix} 0 \\ T \end{bmatrix} w_k \tag{4.3.1.2}$$

Where x_2 refers to the velocity of the system. In this case, assume a full measurement matrix such that the following is the corresponding measurement equation:

$$z_{k+1} = \begin{bmatrix} 1 & 0 \\ 0 & 1 \end{bmatrix} x_{k+1} + v_{k+1} \tag{4.3.1.3}$$

Where v_k refers to measurement noise. Furthermore, assume the following definitions for the damping ratio and natural frequency, respectively:

$$\zeta = 0.2 \tag{4.3.1.4}$$

$$\omega = 5\ rad/s \tag{4.3.1.5}$$

Also, consider the following covariance definitions used to generate the system and measurement noise, respectively:

$$Q = \begin{bmatrix} 1 \times 10^{-6} & 2 \times 10^{-6} \\ 2 \times 10^{-6} & 5 \times 10^{-3} \end{bmatrix} \tag{4.3.1.6}$$

$$R = \begin{bmatrix} 0.01 & 0 \\ 0 & 0.01 \end{bmatrix} \tag{4.3.1.7}$$

The initial state estimates and corresponding error covariance were defined as follows:

$$\hat{x}_{0|0} = [0 \quad 0]^T \tag{4.3.1.8}$$

$$P_{0|0} = \begin{bmatrix} 2 & 0 \\ 0 & 2 \end{bmatrix} \tag{4.3.1.9}$$

For this scenario, the SVSF 'memory' or convergence rate and smoothing boundary layers were defined as follows:

$$\gamma = 0.1 \tag{4.3.1.10}$$

$$\psi = [0.01 \quad 0.001]^T \tag{4.3.1.11}$$

The following figure shows the true position state, with the corresponding KF and SVSF estimates. Note that the estimates are nearly identical, and as such, appear to be overlapping. The second figure shows the position estimation error over time. The KF provides an optimal result (in terms of estimation error) for linear systems; as such, it was expected to outperform the SVSF. A methodology for improving the estimation accuracy of the SVSF is introduced later in Chapter 5.

The following table summarizes the root mean square error (RMSE) for both estimation strategies (for the linear systems example).

Table 4.3.1. RMSE Results for the Linear Systems Example

Filter	Position (m)	Velocity (m/s)
KF	1.07×10^{-5}	7.28×10^{-5}
SVSF	1.11×10^{-5}	9.19×10^{-5}

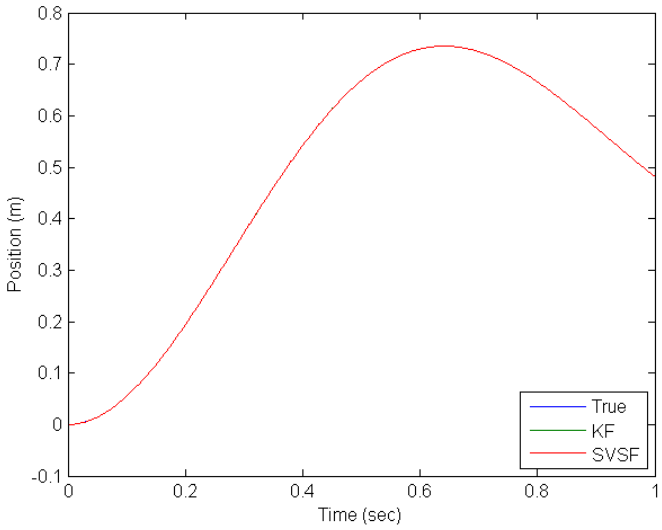

Figure 4.3.1. True and Estimated Position for the Linear System Example

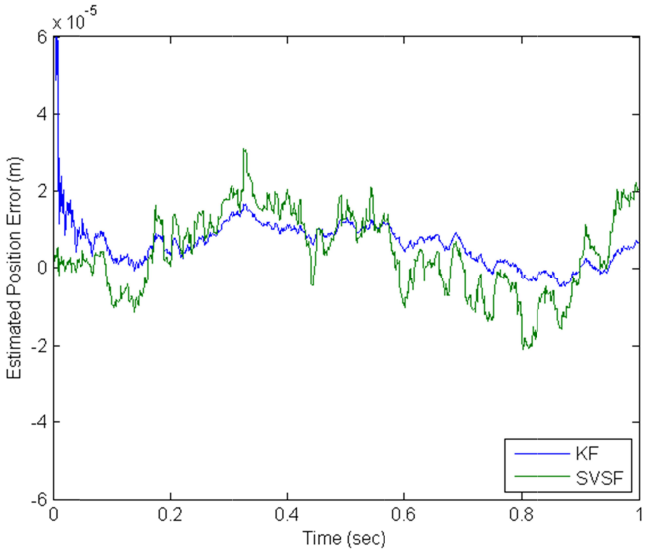

Figure 4.3.2. Estimated Position Error for the Linear System Example

Since this chapter presented a covariance derivation for the SVSF, it is therefore important to look at these results. The following two figures show the position and velocity state error covariance values, respectively. Note that the KF covariance value for the first state converges extremely fast (within two samples), and reaches an area close to its steady-state value within only 25 samples. However, the corresponding SVSF covariance value required a considerable amount of time to converge (roughly 400 samples).

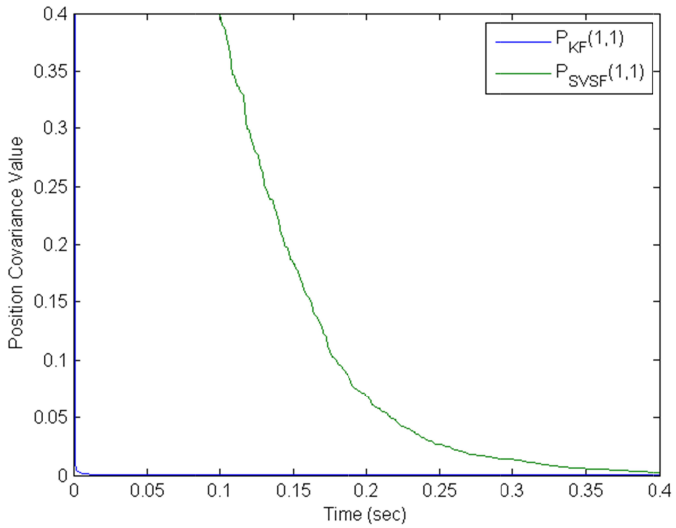

Figure 4.3.3. Position State Error Covariance Value for the Linear System Example

The following figure provides a good visualization for the velocity covariance values. Notice how the SVSF value does not converge to within a region of the KF steady-state value. This gives an indication that the SVSF velocity estimate is not optimal, as further demonstrated by the results of Table 4.3.1. However, an interesting result occurs when the SVSF smoothing boundary layer (SBL) width is changed.

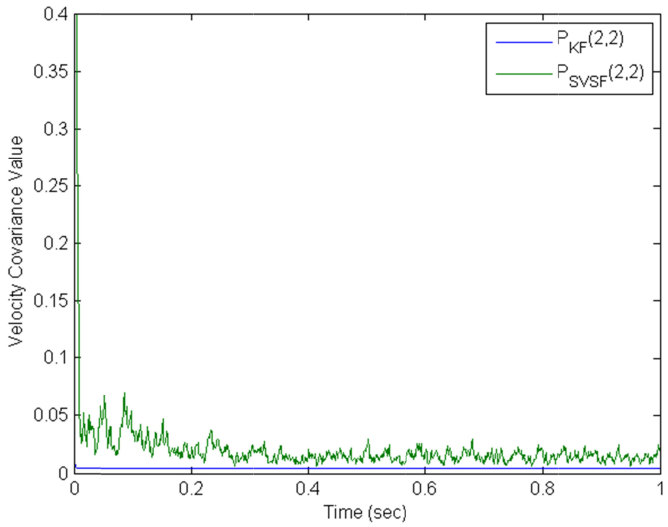

Figure 4.3.4. Velocity State Error Covariance Value for the Linear System Example

Consider the following figure which shows the position state error covariance value for the SVSF when a variety of different SBLs are used. A general trend is found, such that as the SBL value is decreased for the position state estimate**,** the position state error covariance value converges faster and approaches the optimal value (i.e., the KF). Essentially, as the SBL becomes very small, the SVSF simply provides the measured value as the estimate. This may be further explained by the second figure that follows. Figure 4.3.6 shows a closer comparison of the KF and SVSF position covariance values with a very small smoothing boundary layer. The SVSF covariance value converges quickly but becomes saturated at 0.01, which is in fact the corresponding measurement covariance value R_{11}. This may be further explained by the following sets of equations (after the figures).

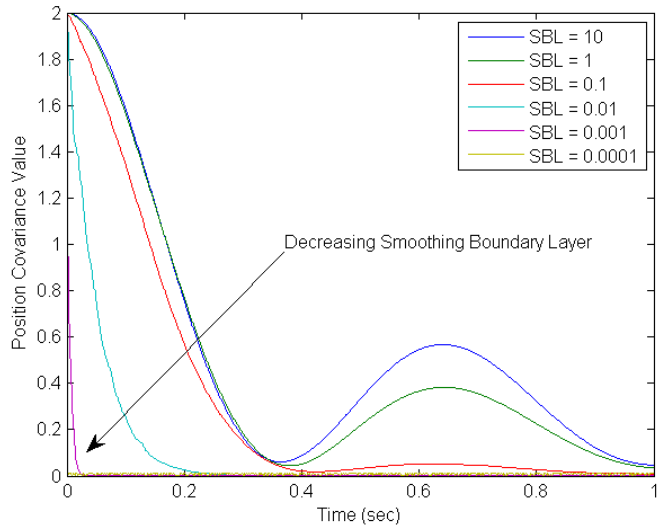

Figure 4.3.5. Relationship of the Covariance and the Smoothing Boundary Layer

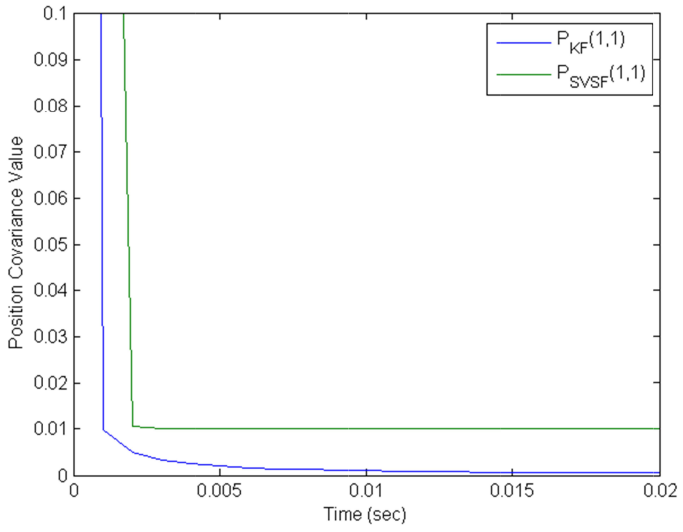

Figure 4.3.6. Covariance Comparison with a Very Small Smoothing Boundary Layer

Consider the following SVSF gain equation:

$$K_{k+1} = C^{+} diag\left[\left(\left|e_{z,k+1|k}\right|_{Abs} + \gamma\left|e_{z,k|k}\right|_{Abs}\right) \circ sat\left(\frac{e_{z,k+1|k}}{\psi}\right)\right]\left[diag\left(e_{z,k+1|k}\right)\right]^{-1} \tag{4.3.1.12}$$

If the corresponding smoothing boundary layer ψ is very small relative to the a priori measurement error $e_{z,k+1|k}$, then $e_{z,k+1|k}/\psi$ will be saturated. Based on the fact that $\gamma = 0.1$ and provided that the a posteriori measurement error $e_{z,k|k}$ is also small, then the resulting SVSF gain will be approximately an identity matrix (however, not exactly!). If the measurement matrix is full and is identity, the first term in the a posteriori state error covariance matrix (4.1.3.6) becomes negligible, such that:

$$(I - K_{k+1}C)P_{k+1|k}(I - K_{k+1}C)^{T} \to 0 \tag{4.3.1.13}$$

This results in the following equation for the updated covariance matrix, based on the fact that the SVSF gain approaches an identity matrix:

$$P_{k+1|k+1} = R_{k+1} \tag{4.3.1.14}$$

Therefore, if the smoothing boundary layer is set too small, the resulting estimate will directly yield the available measurement. This is shown by the state error covariance matrix, which yields the measurement matrix. The purpose of the linear example was to demonstrate that the SVSF covariance derivation yields meaningful and correct results.

4.3.2 Nonlinear System

For completeness, consider a nonlinear system example. One of the most well studied aerospace applications involves ballistic objects on re-entry [31]. In this section, a ballistic target re-entering the atmosphere is considered, as described in [31]. The following figure shows the setup for ballistic target tracking.

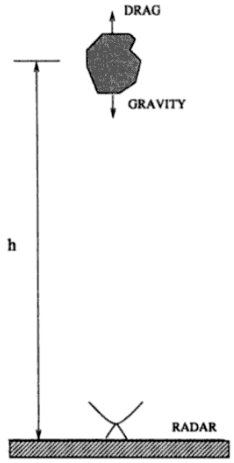

Figure 4.3.7. Ballistic Target Tracking Scenario [31]

Assuming that drag D and gravity g are the only forces acting on the object, the following differential equations govern its motion [31,126]:

$$\dot{h} = v \tag{4.3.2.1}$$

$$\dot{v} = -\frac{\rho(h) g v^2}{2\beta} + g \tag{4.3.2.2}$$

$$\dot{\beta} = 0 \tag{4.3.2.3}$$

The state vector is defined as $x = [h \quad v \quad \beta]^T$, which refers to the target altitude, velocity, and ballistic coefficient, respectively. The air density ρ is modeled as follows:

$$\rho = \gamma e^{-\eta h} \tag{4.3.2.4}$$

Where $\gamma = 1.754$ and $\eta = 1.49 \times 10^{-4}$. The discrete-time state equation is defined as follows [31]:

$$x_{k+1} = F x_k - G[D(x_k) - g] + w_k \tag{4.3.2.5}$$

With matrices F and G defined by:

$$F = \begin{bmatrix} 1 & -T & 0 \\ 0 & 1 & 0 \\ 0 & 0 & 1 \end{bmatrix} \tag{4.3.2.6}$$

$$G = [0 \quad T \quad 0]^T \tag{4.3.2.7}$$

Furthermore, the function for drag $D(x_k)$ (the only nonlinear term) is defined by:

$$D(x_k) = \frac{g\rho(x_{1,k})x_{2,k}^2}{2x_{3,k}} \tag{4.3.2.8}$$

Note that for the EKF approach, the system matrix requires linearization as follows:

$$F_k = \frac{\partial f}{\partial x}\Big|_{\hat{x}_{k|k},u_k} = \begin{bmatrix} 1 & -T & 0 \\ 0 & 1 - \frac{Tg\gamma x_{2,k}}{x_{3,k}e^{\eta x_{1,k}}} & \frac{Tg\gamma x_{2,k}^2}{2x_{3,k}^2 e^{\eta x_{1,k}}} \\ 0 & 0 & 1 \end{bmatrix} \tag{4.3.2.9}$$

As in [31], the system noise w_k is assumed to be zero-mean Gaussian with a covariance matrix Q defined by:

$$Q \approx \begin{bmatrix} q_1\frac{T^3}{3} & q_1\frac{T^2}{2} & 0 \\ q_1\frac{T^2}{2} & q_1 T & 0 \\ 0 & 0 & q_2 T \end{bmatrix} \tag{4.3.2.10}$$

Note that the parameters q_1 and q_2 respectively control the amount of system noise in the target dynamics and the ballistic coefficient [31]. As shown in Figure 4.3.7, a radar is positioned on the ground below the target. The measurement equation in this scenario is defined by:

$$z_k = Hx_k + v_k \tag{4.3.2.11}$$

Where, for simplicity, it is assumed that all three states are measured (i.e., $H = I$).

In this tracking scenario, the initial states are defined as follows: $x_{1,0} = 61{,}000\,m$, $x_{2,0} = 3{,}048\,m/s$, and $x_{3,0} = 19{,}161\,kg/ms^2$. The initial state error covariance matrix was defined by: $P_{0|0} = 10Q$. Other notable parameters were defined as: $q_1 = 10^4$, $q_2 = 10$, $g = 9.81\,m/s^2$, $T = 0.1\,sec$, and $R = diag([10^4 \quad 5\times10^2 \quad 10^4])$.

Furthermore, note that the SVSF 'memory' or convergence rate was set to $\gamma = 0.1$, and the constant smoothing boundary layer widths were defined as $\psi = [1{,}000 \quad 250 \quad 5{,}000]^T$. Also, note that the UKF design parameter was set to $\kappa = 0.001$. For nonlinear systems, as presented earlier, the SVSF may utilize the a priori covariance calculation of the EKF, UKF, or CKF. It is proposed that the a posteriori covariance is calculated as per the EKF strategy for simplicity, and based on the assumption that the measurements are linear (or, at the very least, may be linearized). For this computer experiment, the a priori covariance values were calculated using the EKF, UKF, and CKF strategies. The SVSF gain was then applied, and the covariance was updated as per (4.2.1.4). The following three figures show the covariance values for each state, based on each covariance calculation strategy (P_1 refers to EKF, P_2 refers to UKF, and P_3 refers to CKF).

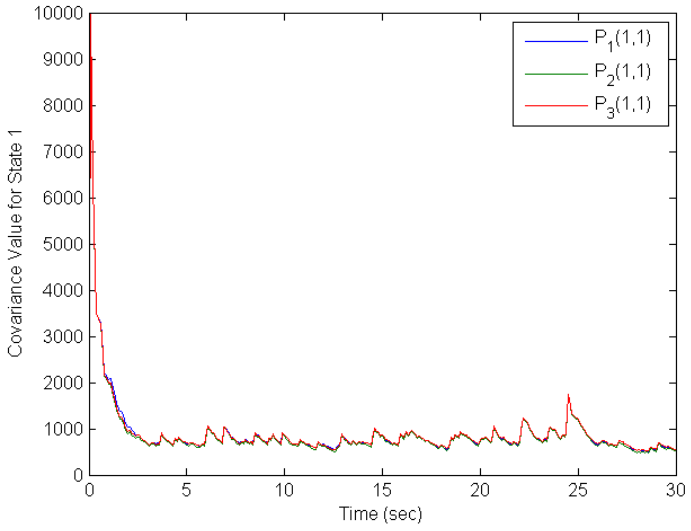

Figure 4.3.8. State 1 Error Covariance Value for the Nonlinear System Example

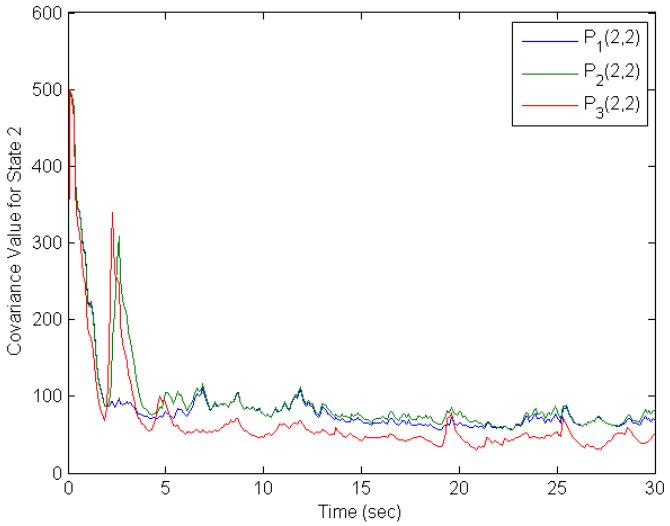

Figure 4.3.9. State 2 Error Covariance Value for the Nonlinear System Example

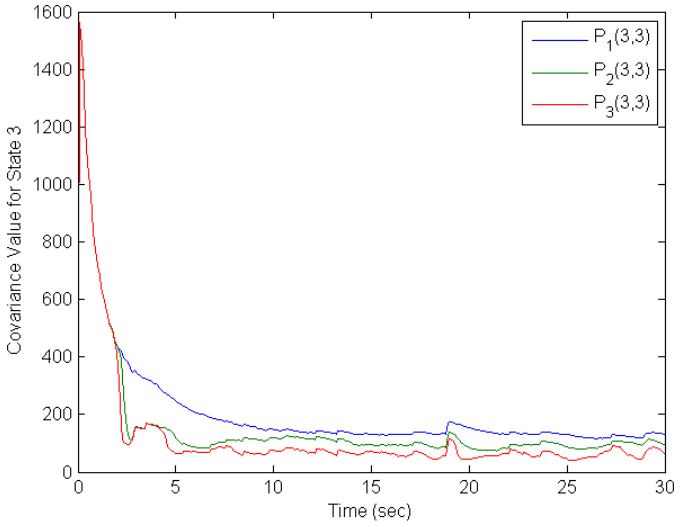

Figure 4.3.10. State 3 Error Covariance Value for the Nonlinear System Example

In general, the covariance values calculated by the CKF strategy were smaller, which was to be expected given that the cubature rule strategy is more accurate than the unscented transform and linearization methods [72]. The covariance values had some 'spikes' or small chattering present, which was due to the nature of the SVSF gain (i.e., switching effect). Furthermore, note that the differences in the above figures were only due to the a priori covariance calculations, since the same gains and update equations were used.

4.4 Summary

In its original form presented in [37], the SVSF is not a classical filter in the sense that it does not make use of a state error covariance matrix. This chapter described the development of a covariance derivation for the SVSF, for both linear and nonlinear systems. A method that makes use of fourth-order moments is provided in Appendix 8.2. However, this method is too cumbersome and tedious to implement effectively. The SVSF update equation is modified in order to provide a simpler covariance derivation. The covariance developed for the SVSF, for both linear and nonlinear systems, are similar to other popular Kalman filtering strategies (KF, EKF, UKF, and CKF). However, it is important to note that the gain used to calculate the SVSF covariance remains different. Two computer experiments have been studied in order to compare the results of the covariance values. It has also been shown that the values for the SVSF smoothing boundary layer play an important role in the estimation process. Note that at this point, determination of the state error covariance matrix does not affect the SVSF estimation process. However, the SVSF estimation methods presented later in Chapters 5 and 6 would not be possible without the development of a state error covariance function.

Chapter 5

A Time-Varying Smoothing Boundary Layer

This chapter presents a novel form of the SVSF which implements a time-varying smoothing boundary layer for increased estimation accuracy (SVSF-VBL). A secondary benefit of this derivation is that it provides the ability to detect changes in the system. The results of the derivation are tested on a computer experiment, and are compared with the popular KF. The latter-half of this chapter utilizes the derivation to combine the SVSF with other popular nonlinear estimation strategies, and compares the results on another computer experiment.

5.1 Derivation of the VBL

The partial derivative of the a posteriori covariance (trace) with respect to the smoothing boundary layer term ψ is the basis for obtaining a strategy for the specification of ψ. The approach taken is similar to determining an optimal gain for the KF. The following derivation is applicable to any measurement case provided that the measurement matrix is completely observable (as defined in Appendix 8.4). For the case when there are fewer measurements than states, one needs to implement a reduced order form of the SVSF as shown in [37], or an alternative method described later in this chapter. This allows the creation of a full measurement matrix, typically in the form of an identity. For the case when there are more measurements than states, the system output can be multiplied by the inverse of the measurement matrix, thus mapping the measurements to the states. One could then use a full measurement matrix (i.e., identity) in the estimation process.

As demonstrated in Chapter 3, previous forms of the SVSF included a vector form of ψ, which had a single smoothing boundary layer term for each corresponding measurement error. Essentially, the boundary layer terms were independent of each other such that the measurement errors would only directly be used for calculating its corresponding gain. The coupling effects are not explicitly considered thus preventing an optimal derivation. A 'near-optimal' formulation of the SVSF could be created using a vector form of ψ, however this would lead to a minimization of only the diagonal elements of the state error covariance matrix [11]. In this chapter, in an effort to obtain a smoothing boundary layer equation that yields optimal state estimates for linear systems (like the KF), a full smoothing boundary layer matrix is proposed. Hence, consider the full matrix form of the smoothing boundary layer:

$$\psi = \begin{bmatrix} \psi_{11} & \psi_{12} & \cdots & \psi_{1m} \\ \psi_{12} & \psi_{22} & \cdots & \psi_{2m} \\ \vdots & \vdots & \ddots & \vdots \\ \psi_{m1} & \psi_{m2} & \cdots & \psi_{mm} \end{bmatrix} \tag{5.1.1}$$

Note that the off-diagonal terms of (5.1.1) are zero for the standard SVSF (presented in Chapter 3), whereas this is not the case for the algorithm presented in this chapter. This definition includes terms that relate one smoothing boundary layer to another (i.e., off-diagonal terms). To solve for a time-varying smoothing boundary layer (VBL) based on (5.1.1), consider:

$$\frac{\partial\big(trace[P_{k+1|k+1}]\big)}{\partial\psi} = 0 \tag{5.1.2}$$

To solve (5.1.2), first consider the following modification of the SVSF gain defined by (4.1.10). Note that the gain structure remains the same.

$$K_{k+1} = C^{-1}\big\{diag(A)\cdot sat\big(\psi^{-1}diag\big[e_{z,k+1|k}\big]\big)\big\}\big[diag\big(e_{z,k+1|k}\big)\big]^{-1} \tag{5.1.3}$$

Where A is a 'vector of errors', defined as follows:

$$A = \Big(\big|e_{z,k+1|k}\big|_{Abs} + \gamma\big|e_{z,k|k}\big|_{Abs}\Big) \tag{5.1.4}$$

In an effort to avoid significant chattering or switching, consider the region only inside the saturation term of the SVSF gain (5.1.5). Furthermore, as will be demonstrated later, this will improve the overall SVSF estimation accuracy. Also, consider the bar notation $\bar{a}$ to signify a diagonal matrix formed of the vector a, such that $\bar{a} = diag(a)$.

$$sat\left(\psi^{-1}\overline{e_{z_{k+1|k}}}\right) = \psi^{-1}\overline{e_{z_{k+1|k}}} \tag{5.1.5}$$

Applying (5.1.5) to (5.1.3) yields:

$$K_{k+1} = C^{-1}\bar{A}\psi^{-1}\overline{e_{z_{k+1|k}}}\left(\overline{e_{z_{k+1|k}}}\right)^{-1} \tag{5.1.6}$$

In an effort to help visualize (5.1.6), consider a system with two states and measurements (where $C = I$), such that (5.1.6) becomes:

$$K_{k+1} = \begin{bmatrix} a_1 & 0 \\ 0 & a_2 \end{bmatrix}\begin{bmatrix} \psi_{11} & \psi_{12} \\ \psi_{21} & \psi_{22} \end{bmatrix}^{-1}\begin{bmatrix} e_{z_1} & 0 \\ 0 & e_{z_2} \end{bmatrix}\begin{bmatrix} \dfrac{1}{e_{z_1}} & 0 \\ 0 & \dfrac{1}{e_{z_2}} \end{bmatrix} = \begin{bmatrix} a_1 & 0 \\ 0 & a_2 \end{bmatrix}\begin{bmatrix} \psi_{11} & \psi_{12} \\ \psi_{21} & \psi_{22} \end{bmatrix}^{-1} \tag{5.1.7}$$

Note that the notation of (5.1.3) does not impact the gain formulations or the state update equation, since the error terms $e_{z,k+1|k}$ eventually cancel out. Simplifying (5.1.6), using (5.1.7) to visualize, yields the following definition for the SVSF gain:

$$K_{k+1} = C^{-1}\bar{A}\psi^{-1} \tag{5.1.8}$$

In evaluating (5.1.2) consider an expansion of the a posteriori covariance equation (4.1.3.6) as follows:

$$\begin{aligned} P_{k+1|k+1} = P_{k+1|k} - K_{k+1}CP_{k+1|k} - P_{k+1|k}C^TK_{k+1}^T + K_{k+1}CP_{k+1|k}C^TK_{k+1}^T \\ + K_{k+1}R_{k+1}K_{k+1}^T \end{aligned} \tag{5.1.9}$$

Note that the measurement covariance R_{k+1} and the state error covariance $P_{k+1|k}$ are symmetric. Furthermore, recall the definition for the innovation (or measurement error) covariance matrix as follows:

$$S_{k+1} = CP_{k+1|k}C^T + R_{k+1} \tag{5.1.10}$$

Equation (5.1.10) can be used to simplify (5.1.9) as follows:

$$P_{k+1|k+1} = P_{k+1|k} - K_{k+1}CP_{k+1|k} - P_{k+1|k}C^T K_{k+1}^T + K_{k+1}S_{k+1}K_{k+1}^T \tag{5.1.11}$$

Substitution of (5.1.8) into (5.1.11) yields:

$$\begin{aligned} P_{k+1|k+1} = P_{k+1|k} - C^{-1}\bar{A}\psi^{-1}CP_{k+1|k} - P_{k+1|k}C^T(C^{-1}\bar{A}\psi^{-1})^T \\ + C^{-1}\bar{A}\psi^{-1}S_{k+1}(C^{-1}\bar{A}\psi^{-1})^T \end{aligned} \tag{5.1.12}$$

Next, to solve for (5.1.2) or $\partial\big(trace\big[P_{k+1|k+1}\big]\big)/\partial\psi$, the individual terms of (5.1.12) will be considered respectively as follows [127]:

$$\frac{\partial\big(trace\big[P_{k+1|k}\big]\big)}{\partial\psi} = 0 \tag{5.1.13}$$

$$\frac{\partial\big(trace\big[-C^{-1}\bar{A}\psi^{-1}CP_{k+1|k}\big]\big)}{\partial\psi} = \psi^{-T}\bar{A}C^{-T}P_{k+1|k}C^T\psi^{-T} \tag{5.1.14}$$

$$\frac{\partial\big(trace\big[-P_{k+1|k}C^T(C^{-1}\bar{A}\psi^{-1})^T\big]\big)}{\partial\psi} = \psi^{-T}\bar{A}C^{-T}P_{k+1|k}C^T\psi^{-T} \tag{5.1.15}$$

$$\frac{\partial(trace[C^{-1}\bar{A}\psi^{-1}S_{k+1}(C^{-1}\bar{A}\psi^{-1})^T])}{\partial\psi} = -2\psi^{-T}\bar{A}C^{-T}C^{-1}\bar{A}\psi^{-1}S_{k+1}\psi^{-T} \tag{5.1.16}$$

Combining (5.1.13) through (5.1.16) into (5.1.2) and (5.1.12) yields:

$$\begin{aligned} \frac{\partial\big(trace[P_{k+1|k+1}]\big)}{\partial\psi} &= 2\psi^{-T}\bar{A}C^{-T}P_{k+1|k}C^T\psi^{-T} - 2\psi^{-T}\bar{A}C^{-T}C^{-1}\bar{A}\psi^{-1}S_{k+1}\psi^{-T} \\ &= 0 \end{aligned} \tag{5.1.17}$$

Now, what remains, is to simplify (5.1.17) and solve for the smoothing boundary layer ψ. First, multiply from the left by $\frac{1}{2}(\psi^{-T})^{-1}$, and then from the right by $(\psi^{-T})^{-1}$:

$$\bar{A}C^{-T}P_{k+1|k}C^T - \bar{A}C^{-T}C^{-1}\bar{A}\psi^{-1}S_{k+1} = 0 \tag{5.1.18}$$

Next, multiply (5.1.18) from the left by $\bar{A}^{-1}$:

$$C^{-T}P_{k+1|k}C^{T} - C^{-T}C^{-1}\bar{A}\psi^{-1}S_{k+1} = 0 \tag{5.1.19}$$

Simplify (5.1.19) further by multiplying from the left by $\bar{A}^{-1}C(C^{-T})^{-1}$, which yields:

$$\bar{A}^{-1}CP_{k+1|k}C^{T} + \psi^{-1}S_{k+1} = 0 \tag{5.1.20}$$

Rearranging (5.1.20) yields a solution for the inverse of the smoothing boundary layer:

$$\psi^{-1} = \bar{A}^{-1}CP_{k+1|k}C^{T}S_{k+1}^{-1} \tag{5.1.21}$$

Finally, a solution for the full smoothing boundary layer matrix may be found as follows:

$$\psi_{k+1} = \left(\bar{A}^{-1}CP_{k+1|k}C^{T}S_{k+1}^{-1}\right)^{-1} \tag{5.1.22}$$

Note that the square matrix (5.1.22) is invertible if $\bar{A}^{-1}CP_{k+1|k}C^{T}S_{k+1}^{-1}$ is non-singular, or if the determinate of the matrix $\bar{A}^{-1}CP_{k+1|k}C^{T}S_{k+1}^{-1}$ is nonzero. Performing a dimensionality check verifies the correct dimension:

$$\psi_{k+1} = \left(\overline{(m \times 1)}^{-1}(m \times n)(n \times n)(n \times m)(m \times m)^{-1}\right)^{-1} = (m \times m) \tag{5.1.23}$$

The proposed smoothing boundary layer equation (5.1.22) is found to be a function of the a priori state error covariance $P_{k+1|k}$, measurement covariance S_{k+1}, measurement matrix C, a priori and previous a posteriori measurement error vectors ($e_{z,k+1|k}$ and $e_{z,k|k}$), and the convergence rate or SVSF 'memory' γ. It appears that the width of the boundary layer is therefore directly related to the level of modeling uncertainties (by virtue of the errors), as well as the estimated system and measurement noise (captured by $P_{k+1|k}$ and S_{k+1}).

The boundary layer widths can now be obtained according to (5.1.22) at each time step, as opposed to the constant (conservative) width presented in Chapter 3. As shown in Appendix 8.5, the units and values of the smoothing boundary layer matrix have been studied. The following subsections look at the saturation term and the revised SVSF gain, introduces a robust filtering strategy, and finally summarizes the proposed SVSF equations with a time varying boundary layer (VBL).

5.1.1 A Closer Look at the Saturation Term

A closer examination of the SVSF gain K_{k+1} defined by (5.1.3) reveals that the derivation of ψ removes the need for the saturation term in the gain, as follows. Consider the saturation term of (5.1.3) with (5.1.21) as follows:

$$sat\left(\psi^{-1}diag\left[e_{z,k+1|k}\right]\right) = sat\left(\bar{A}^{-1}CP_{k+1|k}C^{T}S_{k+1}^{-1}diag\left[e_{z,k+1|k}\right]\right) \tag{5.1.1.1}$$

From (5.1.1.1), consider the following two terms:

$$term_1 = CP_{k+1|k}C^{T}S_{k+1}^{-1} \tag{5.1.1.2}$$

$$term_2 = \bar{A}^{-1}diag\left[e_{z,k+1|k}\right] \tag{5.1.1.3}$$

Analyzing the first term (5.1.1.2) and recalling $S_{k+1} = CP_{k+1|k}C^{T} + R_{k+1}$, consider the following:

$$CP_{k+1|k}C^{T}S_{k+1}^{-1} = (S_{k+1} - R_{k+1})S_{k+1}^{-1} \tag{5.1.1.4}$$

From (5.1.10), it is known that $S_{k+1} \geq R_{k+1}$. Hence, (5.1.1.2) is bounded between 0 and 1 as per (5.1.1.4). Next, the second term defined by (5.1.1.3) will be studied. Note the following definition:

$$\left|e_{z,k+1|k}\right|_{Abs} + \gamma\left|e_{z,k|k}\right|_{Abs} \geq e_{z,k+1|k} \tag{5.1.1.5}$$

Due to the definition of (5.1.1.5), the second term (5.1.1.3) may only yield values equal to or between -1 and 1, depending on the value of the convergence rate γ. This can be confirmed by looking at the diagonal elements i of (5.1.1.3) given any system:

$$\left[\bar{A}^{-1}\overline{e_{z,k+1|k}}\right]_i = \frac{e_{\mathrm{z,k+1|k}_i}}{\left|e_{z,k+1|k}\right|_i + \gamma_i\left|e_{z,k|k}\right|_i} \tag{5.1.1.6}$$

If the convergence rate γ is set to zero, (5.1.1.6) simply yields the sign function of the measurement error (and the answer is -1, 0, or 1). If the convergence rate γ is nonzero (however, bounded between 0_+ and 1), (5.1.1.6) yields a value between -1 and 1.

The argument holds for (5.1.1.3). Given the above discussion, when calculating a time-varying smoothing boundary layer using (5.1.22), the argument inside the saturation term will always be between -1 and 1. Hence, the saturating function used in (5.1.3) is redundant given the definition of ψ as provided in (5.1.22). Note that this also works with the earlier assumption (5.1.5) that the region of interest for the value of the smoothing boundary layer width is inside the saturation term (i.e., between -1 and 1).

5.1.2 Studying the Proposed SVSF Gain

In an effort to study the effects of the time-varying smoothing boundary layer term on the SVSF gain, consider the following. Substituting (5.1.22) into (5.1.8) yields the revised gain, based on the above derivation:

$$K_{k+1} = C^{-1}\bar{A}\left[\bar{A}^{-1}CP_{k+1|k}C^{T}S_{k+1}^{-1}\right] \tag{5.1.2.1}$$

Note that (5.1.2.1) easily simplifies to the following:

$$K_{k+1} = P_{k+1|k}C^{T}S_{k+1}^{-1} \tag{5.1.2.2}$$

Therefore, based on a full smoothing boundary layer matrix defined by (5.1.22), the gain (5.1.8) becomes the KF gain (5.1.2.2), which yields the optimal solution for well-defined linear systems. This is to be expected as the KF yields the best possible estimate for linear, known systems with Gaussian noise. This implies that the robustness of the SVSF is lost with the use of an optimal smoothing boundary layer that would make the saturation function redundant.

5.1.3 A Robust Filtering Strategy for Linear Systems

As per the previous results, it appears that the VBL for the SVSF yields the KF solution (gain) for linear systems. In this case, robustness to modeling uncertainties using the SVSF strategy is lost. It is hence beneficial to propose a combined strategy, referred to here as the SVSF-VBL, such that an accurate estimate is maintained (i.e., using the VBL calculation or KF gain) while ensuring the estimate remains stable (i.e., using the standard SVSF gain).

This strategy is implemented by imposing a saturation limit on the optimal smoothing boundary layer as follows. Outside the limit the robustness and stability of the SVSF is maintained, while inside the boundary layer the optimal gain is applied. Consider the following sets of figures to help describe the overall implementation of the SVSF-VBL strategy.

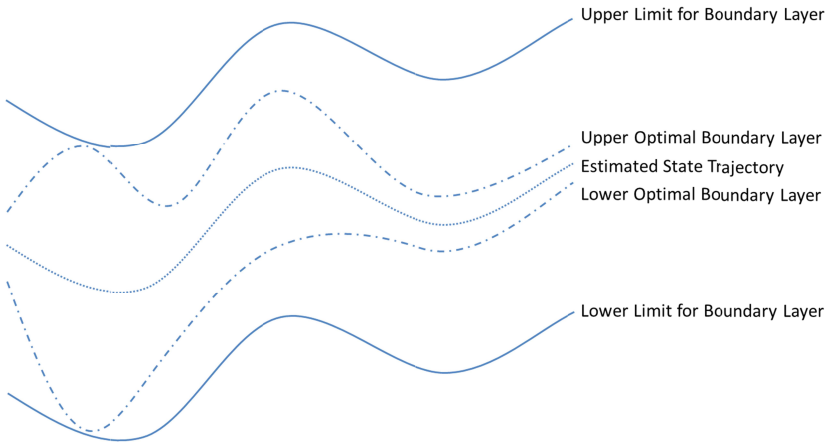

Figure 5.1.1. Well-Defined System Case (SVSF-VBL Strategy)

Figure 5.1.1 illustrates the case when a limit is imposed on the smoothing boundary layer width (a conservative value) and the time varying (optimal) smoothing boundary layer per (5.1.21) follows within this limit. In the standard SVSF, the smoothing boundary layer width is made equal to the limit; such that the difference between the limit and the optimal variable boundary layers quantifies the loss in optimality. Essentially, in this case, the SVSF-VBL (or KF) gain should be used to obtain the best result. Another way to simplify and understand this process is to consider the SVSF-VBL as using a time-varying boundary layer with saturated limits to ensure stability.

Figure 5.1.2 illustrates the case when the optimal time-varying smoothing boundary layer is larger than the limit imposed on the smoothing boundary layer. This typically occurs when there is modeling uncertainty (which leads to a loss in optimality) or when the limit on the smoothing boundary layer is underestimated. This strategy is useful for applications such as fault detection.

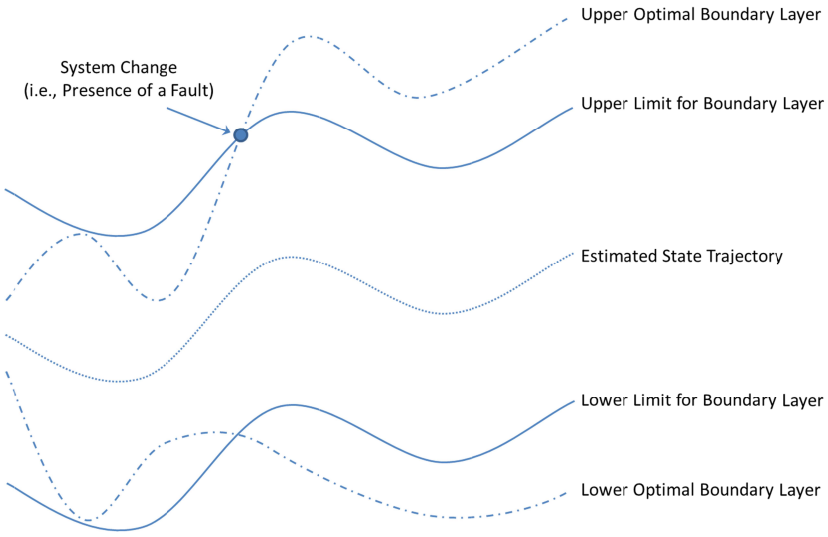

Figure 5.1.2. Presence of a Fault or Poorly-Defined System Case (SVSF-VBL Strategy)

Recall that that the width of the smoothing boundary layer (5.1.22) is directly related to the level of modeling uncertainties (by virtue of the errors), as well as the estimated system and measurement noise (captured by $P_{k+1|k}$ and S_{k+1}). Therefore, the VBL creates another indicator of performance for the SVSF: the widths may be used to determine the presence of modeling uncertainties, as well as detect any changes in the system.

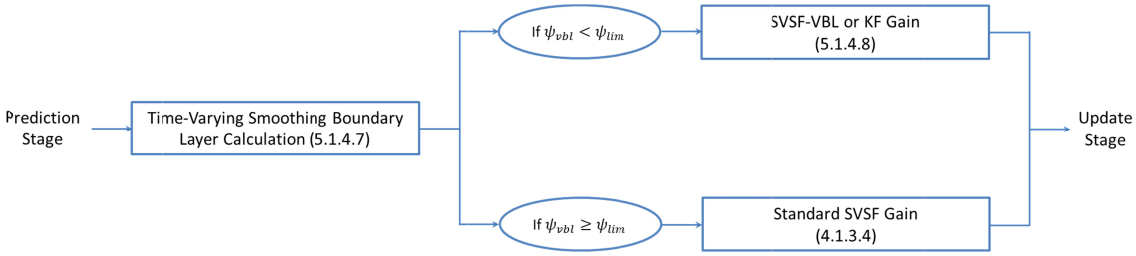

Figure 5.1.3. Summary of the SVSF-VBL Strategy

To summarize the estimation strategy (SVSF-VBL) proposed in this section, consider the above figure. Essentially, in a well-defined case, the gain used to correct the estimate is calculated by the SVSF-VBL or KF gain. When the smoothing boundary layer calculated by (5.1.22) goes beyond the limits, the smoothing boundary layer width requires saturation.

5.1.4 The Computational Process for the SVSF with the VBL

This section briefly summarizes the proposed strategy for the revised SVSF with a time-varying boundary layer (VBL). The equations are primarily the same as the standard SVSF, however with the addition of the boundary layer equation (5.1.22) and corresponding changes in the gain (5.1.8). Consider the prediction stage for a linear system as described earlier, where the state estimates and covariance are first calculated as per (5.1.4.1) and (5.1.4.2), respectively. The following 12 equations summarize the SVSF strategy with a VBL.

$$\hat{x}_{k+1|k} = \hat{A}\hat{x}_{k|k} + \hat{B}u_k \tag{5.1.4.1}$$

$$P_{k+1|k} = CP_{k|k}C^T + Q_k \tag{5.1.4.2}$$

The a priori measurement estimate (5.1.4.3) and errors (5.1.4.4) are then calculated.

$$\hat{z}_{k+1|k} = C\hat{x}_{k+1|k} \tag{5.1.4.3}$$

$$e_{z,k+1|k} = z_{k+1} - \hat{z}_{k+1|k} \tag{5.1.4.4}$$

The update stage is then defined by the following sets of equations. The innovation covariance (5.1.4.5) and combined error vector (5.1.4.6) are calculated, and then used in (5.1.4.7) to determine the smoothing boundary layer matrix. Recall that a 'divide by zero' check should be performed on (5.1.4.6) to avoid inversion of zero in (5.1.4.7). As described earlier, this can be accomplished using a simple if statement with a very small threshold (i.e., 1×10^{-12}).

$$S_{k+1} = CP_{k+1|k}C^T + R_{k+1} \tag{5.1.4.5}$$

$$A_{k+1} = \left|e_{z,k+1|k}\right|_{Abs} + \gamma\left|e_{z,k|k}\right|_{Abs} \tag{5.1.4.6}$$

$$\psi_{k+1} = \left(\bar{A}_{k+1}^{-1}CP_{k+1|k}C^T S_{k+1}^{-1}\right)^{-1} \tag{5.1.4.7}$$

The SVSF gain is then calculated (5.1.4.8), and then used to update the state estimates (5.1.4.9).

$$K_{k+1} = C^{-1}\bar{A}_{k+1}\psi_{k+1}^{-1} \tag{5.1.4.8}$$

$$\hat{x}_{k+1|k+1} = \hat{x}_{k+1|k} + K_{k+1}e_{z,k+1|k} \tag{5.1.4.9}$$

Finally, the a posteriori state error covariance (5.1.4.10), updated measurement estimate (5.1.4.11), and a posteriori errors (5.1.4.12) are calculated.

$$P_{k+1|k+1} = (I - K_{k+1}C)P_{k+1|k}(I - K_{k+1}C)^T + K_{k+1}R_{k+1}K_{k+1}^T \tag{5.1.4.10}$$

$$\hat{z}_{k+1|k+1} = C\hat{x}_{k+1|k+1} \tag{5.1.4.11}$$

$$e_{z,k+1|k+1} = z_{k+1} - \hat{z}_{k+1|k+1} \tag{5.1.4.12}$$

5.2 Computer Experiments for Linear Systems

In this section, the proposed algorithm is applied for state estimation on an electrohydrostatic actuator (EHA). This example uses computer simulations in order to allow a detailed investigation of the effects of parametric uncertainties. The EHA model is based on an actual prototype built for experimentation [37,128]. The purpose of this example is to demonstrate that the new SVSF-VBL estimation process is functional, and that the resulting estimation process is comparable to the KF for linear and known systems. Furthermore, the addition of modeling errors will demonstrate its robustness. For this computer experiment, the input to the system is a random signal with amplitude in the range of $\pm 1\ rad/s$, superimposed onto a unit step occurring at $0.5\ s$ as shown below [37].

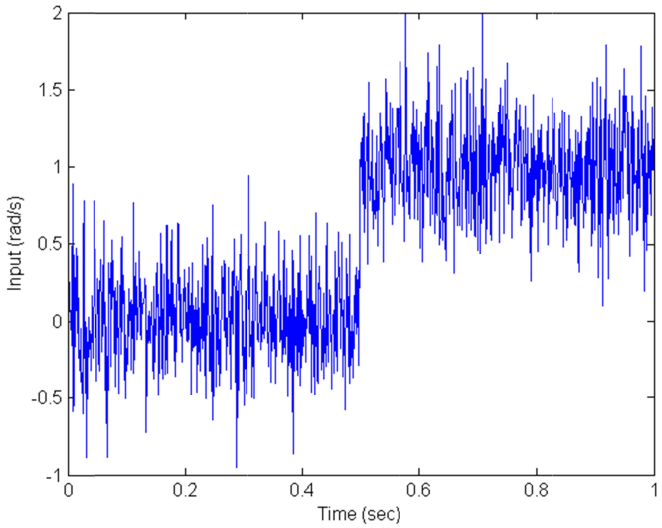

Figure 5.2.1. Input Signal Used in the Computer Experiment

The EHA has been modeled as a third-order linear system with state variables related to its position, velocity, and acceleration [37]. Initially, it is assumed that all three states have measurements associated with them (i.e., $C = I$). The sample time of the system is $T = 0.001\ s$, and the discrete-time state space system equation may be defined as follows [37]:

$$x_{k+1} = \begin{bmatrix} 1 & 0.001 & 0 \\ 0 & 1 & 0.001 \\ -557.02 & -28.616 & 0.9418 \end{bmatrix} x_k + \begin{bmatrix} 0 \\ 0 \\ 557.02 \end{bmatrix} u_k \tag{5.2.1.1}$$

For this case, the corresponding measurement equation is defined by:

$$z_{k+1} = \begin{bmatrix} 1 & 0 & 0 \\ 0 & 1 & 0 \\ 0 & 0 & 1 \end{bmatrix} x_{k+1} \tag{5.2.1.2}$$

The initial state values are set to zero. The system and measurement noises (w and v) are considered to be Gaussian, with zero mean and variances Q and R, respectively. The initial state error covariance $P_{0|0}$, system noise covariance Q, and measurement noise covariance R are defined respectively as follows:

$$P_{0|0} = 10Q \tag{5.2.1.3}$$

$$Q = \begin{bmatrix} 1 \times 10^{-5} & 0 & 0 \\ 0 & 1 \times 10^{-3} & 0 \\ 0 & 0 & 1 \times 10^{-1} \end{bmatrix} \tag{5.2.1.4}$$

$$R = \begin{bmatrix} 1 \times 10^{-4} & 0 & 0 \\ 0 & 1 \times 10^{-2} & 0 \\ 0 & 0 & 1 \end{bmatrix} \tag{5.2.1.5}$$

For the standard SVSF estimation process, the 'memory' or convergence rate was set to $\gamma = 0.1$, and the limits for the smoothing boundary layer widths were defined as $\psi = [0.05 \quad 0.5 \quad 5]^T$. These parameters were selected based on the distribution of the system and measurement noises, which are shown in the following sets of figures. For example, the limit for the smoothing boundary layer width ψ was set to 5 times the maximum system noise, or approximately equal to the measurement noise. The initial state estimates for the filters were defined randomly by a normal distribution, around the true initial state values x_0 and using the initial state error covariance $P_{0|0}$.

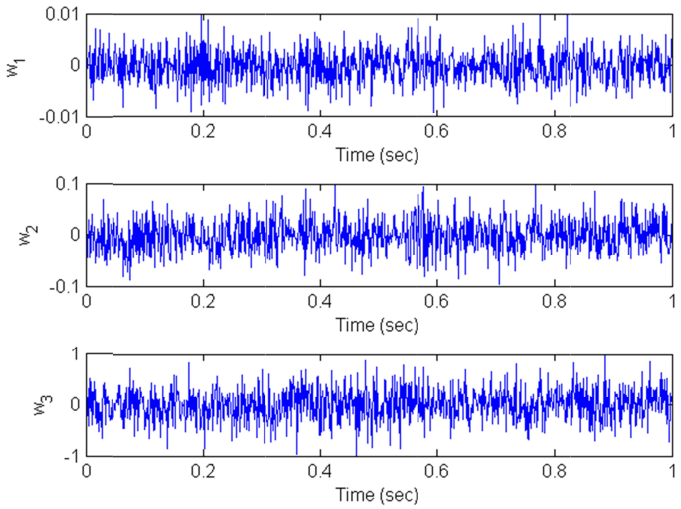

Figure 5.2.2. System Noise Profile

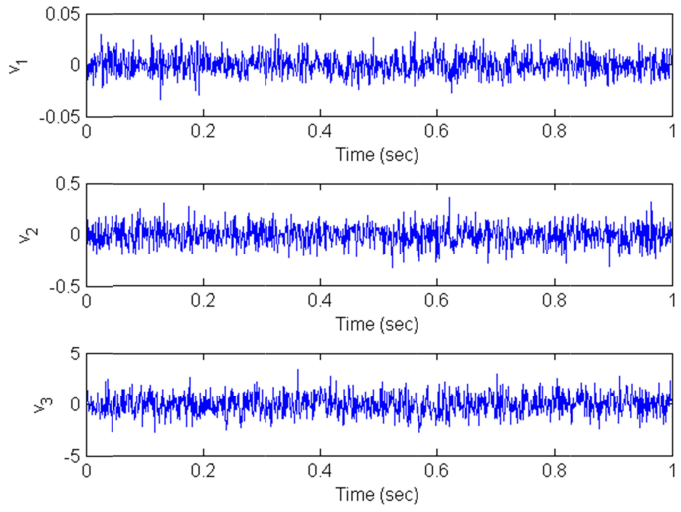

Figure 5.2.3. Measurement Noise Profile

Four different cases were studied. The first case was considered 'normal', and the second included system modeling error half-way through the simulation. The last two cases involved fewer and extra measurements, respectively. The main results of applying the KF, SVSF, and the SVSF-VBL are shown in the following figure.

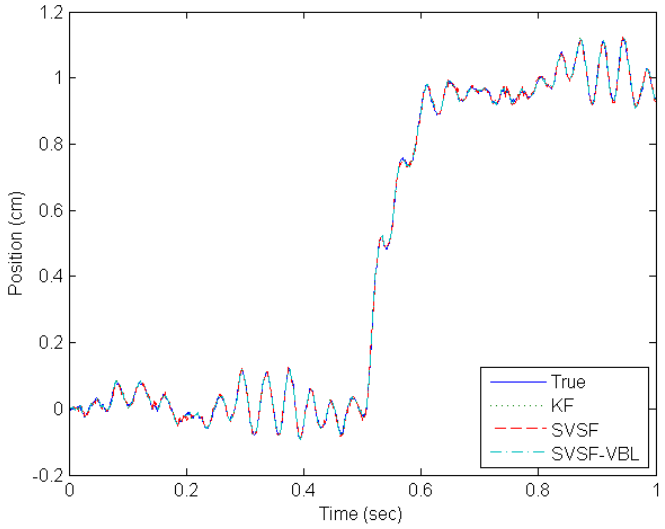

Figure 5.2.4. Position Estimates for the EHA Computer Experiment

This figure shows the true position of the EHA, with the corresponding filter estimates. The estimation results of all filters are practically the same (note that the lines are nearly overlapping and are thus difficult to distinguish). It is important to note that the KF provides the best estimate (i.e., optimal) for a linear and known system, subject to Gaussian noise. Consequently, the SVSF-VBL yielded the same results, since the derived gain (5.1.2.2) is the same as the KF. Although the standard SVSF yielded good results, the estimates were not optimal. The velocity and acceleration estimates were relatively the same, and were thus omitted for space constraints. As shown in the following table, in the normal (standard) case, the KF and SVSF-VBL provide optimal results (in terms of estimation accuracy). The SVSF-VBL improved the SVSF with a constant boundary layer width by roughly 40% (in the position estimate). This is a significant improvement in terms of estimation accuracy. However, note that after some tuning by trial-and-error, it may be possible to improve the SVSF results.

The root mean squared error (RMSE) results of running the simulation are as follows:

Table 5.2.1. RMSE Results (Normal Case)

Filter	Position (m)	Velocity (m/s)	Acceleration (m/s^2)
KF	3.72×10^{-3}	4.89×10^{-2}	0.87
SVSF-VBL	3.72×10^{-3}	4.89×10^{-2}	0.87
SVSF	6.11×10^{-3}	5.93×10^{-2}	1.21

Figure 5.2.5 provides an illustration of the individual smoothing boundary layer widths (found within the ψ matrix), as they evolve with time. The standard SVSF results could be improved if the information contained along the diagonal of the smoothing boundary layer matrix were used to tune the standard SVSF boundary layer widths. In its current form, the SVSF-VBL is equivalent to the KF. However, as shown in the following example, some cases exist such that the KF no longer provides an optimal and reliable estimate.

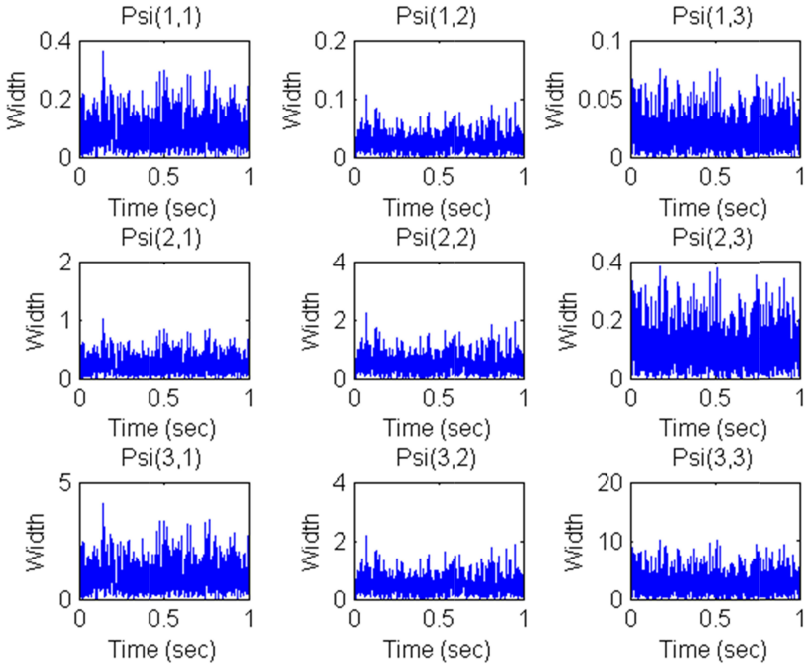

Figure 5.2.5. Smoothing Boundary Layer Widths (Normal Case)

As per [37], consider the introduction of modeling error or uncertainty, such that the system used by the filters is modified (5.2.1.6) at 0.5 seconds. The model changes at this point to coincide with the input step, to exaggerate the effects of modeling uncertainty.

$$x_{k+1} = \begin{bmatrix} 1 & 0.001 & 0 \\ 0 & 1 & 0.001 \\ -240 & -28 & 0.9418 \end{bmatrix} x_k + \begin{bmatrix} 0 \\ 0 \\ 557.02 \end{bmatrix} u_k \tag{5.2.1.6}$$

The corresponding position estimates for this case are shown in the following figure.

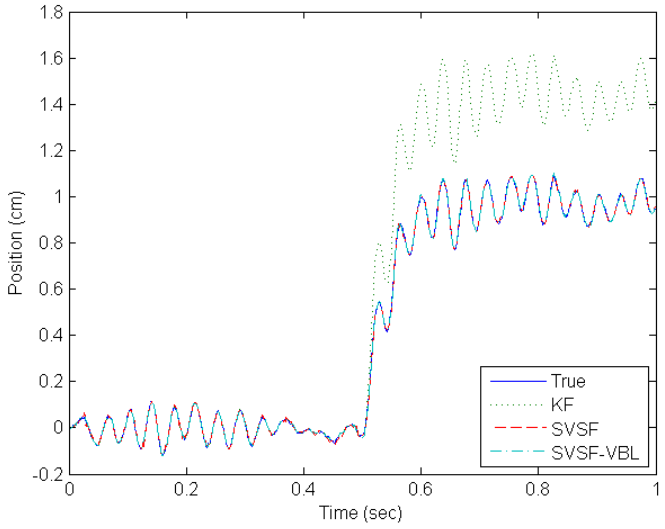

Figure 5.2.6. Position Estimates for the EHA Computer Experiment (Uncertainty Case)

An interesting result occurs when studying the elements of the smoothing boundary layer matrix. As shown in Figure 5.2.7, the smoothing boundary layer widths corresponding to the acceleration state grows larger at the inception of the modeling uncertainty (0.5 seconds). This is due to the fact that the width of the smoothing boundary layer is directly related to the level of modeling uncertainties (by virtue of the errors), as well as the estimated system and measurement noise (captured by $P_{k+1|k}$ and S_{k+1}), as described in (5.1.22). Furthermore, this can be seen by looking at the value of (5.1.4.6) at the onset of modeling uncertainties. The average value in A (corresponding to the third state A_3) increased by nearly 100 times; which in turn, drastically increased the smoothing boundary layer width.

The system modeling error leads to an incorrect a priori state covariance $P_{k+1|k}$, which propagates to the smoothing boundary layer calculation. The smoothing boundary layer matrix ψ_{k+1} therefore provides an alternative method for fault detection, as demonstrated by the immediate changes at the inception of the system modeling uncertainties.

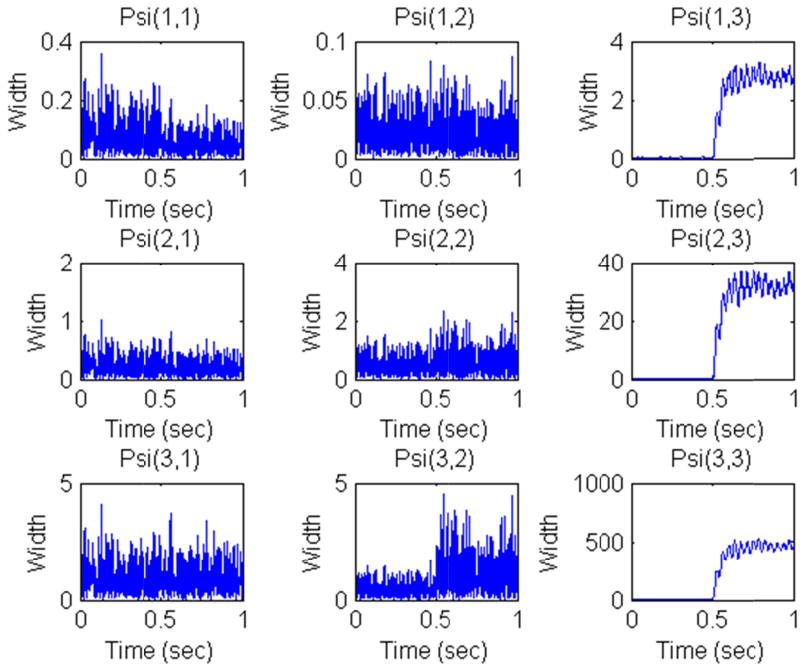

Figure 5.2.7. Smoothing Boundary Layer Widths (Uncertainty Case)

The smoothing boundary layers grow to accommodate for the increased uncertainties at 0.5 seconds. Injection of uncertainties leads to a loss of optimality, as the basic assumption related to having a known model no longer applies. As shown by Figure 5.2.6, at the inception of the modeling error (0.5 seconds), the KF failed to yield a reasonable estimate. However, the SVSF-VBL and SVSF retain their robust stability and their estimates remained bounded to within a region of the true state trajectory. In terms of RMSE, the SVSF-VBL estimation strategy yielded the best results, as shown in the following table.

Table 5.2.2. RMSE Results (Uncertainties Case)

Filter	Position (m)	Velocity (m/s)	Acceleration (m/s^2)
SVSF-VBL	4.96×10^{-3}	5.43×10^{-2}	0.98
SVSF	6.01×10^{-3}	5.75×10^{-2}	1.12
KF	0.31	3.49	17.9

As shown in the above table, the KF provides the worst result (in terms of estimation accuracy). However, the standard SVSF and the SVSF-VBL estimation processes remained relatively stable (when compared with Table 5.2.1). These results would have significant implications when attempting the accurate control of a mechanical or electrical system.

It is not uncommon to have fewer measurements than states. In this case, different strategies may be used to extract the appropriate information. Consider the following revised measurement matrix:

$$C = \begin{bmatrix} 1 & 0 & 0 \\ 0 & 1 & 0 \end{bmatrix} \tag{5.2.1.7}$$

It is required to transform (5.2.1.7) into a square matrix (i.e., identity), such that an 'artificial' measurement is created. Formulating a square measurement matrix allows the implementation of the time-varying smoothing boundary layer strategy. A number of methods exist, such as the reduced order or Luenberger's approach, which are presented in [37,129,120]. Consider a system model involving phase variables. It is possible to derive a third 'artificial' measurement based on the available measurements. For example, in (5.2.1.7) the acceleration measurement is missing. Therefore, consider the following, where y represents an artificial measurement, let:

$$y_{3,k} = \frac{1}{T}\left(z_{2,k+1} - z_{2,k}\right) \tag{5.2.1.8}$$

The accuracy of (5.2.1.8) depends on the sampling rate T. Applying (5.2.1.8) allows a measurement matrix equivalent to the identity matrix. The estimation process would continue as in the previous section, where a full measurement matrix was available.

Note however that the artificial acceleration measurement would be delayed one time step. If the system model (5.2.1.1) is known with complete confidence, then it is possible to derive an artificial measurement for the acceleration from the first two measurements. Hence, consider the following from (5.2.1.1):

$$y_{3,k+1} = -557.02z_{1,k} - 28.616z_{2,k} + 0.9418y_{3,k} + 557.02u_k \tag{5.2.1.9}$$

Note that the artificial measurement would have to be initialized (i.e., 0 is a typical value). Equation (5.2.1.9) essentially propagates the known measurements through the system model to obtain the artificial acceleration measurement. It is conceptually similar to the method presented in [120] and creates a full measurement matrix. To reiterate, the a priori measurement error vector would be calculated as follows:

$$e_{z,k+1|k} = \begin{bmatrix} z_1 \\ z_2 \\ y_3 \end{bmatrix}_{k+1} - \hat{z}_{k+1|k} \tag{5.2.1.10}$$

The estimation strategy continues as described in the previous section with a full measurement matrix. The following table summarizes the results when the system is well defined and has fewer measurements than states.

Table 5.2.3. RMSE Results (Normal Case with Fewer Measurements)

Filter	Position (m)	Velocity (m/s)	Acceleration (m/s^2)
KF	4.79×10^{-3}	5.96×10^{-2}	13.0
SVSF-VBL	4.79×10^{-3}	5.96×10^{-2}	13.0
SVSF	5.78×10^{-3}	7.00×10^{-2}	17.7

The results of the normal case with no modeling uncertainties and with fewer measurements may be summarized in the above table. The KF was able to provide the best estimate in terms of accuracy. The SVSF also yielded relatively good results. This case was repeated with modeling uncertainties added, as before.

It is interesting to point out the differences between applying (5.2.1.8) or (5.2.1.9). Consider the following figure of the artificial acceleration measurement based on the incorrect model applied at 0.5 seconds (5.2.1.9).

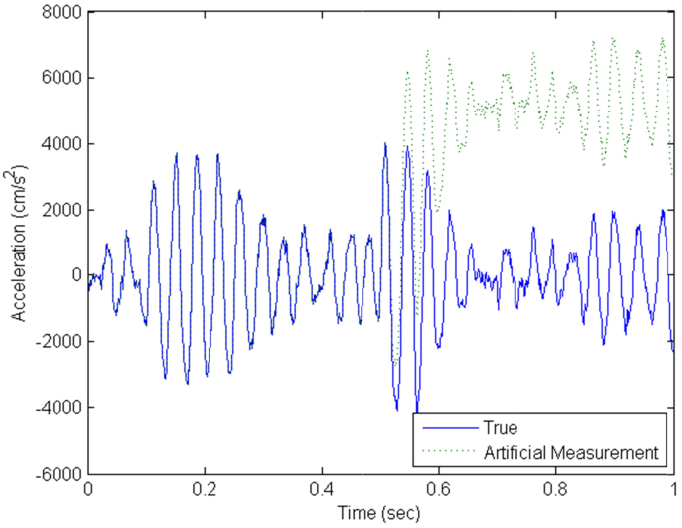

Figure 5.2.8. Artificial Measurement Based on System Model

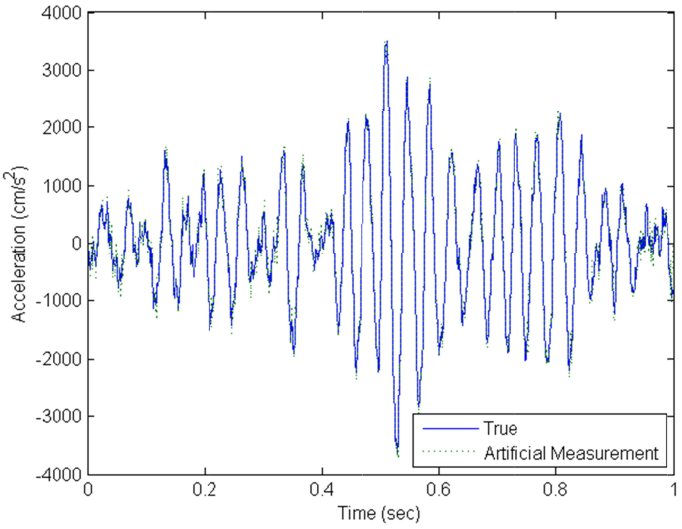

Figure 5.2.9. Artificial Measurement Based on Velocity Derivative

As shown above, the artificial measurement based on the velocity derivative yields a more accurate estimate at the onset of the modeling uncertainty (0.5 seconds). However, prior to this point (i.e., when the system was well defined), the method of (5.2.1.9) yields a less noisy artificial measurement. For this case, the artificial acceleration measurement was calculated as per (5.2.1.8), due to the presence of modeling uncertainty. The following table summarizes these results.

Table 5.2.4. RMSE Results (Uncertainties Case with Fewer Measurements)

Filter	Position (m)	Velocity (m/s)	Acceleration (m/s^2)
SVSF-VBL	5.68×10^{-3}	0.09	126.1
SVSF	6.06×10^{-3}	0.10	151.4
KF	4.08×10^{-2}	4.27	1,612

For this case, the SVSF-VBL provided the best overall estimates in terms of estimation accuracy. It is interesting to point out that the SVSF also worked very well. All three filters had issues with estimating the acceleration, which lacked an appropriate measurement. Note that the KF position estimate was still good; however, the velocity and acceleration measurements were significantly worse.

The final case to be studied involves the presence of more measurements than states. In some situations, extra measurements may be available, such as in neural network applications. In these scenarios, the extra measurements can be used to create artificial measurements, relating the true measurements to the states of interest. Consider the following transformation:

$$y = C^{+}z \tag{5.2.1.11}$$

Performing (5.2.1.11) allows the creation of an identity matrix, to be used by the SVSF and SVSF-VBL estimation processes. For example, consider the case where a differential pressure measurement ΔP_E is available in the EHA system described earlier, such that:

$$\Delta P_E A_E = M\ddot{x} + B_E\dot{x} \tag{5.2.1.12}$$

Equation (5.2.1.12) changes the measurement matrix C used by the KF as follows [37]:

$$C = \begin{bmatrix} 1 & 0 & 0 \\ 0 & 1 & 0 \\ 0 & 0 & 1 \\ 0 & \frac{B_E}{A_E} & \frac{M}{A_E} \end{bmatrix} = \begin{bmatrix} 1 & 0 & 0 \\ 0 & 1 & 0 \\ 0 & 0 & 1 \\ 0 & 15{,}050 & 396.04 \end{bmatrix} \tag{5.2.1.13}$$

Note that the measurement noise covariance matrix is revised as follows:

$$R = \begin{bmatrix} 1 \times 10^{-4} & 0 & 0 & 0 \\ 0 & 1 \times 10^{-2} & 0 & 0 \\ 0 & 0 & 1 & 0 \\ 0 & 0 & 0 & 1 \times 10^{3} \end{bmatrix} \tag{5.2.1.14}$$

The pressure measurement is shown in the following figure. This extra measurement is used to further study and compare the KF, SVSF, and SVSF-VBL. The results of this case may be summarized in the following table. Note that the KF yields the best estimation results in terms of RMSE, followed very closely by the SVSF-VBL. The slight differences may be due to the fact that the SVSF-VBL and SVSF utilize the pseudo-inverse of (5.2.1.13), whereas the KF uses simply (5.2.1.13).

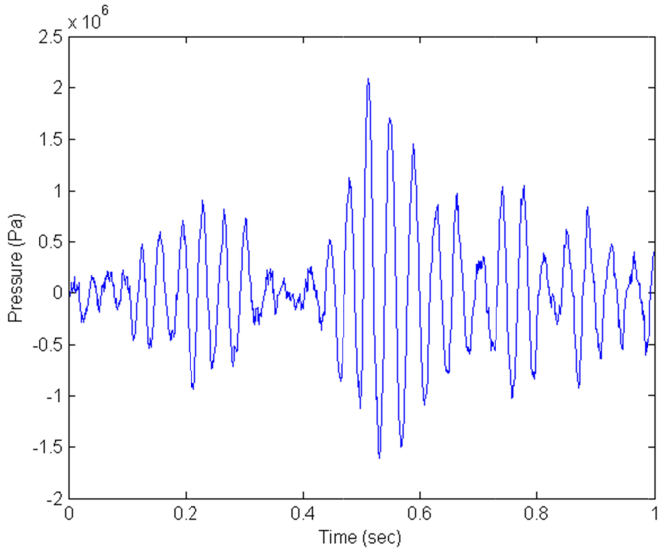

Figure 5.2.10. Extra Measurement (EHA Pressure)

Table 5.2.5. RMSE Results (Normal Case with Extra Measurements)

Filter	Position (m)	Velocity (m/s)	Acceleration (m/s^2)
KF	3.29×10^{-3}	2.07×10^{-2}	0.78
SVSF-VBL	3.29×10^{-3}	2.10×10^{-2}	0.79
SVSF	6.05×10^{-3}	4.45×10^{-2}	1.20

The next table summarizes the extra measurements case with the presence of uncertainties. The SVSF-VBL method provided the best estimate in terms of RMSE, followed by the SVSF. The KF failed to provide a quality estimate at the onset of the modeling uncertainties. The addition of measurements can provide useful information. However, the quality of the additional information should be taken into account; as in some instances, the extra measurements may not be beneficial towards the overall state estimates.

Table 5.2.6. RMSE Results (Uncertainties Case with Extra Measurements)

Filter	Position (m)	Velocity (m/s)	Acceleration (m/s^2)
SVSF-VBL	5.23×10^{-3}	3.26×10^{-2}	0.92
SVSF	6.23×10^{-3}	4.24×10^{-2}	1.11
KF	0.64	0.45	17.2

The aforementioned cases demonstrated the benefits of the new robust filtering strategy for linear systems, referred to as the SVSF-VBL. The optimality of the KF is used in conjunction with the robustness of the SVSF, thus creating an accurate and robust filter.

5.3 Methodology for Combined Nonlinear Filtering Strategies

The SVSF-VBL estimation strategy may be extended further to nonlinear systems and measurements. The variable boundary layer provides a mechanism for combining various forms of the KF with the SVSF in an easy and effective manner. In an effort to utilize the accuracy of the EKF, UKF, and CKF, and the robustness of the SVSF, the filters have been combined resulting in three algorithms referred to as the EK-SVSF, UK-SVSF, and CK-SVSF.

This section describes the concept behind combining the estimation strategies, and then provides the equations for each filter. Finally, a target tracking simulation (an air traffic controller) is used to test, study, and compare the effectiveness of these three algorithms.

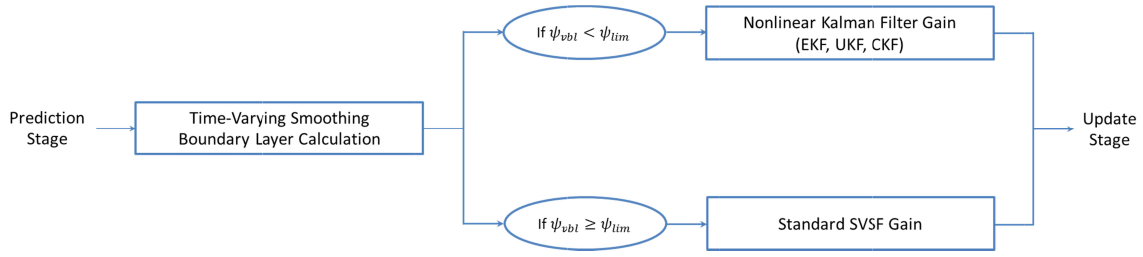

Figure 5.3.1. Methodology for Combing the Nonlinear Filtering Strategies

Essentially, the methodology for combining the filters may be explained with the above figure. Note that it is similar to the SVSF-VBL methodology, except that a nonlinear filter (EKF, UKF, or CKF) is used to update the state estimate if the variable smoothing boundary layer is calculated to exist within the imposed limits of the smoothing boundary layer. The following three sections summarize the three estimation methods (EK-SVSF, UK-SVSF, and CK-SVSF). The last section involves a computer experiment.

5.3.1 The EK-SVSF Equations

For completeness, the EK-SVSF equations are now summarized. The prediction stage begins with an estimation of the states $\hat{x}_{k+1|k}$ and the state error covariance $P_{k+1|k}$, respectively as follows:

$$\hat{x}_{k+1|k} = f\left(\hat{x}_{k|k}, u_k\right) \tag{5.3.1.1}$$

$$P_{k+1|k} = F_k P_{k|k} F_k^T + Q_k \tag{5.3.1.2}$$

The a priori measurement error $e_{z,k+1|k}$ is then found (5.3.1.3), based on the nonlinear measurement model h, followed by the measurement error (innovation) covariance matrix S_{k+1} (5.3.1.4). Furthermore, recall the linearized measurement matrix H defined by (4.2.1.2).

$$e_{z,k+1|k} = z_{k+1} - h\left(\hat{x}_{k+1|k}\right) \tag{5.3.1.3}$$

$$S_{k+1} = H_{k+1}P_{k+1|k}H_{k+1}^T + R_{k+1} \tag{5.3.1.4}$$

At this point, the smoothing boundary layer ψ_{k+1} is calculated as follows:

$$\psi_{k+1} = \left(\bar{A}^{-1}HP_{k+1|k}H^T S_{k+1}^{-1}\right)^{-1} \tag{5.3.1.5}$$

Where:

$$A = \left(\left|e_{z_{k+1|k}}\right|_{Abs} + \gamma \left|e_{z_{k|k}}\right|_{Abs}\right) \tag{5.3.1.6}$$

As suggested by Figure 5.3.1, the values of (5.3.1.5) are compared with the limits for the smoothing boundary layer widths (a designer setting) to determine which gain is used (EKF or SVSF). If the values of (5.3.1.5) are larger than the limits (i.e., $\psi_{k+1} > \psi_{lim}$), the EK-SVSF gain is defined by:

$$K_{k+1} = H^{-1}diag\left[\left(\left|e_{z,k+1|k}\right|_{Abs} + \gamma\left|e_{z,k|k}\right|_{Abs}\right) \circ sat\left(\bar{\psi}^{-1}e_{z,k+1|k}\right)\right] diag\left(e_{z,k+1|k}\right)^{-1} \tag{5.3.1.7}$$

Otherwise, the standard EKF gain may be used (5.3.1.8). Note that this is a seamless transfer as the gain equation does not change but its amplitude changes smoothly as it crosses the boundary layer, ensuring continuity in the estimation process.

$$K_{k+1} = P_{k+1|k}H_{k+1}^T S_{k+1}^{-1} \tag{5.3.1.8}$$

The updated state estimates $\hat{x}_{k+1|k+1}$ and state error covariance matrix $P_{k+1|k+1}$ are determined as:

$$\hat{x}_{k+1|k+1} = \hat{x}_{k+1|k} + K_{k+1}e_{z,k+1|k} \tag{5.3.1.9}$$

$$P_{k+1|k+1} = (I - K_{k+1}H)P_{k+1|k}(I - K_{k+1}H)^T + K_{k+1}R_{k+1}K_{k+1}^T \tag{5.3.1.10}$$

Finally, the updated measurement estimate $\hat{z}_{k+1|k+1}$ is used to calculate the a posteriori measurement error $e_{z,k+1|k+1}$, which is used in later iterations.

$$e_{z,k+1|k+1} = z_{k+1} - h\left(\hat{x}_{k+1|k+1}\right) \tag{5.3.1.11}$$

The EK-SVSF estimation process is iterative, and is summarized by (5.3.1.1) to (5.3.1.11). Note that for the linear systems case, the KF has been combined with the SVSF in a similar fashion, and is referred to as the SVSF-VBL.

5.3.2 The UK-SVSF Equations

For completeness, the UK-SVSF equations are summarized in this section. The sigma points used for the UKF portion of the UK-SVSF method is calculated as per (4.2.2.1) through (4.2.2.6). The majority of the UKF process remains the same. The sigma points are propagated through the nonlinear system model (5.3.2.1), and are used with their corresponding weights to calculate the predicted state estimate (5.3.2.2).

$$\hat{X}_{i,k+1|k} = f\left(X_{i,k|k}, u_k\right) \tag{5.3.2.1}$$

$$\hat{x}_{k+1|k} = \sum_{i=0}^{2n} W_i \hat{X}_{i,k+1|k} \tag{5.3.2.2}$$

From (5.3.2.1) and (5.3.2.2), it is possible to calculate the predicted state error covariance as follows:

$$P_{k+1|k} = \sum_{i=0}^{2n} W_i \left(\hat{X}_{i,k+1|k} - \hat{x}_{k+1|k}\right)\left(\hat{X}_{i,k+1|k} - \hat{x}_{k+1|k}\right)^T \tag{5.3.2.3}$$

Next, the sigma points are propagated through the nonlinear measurement model (5.3.2.4), and the predicted measurement is calculated (5.3.2.5).

$$\hat{Z}_{i,k+1|k} = h\left(\hat{X}_{i,k+1|k}, u_k\right) \tag{5.3.2.4}$$

$$\hat{z}_{k+1|k} = \sum_{i=0}^{2n} W_i \hat{Z}_{i,k+1|k} \tag{5.3.2.5}$$

Next, the a priori measurement error is calculated (5.3.2.6).

$$e_{z,k+1|k} = z_{k+1} - \hat{z}_{k+1|k} \tag{5.3.2.6}$$

The measurement (or innovation) covariance is then calculated as follows:

$$P_{zz.k+1|k} = \sum_{i=0}^{2n} W_i \left(\hat{Z}_{i,k+1|k} - \hat{z}_{k+1|k}\right)\left(\hat{Z}_{i,k+1|k} - \hat{z}_{k+1|k}\right)^T \tag{5.3.2.7}$$

Furthermore, the cross-covariance (between the state and measurement) is then calculated as follows:

$$P_{xz.k+1|k} = \sum_{i=0}^{2n} W_i \left(\hat{X}_{i,k+1|k} - \hat{x}_{k+1|k}\right)\left(\hat{Z}_{i,k+1|k} - \hat{z}_{k+1|k}\right)^T \tag{5.3.2.8}$$

At this point, the smoothing boundary layer ψ_{k+1} is calculated as follows:

$$\psi_{k+1} = \left(\bar{A}^{-1} H P_{k+1|k} H^T P_{zz.k+1|k}^{-1}\right)^{-1} \tag{5.3.2.9}$$

Where:

$$A = \left(\left|e_{z_{k+1|k}}\right|_{Abs} + \gamma \left|e_{z_{k|k}}\right|_{Abs}\right) \tag{5.3.2.10}$$

As suggested by Figure 5.3.1, the values of (5.3.2.9) are compared with the limits for the smoothing boundary layer widths (a designer setting) to determine which gain is used (UKF or SVSF). If the values of (5.3.2.9) are larger than the limits (i.e., $\psi_{k+1} > \psi_{lim}$), the UK-SVSF gain is defined by:

$$K_{k+1} = H^{-1} diag\left[\left(\left|e_{z,k+1|k}\right|_{Abs} + \gamma \left|e_{z,k|k}\right|_{Abs}\right) \circ sat\left(\bar{\psi}^{-1} e_{z,k+1|k}\right)\right] diag\left(e_{z,k+1|k}\right)^{-1} \tag{5.3.2.11}$$

Otherwise, the standard UKF gain is used (5.3.2.12).

$$K_{k+1} = P_{xz.k+1|k} P_{zz.k+1|k}^{-1} \tag{5.3.2.12}$$

Similarly, the updated state estimates $\hat{x}_{k+1|k+1}$ and state error covariance matrix $P_{k+1|k+1}$ are determined respectively as follows:

$$\hat{x}_{k+1|k+1} = \hat{x}_{k+1|k} + K_{k+1} e_{z,k+1|k} \tag{5.3.2.13}$$

$$P_{k+1|k+1} = (I - K_{k+1}H)P_{k+1|k}(I - K_{k+1}H)^T + K_{k+1}R_{k+1}K_{k+1}^T \tag{5.3.2.14}$$

Finally, the updated measurement estimate $\hat{z}_{k+1|k+1}$ is used to calculate the a posteriori measurement error $e_{z,k+1|k+1}$, which is used in later iterations.

$$e_{z,k+1|k+1} = z_{k+1} - h\left(\hat{x}_{k+1|k+1}\right) \tag{5.3.2.15}$$

The UK-SVSF estimation process is iterative, and is summarized by (5.3.2.1) to (5.3.2.15).

5.3.3 The CK-SVSF Equations

For implementation, the CK-SVSF equations are summarized. Note that the integrals found within the CK-SVSF estimation method represent the summation of cubature points used to approximate the state distribution, as suggested by (4.2.3.1). The prediction stage begins with an estimation of the states $\hat{x}_{k+1|k}$ and the state error covariance $P_{k+1|k}$, respectively as follows:

$$\hat{x}_{k+1|k} = \int_{\mathbb{R}^{n_x}} \hat{f}(x_k, u_k)\mathcal{N}\left(x_k; \hat{x}_{k|k}, P_{k|k}\right)dx_k \tag{5.3.3.1}$$

$$P_{k+1|k} = \int_{\mathbb{R}^{n_x}} \hat{f}(x_k, u_k)\hat{f}^T(x_k, u_k)\mathcal{N}\left(x_k; \hat{x}_{k|k}, P_{k|k}\right)dx_k - \hat{x}_{k+1|k}\hat{x}_{k+1|k}^T + Q_{k+1} \tag{5.3.3.2}$$

The estimated measurements $\hat{z}_{k+1|k}$ and corresponding measurement errors $e_{z,k+1|k}$ are then calculated:

$$\hat{z}_{k+1|k} = \int_{\mathbb{R}^{n_x}} \hat{h}(x_{k+1}, u_{k+1})\mathcal{N}\left(x_{k+1}; \hat{x}_{k+1|k}, P_{k+1|k}\right)dx_{k+1} \tag{5.3.3.3}$$

$$e_{z,k+1|k} = z_{k+1} - \hat{z}_{k+1|k} \tag{5.3.3.4}$$

At this point, the smoothing boundary layer ψ_{k+1} is calculated as follows:

$$\psi_{k+1} = \left(\bar{A}^{-1}HP_{k+1|k}H^T S_{k+1}^{-1}\right)^{-1} \tag{5.3.3.5}$$

Where:

$$A = \left(\left| e_{z_{k+1|k}} \right|_{Abs} + \gamma \left| e_{z_{k|k}} \right|_{Abs} \right) \tag{5.3.3.6}$$

As suggested by Figure 5.3.1, the values of (5.3.3.5) are compared with the limits for the smoothing boundary layer widths to determine which gain is used (CKF or SVSF). If the values of (5.3.3.5) are larger than the limits (i.e., $\psi_{k+1} > \psi_{lim}$), the CK-SVSF gain used to update the state is defined by:

$$K_{k+1} = H^{-1} diag\left[\left(\left| e_{z,k+1|k} \right|_{Abs} + \gamma \left| e_{z,k|k} \right|_{Abs} \right) \circ sat\left(\bar{\psi}^{-1} e_{z,k+1|k} \right) \right] diag\left(e_{z,k+1|k} \right)^{-1} \tag{5.3.3.7}$$

Otherwise, the CKF gain (5.3.3.10) is used. In order to calculate the corresponding CKF gain K_{k+1}, the innovation covariance $P_{zz,k+1|k}$ and cross-covariance $P_{xz,k+1|k}$ matrices need to be evaluated, respectively as follows:

$$P_{zz,k+1|k} = \int_{\mathbb{R}^{n_x}} \hat{h}(x_{k+1}, u_{k+1}) \hat{h}^T(x_{k+1}, u_{k+1}) \mathcal{N}\left(x_{k+1}; \hat{x}_{k+1|k}, P_{k+1|k} \right) dx_{k+1} - \hat{z}_{k+1|k} \hat{z}_{k+1|k}^T + R_{k+1} \tag{5.3.3.8}$$

$$P_{xz,k+1|k} = \int_{\mathbb{R}^{n_x}} x_{k+1} \hat{h}^T(x_{k+1}, u_{k+1}) \mathcal{N}\left(x_{k+1}; \hat{x}_{k+1|k}, P_{k+1|k} \right) dx_{k+1} - \hat{x}_{k+1|k} \hat{z}_{k+1|k}^T \tag{5.3.3.9}$$

The CKF gain may now be calculated like before as follows:

$$K_{k+1} = P_{xz,k+1|k} P_{zz,k+1|k}^{-1} \tag{5.3.3.10}$$

The updated state estimates $\hat{x}_{k+1|k+1}$ and state error covariance matrix $P_{k+1|k+1}$ are determined as:

$$\hat{x}_{k+1|k+1} = \hat{x}_{k+1|k} + K_{k+1} e_{z,k+1|k} \tag{5.3.3.11}$$

$$P_{k+1|k+1} = (I - K_{k+1} H) P_{k+1|k} (I - K_{k+1} H)^T + K_{k+1} R_{k+1} K_{k+1}^T \tag{5.3.3.12}$$

Finally, the updated measurement estimate $\hat{z}_{k+1|k+1}$ and measurement errors $e_{z,k+1|k+1}$ are calculated, and are used in later iterations:

$$\hat{z}_{k+1|k+1} = \int_{\mathbb{R}^{n_x}} \hat{h}(x_{k+1}, u_{k+1}) \mathcal{N}\left(x_{k+1}; \hat{x}_{k+1|k+1}, P_{k+1|k+1}\right) dx_{k+1} \tag{5.3.3.13}$$

$$e_{z,k+1|k+1} = z_{k+1} - \hat{z}_{k+1|k+1} \tag{5.3.3.14}$$

The CK-SVSF estimation process is iterative, and is summarized by (5.3.3.1) to (5.3.3.14).

5.3.4 Computer Experiments

In this section, the EK-SVSF, UK-SVSF, and CK-SVSF strategies are applied on a target tracking problem, and are compared with the EKF, UKF, CKF, and SVSF. The purpose of this computer experiment is to demonstrate that the EK-SVSF, UK-SVSF, and CK-SVSF methods provide accurate and stable estimates when compared with their standard counterparts. The target tracking problem is based on a generic air traffic control (ATC) scenario found in [28]. A radar stationed at the origin provides direct position only measurements, with a standard deviation of $50\ m$ in each coordinate. The following figure illustrates the motion of the target.

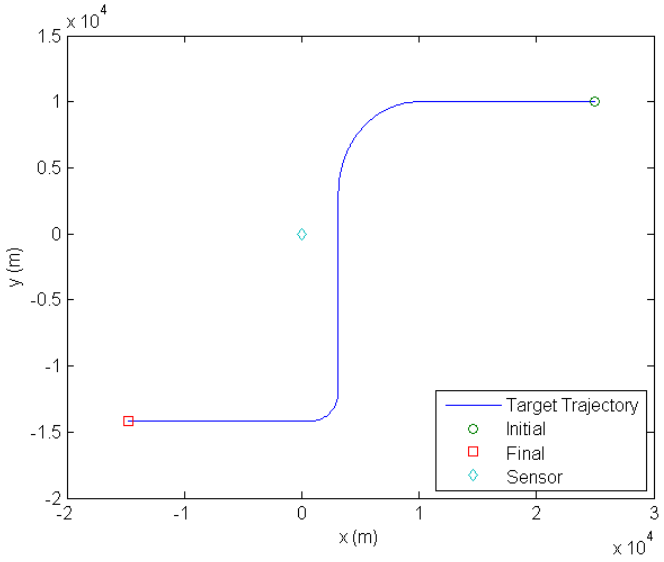

Figure 5.3.2. True Target Trajectory

As shown in the previous figure, an aircraft starts from an initial position of $[25{,}000\ m, 10{,}000\ m]$ at time $t = 0\ s$, and flies westward at $120\ m/s$ for $125\ s$. The aircraft then begins a coordinated turn for a period of $90\ s$ at a rate of $1^{\circ}/s$. It then flies southward at $120\ m/s$ for $125\ s$, followed by another coordinated turn for $30\ s$ at $3^{\circ}/s$. The aircraft then continues to fly westward until it reaches its final destination.

In ATC scenarios, the behaviour of civilian aircraft may be modeled by two different modes: uniform motion (UM) which involves a straight flight path with a constant speed and course, and maneuvering which includes turning or climbing and descending [28]. In this case, maneuvering will refer to a coordinated turn (CT) model, where a turn is made at a constant turn rate and speed. The uniform motion model used for this target tracking problem is given by (5.3.4.1) [28,130].

$$x_{k+1} = \begin{bmatrix} 1 & 0 & T & 0 \\ 0 & 1 & 0 & T \\ 0 & 0 & 1 & 0 \\ 0 & 0 & 0 & 1 \end{bmatrix} x_k + \begin{bmatrix} \frac{1}{2}T^2 & 0 \\ 0 & \frac{1}{2}T^2 \\ T & 0 \\ 0 & T \end{bmatrix} w_k \tag{5.3.4.1}$$

The state vector of the aircraft may be defined as follows:

$$x_k = [\xi_k \quad \eta_k \quad \dot{\xi}_k \quad \dot{\eta}_k]^T \tag{5.3.4.2}$$

The first two states refer to the position along the x-axis and y-axis, respectively, and the last two states refer to the velocity along the x-axis and y-axis, respectively. The sampling time used in this simulation was 5 seconds. When using the CT model, the state vector needs to be augmented to include the turn rate, as shown in (5.3.4.3) [28]. The CT model may be considered nonlinear if the turn rate of the aircraft is not known. Note that a left turn corresponds to a positive turn rate, and a right turn has a negative turn rate. This sign convention follows the commonly used trigonometric convention (the opposite is true for navigation convention) [28]. As per [28,130], the CT model is given by (5.3.4.4).

$$x_k = [\xi_k \quad \eta_k \quad \dot{\xi}_k \quad \dot{\eta}_k \quad \omega_k]^T \tag{5.3.4.3}$$

$$x_{k+1} = \begin{bmatrix} 1 & 0 & \frac{sin\omega_k T}{\omega_k} & -\frac{1-cos\omega_k T}{\omega_k} & 0 \\ 0 & 1 & \frac{1-cos\omega_k T}{\omega_k} & \frac{sin\omega_k T}{\omega_k} & 0 \\ 0 & 0 & cos\omega_k T & -sin\omega_k T & 0 \\ 0 & 0 & sin\omega_k T & cos\omega_k T & 0 \\ 0 & 0 & 0 & 0 & 1 \end{bmatrix} x_k + \begin{bmatrix} \frac{1}{2}T^2 & 0 & 0 \\ 0 & \frac{1}{2}T^2 & 0 \\ T & 0 & 0 \\ 0 & T & 0 \\ 0 & 0 & T \end{bmatrix} w_k \qquad (5.3.4.4)$$

Since the radar stationed at the origin provides direct position measurements only, the measurement equation may be formed linearly as follows:

$$z_k = \begin{bmatrix} 1 & 0 & 0 & 0 & 0 \\ 0 & 1 & 0 & 0 & 0 \end{bmatrix} x_k + v_k \qquad (5.3.4.5)$$

Equations (5.3.4.1) through (5.3.4.5) were used to generate the true state values of the trajectory and the radar measurements for this target tracking scenario. As previously mentioned, the EKF uses a linearized form of the system and measurement matrices. In this case, the system defined by (5.3.4.4) is nonlinear, such that the Jacobian of it yields a linearized form as shown in (5.3.4.6). The terms in the last column of (5.3.4.6) are correspondingly defined in (5.3.4.7) [28].

$$\left[\nabla_x F_{k,x}^T\right]^T\Big|_{x_k=\hat{x}_k} = \begin{bmatrix} 1 & 0 & \frac{sin\hat{\omega}_k T}{\hat{\omega}_k} & -\frac{1-cos\hat{\omega}_k T}{\hat{\omega}_k} & F_{\hat{\omega}1} \\ 0 & 1 & \frac{1-cos\hat{\omega}_k T}{\hat{\omega}_k} & \frac{sin\hat{\omega}_k T}{\hat{\omega}_k} & F_{\hat{\omega}2} \\ 0 & 0 & cos\hat{\omega}_k T & -sin\hat{\omega}_k T & F_{\hat{\omega}3} \\ 0 & 0 & sin\hat{\omega}_k T & cos\hat{\omega}_k T & F_{\hat{\omega}4} \\ 0 & 0 & 0 & 0 & 1 \end{bmatrix} \qquad (5.3.4.6)$$

$$\begin{bmatrix} F_{\hat{\omega}1} \\ F_{\hat{\omega}2} \\ F_{\hat{\omega}3} \\ F_{\hat{\omega}4} \end{bmatrix} = \begin{bmatrix} \frac{(cos\hat{\omega}_k T)T}{\hat{\omega}_k}\widehat{\dot{\xi}_k} - \frac{(sin\hat{\omega}_k T)}{\hat{\omega}_k^2}\widehat{\dot{\xi}_k} - \frac{(sin\hat{\omega}_k T)T}{\hat{\omega}_k}\widehat{\dot{\eta}_k} - \frac{(-1+cos\hat{\omega}_k T)}{\hat{\omega}_k^2}\widehat{\dot{\eta}_k} \\ \frac{(sin\hat{\omega}_k T)T}{\hat{\omega}_k}\widehat{\dot{\xi}_k} - \frac{(1-cos\hat{\omega}_k T)}{\hat{\omega}_k^2}\widehat{\dot{\xi}_k} - \frac{(cos\hat{\omega}_k T)T}{\hat{\omega}_k}\widehat{\dot{\eta}_k} - \frac{(sin\hat{\omega}_k T)}{\hat{\omega}_k^2}\widehat{\dot{\eta}_k} \\ -(sin\hat{\omega}_k T)T\widehat{\dot{\xi}_k} - (cos\hat{\omega}_k T)T\widehat{\dot{\eta}_k} \\ (cos\hat{\omega}_k T)T\widehat{\dot{\xi}_k} - (sin\hat{\omega}_k T)T\widehat{\dot{\eta}_k} \end{bmatrix} \qquad (5.3.4.7)$$

To generate the results for this section, the following values were used for the initial state error covariance matrix $P_{0|0}$, the system noise matrix Q, and the measurement noise matrix R.

$$P_{0|0} = \begin{bmatrix} R_{11} & 0 & 0 & 0 & 0 \\ 0 & R_{22} & 0 & 0 & 0 \\ 0 & 0 & 100 & 0 & 0 \\ 0 & 0 & 0 & 100 & 0 \\ 0 & 0 & 0 & 0 & 1 \end{bmatrix} \tag{5.3.4.8}$$

$$Q = L_1 \begin{bmatrix} \frac{T^3}{3} & 0 & \frac{T^2}{2} & 0 & 0 \\ 0 & \frac{T^3}{3} & 0 & \frac{T^2}{2} & 0 \\ \frac{T^2}{2} & 0 & T & 0 & 0 \\ 0 & \frac{T^2}{2} & 0 & T & 0 \\ 0 & 0 & 0 & 0 & \frac{L_2}{L_1}T \end{bmatrix} \tag{5.3.4.9}$$

$$R = 50^2 \begin{bmatrix} 1 & 0 \\ 0 & 1 \end{bmatrix} \tag{5.3.4.10}$$

Note that L_1 and L_2 are referred to as power spectral densities, and were defined as 0.16 and 0.01, respectively [130]. The system and measurement noise (w_k and v_k) were generated using their respective covariance values (Q and R). Also, when using the UM model, the fifth row and column of (5.3.4.8) and (5.3.4.9) were truncated. For the standalone SVSF estimation process, the limit on the smoothing boundary layer widths were defined as $\psi = [500 \quad 1{,}000 \quad 500 \quad 1{,}000 \quad 1]^T$, and the SVSF 'memory' or convergence rate was set to $\gamma = 0.1$. These parameters were tuned based on some knowledge of the uncertainties (i.e., magnitude of noise) and with the goal of decreasing the estimation error. As per the earlier discussions, it is required to transform the measurement matrix of (5.3.4.5) into a square matrix (i.e., identity), such that an 'artificial' measurement is created. It is possible to derive 'artificial' velocity measurements based on the available position measurements. For example, consider the following artificial measurement vector y_k for the SVSF:

$$y_k = \begin{bmatrix} z_{1,k} \\ z_{2,k} \\ (z_{1,k+1} - z_{1,k})/T \\ (z_{2,k+1} - z_{2,k})/T \\ 0 \end{bmatrix} \tag{5.3.4.11}$$

The accuracy of (5.3.4.11) depends on the sampling rate T. Applying the above type of transformation to non-measured states allows a measurement matrix equivalent to the identity matrix, similar to (5.2.1.7) through (5.2.1.10). The estimation process would continue as in the previous section, where $C = I$. Note however that the artificial velocity measurements would be delayed one time step. Furthermore, it is assumed that the artificial turn rate measurement is set to 0, since no artificial measurement could be created based on the available measurements. A total of 500 Monte Carlo runs were performed, and the results were averaged. The following two figures show the x-position estimation error for both models (uniform motion and coordinated turn, respectively). Notice how the SVSF and combined filtering strategies are bounded within a region of 0 error (which is ideal).

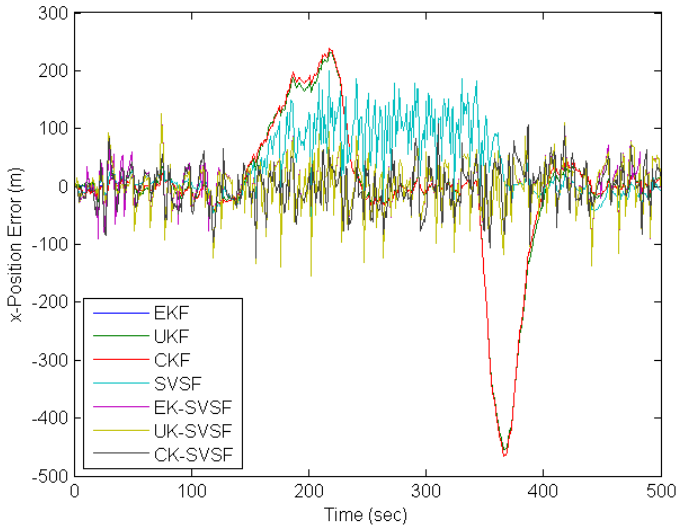

Figure 5.3.3. x-Position Estimation Error (Uniform Motion Model)

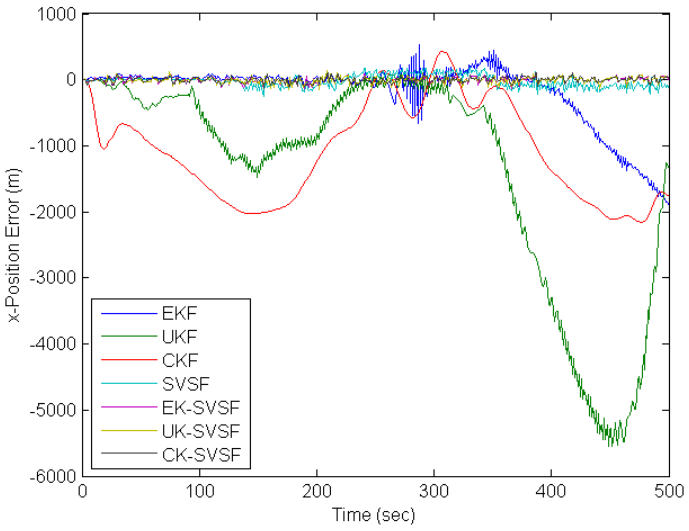

Figure 5.3.4. x-Position Estimation Error (Coordinated Turn Model)

The following two tables summarize the RMSE results for the 500 Monte Carlo runs. Note that the first table corresponds to when the filters used the uniform motion model (5.3.4.1), while the second table corresponds to when the coordinated turn model was implemented (5.3.4.4).

Table 5.3.1. RMSE Results for the Uniform Motion Model (Normal Case)

Filter	Position (m)	Velocity (m/s)
EKF	167	23.6
UKF	155	26.6
CKF	167	23.6
SVSF	107	94.1
EK-SVSF	57.8	30.1
UK-SVSF	56.5	29.1
CK-SVSF	52.3	32.1

Table 5.3.2. RMSE Results for the Coordinated Turn Model (Normal Case)

Filter	Position (m)	Velocity (m/s)	Turn Rate (rad/s)
EKF	2,503	89,258	5.320
UKF	1520	332	1.949
CKF	1168	88.5	0.231
SVSF	130	146	0.063
EK-SVSF	68.8	58.1	0.026
UK-SVSF	67.6	56.7	0.035
CK-SVSF	59.4	50.2	0.025

As shown in the previous tables, the new combined methods performed the best in terms of accuracy (i.e., RMSE). Figure 5.3.3 clearly demonstrates the effects that the uniform motion model has on the EKF, UKF, and CKF when the target is turning. The SVSF switching effect is shown clearly in Figures 5.3.3 and 5.3.4. The switching, inherent to the SVSF gain, ensures that the estimation process is robust and stable. As demonstrated in Figure 5.3.4, the EKF, UKF, and CKF methods were unable to provide a good estimate of the target. Bounding these Kalman-based nonlinear filters to within a region of the measurements by use of the SVSF further increased the stability and the performance, as shown by the results. The strategy effectively combined the accuracy of the EKF, UKF, and CKF with the stability of the SVSF.

The calculation of the smoothing boundary layer term introduces another indicator of performance. For example, consider the following two figures which show the calculated smoothing boundary layer widths corresponding to the x-position and the y-position states. These values were calculated by the EK-SVSF strategy (5.3.1.5), and the state estimates were generated by the uniform motion model (5.3.4.1). For both states, the widths increase approximately when the target was turning; this corresponds to an increase in the uncertainty present in the estimation process (i.e., the filter model does not match the true system model).

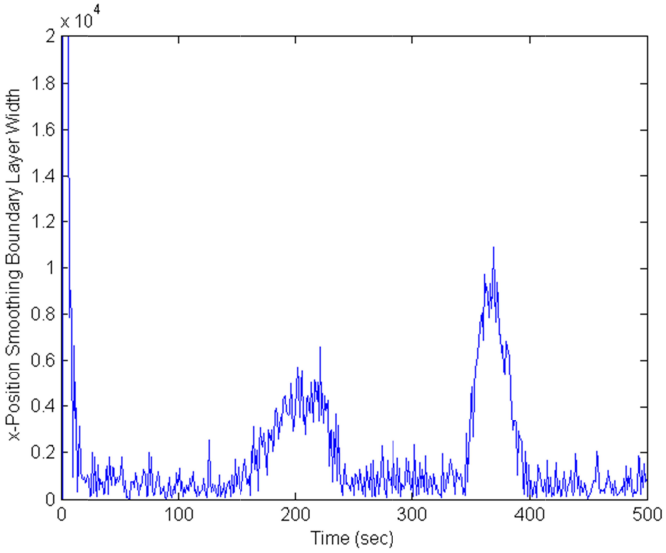

Figure 5.3.5. x-Position Smoothing Boundary Layer ψ_{11}

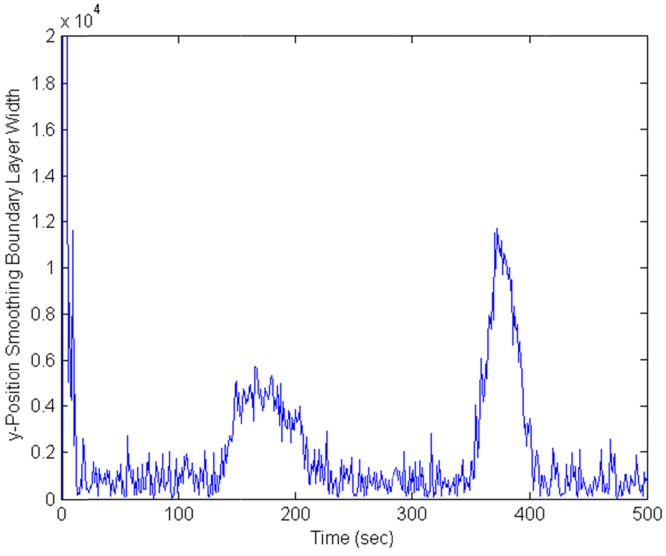

Figure 5.3.6. y-Position Smoothing Boundary Layer ψ_{22}

To further demonstrate the added benefits of combining the filtering strategies, consider the ATC scenario with erroneous measurements introduced half-way through the simulation (i.e., $z_{250} = 500\, z_{250}$). Note that this scenario could be avoided by measurement gating techniques; however, it will be used to study the robustness of the methods [28].

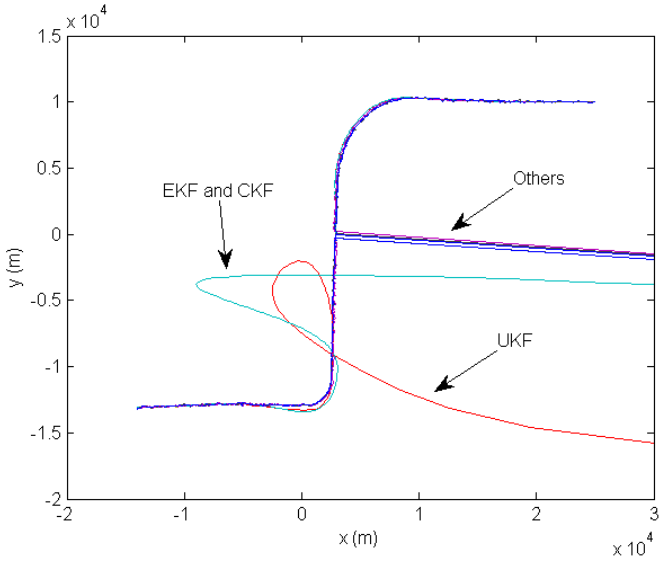

Figure 5.3.7. Estimated Trajectory with Erroneous Measurements (UM Model)

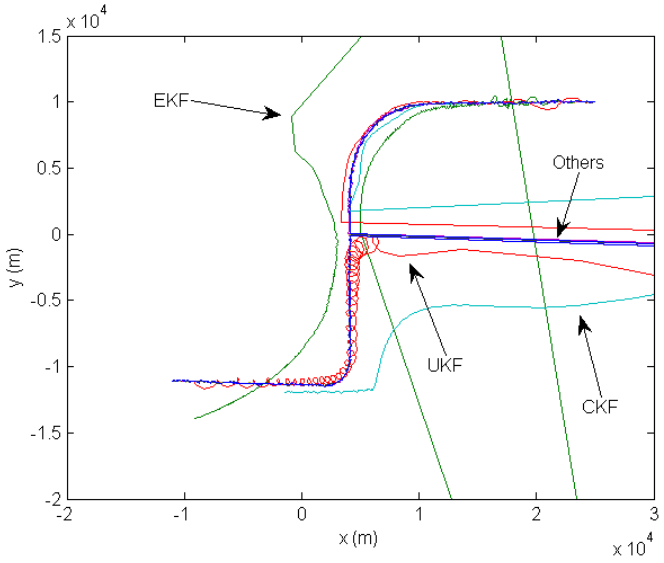

Figure 5.3.8. Estimated Trajectory with Erroneous Measurements (CT Model)

The previous two figures illustrate the estimation results for both the uniform motion and coordinated turn models. The effect of the erroneous measurement is clearly visible. Although all of the filtering strategies remain stable, the recovery time is significantly different. The SVSF, EK-SVSF, UK-SVSF, and CK-SVSF methods utilize the chattering effect of the SVSF gain; which helps keep the estimates bounded to within a region of the true state trajectory. The SVSF chattering effect allows the combined estimation strategies to yield good estimates at the inception of the poor measurement after only 2 or 3 samples. For the uniform motion model case, the UKF recovered in about 35 samples. The EKF and CKF performed the worse, and required about 125 samples to regain the proper target track and yield good state estimates. For the coordinated turn model case, at the inception of the poor measurement, the EKF failed to yield a good estimate of the target. However, the UKF and CKF eventually recovered, but took a significant amount of time.

5.4 Summary

This chapter presented a novel form of the SVSF that implemented a time-varying smoothing boundary layer (VBL), which was derived based on the covariance derivation presented in Chapter 4. For linear systems, it was demonstrated mathematically and on a computer experiment that the VBL formulation yielded the optimal KF gain. It was found that a secondary benefit of the VBL included the ability to detect changes in the system. A methodology was presented based on the VBL which allowed the SVSF to be combined with other nonlinear estimation strategies, such as the EKF, UKF, and CKF. The results were tested and compared on a target tracking problem. The resulting filters (EK-SVSF, UK-SVSF, and CK-SVSF) were found to be more accurate and robust compared with their standalone counterparts. There are two noteworthy drawbacks of the VBL approach. The first involves numerical stability issues that can be caused by dividing by zero, leading to computational and round-off errors. Secondly, the VBL derivation was based on the assumption that the measurement matrix is square. However, this is not always the case. A method presented in [37] and [120] was implemented which creates 'artificial' measurements that allow a full measurement matrix to be created and utilized.

Chapter 6

Interacting Multiple Model Form of the SVSF

This chapter presents a novel interacting multiple model (IMM) strategy based on the SVSF, referred to as the IMM-SVSF. This strategy makes use of the covariance derivation presented earlier in Chapter 4. The new IMM-SVSF method is applied on two applications. The first involves a target tracking computer experiment, based on a state trajectory built from a GPS tracker. The second application involves fault detection and diagnosis of an actual electrohydrostatic actuator (EHA) built for experimentation. The fault detection case made use of three models: normal system, friction fault, and leakage fault. The models were obtained through system identification as well as mathematically modeling the EHA. The results of the IMM-SVSF are compared with the popular KF based IMM (referred to as the IMM-KF).

6.1 Formulation of the IMM-SVSF

As presented earlier in Chapter 2, the interacting multiple model (IMM) strategy makes use of a finite number of models, and is associated with filters that run in parallel. The output from each filter includes the state estimate, the covariance, and the likelihood calculation (which is a function of the measurement error and innovation covariance). The output from the filters is used to calculate mode probabilities, which gives an indication of how close the filter model is to the true model. The IMM has been shown to work significantly better than single model methods, since it is able to make use of more information [28]. It also works extremely well for standard estimation problems such as target tracking, where there are typically two models used to capture the target's trajectory (i.e., uniform motion or coordinated turn) [28].

The motivation for combining the IMM with the SVSF is simple. The SVSF provides an estimation process that is sub-optimal albeit stable. Therefore, utilizing a multiple model (MM) strategy which increases the overall accuracy of the estimation process is beneficial. Furthermore, there was a certain amount of research curiosity present in how the SVSF would perform compared with the KF in terms of model detection probability. The IMM strategy utilizes covariance outputs from the filter; as such, the IMM-SVSF method builds on the results of Chapter 4.

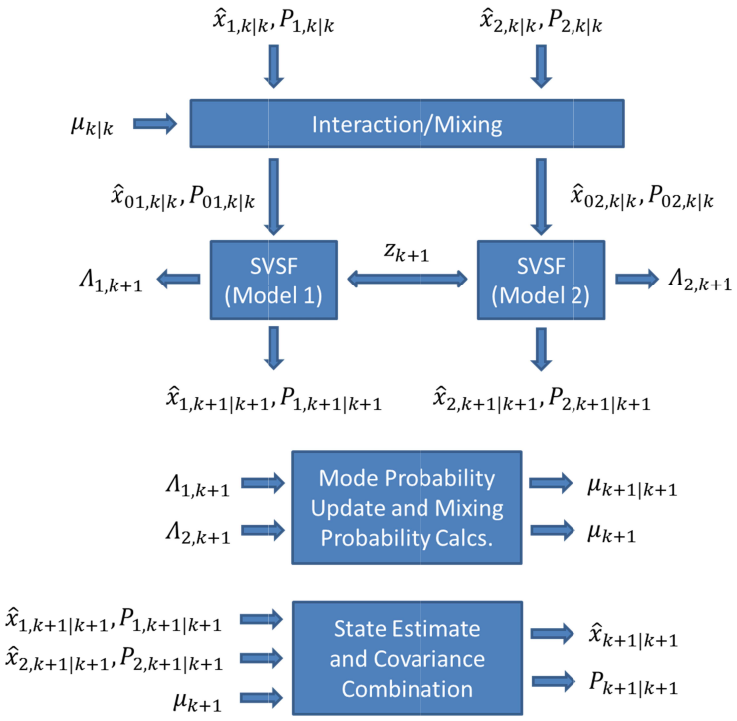

Figure 6.1.1. IMM-SVSF Strategy (Adapted from [28])

The IMM was implemented as per [28], and was presented earlier in Chapter 2. Some portions will be repeated here to help describe the IMM-SVSF strategy. The concept is shown in the above figure. Essentially, the SVSF estimation strategy may be applied on a finite number of models. As an example, the above figure shows two models. The IMM-SVSF estimator consists of five main steps: calculation of the mixing probabilities, mixing stage, mode-matched filtering via the SVSF, mode probability update, and state estimate and covariance combination.

The first step involves calculating the mixing probabilities $\mu_{i|j,k|k}$ (i.e., the probability of the system currently in mode i, and switching to mode j at the next step). These are calculated using the following two equations [28]:

$$\mu_{i|j,k|k} = \frac{1}{\bar{c}_j} p_{ij} \mu_{i,k} \tag{6.1.1}$$

$$\bar{c}_j = \sum_{i=1}^{r} p_{ij}\, \mu_{i,k} \tag{6.1.2}$$

Recall that p_{ij} refers to the mode transition probabilities, and is a designer parameter. Note that $\mu_{i,k}$ refers to the probability of the mode i being correct (with values between 0 and 1), and differs from the mixing probabilities $\mu_{i|j,k|k}$. This notation is standard, and is found in [28]. The mixing probabilities $\mu_{i|j,k|k}$ are used in the mixing stage, next. In addition to the mixing probabilities, the previous mode-matched states $\hat{x}_{i,k|k}$ and covariance's $P_{i,k|k}$ are also used to calculate the mixed initial conditions (states and covariance) for the filter matched to M_j (which consists of A_j and B_j). The mixed initial conditions are found respectively as follows [28]:

$$\hat{x}_{0j,k|k} = \sum_{i=1}^{r} \hat{x}_{i,k|k} \mu_{i|j,k|k} \tag{6.1.3}$$

$$P_{0j,k|k} = \sum_{i=1}^{r} \mu_{i|j,k|k} \left\{ P_{i,k|k} + \left(\hat{x}_{i,k|k} - \hat{x}_{0j,k|k}\right)\left(\hat{x}_{i,k|k} - \hat{x}_{0j,k|k}\right)^T \right\} \tag{6.1.4}$$

The next step involves mode-matched filtering via the SVSF, which involves using (6.1.3) and (6.1.4) as inputs to the SVSF matched to M_j. Each SVSF also uses the measurement z_{k+1} and input to the system u_k (if any), and calculates the corresponding updated state estimates (6.1.10) and corresponding covariance (6.1.11). Adapted from Chapter 4, the modified prediction stage (for linear systems) is as follows. The state estimates $\hat{x}_{0j,k|k}$ (6.1.3) and corresponding covariance $P_{0j,k|k}$ (6.1.4) for each model j are used to predict the state estimate $\hat{x}_{j,k+1|k}$ (6.1.5) and calculate the a priori state error covariance matrix $P_{j,k+1|k}$ (6.1.6).

$$\hat{x}_{j,k+1|k} = A_j \hat{x}_{0j,k|k} + B_j u_k \tag{6.1.5}$$

$$P_{j,k+1|k} = A_j P_{k|k}^{0j} A_j^T + Q_k \tag{6.1.6}$$

From (6.1.5) and (6.1.6), the mode-matched innovation covariance $S_{j,k+1|k}$ (6.1.7) and mode-matched a priori measurement error $e_{j,z,k+1|k}$ (6.1.8) are calculated.

$$S_{j,k+1|k} = C_j P_{j,k+1|k} C_j^T + R_{k+1} \tag{6.1.7}$$

$$e_{j,z,k+1|k} = z_{k+1} - C_j \hat{x}_{j,k+1|k} \tag{6.1.8}$$

The update stage is defined by the following four equations. The mode-matched SVSF gain $K_{j,k+1}$ is calculated (6.1.9) and used to update the state estimates $\hat{x}_{j,k+1|k+1}$ (6.1.10).

$$\begin{aligned} K_{j,k+1} = C_j^+ diag \Big[\Big(\big| e_{j,z,k+1|k} \big|_{Abs} + \gamma_j \big| e_{j,z,k|k} \big|_{Abs} \Big) \\ \circ sat\big(\bar{\psi}_j^{-1} e_{j,z,k+1|k} \big) \Big] diag\big(e_{j,z,k+1|k} \big)^{-1} \end{aligned} \tag{6.1.9}$$

$$\hat{x}_{j,k+1|k+1} = \hat{x}_{j,k+1|k} + K_{j,k+1} e_{j,z,k+1|k} \tag{6.1.10}$$

The corresponding state error covariance matrix $P_{j,k+1|k+1}$ is then calculated (6.1.11) and the a posteriori measurement error $e_{j,z,k+1|k+1}$ may be found (6.1.12).

$$P_{j,k+1|k+1} = \big(I - K_{j,k+1} C_j \big) P_{j,k+1|k} \big(I - K_{j,k+1} C_j \big)^T + K_{j,k+1} R_{k+1} K_{j,k+1}^T \tag{6.1.11}$$

$$e_{j,z,k+1|k+1} = z_{k+1} - C_j \hat{x}_{j,k+1|k+1} \tag{6.1.12}$$

Based on the mode-matched innovation matrix $S_{j,k+1|k}$ (6.1.7) and the mode-matched a priori measurement error $e_{j,z,k+1|k}$ (6.1.8), a corresponding mode-matched likelihood function $\Lambda_{j,k+1}$ based on the SVSF estimation method may be calculated, as follows [28]:

$$\Lambda_{j,k+1} = \mathcal{N}\big(z_{k+1}; \hat{z}_{j,k+1|k}, S_{j,k+1} \big) \tag{6.1.13}$$

Equation (6.1.13) may be solved as follows [28,39]:

$$\Lambda_{j,k+1} = \frac{1}{\sqrt{\big| 2\pi S_{j,k+1} \big|_{Abs}}} exp\left(\frac{-\frac{1}{2} e_{j,z,k+1|k}^T e_{j,z,k+1|k}}{S_{j,k+1}} \right) \tag{6.1.14}$$

Utilizing the mode-matched likelihood functions $\Lambda_{j,k+1}$, the mode probability $\mu_{j,k}$ may be updated by [28]:

$$\mu_{j,k} = \frac{1}{c}\Lambda_{j,k+1}\sum_{i=1}^{r} p_{ij}\,\mu_{i,k} \tag{6.1.15}$$

Where the normalizing constant is defined as [28]:

$$c = \sum_{j=1}^{r}\Lambda_{j,k+1}\sum_{i=1}^{r} p_{ij}\,\mu_{i,k} \tag{6.1.16}$$

Finally, the overall IMM-SVSF state estimates $\hat{x}_{k+1|k+1}$ (6.1.17) and corresponding covariance $P_{k+1|k+1}$ (6.1.17) are calculated.

$$\hat{x}_{k+1|k+1} = \sum_{j=1}^{r}\mu_{j,k+1}\hat{x}_{j,k+1|k+1} \tag{6.1.17}$$

$$\begin{aligned} P_{k+1|k+1} = \sum_{j=1}^{r}\mu_{j,k+1}\Big\{&P_{j,k+1|k+1} \\ &+ \big(\hat{x}_{j,k+1|k+1} - \hat{x}_{k+1|k+1}\big)\big(\hat{x}_{j,k+1|k+1} - \hat{x}_{k+1|k+1}\big)^{T}\Big\} \end{aligned} \tag{6.1.18}$$

The formulation of the IMM-SVSF may be summarized by (6.1.1) through (6.1.18), where there are $i, j = 1, \ldots, r$ models. Note that (6.1.17) and (6.1.18) are used for output purposes only, and are not part of the algorithm recursions [28]. Furthermore, note that the IMM-KF strategy is the same process as above but (6.1.5) through (6.1.12) are replaced with the KF prediction and update equations.

For the remainder of this chapter, the IMM-SVSF and IMM-KF methods are applied on two applications: target tracking, and fault detection and diagnosis of an electrohydrostatic actuator. The results are then compared and discussed.

6.2 Target Tracking Application

This section discusses the application of the IMM-SVSF method on a computer experiment. The air traffic control scenario presented in Chapter 5 will be used here. However, in an effort to provide a more realistic target trajectory, a true state trajectory was generated using a GPS tracker on a vehicle. Artificial system and measurement noise are added in order to provide a more realistic target tracking scenario.

The following figure represents the true state trajectory for this application. A Ford Escape hybrid was driven from McMaster University to the east-end of Hamilton, along the escarpment. This path resulted in a number of turns, uniform directions, and varying velocities. A GPS data logger was used to plot the above path in Google Maps software. The true mode (i.e., uniform motion or coordinated turn) was generated from knowledge of this map. The sample rate for this scenario was $T = 1\ sec$. The relevant equations for this scenario include (5.3.4.1) through (5.3.4.11). To make the estimation problem more difficult, artificial system and measurement noise was added to the true states and measurements, respectively.

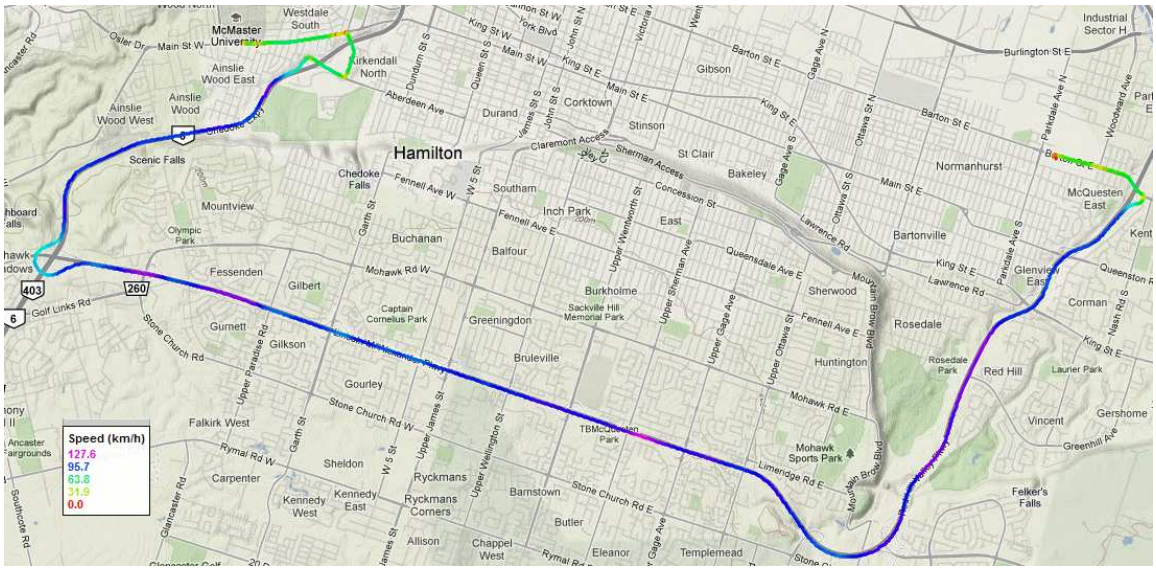

Figure 6.2.1. True State Trajectory for Target Tracking Computer Experiment

The system and measurement noise covariance matrices were defined by:

$$Q = L_1 \begin{bmatrix} \frac{T^3}{3} & 0 & \frac{T^2}{2} & 0 & 0 \\ 0 & \frac{T^3}{3} & 0 & \frac{T^2}{2} & 0 \\ \frac{T^2}{2} & 0 & T & 0 & 0 \\ 0 & \frac{T^2}{2} & 0 & T & 0 \\ 0 & 0 & 0 & 0 & \frac{L_2}{L_1}T \end{bmatrix} \tag{6.2.1}$$

$$R = 10^2 \begin{bmatrix} 1 & 0 \\ 0 & 1 \end{bmatrix} \tag{6.2.2}$$

Note that L_1 and L_2 are referred to as power spectral densities, and were defined as 0.16 and 0.01, respectively [130]. The system and measurement noise (w_k and v_k) were generated using their respective covariance values (Q and R), as per (1.1.3) and (1.1.4).

The initial states and their corresponding estimates were set to zero. The start is assumed to be at McMaster University (i.e., initial position). For the SVSF strategy, the constant smoothing boundary layer widths were defined as $\psi = [100 \quad 500 \quad 100 \quad 500 \quad 1]^T$, and the SVSF 'memory' or convergence rate was set to $\gamma = 0.1$. These parameters were tuned with the goal of decreasing the estimation error. Furthermore, note that the initial mode probability for both the IMM-KF and IMM-SVSF strategies was set to:

$$\mu_{i,0} = [0.75 \quad 0.25] \tag{6.2.3}$$

The mode transition matrix was defined by [28]:

$$p_{ij} = \begin{bmatrix} 0.95 & 0.05 \\ 0.05 & 0.95 \end{bmatrix} \tag{6.2.4}$$

The following figure shows the true state trajectory, along with the corresponding estimates which are fairly close to the true state trajectory, and thus appear overlapping.

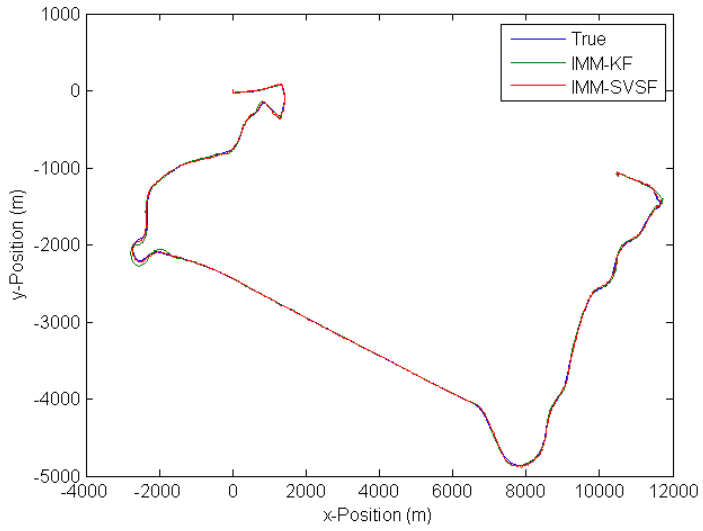

Figure 6.2.2. True and Estimated Target Trajectory

However, a noticeable difference occurs when the vehicle takes a sharp-turn (south west portion of the trajectory). The IMM-KF strategy is unable to accurately estimate the trajectory. The IMM-SVSF method is able to follow the true state trajectory more closely. The following table summarizes the RMSE results for the target tracking simulation. The IMM-SVSF strategy yielded a significant improvement for the position estimates (roughly 42%).

Table 6.2.1. RMSE Results for the Target Tracking Computer Experiment

Filter	Position (m)	Velocity (m/s)	Turn Rate (rad/s)
IMM-SVSF	15.79	6.01	0.001
IMM-KF	27.25	6.14	0.033

However, it is interesting to note that both methods performed relatively the same when estimating the target's velocity. As shown below, this is most likely due to the artificial velocity measurements, which were used to form a full measurement matrix.

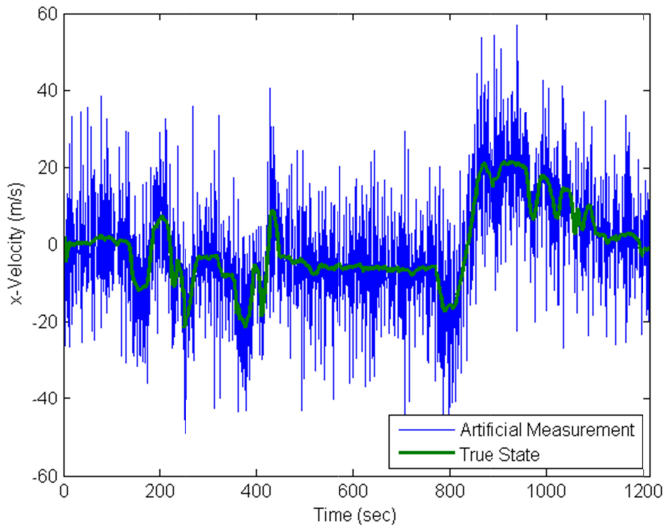

Figure 6.2.3. Artificial Measurement and True x-Velocity Values

The following figure shows the uniform motion mode probability, as calculated by the IMM-KF and IMM-SVSF strategies. Essentially, when the probability value is '1', the vehicle is traveling straight (or relatively straight). When the vehicle turns, this value switches to '0'.

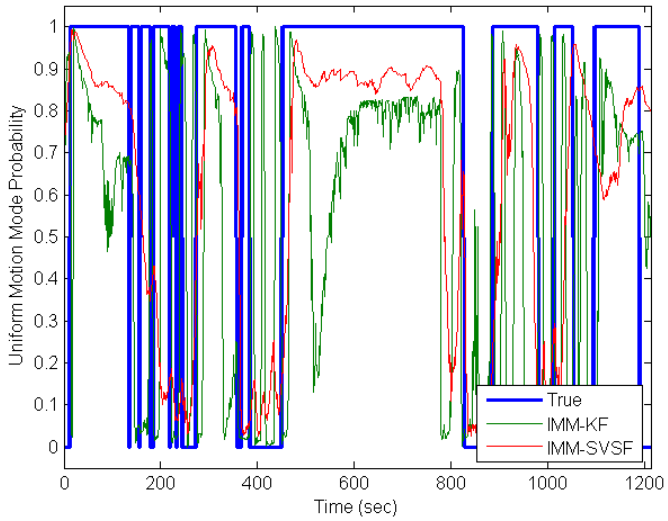

Figure 6.2.4. Uniform Motion Mode Probability

The true mode probability was calculated based on the available knowledge of the vehicle manoeuvres. The IMM strategy is a soft-switching approach, as demonstrated by the results. Overall, the IMM-SVSF strategy yields a more accurate mode probability calculation, when compared with the IMM-KF. This results in an improvement on the overall estimation accuracy. For example, consider the result around 500 seconds. For some period of time, the IMM-KF 'believes' that the vehicle is turning, when in fact it is traveling straight. This results in a less accurate model being implemented by the filter (coordinated turn vs. the uniform motion model), which reduces the overall estimation accuracy. Note that when the vehicle performs mode switches too frequently (i.e., between the time period of 150 to 250 seconds), both IMM strategies have difficulty determining the correct mode probability.

6.3 Fault Detection and Diagnosis Application

This section describes the results of applying the IMM-SVSF and the IMM-KF on an experimental setup for the purposes of fault detection and diagnosis. The experimental setup of the electrohydrostatic actuator is described, followed by methods for obtaining the desired system models. Finally, the results of applying the IMM-SVSF and IMM-KF are shown and discussed.

6.3.1 Experimental Setup

The experimental setup used in this thesis involved an electrohydrostatic actuator (EHA). An EHA is an emerging type of actuator typically used in the aerospace industry. EHAs are self-contained units comprised of their own pump, hydraulic circuit, and actuating cylinder [37]. The main components of an EHA include a variable speed motor, an external gear pump, an accumulator, inner circuitry check valves, a cylinder (or actuator), and a bi-directional pressure relief mechanism. The schematic of the EHA circuitry is shown in Appendix 8.6, as presented in [131]. The EHA can be divided into two subsystems. The first is the inner circuit that includes the accumulator and its surrounding check valves. The second is the high pressure outer circuit which performs the actuation. The inner circuit prevents cavitation which occurs when the inlet pressure reaches near vacuum pressures and provides make-up fluid for any dynamic leakage [37].

Mathematical modeling of the EHA has been performed and can be seen in detail in [37,132]. The EHA experimental setup was developed at McMaster University by Mr. Kevin McCullough, who is a recent M.A.Sc. graduate in the Department of Mechanical Engineering [133]. It is important to remind the reader that the experimental setup was used as a test-bed for the IMM-SVSF strategy; however, the EHA itself was not a part of this thesis research. The following figure shows the experimental setup of the EHA.

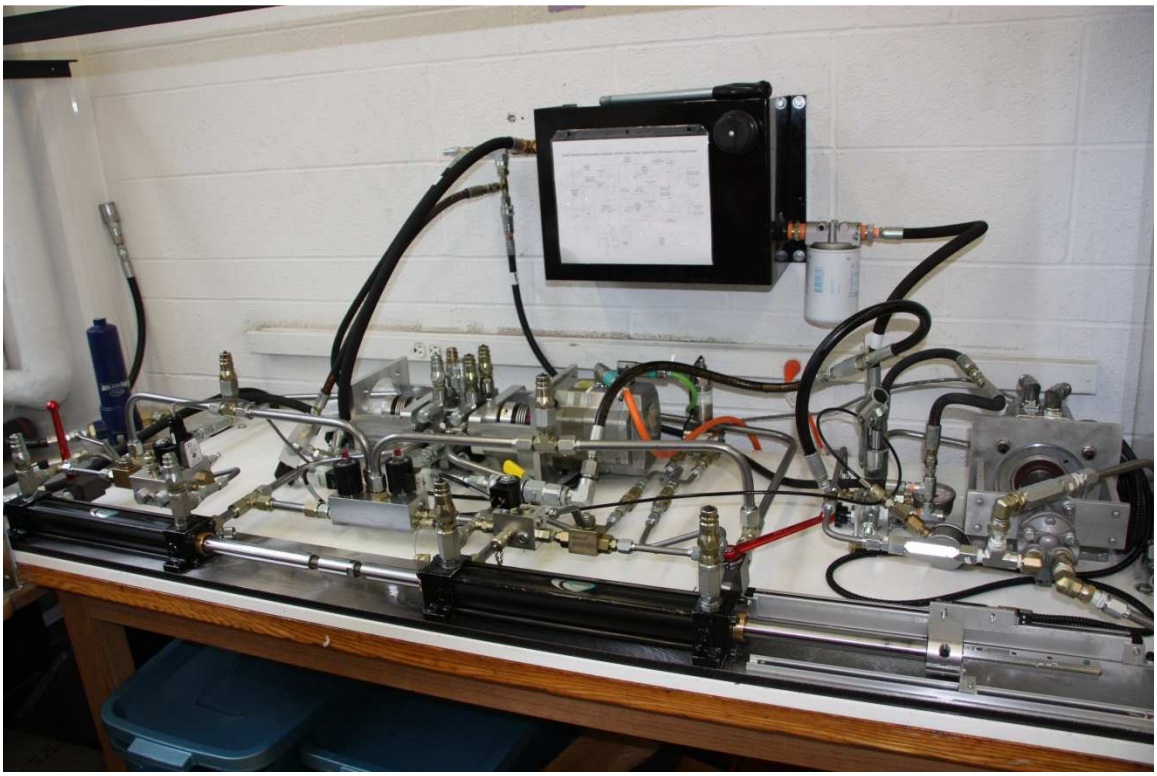

Figure 6.3.1. Experimental Setup of the EHA

In the above figure, the cylinder on the right (foreground) is referred to as Axis A and the cylinder connected to it on the left (foreground) is referred to Axis B. An optical linear encoder attached to Axis A is used to obtain position measurements (which are differentiated to obtain velocity measurements). The gear pump and electric motor are located in the rear (middle) of the table.

The electric motor drives the gear pump, which moves the hydraulic fluid throughout the circuit. A voltage input controls the direction and speed of the pump which affects the velocity of the cylinders (or actuators). This setup is a closed hydrostatic circuit [134]. More details on the design and setup of the EHA may be found in [128,131,133,134]. The computer and electrical cabinet are located off-camera to the right of the setup. The software used to communicate with the EHA setup is MATLAB's Real-Time Windows Target environment.

The two faults that were introduced to the EHA system were increased friction and internal leakage. To incur a friction fault, Axis A was used as the driving mechanism while Axis B acted as a load. To cause internal leakage, the Axis A throttling valve is used (where the Axis A throttle blocking valve is open). As the pump rotates, the Axis A throttling valve incurs cross-port leakage between both chambers of its corresponding cylinder. This action affects the output response of the cylinder.

In order to implement the IMM strategies, three models need to be obtained: normal system operation, and the presence of friction and leakage faults. These models may be obtained either by system identification or mathematical modeling. System identification was performed by Mr. Yu Song, who is currently an M.A.Sc. candidate studying with Dr. Saeid Habibi. For completeness, the results of his identified models are presented in Appendix 8.7. It was found that mathematically modeling the system led to more accurate results when implementing the IMM strategies.

6.3.2 Mathematical Models of the EHA System

A mathematical model for the EHA has been described in detail in [132,134,135]. For the purposes of this thesis, only the main transfer function will be explored. The EHA may be modeled as a third-order, type 1 linear system with state variables related to its position, velocity, and acceleration. The input to the system is the rotational speed of the pump ω_p, with typical units of rad/s. In this experimental setup, the sample rate of the system is $T = 1\,ms$. The significant dynamics of the system may be captured by the following third-order transfer function, obtained from [132]:

$$G_{EHA} = \frac{x}{\omega_p} = \frac{EHA_{Num}}{s^3 + EHA_{Den2}s^2 + EHA_{Den1}s} \tag{6.3.2.1}$$

Where:

$$EHA_{Num} = \frac{A_E D_P \beta_e}{MV_0} \tag{6.3.2.2}$$

$$EHA_{Den1} = \frac{B_E \beta_e L + A_E^2 \beta_e}{MV_0} \tag{6.3.2.3}$$

$$EHA_{Den2} = \frac{B_E V_0 + M\beta_e L}{MV_0} \tag{6.3.2.4}$$

Note that A_E refers to the piston cross-sectional area, B_E represents the load friction present in the system, β_e is the effective bulk modulus (i.e., the 'stiffness' in the hydraulic circuit), D_p refers to the pump displacement, L represents the leakage coefficient, M is the load mass (i.e., weight of the cylinders), and V_0 is the initial cylinder volume. The three main parameters that affect the EHA model are the pump displacement D_p, load friction B_E, and leakage coefficient L. For the three scenarios (normal, friction, and leakage), these parameters need to be determined in order to correctly mathematically model the EHA system. It is important to note that an input of $1\ V$ yields a pump rotation of about $300\ RPM$.

The following table lists the known EHA parameter values, experimentally determined in [133].

Table 6.3.1. EHA Parameter Values

Parameter	Physical Significance	EHA Model Value
A_E	Piston Area	$1.52 \times 10^{-3}\ m^2$
D_P	Pump Displacement	$6.876 \times 10^{-7}\ m^3/rad$
M	Load Mass	$7.376\ kg$
V_0	Initial Cylinder Volume	$2.1789 \times 10^{-4}\ m^3$
x_0	Maximum Cylinder Stroke	$0.14335\ m$
β_e	Effective Bulk Modulus	$2.1 \times 10^8\ Pa$

Three unknown EHA parameters (D_p, B_E, and L) were required in order to obtain mathematical models of the EHA under the three different scenarios (normal operation, and leakage and friction faults). Appendix 8.8 shows how these parameters were experimentally determined. The normal model, leakage model, and friction model are respectively defined as follows:

$$G_{EHA,Normal} = \frac{4{,}250}{s^2 + 3{,}901s + 410{,}250} \tag{6.3.2.5}$$

$$G_{EHA,Leakge} = \frac{4{,}250}{s^2 + 4{,}244s + 452{,}160} \tag{6.3.2.6}$$

$$G_{EHA,Friction} = \frac{3{,}138}{s^2 + 27{,}234s + 404{,}370} \tag{6.3.2.7}$$

Note that the EHA system has become a second-order system, where the input is voltage (V), and the output is the cylinder (Axis A) velocity (m/s).

6.3.3 Experimental Results

The results of applying the IMM-SVSF and IMM-KF are provided in this section. Before applying the methods for the purposes of fault detection and diagnosis, the continuous-time transfer functions of (6.3.2.5) through (6.3.2.7) are converted to discrete-time, with $T = 0.001\ s$. The discrete-time models for normal EHA operation, and the leakage and friction fault models are respectively as follows:

$$G_{EHA,Normal} = \frac{7.960 \times 10^{-4} z + 2.421 \times 10^{-4}}{z^2 - 0.920z + 2.022 \times 10^{-2}} \tag{6.3.3.1}$$

$$G_{EHA,Leakge} = \frac{7.489 \times 10^{-4} z + 2.093 \times 10^{-4}}{z^2 - 0.912z + 1.435 \times 10^{-2}} \tag{6.3.3.2}$$

$$G_{EHA,Friction} = \frac{1.103 \times 10^{-4} z + 4.175 \times 10^{-6}}{z^2 - 0.985z + 1.488 \times 10^{-12}} \tag{6.3.3.3}$$

In order to apply the IMM methods, the discrete-time transfer functions must be converted to state space representation. The corresponding system and input gain matrices for the normal EHA operation are found as follows:

$$A_{Normal} = \begin{bmatrix} 0.9200 & 1 \\ -0.0202 & 0 \end{bmatrix} \tag{6.3.3.4}$$

$$B_{Normal} = \begin{bmatrix} 7.960 \\ 2.421 \end{bmatrix} \times 10^{-4} \tag{6.3.3.5}$$

The system and input gain matrices for the leakage fault model are determined to be:

$$A_{Leakage} = \begin{bmatrix} 0.9124 & 1 \\ -0.0144 & 0 \end{bmatrix} \tag{6.3.3.6}$$

$$B_{Leakage} = \begin{bmatrix} 7.489 \\ 2.093 \end{bmatrix} \times 10^{-4} \tag{6.3.3.7}$$

Finally, the system and input gain matrices for the friction fault model may be found as follows:

$$A_{Friction} = \begin{bmatrix} 0.9853 & 1 \\ -1.4875 \times 10^{-12} & 0 \end{bmatrix} \tag{6.3.3.8}$$

$$B_{Friction} = \begin{bmatrix} 1.103 \\ 0.042 \end{bmatrix} \times 10^{-4} \tag{6.3.3.9}$$

According to the previous state space models, there are two states. Note that for the purposes of fault detection and diagnosis, the states (whether they are kinematic or not) have no bearing on the results, since one is mainly interested in the mode probability. Only the first state that corresponds to the velocity of the EHA cylinder (Axis A) is measured such that the measurement matrix (used by all three models) is defined as follows:

$$C = \begin{bmatrix} 1 & 0 \end{bmatrix} \tag{6.3.3.10}$$

An artificial measurement is derived in an effort to create a full measurement matrix (i.e., an identity), to be used by the SVSF method. Like before, the artificial measurement is created based on the available measurement and knowledge of the system model. As such, each model being used by the IMM will have its own respective artificial measurement based on the following:

$$y_{2,k+1} = A_{21} z_{1,k} + A_{22} y_{2,k} + B_{21} u_k \tag{6.3.3.11}$$

Note that the artificial measurement would have to be initialized (i.e., 0 is a typical value). Equation (6.3.3.11) essentially propagates the known measurements through the system model to obtain an artificial measurement for the second state. It is conceptually similar to the method presented in [120] and creates a full measurement matrix. To reiterate, the a priori measurement error would be calculated as follows:

$$e_{z,k+1|k} = \begin{bmatrix} z_1 \\ y_2 \end{bmatrix}_{k+1} - \hat{z}_{k+1|k} \tag{6.3.3.12}$$

The a posteriori measurement error is calculated in a similar fashion.

Furthermore, note that the system and measurement noise covariance's Q and R of the EHA experimental setup were required to implement the IMM-SVSF and IMM-KF. A number of methods exist in which one can attempt to statistically estimate these values [136,137,138]. However, it was determined that the measurement noise covariance R could be found from a segment of the measured signal, and the system noise covariance Q could be estimated and tuned to refine the results. Consider the following figure of a measurement segment.

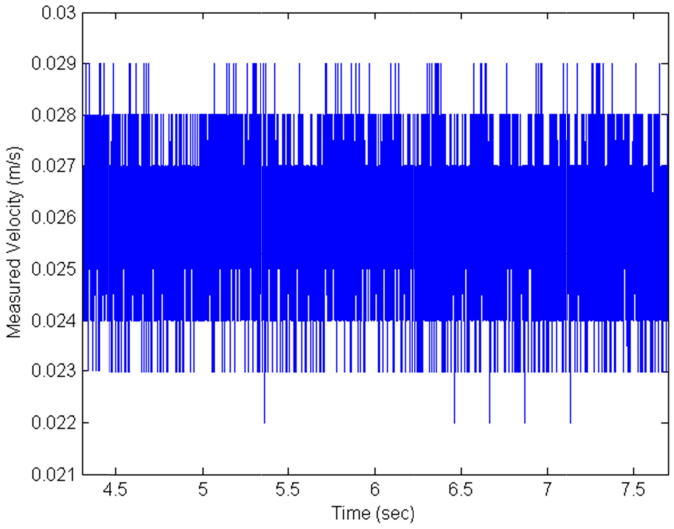

Figure 6.3.2. Segment of the Measurement

The measurement noise covariance may be found using MATLAB through the 'cov' (covariance) command. Alternatively, it may be calculated as follows:

$$R = \frac{(z_i - \bar{z})(z_i - \bar{z})^T}{z_m} = 2.12 \times 10^{-6} \tag{6.3.3.13}$$

Where z_i (a vector) refers to the i^{th} measurement sample, z_m refers to the number of samples in the measurement segment (3,401), and $\bar{z}$ is the measurement mean ($0.0259\ m/s$).

Next, the system noise covariance was determined. An initial estimate of the covariance was made based on earlier work performed on a different EHA [134]. From this starting place, the values were tuned in an effort to yield the best possible estimate for both the KF and the SVSF strategies. It is important to note that a considerable amount of effort was made to ensure a fair comparison between the two strategies. For the following experimental results, the system noise covariance was defined as follows:

$$Q = \begin{bmatrix} 5 \times 10^{-9} & 0 \\ 0 & 1 \times 10^{-7} \end{bmatrix} \tag{6.3.3.14}$$

The initial state estimates and state error covariance were respectively set to:

$$\hat{x}_{0|0} = [z_0 \quad 0]^T \tag{6.3.3.15}$$

$$P_{0|0} = \begin{bmatrix} 20 & 0 \\ 0 & 20 \end{bmatrix} \tag{6.3.3.16}$$

For the SVSF estimation process, the 'memory' or convergence rate was set to $\gamma = 0.1$, and the smoothing boundary layer widths were defined as $\psi = [0.25 \quad 5]^T$. These parameters were tuned based on minimizing the state estimation error. Furthermore, note that the initial mode probability $\mu_{i,0}$ for both the IMM-KF and IMM-SVSF strategies was set to:

$$\mu_{i,0} = [0.90 \quad 0.05 \quad 0.05] \tag{6.3.3.17}$$

It was assumed with a 90% probability that the EHA experienced normal operation at the start (and a 5% probability for each fault). The mode transition matrix p_{ij} was defined by:

$$p_{ij} = \begin{bmatrix} 0.90 & 0.05 & 0.05 \\ 0.05 & 0.90 & 0.05 \\ 0.05 & 0.05 & 0.90 \end{bmatrix} \tag{6.3.3.18}$$

This matrix is a designer parameter. It states, for example, that there is a 90% probability that the EHA will stay in mode 1 (normal operation) if it was in mode 1 at the current time step (i.e., $p_{11} = 0.90$). Furthermore, it also states that there is a 5% probability that the EHA will move to a different mode. For the EHA experimental setup, a sequential step signal with amplitude $\pm 2.5\ V$ (changing every 4 seconds) was inputted into the system, as follows.

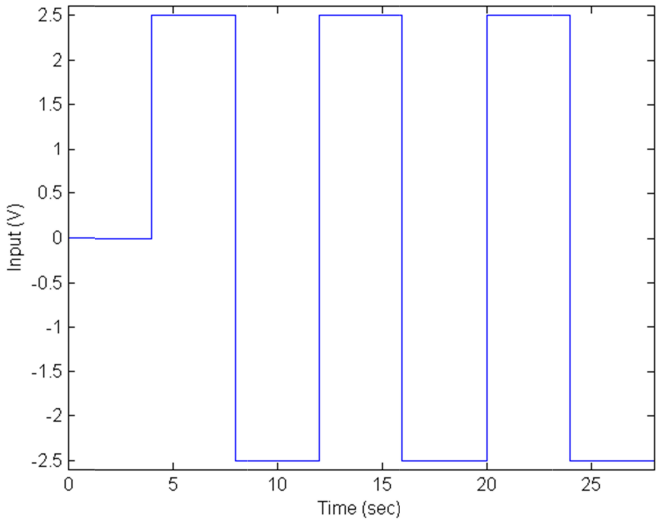

Figure 6.3.3. Sequential Step Input for the EHA

The operating modes for the EHA may be summarized with the following table.

Table 6.3.2. Operating Modes for the EHA Experimental Setup

Time (s)	EHA Mode
$0 - 12$	Normal Operation
$12 - 20$	Leakage Fault
$20 - 28$	Friction Fault

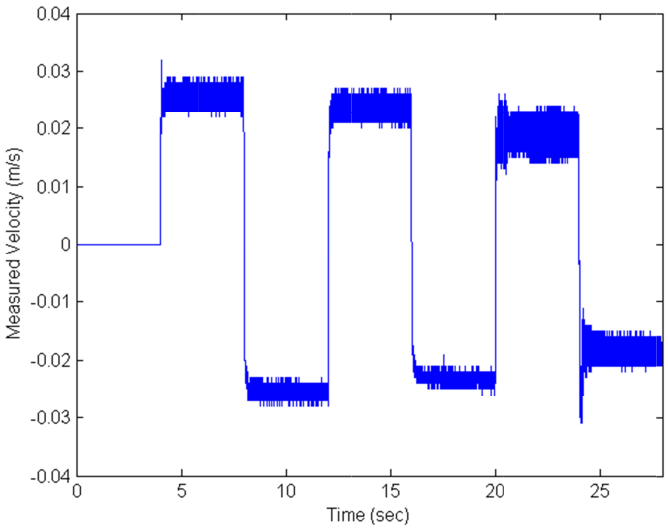

Figure 6.3.4. Unfiltered Measured Output from the EHA

The corresponding (unfiltered) system output is shown in the above figure. Recall that an encoder measured the position of the Axis A cylinder. This value was differentiated to obtain the 'measured' velocity, which resulted in a noisy signal. Two cases were studied on the EHA. For the first case, consider the input of Figure 6.3.3 and the unfiltered measurement of Figure 6.3.4. The second case includes the same input, but the measurement is filtered (using a zero-phase digital filter) in an effort to reduce the measurement noise.

Both the IMM-KF and IMM-SVSF strategies were implemented for each case. The estimated states and corresponding errors for the first case are shown in the following series of figures. Note that the actual 'true' state values were not available (i.e., they cannot be directly measured without any system or measurement noise). As such, the 'true' values were assumed to be calculated from the models used by the filtering strategies.

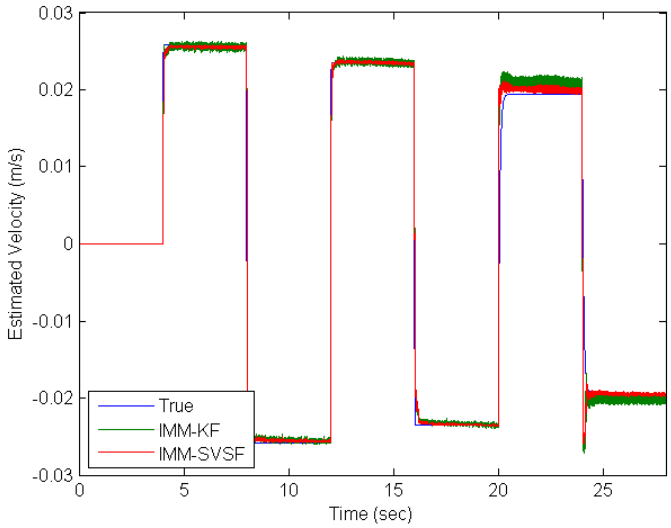

Figure 6.3.5. EHA 'True' Velocity and Estimates

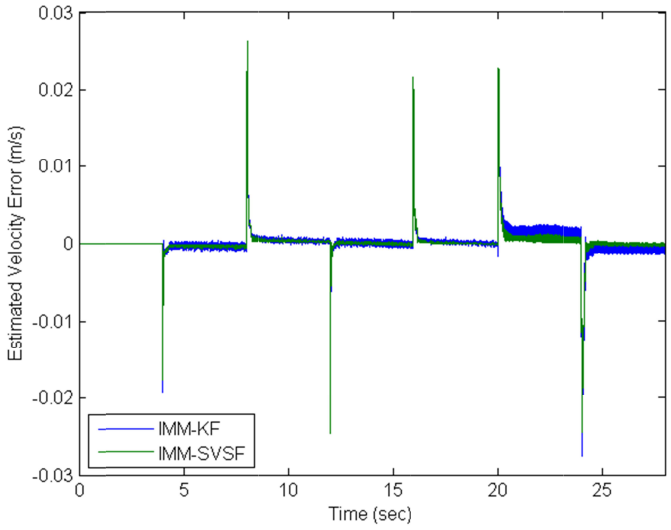

Figure 6.3.6. Errors for the EHA Velocity Estimates

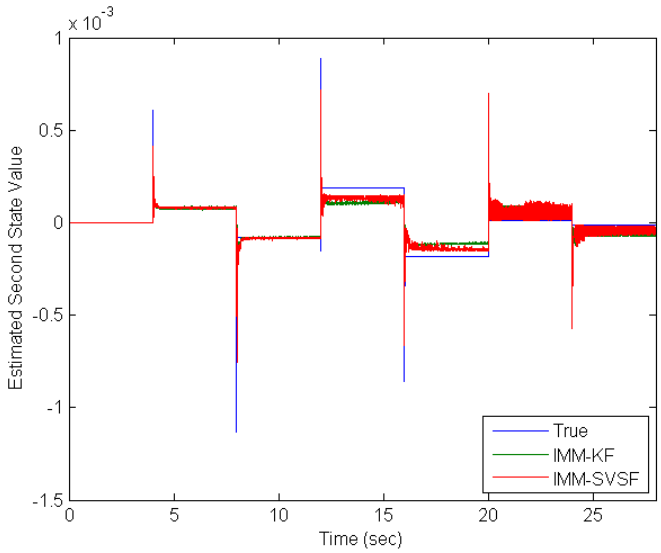

Figure 6.3.7. EHA 'True' Second State and Estimates

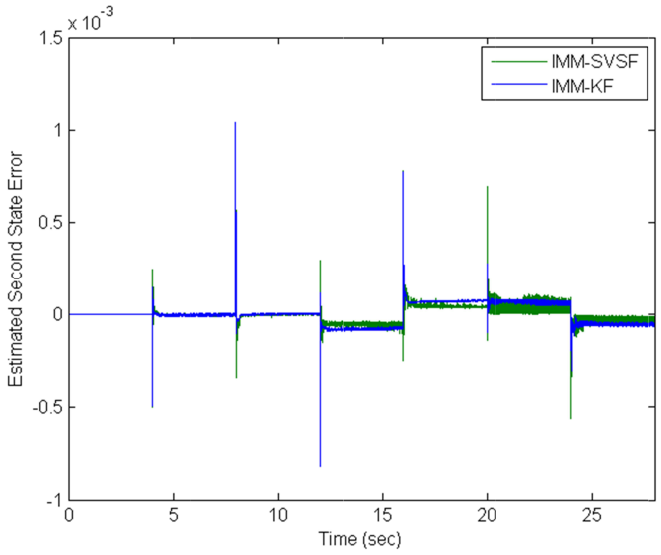

Figure 6.3.8. Errors for the EHA Second State Estimates

For this case, the RMSE was calculated and is summarized in the following table.

Table 6.3.3. RMSE Results for Sequential Step Input

Filter	Velocity (m/s)	Second State
IMM-SVSF	2.07×10^{-3}	4.50×10^{-5}
IMM-KF	2.19×10^{-3}	5.80×10^{-5}

In terms of estimation error, the IMM-SVSF method slightly outperformed the IMM-KF strategy. However, the ability to detect faults and successfully diagnosis them relies on the filters ability to calculate the mode probability. This value gives the user an indication of which mode is present in the EHA.

In the following three figures, a value of '1' refers to a mode probability of 100%, and a value of '0' refers to a mode probability of 0%.

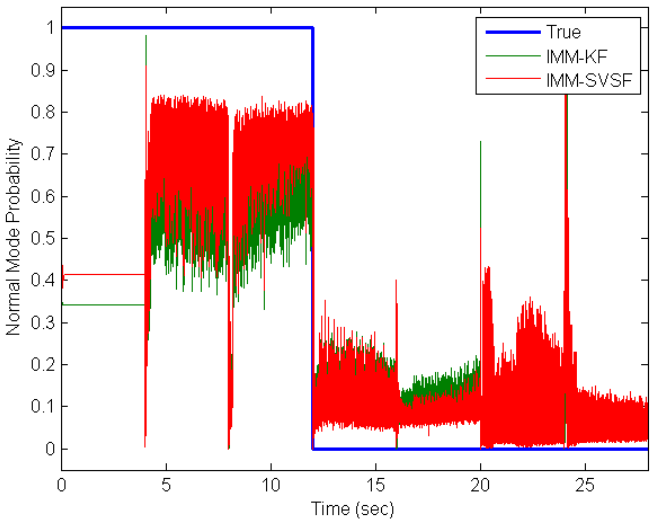

Figure 6.3.9. Normal Mode Probability for the EHA Fault Detection Experiment

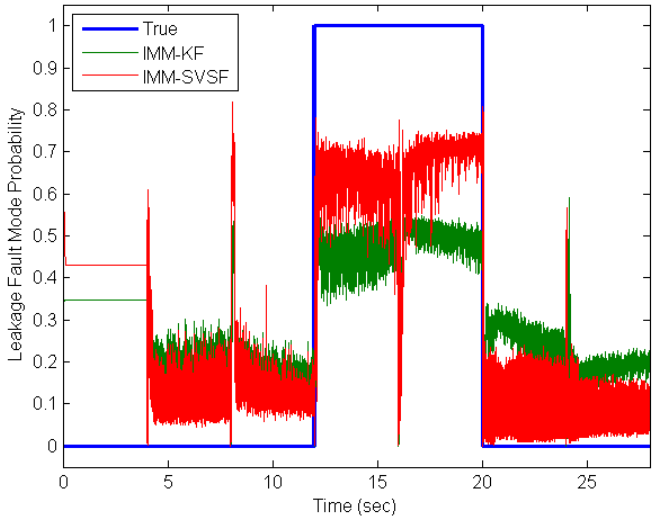

Figure 6.3.10. Leakage Fault Mode Probability for the EHA Fault Detection Experiment

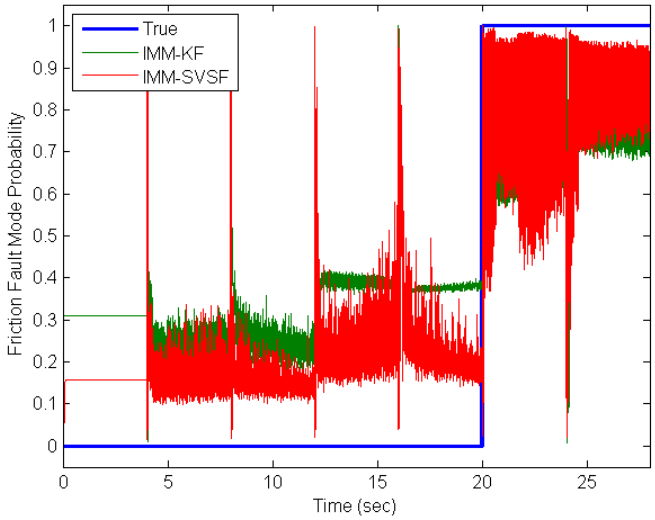

Figure 6.3.11. Friction Fault Mode Probability for the EHA Fault Detection Experiment

Both methods were able to successfully detect changes in the system, and to diagnosis the correct mode that the EHA was experiencing. However, as shown in the following tables, the IMM-SVSF strategy was able to diagnose the modes with a higher probability (about $10-20\%$). Consequently, the 'false detection' probability was lower for the IMM-SVSF than the IMM-KF strategy (i.e., detecting a fault when the EHA system was operating normally). Note that for the first four seconds, there was no input. Furthermore, the spikes present were due to the type of input (sequential step every 4 seconds), as well as the EHA velocity switching across $0\ m/s$. In this region, the three models yielded nearly indistinguishable results.

Table 6.3.4. IMM-KF Averaged Mode Probability Results

	Normal Detected	**Leak Detected**	**Friction Detected**
Normal Present	**58.49** %	16.75 %	24.75 %
Leak Present	13.51 %	**47.03** %	39.46 %
Friction Present	7.68 %	22.10 %	**70.22** %

Table 6.3.5. IMM-SVSF Averaged Mode Probability Results

	Normal Detected	**Leak Detected**	**Friction Detected**
Normal Present	**69.60** %	13.53 %	16.87 %
Leak Present	10.92 %	**64.22** %	24.86 %
Friction Present	8.64 %	9.26 %	**82.10** %

Note that both methods yielded noisy probability calculations due to the amount of noise present in the measurement. Therefore, out of curiosity, a simple digital filter (i.e., zero-phase filter) was added to reduce the amount of measurement noise. The measurement noise covariance was recalculated and was set to $R = 1.68 \times 10^{-8}$. The above experiments were then repeated for this case, and the results are reported as follows.

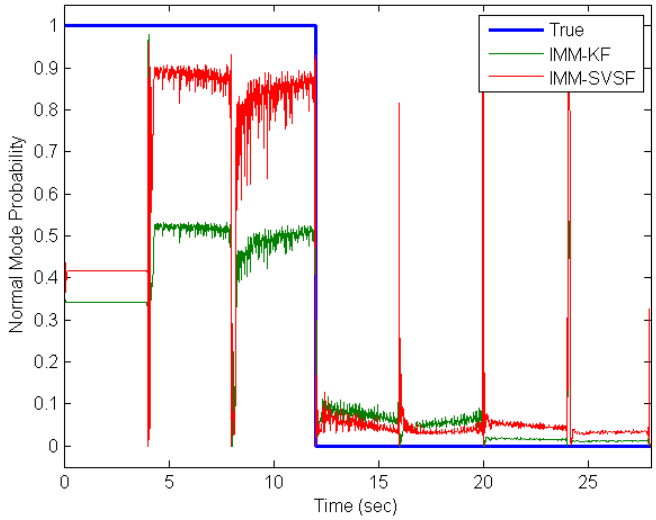

Figure 6.3.12. Normal Mode Probability with Filtered Measurements

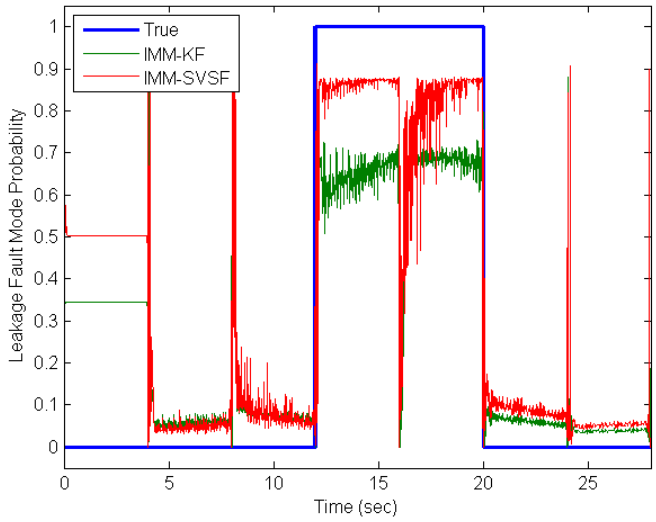

Figure 6.3.13. Leakage Mode Probability with Filtered Measurements

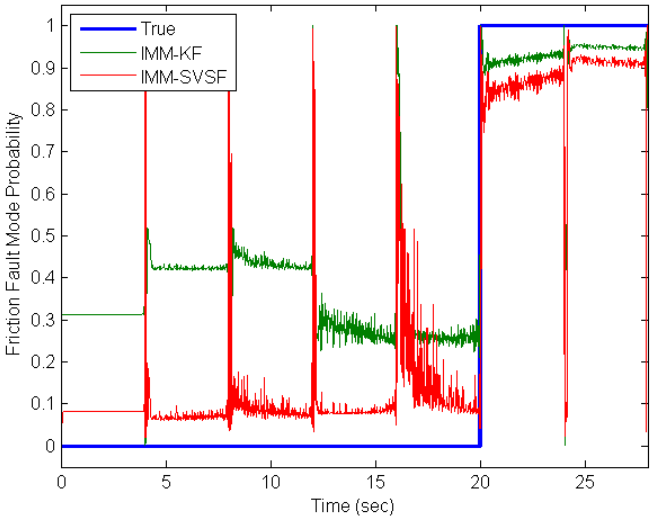

Figure 6.3.14. Friction Mode Probability with Filtered Measurements

The following table shows a summary of the RMSE results for both the IMM-SVSF and IMM-KF, when the measurements were filtered digitally.

Table 6.3.6. RMSE Results for Sequential Step Input (Filtered Measurements)

Filter	Velocity (m/s)	Second State
IMM-SVSF	2.14×10^{-3}	3.41×10^{-5}
IMM-KF	2.22×10^{-3}	4.35×10^{-5}

The estimation results for the velocity state did not change very much compared with the previous case. However, the second state was estimated more accurately, which is to be expected given the reduced measurement noise. The following tables summarize the averaged mode probability results for this case. It is interesting to note how a higher quality measurement improves the results of both IMM strategies. Future recommendations obviously therefore include a better and more suitable sensor to measure the velocity of the EHA cylinder.

Table 6.3.7. IMM-KF Averaged Mode Probability Results (Filtered Measurements)

	Normal Detected	**Leak Detected**	**Friction Detected**
Normal Present	**48.53** %	8.32 %	43.15 %
Leak Present	6.50 %	**64.46** %	29.04 %
Friction Present	2.25 %	5.31 %	**92.44** %

Table 6.3.8. IMM-SVSF Averaged Mode Probability Results (Filtered Measurements)

	Normal Detected	**Leak Detected**	**Friction Detected**
Normal Present	**82.70** %	8.48 %	8.82 %
Leak Present	4.83 %	**81.67** %	13.50 %
Friction Present	5.35 %	7.55 %	**87.10** %

Incorrect model detection was reduced significantly for both methods, as demonstrated by the off-diagonals in the above tables. However, the IMM-KF method had significant difficulty detecting the presence of the friction fault. For example, when the normal mode was present, the IMM-KF correctly identified it with 48.53%; however, it also detected a friction fault with 43.15%. This yields a difference of roughly 5%, which reduces the amount of confidence in correctly identifying the current mode being experienced by the EHA. The IMM-SVSF strategy was able to correctly detect and diagnosis all three modes with over 80% probability. The IMM-SVSF method outperformed the IMM-KF by 34.17% and 17.21% for the first and second mode, respectively. However, it is interesting to note that the IMM-KF yielded a slightly higher friction detection probability than the IMM-SVSF strategy. It is important to remind the reader that the aforementioned scenarios were specific to a certain linear region in the EHA (at $2.5\ V$), such that the developed mathematical models could be implemented. The actual experimental setup is nonlinear (unmodeled hydraulic dynamics, static friction, and so on) [134]. Developing nonlinear models to fit the entire EHA operating range and then applying the IMM strategies is beyond the scope of this thesis.

6.4 Summary

This chapter presented the development of a novel interacting multiple model (IMM) strategy based on the SVSF, referred to as the IMM-SVSF. This strategy makes use of the covariance derivation presented earlier in Chapter 4. The new IMM-SVSF method was applied on two applications. The first involved a target tracking computer experiment. In this case, the IMM-SVSF strategy yielded a significant improvement for the position estimates (roughly 42%) when compared with the popular IMM-KF method. Furthermore, the IMM-SVSF strategy was able to provide more accurate mode probabilities. For some period of time, the IMM-KF 'believes' that the vehicle is turning, when in fact it is traveling straight. This results in a less accurate model being implemented by the filter (coordinated turn vs. the uniform motion model), which reduces the overall estimation accuracy.

The second application involved fault detection and diagnosis of an actual electrohydrostatic actuator (EHA) built for experimentation. The fault detection case made use of three models: normal system, friction fault, and leakage fault. The models were obtained through system identification as well as mathematically modeling the EHA. The results of the IMM-SVSF were compared with the popular IMM-KF. The IMM-SVSF strategy generally outperformed the IMM-KF in terms of estimation accuracy and mode probability determination. The 'false detection' probability was found to be lower for the IMM-SVSF than the IMM-KF strategy (i.e., detecting a fault when the EHA system was operating normally). For the EHA application, it was recommended that a more accurate sensor be implemented in order to obtain better velocity measurements. This would significantly improve the results of both the IMM-SVSF and IMM-KF strategies.

Chapter 7

Concluding Remarks

This short chapter summarizes the major research performed and discussed in this thesis, and also includes recommendations for future work to continue and expand on the research.

7.1 Summary of Research

This research focused on advancing the development and implementation of the SVSF. To reiterate, the SVSF was introduced in 2007, and is based on variable structure theory and sliding mode concepts. It implements a switching gain to converge the estimates to within a boundary of the true states, referred to as the existence subspace. As demonstrated in literature, and reinforced throughout this thesis, the SVSF provides a robust and stable estimate to modeling uncertainties and errors. In its original form, the SVSF did not utilize a state error covariance matrix, which is a measure of the accuracy of the state estimates.

Therefore, the first major contribution of this research was to formulate an SVSF strategy with a covariance derivation. This created a number of research opportunities that could only be pursued and relied on the availability of the error covariance matrix. Chapter 4 presented and summarized the development of the SVSF covariance for both linear and nonlinear systems. A method that makes use of fourth-order moments was provided in Appendix 8.1. However, this method was too cumbersome and tedious to implement effectively. The SVSF update equation was modified in order to provide a simpler covariance derivation.

The covariance developed for the SVSF, for both linear and nonlinear systems, are similar to other popular Kalman filter strategies (KF, EKF, UKF, and CKF). However, it is important to note that the gain used to calculate the SVSF covariance remains different. Two computer experiments were studied in order to compare the results of the covariance values, and demonstrate the functionality of the equations. It was also shown that the values for the SVSF smoothing boundary layer play an important role in the estimation process. Note that the determination of the state error covariance matrix did not affect the SVSF estimation process. However, the SVSF estimation methods presented later in Chapters 5 and 6 would not be possible without the development of a state error covariance function.

A novel form of the SVSF that implemented a time-varying smoothing boundary layer (VBL) was presented in Chapter 5, and was derived based on the covariance derivation presented in Chapter 4. For linear systems, it was demonstrated mathematically and on a computer experiment that the VBL formulation yielded the optimal KF gain. In an effort to develop a robust linear estimation strategy, a new method was created based on the KF's optimality and on the SVSF's robustness. It was found that a secondary benefit of the VBL included the ability to detect changes in the system, based on changing widths. For example, when modeling uncertainty was present, the VBL width would grow larger in order to compensate for the increased modeling error. A methodology was presented based on the VBL which allowed the SVSF to be combined with other nonlinear estimation strategies, such as the EKF, UKF, and CKF. The results were tested and compared on a target tracking problem. The resulting filters (EK-SVSF, UK-SVSF, and CK-SVSF) were found to be more accurate and robust compared with their standalone counterparts. There are two noteworthy drawbacks of the VBL approach. The first involves numerical stability issues that can be caused by dividing by zero; however, this can be prevented with a simple if statement. Secondly, the VBL derivation was based on the assumption that the measurement matrix is square. When applicable, 'artificial' measurements can be used to create a full measurement matrix.

Based on the covariance derivation presented in Chapter 4, a novel interacting multiple model (IMM) strategy based on the SVSF was developed and presented in Chapter 6. The new method, referred to as the IMM-SVSF, was applied on two applications. The first involved a target tracking computer experiment based on a trajectory generated by a vehicle driven through Hamilton with a GPS data logger. Artificial system and measurement noises were added in an effort to make the simulation more realistic. The results of the IMM-SVSF strategy were compared with the popular IMM-KF method. The new strategy was found to outperform the IMM-KF method by nearly 42% in terms of position estimation accuracy. This is considered to be a significant improvement. However, note that both methods yielded relatively the same velocity estimate. It was determined that this was most likely due to the noisy artificial velocity measurements generated to help formulate a square measurement matrix.

The second application involved fault detection and diagnosis of an actual electrohydrostatic actuator (EHA) built for experimentation. The fault detection case made use of three models: normal system, friction fault, and leakage fault. The models were obtained through system identification as well as physical modeling of the EHA. The results of the IMM-SVSF were compared with the popular IMM-KF. Both methods were able to successfully detect changes in the system, and to diagnosis the correct mode that the EHA was experiencing. However, the IMM-SVSF strategy was able to diagnose the modes with a higher probability (about $10 - 20\%$). Consequently, the 'false detection' probability was lower for the IMM-SVSF than the IMM-KF strategy (i.e., detecting a fault when the EHA system was operating normally). Another case was performed with the presence of a digital filter to help reduce the measurement noise. For this case, the IMM-SVSF strategy was able to correctly detect and diagnosis all three modes with over 80% probability. The results of the IMM-KF strategy were also improved from the first case. However, there was a significant amount of 'false detection' probability for the friction model for the IMM-KF. This resulted in a loss of confidence (for the IMM-KF) in correctly identifying the current mode being experienced by the EHA.

7.2 Recommendations and Future Work

This thesis presented a number of improvements on the SVSF. However, since the SVSF is still a relatively new filter, a significant amount of research remains. The first recommendation for the work presented in this thesis involves the derivation for the time-varying smoothing boundary layer. A strict assumption for the derivation presented in Chapter 5 involved a square measurement matrix. This assumption allowed the derivation to be simpler, since taking the 'pseudoinverse' of the measurement matrix could be avoided. Future studies should involve looking at this derivation, and attempting to derive an appropriate VBL calculation for non-square measurement matrices. This is important since most estimation problems do not have measurements associated with each state. Furthermore, it may not always be possible to calculate an appropriate 'artificial' measurement.

For the EHA application, it was recommended that a more accurate sensor be implemented in order to obtain better velocity measurements. This would significantly improve the results of both the IMM-SVSF and IMM-KF strategies. Furthermore, it is important to reiterate that the fault detection and diagnosis scenarios were specific to a certain linear region in the EHA (at $2.5\ V$), such that the developed mathematical models could be implemented. The actual experimental setup is nonlinear (unmodeled hydraulic dynamics, static friction, and so on). Developing nonlinear models to fit the entire EHA operating range and then applying the IMM strategies was beyond the scope of this thesis. However, it is recommended that nonlinear models be studied such that both the IMM strategies may be applied and compared.

The first recommendation for new research involves creating a factored (or square-root) form of the SVSF. The covariance matrix can be broken up into factored terms, which are then propagated forward and updated at each measurement. The factors are multiplied together to reform the covariance matrix, thus ensuring it to be positive definite, while also helping to ensure numerical stability.

Another very important recommendation for future work involves the information form of the SVSF, or the smooth variable structure information filter (SVSIF). An information filter (IF) is one that propagates the inverse of the state error covariance, instead of using the normal covariance in the gain calculation. The term 'information' is based on the Cramer-Rao lower bound (CRLB), where the Fisher information matrix (FIM) is calculated as the inverse of the covariance matrix. There are certain advantages to using the information formulation of a filter. For example, if no prior information is available, one may initialize the information matrix using zeros such that no bias exists in the a priori estimate. Furthermore, the observational update of the information matrix is more robust than the covariance filter form, which makes it a more attractive method when a large number of measurements are available or when round-off errors may be an issue.

The ensemble Kalman filter (EnKF) is a recursive strategy that may be used for systems with a large number of states. It is recommended that an ensemble form of the SVSF be developed (referred to as the EnSVSF). Recently, the SVSF has been combined with artificial neural network (NN) strategies for fault detection and diagnosis [139]. For these scenarios, NNs require a significantly large number of states and measurements. It is recommended that the EnSVSF be developed for this particular application.

Finally, an adaptive SVSF is proposed, based on the adaptive KF. An adaptive filter is one that self-adjusts its system model in an effort to optimize the estimation result. It may also be used to determine system and measurement noise covariance's present in an experimental system. The adaptive method is of particular interest when the system model is not well defined. Furthermore, an adaptive SVSF may be of use when attempting to implement the SVSF strategy with cognitive systems applications.

Although the SVSF is a relatively new filter, it already demonstrates a number of advantages over current methodologies. The results of this thesis should provide a strong starting point for future advances to the SVSF.

Appendices

Index of Supplementary Material

This section provides extra information that was relevant to the overall research, however was omitted from the body of the thesis.

8.1 Proof of SVSF Stability

The following proof of stability for the SVSF is shown exactly as in [42], and has been added here only for completeness. The SVSF guarantees stability by making use of a Lyapunov stability condition [37]. According to Lyapunov stability theory, a Lyapunov function V is said to be stable if V is locally positive definite and the time derivative of V is locally negative semi-definite. Let V be a Lyapunov function defined in terms of the SVSF a posteriori estimation error, such that:

$$V = e_{z,k+1|k+1}^{T} e_{z,k+1|k+1} > 0 \tag{8.1.1}$$

According to Lyapunov stability theory, the estimation process is stable if the following is satisfied [42]:

$$\Delta V \leq 0 \tag{8.1.2}$$

Where ΔV represents the change in the Lyapunov function, and in this case, is defined as follows:

$$\Delta V = e_{z,k+1|k+1}^T e_{z,k+1|k+1} - e_{z,k|k}^T e_{z,k|k} \tag{8.1.3}$$

Substitution of (8.1.3) into (8.1.2), and rearranging, yields the following:

$$e_{z,k+1|k+1}^T e_{z,k+1|k+1} < e_{z,k|k}^T e_{z,k|k} \tag{8.1.4}$$

Equation (8.1.4) is equivalent to the following, which is the stability condition for the SVSF [37]:

$$\left|e_{z,k+1|k+1}\right|_{Abs} < \left|e_{z,k|k}\right|_{Abs} \tag{8.1.5}$$

To remove the absolute operator in (8.1.5), both sides are expressed in the form of diagonal matrices (i.e., $diag(e)$), as follows:

$$diag\left(e_{z,k+1|k+1}\right)diag\left(e_{z,k+1|k+1}\right) < diag\left(e_{z,k|k}\right)diag\left(e_{z,k|k}\right) \tag{8.1.6}$$

Assuming that the measurement function is well-defined (and it may be linearized as C), then the a posteriori measurement error may be calculated as:

$$e_{z,k+1|k+1} = Ce_{x,k+1|k+1} + v_{k+1} \tag{8.1.7}$$

Substitution of (8.1.7) into (8.1.6) yields:

$$\begin{pmatrix} diag\left(Ce_{x,k+1|k+1}\right)diag\left(Ce_{x,k+1|k+1}\right) \\ +diag(v_{k+1})diag(v_{k+1}) \\ +diag\left(Ce_{x,k+1|k+1}\right)diag(v_{k+1}) \\ +diag(v_{k+1})diag\left(Ce_{x,k+1|k+1}\right) \end{pmatrix} < \begin{pmatrix} diag\left(Ce_{x,k|k}\right)diag\left(Ce_{x,k|k}\right) \\ +diag(v_k)diag(v_k) \\ +diag\left(Ce_{x,k|k}\right)diag(v_k) \\ +diag(v_k)diag\left(Ce_{x,k|k}\right) \end{pmatrix} \tag{8.1.8}$$

If the measurement noise v_{k+1} is stationary white, then by taking the expectation of both sides in (8.1.8) and simplifying yields the following:

$$E\begin{bmatrix} diag\left(Ce_{x,k+1|k+1}\right)diag\left(Ce_{x,k+1|k+1}\right) \\ +diag(v_{k+1})diag(v_{k+1}) \end{bmatrix} < E\begin{bmatrix} diag\left(Ce_{x,k|k}\right)diag\left(Ce_{x,k|k}\right) \\ +diag(v_k)diag(v_k) \end{bmatrix} \tag{8.1.9}$$

Where $E\left[diag\left(Ce_{x,k+1|k+1}\right)diag(v_{k+1})\right]$ and $E\left[diag(v_k)diag\left(Ce_{x,k|k}\right)\right]$ vanish due to the white noise assumption. For a diagonal, positive and time-invariant measurement matrix, (8.1.9) becomes:

$$E\left[diag\left(e_{x,k+1|k+1}\right)diag\left(e_{x,k+1|k+1}\right)\right] < E\left[diag\left(e_{x,k|k}\right)diag\left(e_{x,k|k}\right)\right] \tag{8.1.10}$$

Note that the assumptions pertaining to the measurement matrix are realistic since most applications use linear sensors as feedback in their operations. Moreover, these sensors are well calibrated and their structures are well-known [37]. Finally, (8.1.10) becomes:

$$E\left(\left|e_{x,k+1|k+1}\right|_{Abs}\right) < E\left(\left|e_{x,k|k}\right|_{Abs}\right) \tag{8.1.11}$$

Equation (8.1.11) is the proof of stability for the SVSF. It states that the expectation of the a posteriori estimation error is reduced over time (i.e., converges towards a region of the state trajectory referred to as the existence subspace). It is important to reiterate that the above proof of stability for the SVSF was shown exactly as in [42], and has been added here only for completeness. Furthermore, the proof of stability may be used to derive the SVSF gain K_{k+1}^{SVSF}. Define γ to be a diagonal matrix with elements $0 < \gamma_{ii} \leq 1$, such that:

$$\left|e_{z,k|k}\right|_{Abs} > \gamma\left|e_{z,k|k}\right|_{Abs} \tag{8.1.12}$$

Adding the absolute value of the a priori measurement error $\left|e_{z,k+1|k}\right|_{Abs}$ to both sides of (8.1.12) yields:

$$\left|e_{z,k+1|k}\right|_{Abs} + \left|e_{z,k|k}\right|_{Abs} > \left|e_{z,k+1|k}\right|_{Abs} + \gamma\left|e_{z,k|k}\right|_{Abs} \tag{8.1.13}$$

The absolute value of the measurement matrix multiplied with the SVSF gain $\left|CK_{k+1}^{SVSF}\right|_{Abs}$ is set equal to the right side of (8.1.13), such that [42]:

$$\left|CK_{k+1}^{SVSF}\right|_{Abs} = \left|e_{z,k+1|k}\right|_{Abs} + \gamma\left|e_{z,k|k}\right|_{Abs} \tag{8.1.14}$$

Next, consider the following definition:

$$\left|CK_{k+1}^{SVSF}\right|_{Abs} = CK_{k+1}^{SVSF} \circ sign\left(CK_{k+1}^{SVSF}\right) \tag{8.1.15}$$

Furthermore, the sign of the measurement matrix multiplied with the SVSF gain CK_{k+1}^{SVSF} is set equal to the sign of the a priori measurement error $e_{z,k+1|k}$ [37,42]. This leads to the SVSF gain (with a $sign$ function), as follows:

$$K_{k+1}^{SVSF} = C^{+}\left(\left|e_{z,k+1|k}\right|_{Abs} + \gamma\left|e_{z,k|k}\right|_{Abs}\right) \circ sign\left(e_{z,k+1|k}\right) \tag{8.1.16}$$

Note that (8.1.16) satisfies and is derived from inequality (8.1.14), and for $0 < \gamma_{ii} \leq 1$ it satisfies (8.1.14) with the stability condition (8.1.5), as per [37,42].

8.2 Alternative Covariance Derivation for the SVSF

The following is an alternative proof for the a posteriori state error covariance $P_{k+1|k+1}$ used in the SVSF for linear systems. As shown, this derivation is rather involved and too complex to be implemented easily. However, it was included here for completeness, as it provides valuable insight into the SVSF and may be instrumental to devising new improved strategies. Note that the a priori state error covariance $P_{k+1|k}$ derivation is the same as that presented in Chapter 4. The a posteriori state error covariance matrix may be defined as follows:

$$P_{k+1|k+1} = E\left\{\tilde{x}_{k+1|k+1}\tilde{x}_{k+1|k+1}^{T}\right\} \tag{8.2.1}$$

Where the a posteriori state error may be defined by:

$$\tilde{x}_{k+1|k+1} = x_{k+1} - \hat{x}_{k+1|k+1} \tag{8.2.2}$$

The a posteriori state estimate may be described by the following equation:

$$\hat{x}_{k+1|k+1} = \hat{x}_{k+1|k} + K_{k+1} \tag{8.2.3}$$

Substitution of (8.2.3) into (8.2.2) yields:

$$\tilde{x}_{k+1|k+1} = x_{k+1} - \hat{x}_{k+1|k+1} - K_{k+1} \tag{8.2.4}$$

Simplifying (8.2.4) further yields the following a posteriori state error equation:

$$\tilde{x}_{k+1|k+1} = \tilde{x}_{k+1|k} - K_{k+1} \tag{8.2.5}$$

Recall the definition for the SVSF gain as follows:

$$K_{k+1} = C^{-1}\left(\left|e_{z,k+1|k}\right|_{Abs} + \gamma\left|e_{z,k|k}\right|_{Abs}\right) \circ sat\left(\frac{e_{z,k+1|k}}{\psi}\right) \tag{8.2.6}$$

Note that the a priori and previous a posteriori measurement errors may be written respectively as follows:

$$e_{z,k+1|k} = z_{k+1} - \hat{z}_{k+1|k} \tag{8.2.7}$$

$$e_{z,k|k} = z_k - \hat{z}_{k|k} \tag{8.2.8}$$

Furthermore, recall the following discrete measurement equations and their corresponding uncertain measurement estimates:

$$z_{k+1} = Cx_{k+1} + v_{k+1} \tag{8.2.9}$$

$$z_k = Cx_k + v_k \tag{8.2.10}$$

$$\hat{z}_{k+1|k} = \hat{C}\hat{x}_{k+1|k} \tag{8.2.11}$$

$$\hat{z}_{k|k} = \hat{C}\hat{x}_{k|k} \tag{8.2.12}$$

Substitution of (8.2.9) through (8.2.12) into (8.2.7) and (8.2.8) yields, respectively:

$$e_{z,k+1|k} = Cx_{k+1} + v_{k+1} - \hat{C}\hat{x}_{k+1|k} \tag{8.2.13}$$

$$e_{z,k|k} = Cx_k + v_k - \hat{C}\hat{x}_{k|k} \tag{8.2.14}$$

Finally, adding and subtracting $C\hat{x}_{k+1|k}$ to (8.2.13) and $C\hat{x}_{k+1|k}$ to (8.2.14) yields, respectively:

$$e_{z,k+1|k} = C\tilde{x}_{k+1|k} + \tilde{C}\hat{x}_{k+1|k} + v_{k+1} \tag{8.2.15}$$

$$e_{z,k|k} = C\tilde{x}_{k|k} + \tilde{C}\hat{x}_{k|k} + v_k \tag{8.2.16}$$

In general, for some value of a, the following is defined:

$$|a| = asign(a) \tag{8.2.17}$$

Based on (8.2.17), the SVSF gain (8.2.6) may be rewritten as follows:

$$K_{k+1} = C^{-1}\left(e_{z,k+1|k}sign\left(e_{z,k+1|k}\right) + \gamma e_{z,k|k}sign\left(e_{z,k|k}\right)\right) \circ sat\left(\frac{e_{z,k+1|k}}{\psi}\right) \tag{8.2.18}$$

The above saturation term is known to have three possible values:

$$sat\left(\frac{e_{z,k+1|k}}{\psi}\right) = \begin{cases} 1 & e_{z,k+1|k}/\psi \geq 1 \\ e_{z,k+1|k}/\psi & for \quad -1 < e_{z,k+1|k}/\psi < 1 \\ -1 & e_{z,k+1|k}/\psi \leq -1 \end{cases} \tag{8.2.19}$$

In order to attempt and find a generalization of the a posteriori state error covariance, one needs to study the cases (based on the SVSF gain) defined in Table 8.2.1. This is due to the fact that multiple scenarios may arise based on the sigmoidal or saturation functions. Also, note that for the listed cases it is assumed that there is no model mismatch (i.e., the measurement matrix is known), such that the a priori and previous a posteriori measurement errors may be written as follows:

$$e_{z,k+1|k} = C\tilde{x}_{k+1|k} + v_{k+1} \tag{8.2.20}$$

$$e_{z,k|k} = C\tilde{x}_{k|k} + v_k \tag{8.2.21}$$

It is the goal to solve for the a posteriori covariance equation for each of the 12 cases, and then attempt to find a generalized formulation. A general form was not found; however, it was determined that they all collapsed to two cases (inside and outside the boundary layer).

Table 8.2.1. Cases for the Alternative Updated Covariance Derivation

Case	$sign(e_{z,k+1\|k})$	$sign(e_{z,k\|k})$	$sat(e_{z,k+1\|k}/\psi)$	Possible
1	$+1$	$+1$	$+1$	Yes
2	$+1$	$+1$	$e_{z,k+1\|k}/\psi$	Yes
3	$+1$	$+1$	-1	No
4	$+1$	-1	$+1$	Yes
5	$+1$	-1	$e_{z,k+1\|k}/\psi$	Yes

Table 8.2.1. Cases for the Alternative Updated Covariance Derivation (Continued)

6	$+1$	-1	-1	No
7	-1	$+1$	$+1$	No
8	-1	$+1$	$e_{z,k+1\|k}/\psi$	Yes
9	-1	$+1$	-1	Yes
10	-1	-1	$+1$	No
11	-1	-1	$e_{z,k+1\|k}/\psi$	Yes
12	-1	-1	-1	Yes

Consider the first case, where there are positive measurement errors and upper saturation. For this case, the SVSF gain (8.2.18) becomes:

$$K_{k+1} = C^{-1}\left(e_{z,k+1|k} + \gamma e_{z,k|k}\right) \tag{8.2.22}$$

Substitution of (8.2.20) and (8.2.21) into (8.2.22) yields:

$$K_{k+1} = C^{-1}\left(C\tilde{x}_{k+1|k} + v_{k+1} + \gamma C\tilde{x}_{k|k} + \gamma v_k\right) \tag{8.2.23}$$

Substitution of (8.2.23) into the equation for the a posteriori state error (8.2.5) yields the following:

$$\tilde{x}_{k+1|k+1} = \tilde{x}_{k+1|k} - C^{-1}\left(C\tilde{x}_{k+1|k} + v_{k+1} + \gamma C\tilde{x}_{k|k} + \gamma v_k\right) \tag{8.2.24}$$

Simplifying (8.2.24) assuming that γ is a scalar:

$$\tilde{x}_{k+1|k+1} = -\gamma\tilde{x}_{k|k} - C^{-1}v_{k+1} - C^{-1}\gamma v_k \tag{8.2.25}$$

The transpose of (8.2.25) is written as follows:

$$\tilde{x}^T_{k+1|k+1} = -\tilde{x}^T_{k|k}\gamma^T - v^T_{k+1}C^{-T} - v^T_k\gamma^T C^{-T} \tag{8.2.26}$$

Multiplying (8.2.25) and (8.2.26) together (and ignoring the cross-terms that go to zero after the expectation) yields the following:

$$\tilde{x}_{k+1|k+1}\tilde{x}^T_{k+1|k+1} = \gamma\tilde{x}_{k|k}\tilde{x}^T_{k|k}\gamma^T + C^{-1}v_{k+1}v^T_{k+1}C^{-T} + C^{-1}\gamma v_k v^T_k\gamma^T C^{-T} \tag{8.2.27}$$

Finally, taking the expectation of (8.2.27) and simplifying yields an equation for the a posteriori state error covariance, for the first case:

$$P_{k+1|k+1} = \gamma P_{k|k} \gamma^T + C^{-1}(R_{k+1} + \gamma R_k \gamma^T) C^{-T} \tag{8.2.28}$$

In this case, it is shown that the a posteriori state error covariance $P_{k+1|k+1}$ is a function of the previous a posteriori state error covariance $P_{k|k}$, the measurement (output) model C, the SVSF parameter γ, and the measurement noise covariance R_k. The other cases (4, 9, and 12) remaining outside the saturation region yield the same solution (8.2.28). Therefore, when outside the smoothing boundary layer (i.e., a saturation of $+1$ or -1), it is proposed that (8.2.28) should be used to derive the updated covariance. Consider the second case of Table 8.2.1, where one has positive errors but within the saturation limits. For this case, the SVSF gain (8.2.18) becomes:

$$K_{k+1} = C^{-1}\left(e_{z,k+1|k} + \gamma e_{z,k|k}\right) \circ \left(\frac{e_{z,k+1|k}}{\psi}\right) \tag{8.2.29}$$

The above equation may be written as follows (to remove the Schur product):

$$\begin{aligned} K_{k+1} = {} & C^{-1}\big(diag(\psi)\big)^{-1} diag\big(e_{z,k+1|k}\big) e_{z,k+1|k} \\ & + C^{-1}\big(diag(\psi)\big)^{-1} diag(\gamma) diag\big(e_{z,k|k}\big) e_{z,k+1|k} \end{aligned} \tag{8.2.30}$$

Collecting like terms:

$$K_{k+1} = C^{-1}\big(diag(\psi)\big)^{-1} \Big(diag\big(e_{z,k+1|k}\big) + diag(\gamma) diag\big(e_{z,k|k}\big)\Big) e_{z,k+1|k} \tag{8.2.31}$$

Rewriting the diagonal terms in another notation for simplicity (with an over-bar):

$$K_{k+1} = C^{-1} \bar{\psi}^{-1}\big(\bar{e}_{z,k+1|k} + \bar{\gamma} \bar{e}_{z,k|k}\big) e_{z,k+1|k} \tag{8.2.32}$$

Recall that the a posteriori error (for no model mismatch) may be calculated as follows:

$$\tilde{x}_{k+1|k+1} = \tilde{x}_{k+1|k} - K_{k+1} \tag{8.2.33}$$

Substitution of (8.2.32) into (8.2.33) yields:

$$\tilde{x}_{k+1|k+1} = \tilde{x}_{k+1|k} - C^{-1}\bar{\psi}^{-1}\left(\bar{e}_{z,k+1|k} + \bar{\gamma}\bar{e}_{z,k|k}\right)e_{z,k+1|k} \tag{8.2.34}$$

Performing the transpose of (8.2.34), where the transpose of a diagonal of itself, yields:

$$\tilde{x}^T_{k+1|k+1} = \tilde{x}^T_{k+1|k} - e^T_{z,k+1|k}\left(\bar{e}_{z,k+1|k} + \bar{\gamma}\bar{e}_{z,k|k}\right)\bar{\psi}^{-1}C^{-T} \tag{8.2.35}$$

Furthermore, the a posteriori covariance function for this case is calculated by:

$$P_{k+1|k+1} = E\left\{\tilde{x}_{k+1|k+1}\tilde{x}^T_{k+1|k+1}\right\} \tag{8.2.36}$$

Hence, utilizing (8.2.34) and (8.2.35) yields:

$$\begin{aligned}\tilde{x}_{k+1|k+1}\tilde{x}^T_{k+1|k+1} &= \tilde{x}_{k+1|k}\tilde{x}^T_{k+1|k} - \tilde{x}_{k+1|k}e^T_{z,k+1|k}\left(\bar{e}_{z,k+1|k} + \bar{\gamma}\bar{e}_{z,k|k}\right)\bar{\psi}^{-1}C^{-T} \\ &- C^{-1}\bar{\psi}^{-1}\left(\bar{e}_{z,k+1|k} + \bar{\gamma}\bar{e}_{z,k|k}\right)e_{z,k+1|k}\tilde{x}^T_{k+1|k} \\ &+ C^{-1}\bar{\psi}^{-1}\left(\bar{e}_{z,k+1|k} + \bar{\gamma}\bar{e}_{z,k|k}\right)e_{z,k+1|k}e^T_{z,k+1|k}\left(\bar{e}_{z,k+1|k}\right. \\ &\left.+ \bar{\gamma}\bar{e}_{z,k|k}\right)\bar{\psi}^{-1}C^{-T}\end{aligned} \tag{8.2.37}$$

To continue with the derivation, the four main terms in (8.2.37) need to be solved by taking their corresponding expectations. This process is tedious and eventually yields 81 separate terms! However, note that a good proportion of the terms are found to be zero. To aid this process, consider the following assumptions and conditions:

$$\begin{aligned}E\left\{\tilde{x}_{k+1|k}w^T_{k+1}\right\} = E\left\{\tilde{x}_{k+1|k}v^T_{k+1}\right\} = E\left\{w_{k+1}v^T_{k+1}\right\} = E\left\{w_{k+1}w^T_k\right\} = E\left\{v_{k+1}v^T_k\right\} \\ = 0\end{aligned} \tag{8.2.38}$$

The task at this point is to expand and simplify the expectations of the four main terms of (8.2.37), which will then lead to a final solution. Taking the expectation of the first term in (8.2.37) yields:

$$E\left\{\tilde{x}_{k+1|k}\tilde{x}^T_{k+1|k}\right\} = P_{k+1|k} \tag{8.2.39}$$

Utilizing (8.2.20) and (8.2.21), the second main term in (8.2.37) becomes:

$$-\tilde{x}_{k+1|k}\left(\tilde{x}_{k+1|k}^{T}C^{T}+v_{k+1}^{T}\right)\left(\overline{C\tilde{x}}_{k+1|k}+\bar{v}_{k+1}+\bar{\gamma}\overline{C\tilde{x}}_{k|k}+\bar{\gamma}\bar{v}_{k}\right)\bar{\psi}^{-1}C^{-T} \tag{8.2.40}$$

Expanding the terms in (8.2.40) and solving for their corresponding expectation yields the following table of results.

Table 8.2.2. Expectations of the Second Main Term in (8.2.37)

Term	Expectations
(1)	$-E\{\tilde{x}_{k+1\|k}\tilde{x}_{k+1\|k}^{T}C^{T}\overline{C\tilde{x}}_{k+1\|k}\}\bar{\psi}^{-1}C^{-T}=-M_{3,1}\bar{\psi}^{-1}C^{-T}$ Where $M_{3,1}=E\{\tilde{x}_{k+1\|k}\tilde{x}_{k+1\|k}^{T}C^{T}\overline{C\tilde{x}}_{k+1\|k}\}$
(2)	$-E\{\tilde{x}_{k+1\|k}\tilde{x}_{k+1\|k}^{T}C^{T}\bar{v}_{k+1}\}\bar{\psi}^{-1}C^{-T}=0$
(3)	$-E\{\tilde{x}_{k+1\|k}\tilde{x}_{k+1\|k}^{T}C^{T}\bar{\gamma}\overline{C\tilde{x}}_{k\|k}\}\bar{\psi}^{-1}C^{-T}=-M_{3,2}\bar{\psi}^{-1}C^{-T}$ Where $M_{3,2}=E\{\tilde{x}_{k+1\|k}\tilde{x}_{k+1\|k}^{T}C^{T}\bar{\gamma}\overline{C\tilde{x}}_{k\|k}\}$
(4)	$-E\{\tilde{x}_{k+1\|k}\tilde{x}_{k+1\|k}^{T}C^{T}\bar{\gamma}\bar{v}_{k}\}\bar{\psi}^{-1}C^{-T}=0$
(5)	$-E\{\tilde{x}_{k+1\|k}v_{k+1}^{T}\overline{C\tilde{x}}_{k+1\|k}\}\bar{\psi}^{-1}C^{-T}=0$
(6)	$-E\{\tilde{x}_{k+1\|k}v_{k+1}^{T}\bar{v}_{k+1}\}\bar{\psi}^{-1}C^{-T}=0$
(7)	$-E\{\tilde{x}_{k+1\|k}v_{k+1}^{T}\bar{\gamma}\overline{C\tilde{x}}_{k\|k}\}\bar{\psi}^{-1}C^{-T}=0$
(8)	$-E\{\tilde{x}_{k+1\|k}v_{k+1}^{T}\bar{\gamma}\bar{v}_{k}\}\bar{\psi}^{-1}C^{-T}=0$

The third main term in (8.2.37) may be written as follows:

$$-C^{-1}\bar{\psi}^{-1}\left(\overline{C\tilde{x}}_{k+1|k}+\bar{v}_{k+1}+\bar{\gamma}\overline{C\tilde{x}}_{k|k}+\bar{\gamma}\bar{v}_{k}\right)\left(C\tilde{x}_{k+1|k}+v_{k+1}\right)\tilde{x}_{k+1|k}^{T} \tag{8.2.41}$$

Expanding the terms in (8.2.41) and solving for the expectations yields the following table.

Table 8.2.3. Expectations of the Third Main Term in (8.2.37)

Term	Expectations
(1)	$-C^{-1}\bar{\psi}^{-1}E\{\overline{C\tilde{x}}_{k+1\|k}C\tilde{x}_{k+1\|k}\tilde{x}_{k+1\|k}^{T}\}=-C^{-1}\bar{\psi}^{-1}M_{3,3}$ Where $M_{3,3}=E\{\overline{C\tilde{x}}_{k+1\|k}C\tilde{x}_{k+1\|k}\tilde{x}_{k+1\|k}^{T}\}$
(2)	$-C^{-1}\bar{\psi}^{-1}E\{\bar{v}_{k+1}C\tilde{x}_{k+1\|k}\tilde{x}_{k+1\|k}^{T}\}=0$
(3)	$-C^{-1}\bar{\psi}^{-1}E\{\bar{\gamma}\overline{C\tilde{x}}_{k\|k}C\tilde{x}_{k+1\|k}\tilde{x}_{k+1\|k}^{T}\}=-C^{-1}\bar{\psi}^{-1}M_{3,4}$ Where $M_{3,4}=E\{\bar{\gamma}\overline{C\tilde{x}}_{k\|k}C\tilde{x}_{k+1\|k}\tilde{x}_{k+1\|k}^{T}\}$
(4)	$-C^{-1}\bar{\psi}^{-1}E\{\bar{\gamma}\bar{v}_{k}C\tilde{x}_{k+1\|k}\tilde{x}_{k+1\|k}^{T}\}=0$
(5)	$-C^{-1}\bar{\psi}^{-1}E\{\overline{C\tilde{x}}_{k+1\|k}v_{k+1}\tilde{x}_{k+1\|k}^{T}\}=0$

Table 8.2.3. Expectations of the Third Main Term in (8.2.37) (Continued)

(6)	$-C^{-1}\bar{\psi}^{-1}E\{\bar{v}_{k+1}v_{k+1}\tilde{x}_{k+1\|k}^{T}\}=0$
(7)	$-C^{-1}\bar{\psi}^{-1}E\{\bar{\gamma}\overline{C\tilde{x}}_{k\|k}v_{k+1}\tilde{x}_{k+1\|k}^{T}\}=0$
(8)	$-C^{-1}\bar{\psi}^{-1}E\{\bar{\gamma}\bar{v}_{k}v_{k+1}\tilde{x}_{k+1\|k}^{T}\}=0$

Expanding the fourth main term of (8.2.37) yields the following:

$$C^{-1}\bar{\psi}^{-1}\big(\overline{C\tilde{x}}_{k+1|k}+\bar{v}_{k+1}+\bar{\gamma}\overline{C\tilde{x}}_{k|k}+\bar{\gamma}\bar{v}_{k}\big)\big(C\tilde{x}_{k+1|k}\tilde{x}_{k+1|k}^{T}C^{T}+C\tilde{x}_{k+1|k}v_{k+1}^{T}+v_{k+1}\tilde{x}_{k+1|k}^{T}C^{T}+v_{k+1}v_{k+1}^{T}\big)\big(\overline{C\tilde{x}}_{k+1|k}+\bar{v}_{k+1}+\bar{\gamma}\overline{C\tilde{x}}_{k|k}+\bar{\gamma}\bar{v}_{k}\big)\bar{\psi}^{-1}C^{-T} \tag{8.2.42}$$

Equation (8.2.42) leads to 64 (4^4) terms. Expectations were performed; leading to second, third, and fourth-order moments. The results are shown in the following table.

Table 8.2.4. Expectations of the Fourth Main Term in (8.2.37)

Term	Expectations
(1)	$C^{-1}\bar{\psi}^{-1}E\{\overline{C\tilde{x}}_{k+1\|k}C\tilde{x}_{k+1\|k}\tilde{x}_{k+1\|k}^{T}C^{T}\overline{C\tilde{x}}_{k+1\|k}\}\bar{\psi}^{-1}C^{-T}=C^{-1}\bar{\psi}^{-1}M_{4,1}\bar{\psi}^{-1}C^{-T}$ Where $M_{4,1}=E\{\overline{C\tilde{x}}_{k+1\|k}C\tilde{x}_{k+1\|k}\tilde{x}_{k+1\|k}^{T}C^{T}\overline{C\tilde{x}}_{k+1\|k}\}$
(2)	$C^{-1}\bar{\psi}^{-1}E\{\overline{C\tilde{x}}_{k+1\|k}C\tilde{x}_{k+1\|k}\tilde{x}_{k+1\|k}^{T}C^{T}\bar{v}_{k+1}\}\bar{\psi}^{-1}C^{-T}=0$
(3)	$C^{-1}\bar{\psi}^{-1}E\{\overline{C\tilde{x}}_{k+1\|k}C\tilde{x}_{k+1\|k}\tilde{x}_{k+1\|k}^{T}C^{T}\bar{\gamma}\overline{C\tilde{x}}_{k\|k}\}\bar{\psi}^{-1}C^{-T}=C^{-1}\bar{\psi}^{-1}M_{4,2}\bar{\psi}^{-1}C^{-T}$ Where $M_{4,2}=E\{\overline{C\tilde{x}}_{k+1\|k}C\tilde{x}_{k+1\|k}\tilde{x}_{k+1\|k}^{T}C^{T}\bar{\gamma}\overline{C\tilde{x}}_{k\|k}\}$
(4)	$C^{-1}\bar{\psi}^{-1}E\{\overline{C\tilde{x}}_{k+1\|k}C\tilde{x}_{k+1\|k}\tilde{x}_{k+1\|k}^{T}C^{T}\bar{\gamma}\bar{v}_{k}\}\bar{\psi}^{-1}C^{-T}=0$
(5)	$C^{-1}\bar{\psi}^{-1}E\{\overline{C\tilde{x}}_{k+1\|k}C\tilde{x}_{k+1\|k}v_{k+1}^{T}\overline{C\tilde{x}}_{k+1\|k}\}\bar{\psi}^{-1}C^{-T}=0$
(6)	$C^{-1}\bar{\psi}^{-1}E\{\overline{C\tilde{x}}_{k+1\|k}C\tilde{x}_{k+1\|k}v_{k+1}^{T}\bar{v}_{k+1}\}\bar{\psi}^{-1}C^{-T}=C^{-1}\bar{\psi}^{-1}M_{2,1}\bar{R}_{k+1}^{T}\bar{\psi}^{-1}C^{-T}$ Where $M_{2,1}=E\{\overline{C\tilde{x}}_{k+1\|k}C\tilde{x}_{k+1\|k}\}$
(7)	$C^{-1}\bar{\psi}^{-1}E\{\overline{C\tilde{x}}_{k+1\|k}C\tilde{x}_{k+1\|k}v_{k+1}^{T}\bar{\gamma}\overline{C\tilde{x}}_{k\|k}\}\bar{\psi}^{-1}C^{-T}=0$
(8)	$C^{-1}\bar{\psi}^{-1}E\{\overline{C\tilde{x}}_{k+1\|k}C\tilde{x}_{k+1\|k}v_{k+1}^{T}\bar{\gamma}\bar{v}_{k}\}\bar{\psi}^{-1}C^{-T}=0$
(9)	$C^{-1}\bar{\psi}^{-1}E\{\overline{C\tilde{x}}_{k+1\|k}v_{k+1}\tilde{x}_{k+1\|k}^{T}C^{T}\overline{C\tilde{x}}_{k+1\|k}\}\bar{\psi}^{-1}C^{-T}=0$
(10)	$C^{-1}\bar{\psi}^{-1}E\{\overline{C\tilde{x}}_{k+1\|k}v_{k+1}\tilde{x}_{k+1\|k}^{T}C^{T}\bar{v}_{k+1}\}\bar{\psi}^{-1}C^{-T}=C^{-1}\bar{\psi}^{-1}M_{2,2}\bar{\psi}^{-1}C^{-T}$ Where $M_{2,2}=E\{\overline{C\tilde{x}}_{k+1\|k}v_{k+1}\tilde{x}_{k+1\|k}^{T}C^{T}\bar{v}_{k+1}\}$
(11)	$C^{-1}\bar{\psi}^{-1}E\{\overline{C\tilde{x}}_{k+1\|k}v_{k+1}\tilde{x}_{k+1\|k}^{T}C^{T}\bar{\gamma}\overline{C\tilde{x}}_{k\|k}\}\bar{\psi}^{-1}C^{-T}=0$
(12)	$C^{-1}\bar{\psi}^{-1}E\{\overline{C\tilde{x}}_{k+1\|k}v_{k+1}\tilde{x}_{k+1\|k}^{T}C^{T}\bar{\gamma}\bar{v}_{k}\}\bar{\psi}^{-1}C^{-T}=0$
(13)	$C^{-1}\bar{\psi}^{-1}E\{\overline{C\tilde{x}}_{k+1\|k}v_{k+1}v_{k+1}^{T}\overline{C\tilde{x}}_{k+1\|k}\}\bar{\psi}^{-1}C^{-T}=C^{-1}\bar{\psi}^{-1}M_{2,3}\bar{\psi}^{-1}C^{-T}$ Where $M_{2,3}=E\{\overline{C\tilde{x}}_{k+1\|k}v_{k+1}v_{k+1}^{T}\overline{C\tilde{x}}_{k+1\|k}\}$

Table 8.2.4. Expectations of the Fourth Main Term in (8.2.37) (Continued)

(14)	$C^{-1}\bar{\psi}^{-1}E\{\overline{C\tilde{x}}_{k+1\|k}v_{k+1}v_{k+1}^{T}\bar{v}_{k+1}\}\bar{\psi}^{-1}C^{-T}=0$
(15)	$C^{-1}\bar{\psi}^{-1}E\{\overline{C\tilde{x}}_{k+1\|k}v_{k+1}v_{k+1}^{T}\bar{\gamma}\overline{C\tilde{x}}_{k\|k}\}\bar{\psi}^{-1}C^{-T}=C^{-1}\bar{\psi}^{-1}M_{2,4}\bar{\psi}^{-1}C^{-T}$ Where $M_{2,4}=E\{\overline{CA\tilde{x}}_{k\|k}v_{k+1}v_{k+1}^{T}\bar{\gamma}\overline{C\tilde{x}}_{k\|k}\}$
(16)	$C^{-1}\bar{\psi}^{-1}E\{\overline{C\tilde{x}}_{k+1\|k}v_{k+1}v_{k+1}^{T}\bar{\gamma}\bar{v}_{k}\}\bar{\psi}^{-1}C^{-T}=0$
(17)	$C^{-1}\bar{\psi}^{-1}E\{\bar{v}_{k+1}C\tilde{x}_{k+1\|k}\tilde{x}_{k+1\|k}^{T}C^{T}\overline{C\tilde{x}}_{k+1\|k}\}\bar{\psi}^{-1}C^{-T}=0$
(18)	$C^{-1}\bar{\psi}^{-1}E\{\bar{v}_{k+1}C\tilde{x}_{k+1\|k}\tilde{x}_{k+1\|k}^{T}C^{T}\bar{v}_{k+1}\}\bar{\psi}^{-1}C^{-T}=C^{-1}\bar{\psi}^{-1}M_{2,5}\bar{\psi}^{-1}C^{-T}$ Where $M_{2,5}=E\{\bar{v}_{k+1}C\tilde{x}_{k+1\|k}\tilde{x}_{k+1\|k}^{T}C^{T}\bar{v}_{k+1}\}$
(19)	$C^{-1}\bar{\psi}^{-1}E\{\bar{v}_{k+1}C\tilde{x}_{k+1\|k}\tilde{x}_{k+1\|k}^{T}C^{T}\bar{\gamma}\overline{C\tilde{x}}_{k\|k}\}\bar{\psi}^{-1}C^{-T}=0$
(20)	$C^{-1}\bar{\psi}^{-1}E\{\bar{v}_{k+1}C\tilde{x}_{k+1\|k}\tilde{x}_{k+1\|k}^{T}C^{T}\bar{\gamma}\bar{v}_{k}\}\bar{\psi}^{-1}C^{-T}=0$
(21)	$C^{-1}\bar{\psi}^{-1}E\{\bar{v}_{k+1}C\tilde{x}_{k+1\|k}v_{k+1}^{T}\overline{C\tilde{x}}_{k+1\|k}\}\bar{\psi}^{-1}C^{-T}=C^{-1}\bar{\psi}^{-1}M_{2,6}\bar{\psi}^{-1}C^{-T}$ Where $M_{2,6}=E\{\bar{v}_{k+1}C\tilde{x}_{k+1\|k}v_{k+1}^{T}\overline{C\tilde{x}}_{k+1\|k}\}$
(22)	$C^{-1}\bar{\psi}^{-1}E\{\bar{v}_{k+1}C\tilde{x}_{k+1\|k}v_{k+1}^{T}\bar{v}_{k+1}\}\bar{\psi}^{-1}C^{-T}=0$
(23)	$C^{-1}\bar{\psi}^{-1}E\{\bar{v}_{k+1}C\tilde{x}_{k+1\|k}v_{k+1}^{T}\bar{\gamma}\overline{C\tilde{x}}_{k\|k}\}\bar{\psi}^{-1}C^{-T}=C^{-1}\bar{\psi}^{-1}M_{2,7}\bar{\psi}^{-1}C^{-T}$ Where $M_{2,7}=E\{\bar{v}_{k+1}C\tilde{x}_{k+1\|k}v_{k+1}^{T}\bar{\gamma}\overline{C\tilde{x}}_{k\|k}\}$
(24)	$C^{-1}\bar{\psi}^{-1}E\{\bar{v}_{k+1}C\tilde{x}_{k+1\|k}v_{k+1}^{T}\bar{\gamma}\bar{v}_{k}\}\bar{\psi}^{-1}C^{-T}=0$
(25)	$C^{-1}\bar{\psi}^{-1}E\{\bar{v}_{k+1}v_{k+1}\tilde{x}_{k+1\|k}^{T}C^{T}\overline{C\tilde{x}}_{k+1\|k}\}\bar{\psi}^{-1}C^{-T}=C^{-1}\bar{\psi}^{-1}\bar{R}_{k+1}M_{2,8}\bar{\psi}^{-1}C^{-T}$ Where $M_{2,8}=E\{\bar{v}_{k+1}v_{k+1}\tilde{x}_{k+1\|k}^{T}C^{T}\overline{C\tilde{x}}_{k+1\|k}\}$
(26)	$C^{-1}\bar{\psi}^{-1}E\{\bar{v}_{k+1}v_{k+1}\tilde{x}_{k+1\|k}^{T}C^{T}\bar{v}_{k+1}\}\bar{\psi}^{-1}C^{-T}=0$
(27)	$C^{-1}\bar{\psi}^{-1}E\{\bar{v}_{k+1}v_{k+1}\tilde{x}_{k+1\|k}^{T}C^{T}\bar{\gamma}\overline{C\tilde{x}}_{k\|k}\}\bar{\psi}^{-1}C^{-T}=C^{-1}\bar{\psi}^{-1}\bar{R}_{k+1}M_{2,9}\bar{\psi}^{-1}C^{-T}$ Where $M_{2,9}=E\{\bar{v}_{k+1}v_{k+1}\tilde{x}_{k+1\|k}^{T}C^{T}\bar{\gamma}\overline{C\tilde{x}}_{k\|k}\}$
(28)	$C^{-1}\bar{\psi}^{-1}E\{\bar{v}_{k+1}v_{k+1}\tilde{x}_{k+1\|k}^{T}C^{T}\bar{\gamma}\bar{v}_{k}\}\bar{\psi}^{-1}C^{-T}=0$
(29)	$C^{-1}\bar{\psi}^{-1}E\{\bar{v}_{k+1}v_{k+1}v_{k+1}^{T}\overline{C\tilde{x}}_{k+1\|k}\}\bar{\psi}^{-1}C^{-T}=0$
(30)	$C^{-1}\bar{\psi}^{-1}E\{\bar{v}_{k+1}v_{k+1}v_{k+1}^{T}\bar{v}_{k+1}\}\bar{\psi}^{-1}C^{-T}=C^{-1}\bar{\psi}^{-1}R_{k+1}\circ R_{k+1}\bar{\psi}^{-1}C^{-T}$
(31)	$C^{-1}\bar{\psi}^{-1}E\{\bar{v}_{k+1}v_{k+1}v_{k+1}^{T}\bar{\gamma}\overline{C\tilde{x}}_{k\|k}\}\bar{\psi}^{-1}C^{-T}=0$
(32)	$C^{-1}\bar{\psi}^{-1}E\{\bar{v}_{k+1}v_{k+1}v_{k+1}^{T}\bar{\gamma}\bar{v}_{k}\}\bar{\psi}^{-1}C^{-T}=0$
(33)	$C^{-1}\bar{\psi}^{-1}E\{\bar{\gamma}\overline{C\tilde{x}}_{k\|k}C\tilde{x}_{k+1\|k}\tilde{x}_{k+1\|k}^{T}C^{T}\overline{C\tilde{x}}_{k+1\|k}\}\bar{\psi}^{-1}C^{-T}=C^{-1}\bar{\psi}^{-1}M_{4,3}\bar{\psi}^{-1}C^{-T}$ Where $M_{4,3}=E\{\bar{\gamma}\overline{C\tilde{x}}_{k\|k}CA\tilde{x}_{k\|k}\tilde{x}_{k\|k}^{T}A^{T}C^{T}\overline{CA\tilde{x}}_{k\|k}\}$
(34)	$C^{-1}\bar{\psi}^{-1}E\{\bar{\gamma}\overline{C\tilde{x}}_{k\|k}C\tilde{x}_{k+1\|k}\tilde{x}_{k+1\|k}^{T}C^{T}\bar{v}_{k+1}\}\bar{\psi}^{-1}C^{-T}=0$
(35)	$C^{-1}\bar{\psi}^{-1}E\{\bar{\gamma}\overline{C\tilde{x}}_{k\|k}C\tilde{x}_{k+1\|k}\tilde{x}_{k+1\|k}^{T}C^{T}\bar{\gamma}\overline{C\tilde{x}}_{k\|k}\}\bar{\psi}^{-1}C^{-T}=C^{-1}\bar{\psi}^{-1}M_{4,4}\bar{\psi}^{-1}C^{-T}$ Where $M_{4,4}=E\{\bar{\gamma}\overline{C\tilde{x}}_{k\|k}CA\tilde{x}_{k\|k}\tilde{x}_{k\|k}^{T}A^{T}C^{T}\bar{\gamma}\overline{C\tilde{x}}_{k\|k}\}$
(36)	$C^{-1}\bar{\psi}^{-1}E\{\bar{\gamma}\overline{C\tilde{x}}_{k\|k}C\tilde{x}_{k+1\|k}\tilde{x}_{k+1\|k}^{T}C^{T}\bar{\gamma}\bar{v}_{k}\}\bar{\psi}^{-1}C^{-T}=0$
(37)	$C^{-1}\bar{\psi}^{-1}E\{\bar{\gamma}\overline{C\tilde{x}}_{k\|k}C\tilde{x}_{k+1\|k}v_{k+1}^{T}\overline{C\tilde{x}}_{k+1\|k}\}\bar{\psi}^{-1}C^{-T}=0$
(38)	$C^{-1}\bar{\psi}^{-1}E\{\bar{\gamma}\overline{C\tilde{x}}_{k\|k}C\tilde{x}_{k+1\|k}v_{k+1}^{T}\bar{v}_{k+1}\}\bar{\psi}^{-1}C^{-T}=C^{-1}\bar{\psi}^{-1}M_{2,10}\bar{\psi}^{-1}C^{-T}$ Where $M_{2,10}=E\{\bar{\gamma}\overline{C\tilde{x}}_{k\|k}C\tilde{x}_{k+1\|k}v_{k+1}^{T}\bar{v}_{k+1}\}$
(39)	$C^{-1}\bar{\psi}^{-1}E\{\bar{\gamma}\overline{C\tilde{x}}_{k\|k}C\tilde{x}_{k+1\|k}v_{k+1}^{T}\bar{\gamma}\overline{C\tilde{x}}_{k\|k}\}\bar{\psi}^{-1}C^{-T}=0$

Table 8.2.4. Expectations of the Fourth Main Term in (8.2.37) (Continued)

(40)	$C^{-1}\bar{\psi}^{-1}E\{\bar{\gamma}\overline{C\tilde{x}}_{k\|k}C\tilde{x}_{k+1\|k}v_{k+1}^{T}\bar{\gamma}\bar{v}_{k}\}\bar{\psi}^{-1}C^{-T}=0$
(41)	$C^{-1}\bar{\psi}^{-1}E\{\bar{\gamma}\overline{C\tilde{x}}_{k\|k}v_{k+1}\tilde{x}_{k+1\|k}^{T}C^{T}\overline{C\tilde{x}}_{k+1\|k}\}\bar{\psi}^{-1}C^{-T}=0$
(42)	$C^{-1}\bar{\psi}^{-1}E\{\bar{\gamma}\overline{C\tilde{x}}_{k\|k}v_{k+1}\tilde{x}_{k+1\|k}^{T}C^{T}\bar{v}_{k+1}\}\bar{\psi}^{-1}C^{-T}=C^{-1}\bar{\psi}^{-1}M_{2,11}\bar{\psi}^{-1}C^{-T}$ Where $M_{2,11}=E\{\bar{\gamma}\overline{C\tilde{x}}_{k\|k}v_{k+1}\tilde{x}_{k\|k}^{T}A^{T}C^{T}\bar{v}_{k+1}\}$
(43)	$C^{-1}\bar{\psi}^{-1}E\{\bar{\gamma}\overline{C\tilde{x}}_{k\|k}v_{k+1}\tilde{x}_{k+1\|k}^{T}C^{T}\bar{\gamma}\overline{C\tilde{x}}_{k\|k}\}\bar{\psi}^{-1}C^{-T}=0$
(44)	$C^{-1}\bar{\psi}^{-1}E\{\bar{\gamma}\overline{C\tilde{x}}_{k\|k}v_{k+1}\tilde{x}_{k+1\|k}^{T}C^{T}\bar{\gamma}\bar{v}_{k}\}\bar{\psi}^{-1}C^{-T}=0$
(45)	$C^{-1}\bar{\psi}^{-1}E\{\bar{\gamma}\overline{C\tilde{x}}_{k\|k}v_{k+1}v_{k+1}^{T}\overline{C\tilde{x}}_{k+1\|k}\}\bar{\psi}^{-1}C^{-T}=C^{-1}\bar{\psi}^{-1}M_{2,12}\bar{\psi}^{-1}C^{-T}$ Where $M_{2,12}=E\{\bar{\gamma}\overline{C\tilde{x}}_{k\|k}v_{k+1}v_{k+1}^{T}\overline{CA\tilde{x}}_{k\|k}\}$
(46)	$C^{-1}\bar{\psi}^{-1}E\{\bar{\gamma}\overline{C\tilde{x}}_{k\|k}v_{k+1}v_{k+1}^{T}\bar{v}_{k+1}\}\bar{\psi}^{-1}C^{-T}=0$
(47)	$C^{-1}\bar{\psi}^{-1}E\{\bar{\gamma}\overline{C\tilde{x}}_{k\|k}v_{k+1}v_{k+1}^{T}\bar{\gamma}\overline{C\tilde{x}}_{k\|k}\}\bar{\psi}^{-1}C^{-T}=C^{-1}\bar{\psi}^{-1}M_{2,13}\bar{\psi}^{-1}C^{-T}$ Where $M_{2,13}=E\{\bar{\gamma}\overline{C\tilde{x}}_{k\|k}v_{k+1}v_{k+1}^{T}\bar{\gamma}\overline{C\tilde{x}}_{k\|k}\}$
(48)	$C^{-1}\bar{\psi}^{-1}E\{\bar{\gamma}\overline{C\tilde{x}}_{k\|k}v_{k+1}v_{k+1}^{T}\bar{\gamma}\bar{v}_{k}\}\bar{\psi}^{-1}C^{-T}=0$
(49)	$C^{-1}\bar{\psi}^{-1}E\{\bar{\gamma}\bar{v}_{k}C\tilde{x}_{k+1\|k}\tilde{x}_{k+1\|k}^{T}C^{T}\overline{C\tilde{x}}_{k+1\|k}\}\bar{\psi}^{-1}C^{-T}=0$
(50)	$C^{-1}\bar{\psi}^{-1}E\{\bar{\gamma}\bar{v}_{k}C\tilde{x}_{k+1\|k}\tilde{x}_{k+1\|k}^{T}C^{T}\bar{v}_{k+1}\}\bar{\psi}^{-1}C^{-T}=0$
(51)	$C^{-1}\bar{\psi}^{-1}E\{\bar{\gamma}\bar{v}_{k}C\tilde{x}_{k+1\|k}\tilde{x}_{k+1\|k}^{T}C^{T}\bar{\gamma}\overline{C\tilde{x}}_{k\|k}\}\bar{\psi}^{-1}C^{-T}=0$
(52)	$C^{-1}\bar{\psi}^{-1}E\{\bar{\gamma}\bar{v}_{k}C\tilde{x}_{k+1\|k}\tilde{x}_{k+1\|k}^{T}C^{T}\bar{\gamma}\bar{v}_{k}\}\bar{\psi}^{-1}C^{-T}=C^{-1}\bar{\psi}^{-1}M_{2,14}\bar{\psi}^{-1}C^{-T}$ Where $M_{2,14}=E\{\bar{\gamma}\bar{v}_{k}C\tilde{x}_{k+1\|k}\tilde{x}_{k+1\|k}^{T}C^{T}\bar{\gamma}\bar{v}_{k}\}$
(53)	$C^{-1}\bar{\psi}^{-1}E\{\bar{\gamma}\bar{v}_{k}C\tilde{x}_{k+1\|k}v_{k+1}^{T}\overline{C\tilde{x}}_{k+1\|k}\}\bar{\psi}^{-1}C^{-T}=0$
(54)	$C^{-1}\bar{\psi}^{-1}E\{\bar{\gamma}\bar{v}_{k}C\tilde{x}_{k+1\|k}v_{k+1}^{T}\bar{v}_{k+1}\}\bar{\psi}^{-1}C^{-T}=0$
(55)	$C^{-1}\bar{\psi}^{-1}E\{\bar{\gamma}\bar{v}_{k}C\tilde{x}_{k+1\|k}v_{k+1}^{T}\bar{\gamma}\overline{C\tilde{x}}_{k\|k}\}\bar{\psi}^{-1}C^{-T}=0$
(56)	$C^{-1}\bar{\psi}^{-1}E\{\bar{\gamma}\bar{v}_{k}C\tilde{x}_{k+1\|k}v_{k+1}^{T}\bar{\gamma}\bar{v}_{k}\}\bar{\psi}^{-1}C^{-T}=0$
(57)	$C^{-1}\bar{\psi}^{-1}E\{\bar{\gamma}\bar{v}_{k}v_{k+1}\tilde{x}_{k+1\|k}^{T}C^{T}\overline{C\tilde{x}}_{k+1\|k}\}\bar{\psi}^{-1}C^{-T}=0$
(58)	$C^{-1}\bar{\psi}^{-1}E\{\bar{\gamma}\bar{v}_{k}v_{k+1}\tilde{x}_{k+1\|k}^{T}C^{T}\bar{v}_{k+1}\}\bar{\psi}^{-1}C^{-T}=0$
(59)	$C^{-1}\bar{\psi}^{-1}E\{\bar{\gamma}\bar{v}_{k}v_{k+1}\tilde{x}_{k+1\|k}^{T}C^{T}\bar{\gamma}\overline{C\tilde{x}}_{k\|k}\}\bar{\psi}^{-1}C^{-T}=0$
(60)	$C^{-1}\bar{\psi}^{-1}E\{\bar{\gamma}\bar{v}_{k}v_{k+1}\tilde{x}_{k+1\|k}^{T}C^{T}\bar{\gamma}\bar{v}_{k}\}\bar{\psi}^{-1}C^{-T}=0$
(61)	$C^{-1}\bar{\psi}^{-1}E\{\bar{\gamma}\bar{v}_{k}v_{k+1}v_{k+1}^{T}\overline{C\tilde{x}}_{k+1\|k}\}\bar{\psi}^{-1}C^{-T}=0$
(62)	$C^{-1}\bar{\psi}^{-1}E\{\bar{\gamma}\bar{v}_{k}v_{k+1}v_{k+1}^{T}\bar{v}_{k+1}\}\bar{\psi}^{-1}C^{-T}=0$
(63)	$C^{-1}\bar{\psi}^{-1}E\{\bar{\gamma}\bar{v}_{k}v_{k+1}v_{k+1}^{T}\bar{\gamma}\overline{C\tilde{x}}_{k\|k}\}\bar{\psi}^{-1}C^{-T}=0$
(64)	$C^{-1}\bar{\psi}^{-1}E\{\bar{\gamma}\bar{v}_{k}v_{k+1}v_{k+1}^{T}\bar{\gamma}\bar{v}_{k}\}\bar{\psi}^{-1}C^{-T}=C^{-1}\bar{\psi}^{-1}M_{2,15}\bar{\psi}^{-1}C^{-T}$ Where $M_{2,15}=E\{\bar{\gamma}\bar{v}_{k}v_{k+1}v_{k+1}^{T}\bar{\gamma}\bar{v}_{k}\}$

The following equation for the a posteriori state error covariance (while inside the saturation boundary) may be formed by combining the non-zero terms (from the above 81 terms).

$$P_{k+1|k+1} = P_{k+1|k} - \left(M_{3,1} + M_{3,2}\right)\bar{\psi}^{-1}C^{-T} - C^{-1}\bar{\psi}^{-1}\left(M_{3,3} + M_{3,4}\right) + C^{-1}\bar{\psi}^{-1}M_P\bar{\psi}^{-1}C^{-T} \tag{8.2.43}$$

Where the following is defined:

$$M_P = M_{4,1} + M_{4,2} + M_{4,3} + M_{4,4} + M_{2,1}\bar{R}_{k+1}^T + M_{2,2} + M_{2,3} + M_{2,4} + M_{2,5} + M_{2,6} + M_{2,7} + \bar{R}_{k+1}\left(M_{2,8} + M_{2,9}\right) + R_{k+1} \circ R_{k+1} + M_{2,10} + M_{2,11} + M_{2,12} + M_{2,13} + M_{2,14} + M_{2,15} \tag{8.2.44}$$

Note that some of the non-zero elements yield the same final solution, such as:

$$M_{2,2} = M_{2,3} = M_{2,5} = M_{2,6} \tag{8.2.45}$$

$$M_{2,4} = M_{2,7} \tag{8.2.46}$$

$$M_{2,11} = M_{2,12} \tag{8.2.47}$$

From these definitions, (8.2.44) can thus be simplified as follows:

$$M_P = M_{4,1} + M_{4,2} + M_{4,3} + M_{4,4} + 4M_{2,2} + 2M_{2,4} + M_{2,10} + 2M_{2,11} + M_{2,13} + M_{2,14} + M_{2,1}\bar{R}_{k+1}^T + \bar{R}_{k+1}\left(M_{2,8} + M_{2,9}\right) + R_{k+1} \circ R_{k+1} + \bar{\gamma}R_{k+1} \circ R_k\bar{\gamma} \tag{8.2.48}$$

The supporting equations for the second, third, and fourth-order matrices ($M_{2,\#}$, $M_{3,\#}$, and $M_{4,\#}$) are defined in the previous three tables. Note that these equations contain third and fourth-order moments of the state error. These third and fourth-order moments (defined as M_3 and M_4 respectively) need to be calculated in a recursive format in order to obtain a recursive a posteriori state error covariance. Consider the third-order moment matrix as follows:

$$M_{3,k+1|k} = \begin{bmatrix} M_{3,11} + M_{3,12} + \cdots + M_{3,1n} \\ M_{3,21} + M_{3,22} + \cdots + M_{3,2n} \\ M_{3,n1} + M_{3,n2} + \cdots + M_{3,nn} \end{bmatrix}_{k+1|k} = \begin{bmatrix} E\{\tilde{x}_1^3\} + E\{\tilde{x}_1\tilde{x}_2^2\} + \cdots + E\{\tilde{x}_1\tilde{x}_n^2\} \\ E\{\tilde{x}_2\tilde{x}_1^2\} + E\{\tilde{x}_2^3\} + \cdots + E\{\tilde{x}_2\tilde{x}_n^2\} \\ E\{\tilde{x}_n\tilde{x}_1^2\} + \cdots + E\{\tilde{x}_n\tilde{x}_{n-1}^2\} + E\{\tilde{x}_n^3\} \end{bmatrix}_{k+1|k} \tag{8.2.49}$$

Recall the following definition for the a priori state error (with no model mismatch):

$$\tilde{x}_{k+1|k} = A\tilde{x}_{k|k} + w_k \tag{8.2.50}$$

The above definition may be rewritten as an element-by-element expansion:

$$\begin{bmatrix} \tilde{x}_1 \\ \tilde{x}_2 \\ \vdots \\ \tilde{x}_n \end{bmatrix}_{k+1|k} = \begin{bmatrix} A_{11} & A_{12} & \dots & A_{1n} \\ A_{21} & A_{22} & \dots & A_{2n} \\ \vdots & \vdots & \ddots & \vdots \\ A_{n1} & A_{n2} & \dots & A_{nn} \end{bmatrix} \begin{bmatrix} \tilde{x}_1 \\ \tilde{x}_2 \\ \vdots \\ \tilde{x}_n \end{bmatrix}_{k|k} + \begin{bmatrix} w_1 \\ w_2 \\ \vdots \\ w_n \end{bmatrix}_k \tag{8.2.51}$$

Utilizing this notation, the elements within the a priori third-order moment matrix (8.2.49) may be found as follows (supposing that $n = 2$):

$$\begin{aligned} M_{3,11_{k+1|k}} &= E\{\tilde{x}_{1,k+1|k}^3\} \\ &= A_{11}^3 M_{3,11_{k|k}} + 3A_{11}A_{12}^2 M_{3,12_{k|k}} + 3A_{11}^2 A_{12} M_{3,21_{k|k}} + A_{12}^3 M_{3,22_{k|k}} \end{aligned} \tag{8.2.52}$$

$$\begin{aligned} M_{3,12_{k+1|k}} &= E\{\tilde{x}_{1,k+1|k}\tilde{x}_{2,k+1|k}^2\} \\ &= A_{11}A_{21}^2 M_{3,11_{k|k}} + (2A_{12}A_{21}A_{22} + A_{11}A_{22}^2) M_{3,12_{k|k}} \\ &\quad + (2A_{11}A_{21}A_{22} + A_{12}A_{21}^2) M_{3,21_{k|k}} + A_{12}A_{22}^2 M_{3,22_{k|k}} \end{aligned} \tag{8.2.53}$$

$$\begin{aligned} M_{3,21_{k+1|k}} &= E\{\tilde{x}_{1,k+1|k}^2\tilde{x}_{2,k+1|k}\} \\ &= A_{11}A_{21}^2 M_{3,11_{k|k}} + (2A_{12}A_{21}A_{22} + A_{11}A_{22}^2) M_{3,12_{k|k}} \\ &\quad + (2A_{11}A_{21}A_{22} + A_{12}A_{21}^2) M_{3,21_{k|k}} + A_{12}A_{22}^2 M_{3,22_{k|k}} \end{aligned} \tag{8.2.54}$$

$$\begin{aligned} M_{3,22_{k+1|k}} &= E\{\tilde{x}_{2,k+1|k}^3\} \\ &= A_{21}^3 M_{3,11_{k|k}} + 3A_{21}A_{22}^2 M_{3,12_{k|k}} + 3A_{21}^2 A_{22} M_{3,21_{k|k}} + A_{22}^3 M_{3,22_{k|k}} \end{aligned} \tag{8.2.55}$$

Equations (8.2.52) through (8.2.55) may be used to solve the a priori third-order moments for a system with two states. The equations may be expanded depending on the number of states. The a posteriori third-order moment equations may be found next, in a similar manner. Note the following:

$$\tilde{x}_{k+1|k+1} = \tilde{x}_{k+1|k} - K_{k+1} \tag{8.2.56}$$

Such that, on an element by element basis, the a posteriori third-order moment equations (for $n = 2$) may be found as follows:

$$M_{3,11_{k+1|k+1}} = E\{\tilde{x}_{1,k+1|k+1}^3\} = M_{3,11_{k+1|k}} - 3K_{1,k+1}P_{11,k+1|k} - K_{1,k+1}^3 \tag{8.2.57}$$

$$\begin{aligned} M_{3,12_{k+1|k+1}} &= E\{\tilde{x}_{1,k+1|k+1}\tilde{x}_{2,k+1|k+1}^2\} \\ &= M_{3,12_{k+1|k}} - K_{1,k+1}\left(K_{2,k+1}^2 + P_{22,k+1|k}\right) - 2K_{2,k+1}P_{12,k+1|k} \end{aligned} \tag{8.2.58}$$

$$\begin{aligned} M_{3,21_{k+1|k+1}} &= E\{\tilde{x}_{1,k+1|k+1}^2\tilde{x}_{2,k+1|k+1}\} \\ &= M_{3,21_{k+1|k}} - K_{2,k+1}\left(K_{1,k+1}^2 + P_{11,k+1|k}\right) - 2K_{1,k+1}P_{12,k+1|k} \end{aligned} \tag{8.2.59}$$

$$M_{3,22_{k+1|k+1}} = E\{\tilde{x}_{2,k+1|k+1}^3\} = M_{3,22_{k+1|k}} - 3K_{2,k+1}P_{22,k+1|k} - K_{2,k+1}^3 \tag{8.2.60}$$

Next, consider the following definition for the fourth-order moment matrix:

$$M_{4,k+1|k} = \begin{bmatrix} M_{4,11} & M_{4,12} & \cdots & M_{4,1n} \\ M_{4,21} & M_{4,22} & \cdots & M_{4,2n} \\ \vdots & \vdots & \ddots & \vdots \\ M_{4,n1} & M_{4,n2} & \cdots & M_{4,nn} \end{bmatrix}_{k+1|k} \tag{8.2.61}$$

Where the diagonal elements of (8.2.61) may be found as follows (omitting the time subscript for ease of notation:

$$M_{4,11} = E\{\tilde{x}_1^4\} + E\{\tilde{x}_1^2\tilde{x}_2^2\} + \cdots + E\{\tilde{x}_1^2\tilde{x}_n^2\} \tag{8.2.62}$$

$$M_{4,nn} = E\{\tilde{x}_1^2\tilde{x}_n^2\} + \cdots + E\{\tilde{x}_{n-1}^2\tilde{x}_n^2\} + E\{\tilde{x}_n^4\} \tag{8.2.63}$$

The off-diagonal elements of (8.2.61) are found in a similar fashion, where one calculates $\tilde{x}\tilde{x}^T\tilde{x}\tilde{x}^T$ and looks at the expectation of each off-diagonal element. As an example, consider a system with only two states, such that one has the following a priori fourth-order moment matrix:

$$\begin{aligned} M_{4,k+1|k} &= \begin{bmatrix} M_{4,11} & M_{4,12} \\ M_{4,21} & M_{4,22} \end{bmatrix}_{k+1|k} \\ &= \begin{bmatrix} E\{\tilde{x}_1^4\} + E\{\tilde{x}_1^2\tilde{x}_2^2\} & E\{\tilde{x}_1^3\tilde{x}_2\} + E\{\tilde{x}_1\tilde{x}_2^3\} \\ E\{\tilde{x}_1^3\tilde{x}_2\} + E\{\tilde{x}_1\tilde{x}_2^3\} & E\{\tilde{x}_1^2\tilde{x}_2^2\} + E\{\tilde{x}_2^4\} \end{bmatrix}_{k+1|k} \end{aligned} \tag{8.2.64}$$

Note that one can label each expectation within each matrix cell of (8.2.64) as a, b, c, and so on. From the above equations, in particular $\tilde{x}_{k+1|k} = A\tilde{x}_{k|k} + w_k$, one then has the following a priori fourth-order moment equations:

$$\begin{aligned} M_{4,11a_{k+1|k}} &= E\{\tilde{x}_{1,k+1|k}^4\} \\ &= A_{11}^4 M_{4,11a_{k|k}} + 4A_{11}^3 A_{12} M_{4,12a_{k|k}} + 6A_{11}^2 A_{12}^2 M_{4,11b_{k|k}} \\ &+ 6A_{11}^2 Q_{11,k} P_{11,k|k} + 4A_{11} A_{12}^3 M_{4,12b_{k|k}} + 12A_{11} A_{12} Q_{11,k} P_{12,k|k} \\ &+ A_{12}^4 M_{4,22b_{k|k}} + 6A_{12}^2 Q_{11,k} P_{22,k|k} + 3Q_{11,k}^2 \end{aligned} \tag{8.2.65}$$

$$\begin{aligned} M_{4,11b_{k+1|k}} &= E\{\tilde{x}_{1,k+1|k}^2 \tilde{x}_{2,k+1|k}^2\} \\ &= A_{11}^2 A_{21}^2 M_{4,11a_{k|k}} + 2A_{11}^2 A_{21} A_{22} M_{4,12a_{k|k}} + A_{11}^2 A_{22}^2 M_{4,11b_{k|k}} \\ &+ A_{11}^2 Q_{22,k} P_{11,k|k} + 2A_{11} A_{12} A_{21}^2 M_{4,12a_{k|k}} \\ &+ 4A_{11} A_{12} A_{21} A_{22} M_{4,11b_{k|k}} + 2A_{11} A_{12} A_{22}^2 M_{4,12b_{k|k}} \\ &+ 2A_{11} A_{12} Q_{22,k} P_{12,k|k} + 4A_{11} A_{21} Q_{12,k} P_{11,k|k} \\ &+ 4A_{11} A_{22} Q_{12,k} P_{12,k|k} + A_{12}^2 A_{21}^2 M_{4,11b_{k|k}} + 2A_{12}^2 A_{21} A_{22} M_{4,12b_{k|k}} \\ &+ A_{12}^2 A_{22}^2 M_{4,22b_{k|k}} + A_{12}^2 Q_{22,k} P_{22,k|k} + 4A_{12} A_{21} Q_{12,k} P_{12,k|k} \\ &+ 4A_{12} A_{22} Q_{12,k} P_{22,k|k} + A_{21}^2 Q_{11,k} P_{11,k|k} + 2A_{21} A_{22} Q_{11,k} P_{12,k|k} \\ &+ A_{22}^2 Q_{11,k} P_{22,k|k} \end{aligned} \tag{8.2.66}$$

$$\begin{aligned} M_{4,22b_{k+1|k}} &= E\{\tilde{x}_{2,k+1|k}^4\} \\ &= A_{21}^4 M_{4,11a_{k|k}} + 4A_{21}^3 A_{22} M_{4,12a_{k|k}} + 6A_{21}^2 A_{22}^2 M_{4,11b_{k|k}} \\ &+ 6A_{21}^2 Q_{22,k} P_{11,k|k} + 4A_{21} A_{22}^3 M_{4,12b_{k|k}} + 12A_{21} A_{22} Q_{22,k} P_{12,k|k} \\ &+ A_{22}^4 M_{4,22b_{k|k}} + 6A_{22}^2 Q_{22,k} P_{22,k|k} + 3Q_{22,k}^2 \end{aligned} \tag{8.2.67}$$

The remaining two a priori fourth-order moments $M_{4,12a_{k+1|k}}$ and $M_{4,12b_{k+1|k}}$ may be found in a similar fashion. Likewise, the a posteriori fourth-order moment equations (for a second order system) may be found as follows:

$$\begin{aligned} M_{4,11a_{k+1|k+1}} &= E\{\tilde{x}_{1,k+1|k+1}^4\} \\ &= M_{4,11a_{k+1|k}} + 4K_{1,k+1} M_{3,11_{k+1|k}} + 6K_{1,k+1}^2 P_{11,k+1|k} + K_{1,k+1}^4 \end{aligned} \tag{8.2.68}$$

$$\begin{aligned} M_{4,11b_{k+1|k+1}} &= \{\tilde{x}^2_{1,k+1|k+1}\tilde{x}^2_{2,k+1|k+1}\} \\ &= M_{4,11b_{k+1|k}} - 2K_{2,k+1}M_{3,21_{k+1|k}} - 2K_{1,k+1}M_{3,21_{k+1|k}} \\ &+ K^2_{2,k+1}P_{11,k+1|k} + 4K_{1,k+1}K_{2,k+1} + K^2_{1,k+1}P_{22,k+1|k} \\ &+ K^2_{1,k+1}K^2_{2,k+1} \end{aligned} \tag{8.2.69}$$

$$\begin{aligned} M_{4,12a_{k+1|k+1}} &= \{\tilde{x}^3_{1,k+1|k+1}\tilde{x}_{2,k+1|k+1}\} \\ &= M_{4,12a_{k+1|k}} + 3K_{1,k+1}K_{2,k+1}P_{11,k+1|k} - K_{2,k+1}M_{3,11_{k+1|k}} \\ &+ K^3_{1,k+1}K_{2,k+1} - 3K_{1,k+1}M_{3,21_{k+1|k}} + 3K^2_{1,k+1}P_{12,k+1|k} \end{aligned} \tag{8.2.70}$$

$$\begin{aligned} M_{4,12b_{k+1|k+1}} &= \{\tilde{x}_{1,k+1|k+1}\tilde{x}^3_{2,k+1|k+1}\} \\ &= M_{4,12b_{k+1|k}} + 3K_{1,k+1}K_{2,k+1}P_{22,k+1|k} - K_{1,k+1}M_{3,22_{k+1|k}} \\ &+ K_{1,k+1}K^3_{2,k+1} - 3K_{2,k+1}M_{3,12_{k+1|k}} + 3K^2_{2,k+1}P_{12,k+1|k} \end{aligned} \tag{8.2.71}$$

$$\begin{aligned} M_{4,22b_{k+1|k+1}} &= E\{\tilde{x}^4_{2,k+1|k+1}\} \\ &= M_{4,22b_{k+1|k}} + 4K_{2,k+1}M_{3,22_{k+1|k}} + 6K^2_{2,k+1}P_{22,k+1|k} + K^4_{2,k+1} \end{aligned} \tag{8.2.72}$$

Equations (8.2.1) through (8.2.72) represent an alternative derivation for the a posteriori SVSF covariance equation. Note that the a posteriori covariance when inside the smoothing boundary layer was found to be a function of second, third, and fourth-order moments. While outside the smoothing boundary layer, the a posteriori covariance was found to be a function of only second-order moments. This is an important observation. The above derivation is complex, and becomes even more so with an increased number of states. This led to revised forms of the SVSF gain and state update equations, creating a significantly simpler covariance derivation, as described in Chapter 4.

8.3 SVSF Strategy with Linearized Nonlinear Functions

This section summarizes the SVSF strategy with linearized nonlinear functions, which was introduced in Chapter 4. There are two stages: prediction and update. The first step is to predict the state estimates (8.3.1), calculate the a priori state error covariance (8.3.2), and find the corresponding estimation error (8.3.3).

$$\hat{x}_{k+1|k} = f\left(\hat{x}_{k|k}, u_k\right) \tag{8.3.1}$$

$$P_{k+1|k} = F_k P_{k|k} F_k^T + Q_k \tag{8.3.2}$$

$$e_{z,k+1|k} = z_{k+1} - h\left(\hat{x}_{k+1|k}\right) \tag{8.3.3}$$

Where partial derivatives are used to compute linearized system and measurement matrices F and H, respectively found as follows [32]:

$$F_k = \left.\frac{\partial f}{\partial x}\right|_{\hat{x}_{k|k}, u_k} \tag{8.3.4}$$

$$H_{k+1} = \left.\frac{\partial h}{\partial x}\right|_{\hat{x}_{k+1|k}} \tag{8.3.5}$$

The next step involves calculating the corresponding SVSF gain (8.3.6), updating the state estimate (8.3.7), finding the a posteriori state error covariance (8.3.8), and determining the a posteriori measurement error (8.3.9) which is to be used in the next iteration.

$$K_{k+1} = H^+ diag\left[\left(\left|e_{z,k+1|k}\right|_{Abs} + \gamma\left|e_{z,k|k}\right|_{Abs}\right) \circ sat\left(\frac{e_{z,k+1|k}}{\psi}\right)\right]\left[diag\left(e_{z,k+1|k}\right)\right]^{-1} \tag{8.3.6}$$

$$\hat{x}_{k+1|k+1} = \hat{x}_{k+1|k} + K_{k+1} e_{z,k+1|k} \tag{8.3.7}$$

$$P_{k+1|k+1} = (I - K_{k+1}C)P_{k+1|k}(I - K_{k+1}C)^T + K_{k+1}R_{k+1}K_{k+1}^T \tag{8.3.8}$$

$$e_{z,k+1|k+1} = z_{k+1} - C\hat{x}_{k+1|k+1} \tag{8.3.9}$$

It is important to remind the reader that a 'divide by zero' check should be performed on (8.3.6) to avoid division by zero. The proposed SVSF estimation strategy with linearized nonlinear functions may be summarized by (8.3.1) through (8.3.9).

8.4 Definitions for Observability and Controllability

As described in [122], consider an n^{th}-order system whose state and measurement equations are respectively defined by:

$$\dot{x} = Ax + Bu \tag{8.4.1}$$

$$z = Cx \tag{8.4.2}$$

Then the system is considered completely observable if the following matrix is of rank n, where O_M is called the observability matrix [122]:

$$O_M = \begin{bmatrix} C \\ CA \\ \vdots \\ CA^{n-1} \end{bmatrix} \tag{8.4.3}$$

Similarly, if the following matrix is of rank n, then the system is considered to be completely controllable [122]:

$$C_M = [B \quad AB \quad \dots \quad A^{n-1}B] \tag{8.4.4}$$

Where C_M refers to the controllability matrix.

8.5 A Look at the Values of the Smoothing Boundary Layer Matrix

It is important to study the units of the smoothing boundary layer matrix in an effort to better understand the values. As an example, consider a system with two fully measured states corresponding to position (m) and velocity (m/s). From (5.1.22), one then has the following units:

$$\psi_{k+1} = \left(\begin{bmatrix} \frac{1}{m} & 0 \\ 0 & \frac{s}{m} \end{bmatrix} \begin{bmatrix} m^2 & m^2/s \\ m^2/s & m^2/s^2 \end{bmatrix} \begin{bmatrix} m^2 & \frac{m^2}{s} \\ \frac{m^2}{s} & \frac{m^2}{s^2} \end{bmatrix}^{-1} \right)^{-1} \tag{8.5.1}$$

Combining the first two matrices yields:

$$\psi_{k+1} = \left(\begin{bmatrix} m & \frac{m}{s} \\ m & \frac{m}{s} \end{bmatrix} \begin{bmatrix} m^2 & \frac{m^2}{s} \\ \frac{m^2}{s} & \frac{m^2}{s^2} \end{bmatrix}^{-1} \right)^{-1} \tag{8.5.2}$$

Performing the matrix inverse of the second matrix in (8.5.2) yields the following:

$$\psi_{k+1} = \left(\begin{bmatrix} m & \frac{m}{s} \\ m & \frac{m}{s} \end{bmatrix} \begin{bmatrix} \frac{1}{m^2} & \frac{s}{m^2} \\ \frac{s}{m^2} & \frac{s^2}{m^2} \end{bmatrix} \right)^{-1} \tag{8.5.3}$$

Next, combining the two matrices in (8.5.3) yields:

$$\psi_{k+1} = \begin{bmatrix} \frac{1}{m} & \frac{s}{m} \\ \frac{1}{m} & \frac{s}{m} \end{bmatrix}^{-1} \tag{8.5.4}$$

Finally, performing a matrix inverse and simplifying yields the units of the smoothing boundary layer matrix for a system with two states (position and velocity):

$$\psi_{k+1} = \begin{bmatrix} m & m \\ m/s & m/s \end{bmatrix} \tag{8.5.5}$$

Therefore, it appears that the units may be generalized as follows:

$$\psi_{k+1} = \begin{bmatrix} x_1 & x_1 \\ x_2 & x_2 \end{bmatrix} \tag{8.5.6}$$

Where x_1 refers to the units of the first state, and x_2 refers to the units of the second state. For completeness, the units of the corresponding SVSF gain and update equation are then studied. Consider the units of the SVSF gain (5.1.8), as follows:

$$K_{k+1} = \begin{bmatrix} m & 0 \\ 0 & \frac{m}{s} \end{bmatrix} \begin{bmatrix} m & m \\ \frac{m}{s} & \frac{m}{s} \end{bmatrix}^{-1} \tag{8.5.7}$$

Performing the matrix inverse of the second matrix in (8.5.7), and then combining the resulting matrices and simplifying yields:

$$K_{k+1} = \begin{bmatrix} 1 & s \\ \frac{1}{s} & 1 \end{bmatrix} \tag{8.5.8}$$

Next, studying the units of the state update equation defined earlier:

$$\begin{bmatrix} m \\ \frac{m}{s} \end{bmatrix} = \begin{bmatrix} m \\ \frac{m}{s} \end{bmatrix} + \begin{bmatrix} 1 & s \\ \frac{1}{s} & 1 \end{bmatrix} \begin{bmatrix} m \\ \frac{m}{s} \end{bmatrix} \tag{8.5.9}$$

Equation (8.5.9) simplifies to the following correct units:

$$\begin{bmatrix} m \\ \frac{m}{s} \end{bmatrix} = \begin{bmatrix} m \\ \frac{m}{s} \end{bmatrix} \tag{8.5.10}$$

Therefore, the units of the smoothing boundary layer matrix are shown to be correct, as the resulting equations yield the correct units for the state estimates (in this case, position and velocity). It is also important to note that the actual values of the smoothing boundary layer matrix are positive along the diagonal, whereas the off-diagonal terms may be positive or negative. This is due to the fact that (5.1.22) is a function of $P_{k+1|k}$ and S_{k+1}, which are both positive along the diagonal, but the terms on the off-diagonal may be positive or negative. For example, consider the following example using (5.1.22) with a fully measured two-state system:

$$\psi_{k+1} = \left(\begin{bmatrix} 6 & 0 \\ 0 & 1.5 \end{bmatrix}^{-1} \begin{bmatrix} 5 & -9 \\ -9 & 7 \end{bmatrix} \begin{bmatrix} 6 & -9 \\ -9 & 8 \end{bmatrix}^{-1} \right)^{-1} \tag{8.5.11}$$

Solving (8.5.11) yields the following:

$$\psi_{k+1} = \begin{bmatrix} 5.1 & -0.3 \\ -1.2 & 1.3 \end{bmatrix} \tag{8.5.12}$$

Therefore, as shown in the above example, the smoothing boundary layer matrix may sometimes have negative terms on the off-diagonal.

8.6 EHA Circuit Diagram

The following is a circuit diagram of the EHA used for fault detection and diagnosis in Chapter 6, as presented in [131].

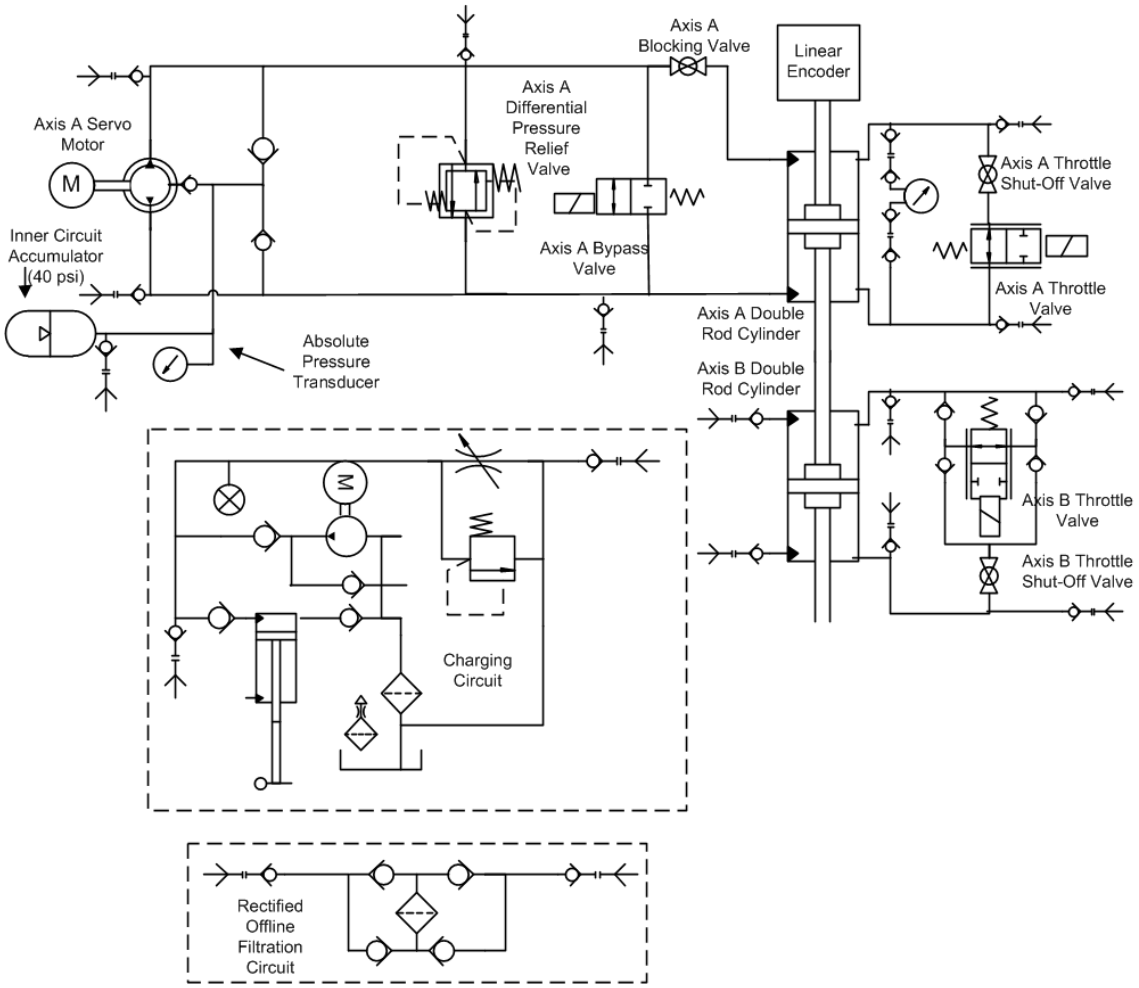

Figure 8.6.1. EHA Circuit Diagram [131]

8.7 Identifying the System Models

This section presents system identification results performed on the EHA by Mr. Yu Song. System identification is performed in an effort to extract a 'black box model' of a dynamic system by fitting a statistical model with experimental measurements and designer knowledge of the system. The prior knowledge of the system includes the frequency range of interest, saturation, and knowledge of the piece-wise linear regions. To create an accurate model, the frequency of interest should be well past the cross-over frequency range, and preferably to where the signal-to-noise ratio drops dramatically and stops offering valuable information.

The three scenarios (normal operation, friction and leakage faults) were setup and run on the EHA. For each case, a chirp signal with amplitude $2.5\ V$ and maximum frequency $10\ Hz$ was sent as an input to the system. Two system transfer functions were created by fitting Box-Jenkins models with experimental data. The normal EHA transfer function (in discrete-time) was found to be third-order, as follows:

$$G_{EHA,Normal} = \frac{1.072 \times 10^{-3} z^2 - 1.770 \times 10^{-3} z + 7.075 \times 10^{-3}}{z^3 - 2.711 z^2 + 2.459 z - 0.747} \tag{8.7.1}$$

The corresponding model with leakage fault was found to be:

$$G_{EHA,Leakage} = \frac{-1.588 \times 10^{-3} z + 1.877 \times 10^{-3}}{z^3 - 0.641 z^2 - 0.605 z + 0.276} \tag{8.7.2}$$

Finally, the model with a friction fault present was experimentally identified as:

$$G_{EHA,Friction} = \frac{9.392 \times 10^{-3} z^2 - 1.722 \times 10^{-3} z + 7.910 \times 10^{-3}}{z^3 - 2.757 z^2 + 2.545 z - 0.787} \tag{8.7.3}$$

Based on the above three EHA models and a sequential step input (magnitude $\pm 2.5\ V$, changing every four seconds), the output from each model may be simulated and compared with actual experimental measurements for validation as shown in the following two figures. In this scenario, the EHA is run normally for the first 12 seconds. During the following 8 seconds, a leak is introduced. A friction fault is produced during the last 8 seconds of the setup.

As shown in the following figure, the obtained EHA models match the actual measurement fairly well during the steady-state regions. However, there appears to be significant overshoot or oscillations present during the transient regions. An encoder measured the position of the Axis A cylinder. This value was differentiated to obtain the 'measured' velocity, which resulted in a noisy signal. Future work on the EHA should involve the use of an accelerometer to obtain the velocity measurement (through integration), in an effort to minimize the effects of noise, such that more distinct models may be obtained and studied. More information on performing system identification on the EHA is available in [133].

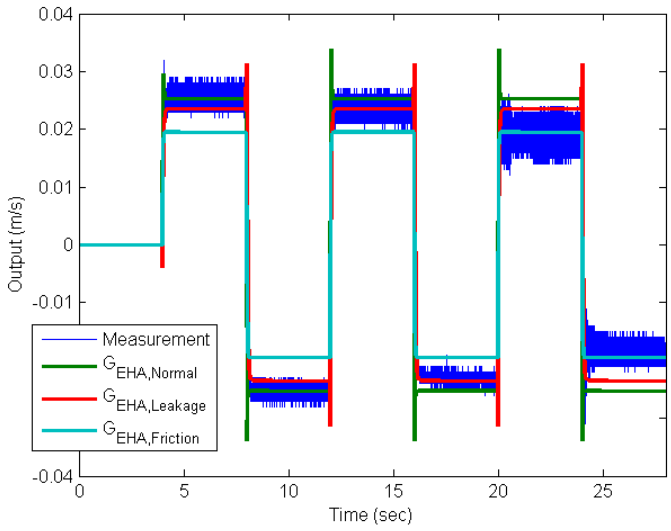

Figure 8.7.1. Measurements and the Outputs from the System Identification Models

The following figure shows the errors between the model outputs and the measurement. This helps clarify the above figure and the modes that the EHA is operating under for each segment.

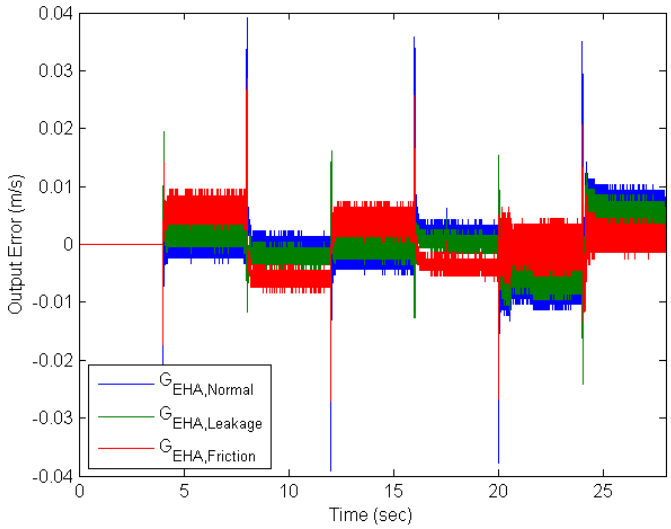

Figure 8.7.2. Measurement and Output Errors from the System Identification Models

It was found that mathematically modeling the system rather than performing system identification led to more accurate results. Hence, in an effort to obtain more accurate system models, the mathematical model of the EHA was explored and implemented on both the IMM-KF and IMM-SVSF strategies.

8.8 Mathematically Modeling the EHA System

In an effort to obtain approximate values for the unknown EHA parameters (D_p, B_E, and L), a sequential step signal with amplitude $\pm 2.5\ V$ (changing every 4 seconds) was inputted into the system, as shown below. Note that this corresponds to a pump rotation of $\pm 750\ RPM$. The corresponding (unfiltered) system output is shown in the second following figure. Recall that an encoder measured the position of the Axis A cylinder. This value was differentiated to obtain the 'measured' velocity, which resulted in a noisy signal. Note that for the first 12 seconds, the EHA was in normal operation. From 12 seconds to 20 seconds, the EHA experienced the leakage fault. During the final 8 seconds, the friction fault was present.

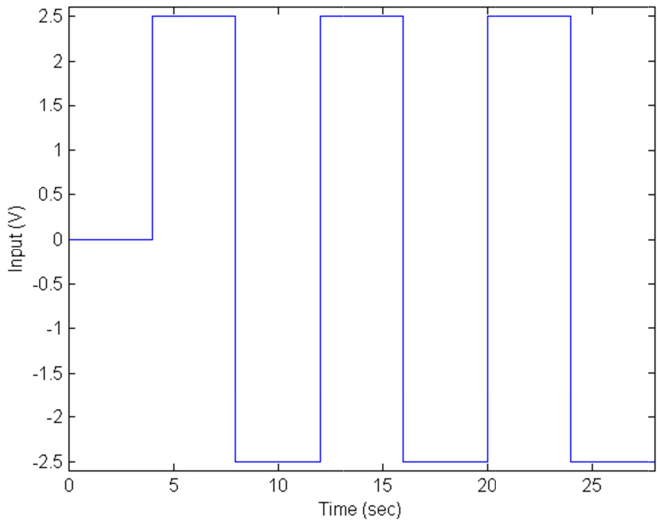

Figure 8.8.1. Sequential Step Input for the EHA

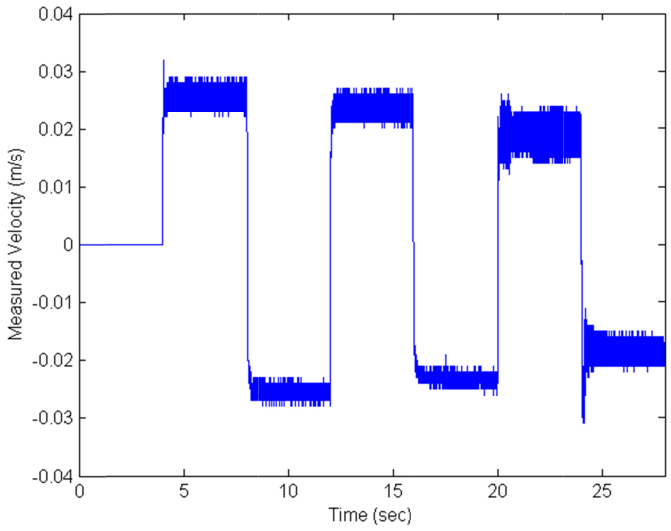

Figure 8.8.2. Unfiltered Measured Output from the EHA

The differential pressure ΔP_A (across the Axis A cylinder) was measured during the data collection for each case. Furthermore, the measured velocity x_∞ (for $+2.5\ V$) was averaged for each case, once steady-state was reached (i.e., the final step value). These values, among those found in Table 6.3.1, are used to determine the unknown EHA parameters.

The first step is to calculate the pump displacement parameter D_p. This can be accomplished using the following formula obtained from [133]:

$$D_p = \frac{Q_E}{\omega_{rad/s}} \tag{8.8.1}$$

Essentially (8.8.1) defines the pump displacement as a function of volumetric flow rate Q_E and pump turn rate $\omega_{rad/s}$. The volumetric flow rate may be determined from its relationship with pressure, and a series of experimental trials. This relationship is shown in the following figure, as reported in [133].

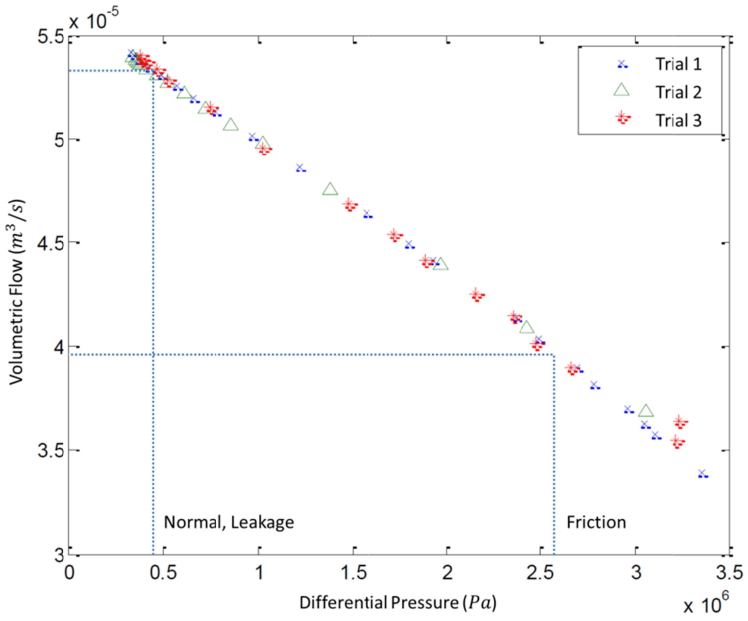

Figure 8.8.3. Relationship Between Volumetric Flow Rate and Differential Pressure [133]

For the normal case, the differential pressure was found to be $70.6\ psi$ or $486.8\ kPa$. From the above figure, this results in an approximate volumetric flow rate of $5.35 \times 10^{-5}\ m^3/s$. These values result in the following pump displacement, for the normal case:

$$D_p = \frac{(60\ s)\left(5.35 \times 10^{-5}\frac{m^3}{s}\right)}{2\pi(750\ rad)} = 6.812 \times 10^{-7} m^3/rad \tag{8.8.2}$$

The pump displacement for the friction and leakage cases may be found in a similar fashion. Next, the load friction B_E will be determined for each scenario. Consider the following equation which simplifies the forces present in the EHA cylinder:

$$F_E = M\ddot{x} + B_E\dot{x} \tag{8.8.3}$$

Recall the sequential input to the system as presented earlier. Notice that the measured velocity reaches a steady-state value after a short period of time. At this point, there is no longer acceleration present, such that the force required to overcome friction may be calculated as follows:

$$F_E = \Delta P_A A_E = B_E \dot{x}_\infty \tag{8.8.4}$$

Rearranging and simplifying yields:

$$B_E = \frac{\Delta P_A A_E}{\dot{x}_\infty} \tag{8.8.5}$$

For the normal case, the averaged steady-state velocity was found to be $0.0259\ m/s$. Substituting the remaining values into (8.8.5) yields the following load friction value for the normal case:

$$B_E = \frac{(486.8 \times 10^3\ Pa)(1.52 \times 10^{-3}\ m^2)}{0.0259\ m/s} = 28{,}569\ Ns/m \tag{8.8.6}$$

Finally, the leakage coefficient L may be solved. In order to find an approximate leakage coefficient, consider multiplying the EHA transfer function (6.3.2.1) by s (the Laplace variable), and then solving for L when $s \to 0$. This allows the steady-state value of the velocity $\dot{x}_\infty$ to be used, as follows:

$$\frac{\dot{x}_\infty}{\omega_p} = \frac{EHA_{Num} s}{s^3 + EHA_{Den2} s^2 + EHA_{Den1} s} \tag{8.8.7}$$

Then, allowing $s \to 0$ in (8.8.7) yields:

$$\left.\frac{EHA_{Num}}{EHA_{Den1}}\right|_{s \to 0} = \dot{x}_\infty = \frac{2.5(10\pi) A_E D_p}{B_E L + A_E^2} \tag{8.8.8}$$

Rearranging (8.8.8) for the leakage coefficient yields the following:

$$L = \frac{2.5(10\pi) A_E D_p}{B_E \dot{x}_\infty} - \frac{A_E^2}{B_E} \tag{8.8.9}$$

Substitution of the known values, as well as (8.8.2) and (8.8.6), yields:

$$L = \frac{2.5(10\pi)(1.52 \times 10^{-3}\ m^2)(6.812 \times 10^{-7} m^3/rad)}{(28{,}569\ Ns/m)(0.0259\ m/s)} - \frac{(1.52 \times 10^{-3}\ m^2)^2}{28{,}569\ Ns/m} \tag{8.8.10}$$

An approximation for the leakage coefficient for the normal case is then found as:

$$L = 2.903 \times 10^{-11}\ Nm/s \tag{8.8.11}$$

The above procedures may be repeated for the friction and leakage faults. The following table summarizes the important data used to obtain the desired parameters (D_p, B_E, and L), which are used to model the EHA under the three scenarios.

Table 8.8.1. Measured and Calculated EHA Parameters

Parameter	Normal	Leakage	Friction
ΔP_A	$486.8\ kPa$	$479.9\ kPa$	$2{,}563.5\ kPa$
$\dot{x}_\infty$	$0.0259\ m/s$	$0.0235\ m/s$	$0.0194\ m/s$
Q_E	$5.35 \times 10^{-5}\ m^3/s$	$5.35 \times 10^{-5}\ m^3/s$	$3.95 \times 10^{-5}\ m^3/s$
D_p	$6.812 \times 10^{-7} m^3/rad$	$6.812 \times 10^{-7} m^3/rad$	$5.029 \times 10^{-7} m^3/rad$
B_E	$28{,}569\ Ns/m$	$31{,}040\ Ns/m$	$200{,}850\ Ns/m$
L	$2.903 \times 10^{-11}\ Nm/s$	$3.705 \times 10^{-11}\ Nm/s$	$3.905 \times 10^{-12}\ Nm/s$

Finally, based on the aforementioned mathematical modeling, three different transfer functions may be created from (6.3.2.1) through (6.3.2.4). The normal model, leakage model, and friction model are respectively defined as follows:

$$G_{EHA,Normal} = \frac{4{,}250}{s^2 + 3{,}901s + 410{,}250} \tag{8.8.12}$$

$$G_{EHA,Leakge} = \frac{4{,}250}{s^2 + 4{,}244s + 452{,}160} \tag{8.8.13}$$

$$G_{EHA,Friction} = \frac{3{,}138}{s^2 + 27{,}234s + 404{,}370} \tag{8.8.14}$$

Note that the EHA system has become a second-order system, where the input is voltage (V), and the output is the cylinder (Axis A) velocity (m/s). Based on the above three EHA models and the sequential step input defined earlier, the output from each model may be simulated and compared with the measurement.

As shown in the following two figures, the obtained EHA models match the actual measurement very well. These models are used for the fault detection and diagnosis example in Chapter 6.

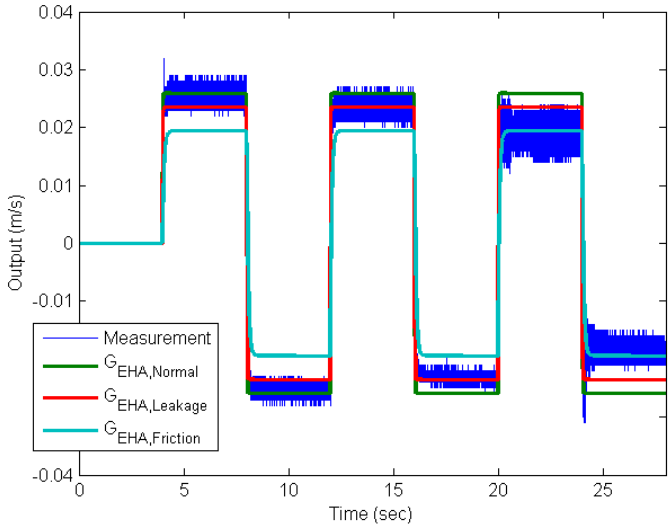

Figure 8.8.4. Measurements and the Outputs from the EHA Mathematical Models

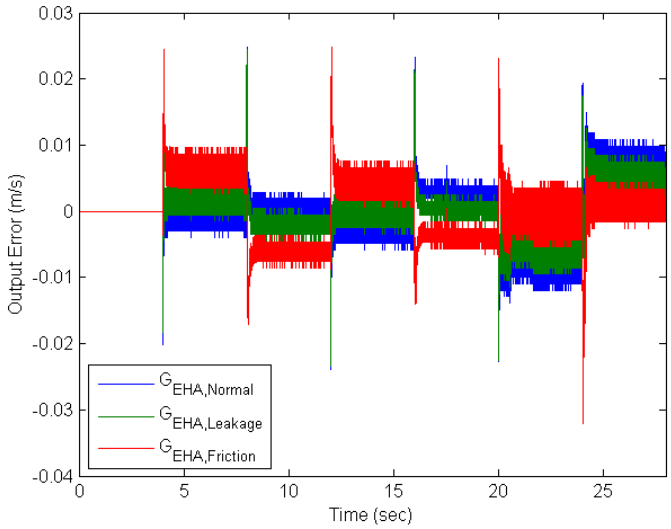

Figure 8.8.5. Measurement and Output Errors from the EHA Mathematical Models

Bibliography

List of References

[1] S. A. Gadsden, M. Al-Shabi, and S. R. Habibi, "Estimation Strategies for the Condition Monitoring of a Battery System in a Hybrid Electric Vehicle," ISRN Signal Processing, 2011.

[2] S. A. Gadsden, M. Al-Shabi, I. Arasaratnam, and S. R. Habibi, "Combined Cubature Kalman and Smooth Variable Structure Filtering for Nonlinear Estimation with Modeling Uncertainties," IEEE Transactions on Automatic Control, Submitted March 30, 2011 (FP-11-187).

[3] S. A. Gadsden and S. R. Habibi, "An Optimal Smoothing Boundary Layer for the Smoth Variable Structure Filter," Journal of Dynamic Systems, Measurements and Control (ASME), Submitted February 2, 2011 (DS-11-1025).

[4] S. A. Gadsden, D. Dunne, S. R. Habibi, and T. Kirubarajan, "Nonlinear Estimation Techniques Applied on Target Tracking Problems," Journal of Dynamic Systems, Measurements and Control (ASME), Submitted October 5, 2009 (DS-09-1266).

[5] S. A. Gadsden, Y. Song, K. R. McCullough, and S. R. Habibi, "Friction Fault Detection of an Electrohydrostatic Actuator," in ASME/Bath Symposium on Fluid Power and Motion Control (FPMC), Washington, D.C., 2011.

[6] S. A. Gadsden, D. Dunne, S. R. Habibi, and T. Kirubarajan, "Combined Particle and Smooth Variable Structure Filter for Nonlinear Estimation Problems," in 14th International Conference on Information Fusion, Chicago, Illinois, 2011.

[7] S. A. Gadsden and S. R. Habibi, "Model-Based Fault Detection of a Battery System in a Hybrid Electric Vehicle," in IEEE Vehicle Power and Propulsion Conference (VPCC), Chicago, Illinois, 2011.

[8] R. M. Ahmed, M. El Sayed, S. A. Gadsden, and S. R. Habibi, "Fault Detection of an Engine Using a Neural Network Trained by the Smooth Variable Structure Filter," in IEEE Multi-Conference on Systems and Control, Denver, Colorado, 2011.

[9] S. A. Gadsden, M. El Sayed, and S. R. Habibi, "The Continuous-Time Smooth Variable Structure Filter," in 23rd Canadian Congress of Applied Mechanics (CANCAM), Vancouver, British Columbia, 2011.

[10] R. M. Ahmed, S. A. Gadsden, M. El Sayed, and S. R. Habibi, "Fault Detection and Classification of an Electrohydrostatic Actuator Using a Neural Network Trained by the Smooth Variable Structure Filter," in 23rd Canadian Congress of Applied Mechanics (CANCAM), Vancouver, British Columbia, 2011.

[11] S. A. Gadsden, M. El Sayed, and S. R. Habibi, "Derivation of an Optimal Boundary Layer Width for the Smooth Variable Structure Filter," in American Control Conference (ACC), San Francisco, California, 2011.

[12] S. A. Gadsden, K. R. McCullough, and S. R. Habibi, "Fault Detection and Diagnosis of an Electrohydrostatic Actuator Using a Novel Interacting Multiple Model Approach," in American Control Conference (ACC), San Francisco, California, 2011.

[13] S. A. Gadsden, D. Dunne, S. R. Habibi, and T. Kirubarajan, "Application of the Smooth Variable Structure Filter to a Multi-Target Tracking Problem," in Signal Processing, Sensor Fusion, and Target Recognition, Society of Photo-Optical Instrumentation Engineers (SPIE), Orlando, Florida, 2011.

[14] S. A. Gadsden and S. R. Habibi, "Derivation of the Smooth Variable Structure Information Filter," in ASME International Mechanical Engineering Congress and Exposition (IMECE), Vancouver, British Columbia, 2010.

[15] S. A. Gadsden, M. Al-Shabi, I. Arasaratnam, and S. R. Habibi, "Estimation of an Electrohydrostatic Actuator Using a Combined Cubature Kalman and Smooth Variable Structure Filter," in ASME International Mechanical Engineering Congress and Exposition (IMECE), Vancouver, British Columbia, 2010.

[16] S. A. Gadsden and S. R. Habibi, "A New Form of the Smooth Variable Structure Filter with a Covariance Derivation," in IEEE Conference on Decision and Control, Atlanta, Georgia, 2010.

[17] S. A. Gadsden, S. R. Habibi, and T. Kirubarajan, "A Novel Interacting Multiple Model Method for Target Tracking," in 13th International Conference on Information Fusion, Edinburgh, UK, 2010.

[18] V. Jouppila, S. A. Gadsden, and A. Ellman, "Modeling and Identification of a Pneumatic Muscle Actuator System Controlled by an On/Off Solenoid Valve," in 7th International Fluid Power Conference (IFP), Aachen, Germany, 2010.

[19] S. A. Gadsden and S. R. Habibi, "Target Tracking Using the Smooth Variable Structure Filter," in ASME Dynamic Systems and Control Conference (DSCC), Hollywood, California, 2009.

[20] S. A. Gadsden, D. Dunne, S. R. Habibi, and T. Kirubarajan, "Comparison of Extended and Unscented Kalman, Particle, and Smooth Variable Structure Filters on a Bearing-Only Target Tracking Problem," in Signal and Data Processing of Small Targets, Society of Photo-Optical Instrumentation Engineers (SPIE), San Diego, California, 2009.

[21] V. Jouppila, S. A. Gadsden, G. Bone, and S. R. Habibi, "Sliding Mode Controller and Filter Applied to a Pneumatic McKibben Muscle Actuator," in ASME International Mechanical Engineering Congress and Exposition (IMECE), Lake Buena Vista, Florida, 2009.

[22] S. A. Gadsden, D. Mohammed, and M. Al-Shabi, "Regularized Least Squares: A Useful (Forgotten) Tool for Supervised and Semi-Supervised Learning," in 13th World Multi-Conference on Systemics, Cybernetics and Informatics (WMSCI), Orlando, Florida, 2009.

[23] S. A. Gadsden and S. R. Habibi, "The Future of Automobiles: Cognitive Cars," in 22nd Canadian Congress of Applied Mechanics (CANCAM), Halifax, Nova Scotia, 2009.

[24] S. A. Gadsden and S. R. Habibi, "Aircraft Tracking Using a Radar and the Smooth Variable Structure Filter," in 22nd Canadian Congress of Applied Mechanics (CANCAM), Halifax, Nova Scotia, 2009.

[25] S. A. Gadsden and S. R. Habibi, "Aerodynamic Flutter and Flight Surface Actuation," in ASME International Mechanical Engineering Congress and Exposition (IMECE), Seattle, Washington, 2007.

[26] S. A. Gadsden, "A Brief History and Philosophy of Mechanics," in 21st Canadian Congress of Applied Mechanics (CANCAM), Toronto, Ontario, 2007.

[27] S. A. Gadsden and S. R. Habibi, "Effects of Aerodynamic Flutter on a Flight Surface Actuator," in 21st Canadian Congress of Applied Mechanics (CANCAM), Toronto, Ontario, 2007.

[28] Y. Bar-Shalom, X. Rong Li, and T. Kirubarajan, Estimation with Applications to Tracking and Navigation. New York: John Wiley and Sons, Inc., 2001.

[29] R. E. Kalman, "A New Approach to Linear Filtering and Prediction Problems," Journal of Basic Engineering, Transactions of ASME, vol. 82, pp. 35-45, 1960.

[30] B. D. O. Anderson and J. B. Moore, Optimal Filtering. Englewood Cliffs, NJ: Prentice-Hall, 1979.

[31] B. Ristic, S. Arulampalam, and N. Gordon, Beyond the Kalman Filter: Particle Filters for Tracking Applications. Boston: Artech House, 2004.

[32] S. Haykin, Kalman Filtering and Neural Networks. New York, U.S.A.: John Wiley and Sons, Inc., 2001.

[33] A. Gelb, Applied Optimal Estimation. Cambridge, MA: MIT Press, 1974.

[34] D. Simon, Optimal State Estimation: Kalman, H-Infinity, and Nonlinear Approaches.: Wiley-

Interscience, 2006.

[35] G. Welch and G. Bishop, "An Introduction to the Kalman Filter," Department of Computer Science, University of North Carolina, 2006.

[36] S. J. Julier, J. K. Ulhmann, and H. F. Durrant-Whyte, "A New Method for Nonlinear Transformation of Means and Covariances in Filters and Estimators," IEEE Transactions on Automatic Control, vol. 45, pp. 472-482, March 2000.

[37] S. R. Habibi, "The Smooth Variable Structure Filter," Proceedings of the IEEE, vol. 95, no. 5, pp. 1026-1059, 2007.

[38] S. R. Habibi and R. Burton, "The Variable Structure Filter," Journal of Dynamic Systems, Measurement, and Control (ASME), vol. 125, pp. 287-293, September 2003.

[39] M. S. Grewal and A. P. Andrews, Kalman Filtering: Theory and Practice Using MATLAB, 3rd ed. New York: John Wiley and Sons, Inc., 2008.

[40] N. Wiener, Extrapolation, Interpolation, and Smoothing of Stationary Time Series. Cambridge, Massachusetts, USA: MIT Press, 1964.

[41] A. Kolmogorov, Interpolation and Extrapolation of Stationary Random Sequences (Selected Works of A. N. Kolmogorov), V. Tikhomirov, Ed. Dordrecht, The Netherlands: Kluwer Academic Publishers, 1941 (1992), vol. II.

[42] M. Al-Shabi, "The General Toeplitz/Observability SVSF," Department of Mechanical Engineering, McMaster University, Hamilton, Ontario, Ph.D. Thesis 2011.

[43] L. Zadeh and J. Ragazzini, "An Extension of Wiener's Theory of Prediction," Journal of Applied Physics, vol. 21, pp. 645-655, July 1950.

[44] R. Booton, "An Optimization Theory for Time-Varying Linear Systems with Non-Stationary Statistical Inputs," Proceedings of the IRE, vol. 40, pp. 977-981, August 1952.

[45] S. Schmidt, "The Kalman Filter: Its Recognition and Development for Aerospace Applications," Journal of Guidance and Control, vol. 4, no. 1, pp. 4-7, January and February 1981.

[46] L. McGee and S. Schmidt, "Discovery of the Kalman Filter as a Practical Tool for Aerospace and Industry," NASA, Technical Memo 86847, 1985.

[47] R. Kalman and R. Bucy, "New Results in Linear Filtering and Prediction Theory," ASME Journal of Basic Engineering, vol. 83, pp. 95-108, March 1961.

[48] M. S. Grewal and K. James, "Kalman Filter Implementation with Improved Numerical Properties," IEEE Transactions on Automatic Control, vol. 55, no. 9, pp. 2058-2068, September 2010.

[49] J. E. Potter and R. G. Stern, "Statistical Filtering of Space Navigation Measurements," in Proceedings of 1963 AIAA Guidance and Control Conference, New York, 1963.

[50] N. A. Carlson, "Fast Triangular Formulation of the Square Root Filter," AIAA Journal, vol. 11, no. 9, pp. 1259-1265, 1973.

[51] G. J. Bierman, Factorization Methods for Discrete Sequential Estimation. New York, USA: Academic Press, Inc., 1977.

[52] R. Van der Merwe and E. A. Wan, "The Square-Root Unscented Kalman Filter for State and Parameter-Estimation," in IEEE International Conference on Acoustics, Speech, and Signal Processing, 2001, pp. 3461-3464.

[53] W. H. Press, S. A. Teukolsky, W. T. Vetterling, and B. P. Flannery, Numerical Recipes: The Art of Scientific Computing. New York, USA: Cambridge University Press, 2007.

[54] K. Lemon and B. W. Welch, "Comparison of Nonlinear Filtering Techniques for Lunar Surface Roving Navigation," Glenn Research Center, NASA, Cleveland, Ohio, NASA/TM-2008-215152, 2008.

[55] G. J. Bierman, "Measurement Updating Using the U-D Factorization," in IEEE Conference on Decision and Control, 1975, pp. 337-346.

[56] C. L. Thornton and G. J. Bierman, "Givens Transformation Techniques for Kalman Filtering," Acta Astronautica, vol. 4, no. 7-8, pp. 847-863, July-August 1977.

[57] A. Andrews, "A Square Root Formulation of the Kalman Covariance Equations," AIAA Journal, vol. 6, pp. 1165-1166, 1968.

[58] J. M. Bennet, "Triangular Factors of Modified Matrices," Numerische Mathematik, vol. 7, pp. 217-221, 1963.

[59] A. Jazwinski, "Adaptive Filtering," Automatica, vol. 5, no. 4, pp. 475-485, July 1969.

[60] A. Jazwinski, Stochastic Processes and Filtering Theory. New York, USA: Academic Press, 1970.

[61] F. Schlee, C. Standish, and N. Toda, "Divergence in the Kalman Filter," AIAA Journal, vol. 5, pp. 1114-1120, June 1967.

[62] H. Sorenson and J. Sacks, "Recursive Fading Memory Filtering," Information Science, vol. 3, pp. 101-119, January 1971.

[63] R. Bucy and P. Joseph, Filtering for Stochastic Processes with Applications to Guidance. New York, USA: John Wiley & Sons, 1968.

[64] J. Crassidis and J. Junkins, Optimal Estimation of Dynamic Systems. New York, USA: CRC Press, 2004.

[65] B. Berndt, R. Evans, and K. Williams, Gauss and Jacobi Sums. New York, U.S.A.: John Wiley & Sons, Inc., 1998.

[66] R. Fitzgerald, "Divergence of the Kalman Filter," IEEE Transactions on Automatic Control, vol. AC-16, pp. 736-747, December 1971.

[67] A. L. Barker, D. E. Brown, and W. N. Martin, "Bayesian Estimation and the Kalman Filter," Computers and Mathematics with Applications, vol. 30, no. 10, p. 55, November 1995.

[68] R. Negenborn, "Robot Localization and Kalman Filters: On Finding Your Position in a Noisy World," Urtecht University, M.A.Sc. Thesis INF/SCR-03-09, 2003.

[69] P. S. Maybeck, Stochastic Models, Estimation and Control. New York, USA: Academic Press, 1979.

[70] J. Bellantoni and K. Dodge, "A Square Root Formulation of the Kalman-Schmidt Filter," AIAA Journal, vol. 5, pp. 1309-1314, 1967.

[71] S. J. Julier and J. K. Uhlmann, "Unscented Filtering and Nonlinear Estimation," Proceedings of the IEEE, vol. 92, no. 3, pp. 401-422, March 2004.

[72] I. Arasaratnam and S. Haykin, "Cubature Kalman Filters," IEEE Transactions on Automatic Control, vol. 54, no. 6, June 2009.

[73] B. Hassibi and T. Kailath, "H-infinity Adaptive Filtering," in IEEE International Conference on Acoustics, Speech, and Signal Processing, 1995, pp. 949-952.

[74] D. Moral., "Measure Valued Processes and Interacting Particle Systems: Application to Non-Linear Filtering Problems," Annals of Applied Probability, vol. 8, no. 2, pp. 438-495, 1998.

[75] N. J. Gordon, D. J. Salmond, and A. F. M. Smith, "Novel Approach to Nonlinear/Non-Gaussian Bayesian State Estimation," IEEE Proceedings - F, vol. 140, no. 2, pp. 107-113, 1993.

[76] J. MacCormick and A. Blake, "A Probabilistic Exclusion Principle for Tracking Multiple Objects," in Proceedings of International Conference on Computer Vision, 1999, pp. 572-578.

[77] K. Kanazawa, D. Koller, and S. J. Russell, "Stochastic Simulation Algorithms for Dynamic Probabilistic Networks," in Proceedings of the Eleventh Annual Conference on Uncertainty in Artificial Intelligence, 1995, pp. 346-351.

[78] R. Van der Merwe and E. Wan, "Sigma-Point Kalman Filters for Integrated Navigation," in Proceedings of the Institute of Navigation Annual Meeting, 2004, pp. 641-654.

[79] R. Van der Merwe, "Sigma-Point Kalman Filters for Probabilistic Inference in Dynamic State Space Models," OGI School of Science and Engineering, Oregon Health and Science Univeristy, Ph.D. Thesis 2004.

[80] J. Ambadan and Y. Tang, "Sigma-Point Kalman Filter Data Assimilation Methods for Strongly Nonlinear Systems," Journal of the Atmospheric Sciences, vol. 66, no. 2, 2009.

[81] X. Tang, X. Zhao, and X. Zhang, "The Square-Root Spherical Simplex Unscented Kalman Filter for State and Parameter Estimation," in Proceedings of the International Conference

on Signal Processing, 2008, pp. 260-263.

[82] S. Kim and W. Han, "Joint Estimation of Time Delay and Channel Amplitude by Simplex Unscented Filter without Assisted Pilot in CDMA Systems," in The 7th International Conference on Advanced Communications Technology, 2005, pp. 233-240.

[83] S. Julier, "The Spherical Simplex Unscented Transformation," in Proceedings of the American Conference Conference, 2003, pp. 2430-2434.

[84] I. Arasaratnam, S. Haykin, and R. Elliott, "Discrete-Time Nonlinear Filtering Algorithms Using Gauss-Hermite Quadrature," Proceedings of the IEEE, vol. 95, no. 5, pp. 953-977, 2007.

[85] X. R. Li, Advances in Aerospace Systems Dynamics and Control Systems (Volume 76), C. T. Leondes, Ed. New York, USA: Academic Press, 1996.

[86] D. T. Magill, "Optimal Adaptive Estimation of Sampled Stochastic Processes," IEEE Transactions on Automatic Control, vol. AC-10, pp. 434-439, 1965.

[87] G. A. Ackerson and K. S. Fu, "On State Estimation in Switching Environments," IEEE Transactions on Automatic Control, vol. AC-15, no. 1, pp. 10-17, January 1970.

[88] A. G. Jaffer and S. C. Gupta, "Recursive Bayesian Estimation with Uncertain Observation," IEEE Transactions on Information Theory, vol. IT-17, pp. 614-616, September 1971.

[89] A. G. Jaffer and S. C. Gupta, "Optimal Sequential Estimation of Discrete Processes with Markov Interrupted Observations," IEEE Transactions on Automatic Control, vol. AC-16, pp. 417-475, October 1971.

[90] C. B. Chang and M. Athans, "State Estimation for Discrete Systems with Switching Parameters," IEEE Transactions on Aerospace and Electronic Systems, vol. AES-14, no. 5, pp. 418-425, May 1978.

[91] H. A. P. Blom, "An Efficient Filter for Abruptly Changing Systems," in 23rd IEEE Conference on Decision and Control, Las Vegas, Nevada, December, 1984.

[92] H. A. P. Blom and Y. Bar-Shalom, "The Interacting Multiple Model Algorithm for Systems with Markovian Switching Coefficients," IEEE Transactions on Automatic Control, vol. AC-33, no. 8, pp. 780-783, August 1988.

[93] E. Mazor, A. Averbuch, Y. Bar-Shalom, and J. Dayan, "Interacting Multiple Model Methods in Target Tracking: A Survey," IEEE Transactions on Aerospace and Electronic Systems, vol. 34, no. 1, pp. 103-123, January 1998.

[94] H. Wang, T. Kirubarajan, and Y. Bar-Shalom, "Precision Large Scale Air Traffic Surveillance Using an IMM Estimator with Assignment," IEEE Transactions on Aerospace and Electronic Systems, vol. 35, no. 1, pp. 255-266, January 1999.

[95] Y. M. Zhang and X. R. Li, "Detection and Diagnosis of Sensor and Actuator Failures Using

IMM Estimator," IEEE Transactions on Aerospace and Electronic Systems, vol. 34, pp. 1293-1313, October 1998.

[96] S. Kim, J. Choi, and Y. Kim, "Fault Detection and Diagnosis of Aircraft Actuators Using Fuzzy-Tuning IMM Filter," IEEE Transactions on Aerospace and Electronic Systems, vol. 44, no. 3, pp. 940-952, July 2008.

[97] V. I. Utkin, "Variable Structure Systems With Sliding Mode: A Survey," IEEE Transactions on Automatic Control, vol. 22, pp. 212-222, 1977.

[98] V. I. Utkin, Sliding Mode and Their Application in Variable Structure Systems, English Translation ed.: Mir Publication, 1978.

[99] A. F. Fillipov, "Differential Equation with Discontinuous Right Hand Side," American Mathematical Society Transactions, vol. 62, 1969.

[100] V. Utkin, Sliding Modes in Control Optimization. New York, USA: Springer-Verlag, 1992.

[101] J. J. E. Slotine and W. Li, Applied Nonlinear Control. Englewood Cliffs, NJ, USA: Prentice-Hall, 1991.

[102] C. Milosavlejic, "General Conditions for the Existence of a Quasi-Sliding Mode on the Switching Hyperplane in Discrete Variable Structure Systems," Automatic Rmote Control, vol. 46, pp. 307-315, 1985.

[103] S. Z. Sarpturk, Y. Istefanopoulos, and O. Kaynak, "On the Stability of Discrete-Time Sliding Mode Control Systems," IEEE Transactions on Automatic Control, vol. AC-32, no. 10, pp. 930-932, October 1987.

[104] K. Furuta, "Sliding Mode Control of a Discrete System," Systems Control Letters, vol. 14, pp. 145-152, 1990.

[105] S. K. Spurgeon, "Sliding Mode Observers: A Survey," International Journal of Systems Science, pp. 751-764, 2008.

[106] S. H. Qaiser, A. I. Bhatti, M. Iqbal, R. Samar, and J. Qadir, "Estimation of Precursor Concentration in a Research Reactor by Using Second Order Sliding Mode Observer," Nuclear Engineering and Design, vol. 239, pp. 2134-2140, 2009.

[107] S. Qaiser, A. Bhatti, R. Samar, M. Iqbal, and J. Qadir, "Higher Order Sliding Mode Observer Based Estimation of Precursor Concentration in a Research Reactor," in 4th IEEE Conference on Emerging Technologies, 208, pp. 338-343.

[108] C. Edwards and S. Spurgeon, "On the Development of Discontinuous Observers," International Journal of Control, vol. 59, pp. 1211-1229, 1994.

[109] J. J. E. Slotine, J. Hedrick, and E. Misawa, "On Sliding Observers for Nonlinear Systems," in American Control Conference, Seattle, Washington, 1986, pp. 1794-1800.

[110] J. J. E. Slotine, J. Hedrick, and E. Misawa, "On Sliding Observers for Nonlinear Systems,"

ASME Journal of Dynamic Systems, Measurement and Control, vol. 109, no. 3, pp. 245-252, September 1987.

[111] B. Walcott and S. Zak, "State Observation of Nonlinear Uncertain Dynamical Systems," IEEE Transactions on Automatic Control, vol. AC-32, no. 2, pp. 166-170, February 1987.

[112] B. Walcott, M. Corless, and S. Zak, "Comparative Study of State Observation Techniques," International Journal of Control, vol. 45, no. 6, pp. 2109-2132, June 1987.

[113] C. Tan and C. Edwards, "Sliding Mode Observers for Robust Detection and Reconstruction of Actuator and Sensor Faults," International Journal of Robust and Nonlinear Control, vol. 13, no. 1, pp. 443-463, January 2003.

[114] S. R. Habibi, R. Burton, and Y. Chinniah, "Estimation Using a New Variable Structure Filter," in American Control Conference, Anchorage, AK, 2002, pp. 2937-2942.

[115] E. P. Ryan and M. Corless, "Ultimate Boundedness and Asymptotic Stability of a Class of Uncertain Dynamical Systems via Continuous and Discontinuous Feedback Control," Journal of Mathematics Control and Information, vol. 1, pp. 223-242.

[116] J. J. E. Slotine, "Sliding Controller Design for Nonlinear Systems," International Journal of Control, vol. 40, no. 2, pp. 421-434, 1984.

[117] J. J. E. Slotine, "The Robust Control of Robot Manipulators," International Journal of Robotic Research, vol. 4, no. 2, pp. 49-64, 1985.

[118] H. Asada and J. J. E. Slotine, Robot Analysis and Control. New York, U.S.A.: John Wiley Publications, 1986.

[119] S. R. Habibi, "The Extended Variable Structure Filter," ASME Journal of Dynamic Systems, Measurement, and Control, vol. 128, no. 2, pp. 341-351, June 2006.

[120] D. G. Luenberger, Introduction to Dynamic Systems. U.S.A.: John Wiley, 1979.

[121] S. Li, A. J. Jarvis, and D. T. Leedal, "Are Response Function Representations of the Global Carbon Cycle Ever Interpretable?," Tellus, vol. 61B, pp. 361-371, 2009.

[122] N. Nise, Control Systems Engineering, 6th ed. New York: John Wiley and Sons, Inc., 2011.

[123] M. L. Hernandez, T. Kirubarajan, and Y. Bar-Shalom, "Multisensor Resource Management in the Presence of Clutter Using Cramér-Rao Lower Bounds," IEEE Transactions on Aerospace and Electronic Systems, vol. 40, no. 2, April 2004.

[124] X. Zhang and P. Willett, "Cramér-Rao Bounds for Discrete-Time Linear Filtering with Measurement Origin Uncertainties," in Proceedings of the Workshop on Estimation, Tracking and Fusion: A Tribute to Yaakov Bar-Shalom, California, 2001.

[125] P. Tichavsky, "Posterior Cramér-Rao Bounds for Discrete-Time Nonlinear Filtering," IEEE Transactions on Signal Processing, vol. 46, no. 5, May 1998.

[126] P. Zarchan, "Tactical and Strategic Missile Guidance," Progress in Astronautics and

Aeronautics, vol. 157, 1994.

[127] K. B. Petersen and M. S. Pedersen, The Matrix Cookbook.: Technical University of Denmark, 2008.

[128] S. R. Habibi and R. Burton, "Parameter Identification for a High Performance Hydrostatic Actuation System using the Variable Structure Filter Concept," ASME Journal of Dynamic Systems, Measurement, and Control, 2007.

[129] T. Kailath, Linear Systems. U.S.A.: Prentice Hall, 1980.

[130] H. Wang, T. Kirubarajan, and Y. Bar-Shalom, "Precision Large Scale Air Traffic Surveillance Using an IMM Estimator with Assignment," Transaction of the IEEE, Aerospace and Electronic Systems Journal, vol. 35, no. 1, pp. 255-266, 1999.

[131] M. El Sayed, "Multiple Sliding Mode Control for Electro-Hydraulic Actuation (EHA) Systems," Article Under Preparation, 2011.

[132] M. El Sayed and S. R. Habibi, "Inner-Loop Control for Electro-Hydraulic Actuation (EHA) Systems," ASME Journal of Dynamic Systems, Measurement and Control, 2011 (In Press).

[133] K. McCullough, "Design and Characterization of a Dual Electro-Hydrostatic Actuator," Department of Mechanical Engineering, McMaster University, Hamilton, Ontario, M.A.Sc. Thesis 2011.

[134] Y. A. Chinniah, "Fault Detection in the Electrohydraulic Actuator Using the Extended Kalman Filter," Department of Mechanical Engineering, University of Saskatchewan, Saskatoon, Saskatchewan, Ph.D. Thesis 2004.

[135] S. Wang, "Integrated Control and Estimation Based on Sliding Mode Control Applied to Electrohydraulic Actuator," Department of Mechanical Engineering, University of Saskatchewan, Saskatoon, Saskatchewan, Ph.D. Thesis 2007.

[136] R. K. Mehra, "On the Identification of Variances and Adaptive Kalman Filtering," IEEE Transactions on Automatic Control, vol. AC-15, no. 2, pp. 175-184, April 1970.

[137] R. T. Morein and P. Kalata, "A Polynomial Algorithm for Noise Identification in Linear Systems," in 5th IEEE International Symposium on Intelligent Control, 1990, pp. 595-600.

[138] J. Dunik and M. Simandl, "Estimation of State and Measurement Noise Covariance Matrices by Multi-Step Prediction," in 17th World Congress, International Federation of Automatic Control, Seoul, Korea, 2008, pp. 3689-3694.

[139] R. Ahmed, "Training of Neural Networks Using the Smooth Variable Structure Filter with Application to Fault Detection," Department of Mechanical Engineering, McMaster University, Hamilton, Ontario, Canada, M.A.Sc. Thesis 2011.